CENTRAL RESEARCH LIBRARY
DOCUMENT COLLECTION

7

MARTIN MARIETTA ENERGY SYSTEMS LIBRARIES
3 4456 0049752 1

ORNL-2743
Reactors–Power
TID-4500 (14th ed.)

HOMOGENEOUS REACTOR PROJECT

QUARTERLY PROGRESS REPORT

FOR PERIOD ENDING APRIL 30, 1959

CENTRAL RESEARCH LIBRARY
DOCUMENT COLLECTION
LIBRARY LOAN COPY
DO NOT TRANSFER TO ANOTHER PERSON
If you wish someone else to see this document, send in name with document and the library will arrange a loan.

OAK RIDGE NATIONAL LABORATORY
operated by
UNION CARBIDE CORPORATION
for the
U.S. ATOMIC ENERGY COMMISSION

Printed in USA. Price $4.00. Available from the
Office of Technical Services
Department of Commerce
Washington 25, D.C.

LEGAL NOTICE

This report was prepared as an account of Government sponsored work. Neither the United States, nor the Commission, nor any person acting on behalf of the Commission:

A. Makes any warranty or representation, expressed or implied, with respect to the accuracy, completeness, or usefulness of the information contained in this report, or that the use of any information, apparatus, method, or process disclosed in this report may not infringe privately owned rights; or

B. Assumes any liabilities with respect to the use of, or for damages resulting from the use of any information, apparatus, method, or process disclosed in this report.

As used in the above, "person acting on behalf of the Commission" includes any employee or contractor of the Commission, or employee of such contractor, to the extent that such employee or contractor of the Commission, or employee of such contractor prepares, disseminates, or provides access to, any information pursuant to his employment or contract with the Commission, or his employment with such contractor.

ORNL-2743
Reactors–Power
TID-4500 (14th ed.)

Contract No. W-7405-eng-26

HOMOGENEOUS REACTOR PROJECT

QUARTERLY PROGRESS REPORT

for Period Ending April 30, 1959

Project Director – R. B. Briggs
Associate Director – C. E. Winters

Homogeneous Reactor Test – S. E. Beall
Reactor Analysis, Research, and Design – R. N. Lyon
Engineering Development – R. N. Lyon
Reactor Materials Research – E. G. Bohlmann
Chemical Engineering Development – D. E. Ferguson
Supporting Chemical Research – H. F. McDuffie
Analytical Chemistry – M. T. Kelley

DATE ISSUED

JUL 30 1959

OAK RIDGE NATIONAL LABORATORY
Oak Ridge, Tennessee
operated by
UNION CARBIDE CORPORATION
for the
U.S. ATOMIC ENERGY COMMISSION

MARTIN MARIETTA ENERGY SYSTEMS LIBRARIES
3 4456 0049752 1

SUMMARY

PART I. HOMOGENEOUS REACTOR TEST

1. HRT Operations

HRT run 18 was terminated after 1281 hr by the first scram in the history of the reactor. After several components were replaced or repaired, run 19 was begun, and it was discovered that neither circulating pump was pumping at the normal rate. After several weeks of investigation during which pressure taps were installed and measurements made in both systems, it was determined that the blanket pump was indeed faulty but that the fuel pump had not performed correctly because it had been improperly wired during the maintenance period preceding run 19.

The blanket pump was removed and replaced with a new pump. When the old pump was disassembled, it was found that about three-fourths of the titanium impeller had disappeared, apparently having been ignited. Deposits of slag and solidified metal droplets were scattered over the suction nozzle and scroll liner. The burning of the titanium probably resulted when the pump became oxygen-gas-bound at the startup for run 19. The impeller must have been scratched, exposing new metal which ignited in the oxygen atmosphere.

Preparations are being completed for run 20, in which fuel-stability problems will be investigated.

2. HRT Processing Plant

The results of three additional hydroclone-system runs reported this quarter were not significantly different from previous runs. Solids removal rates were comparable (0.3 - 0.6 g/hr), and the chemical composition of solids removed was essentially identical (Fe, 23%; Zr, 41%; Cr, 7%; U, 4.8%) to the results of the earlier runs. Revised estimates of total zirconium corrosion in the reactor, based on known stainless steel corrosion rates and the composition of solids removed in the chemical plant, indicate that 21 kg of ZrO_2 has been produced. Similar calculations based on the fraction of Zr^{95} removed are in excellent agreement.

A multiple hydroclone unit containing 13 hydroclones was designed and fabricated for installation in HRT. A bypass stream of greater than 10 gpm will be continuously routed through the unit. Solids concentrated in the underflow stream will be collected by the existing chemical plant hydroclone and underflow pot.

A complete analysis of all rare-earth spectrographic data shows that, at present concentrations, limits imposed by analytical sensitivity prevent a

complete study of rare-earth behavior under reactor conditions. An addition of nonradioactive rare earths which would increase concentrations equivalent to approximately one year's full power operation has been proposed.

The radioactivity in 1,420,000 gal of reactor-cell shield water discharged this quarter was reduced from 350 to 2.2 curies of beta activity by adsorption on a calcium phosphate precipitate before disposal of the water from the retention pond.

3. Design and Development of Tools for HRT Remote Operations

The tooling required to remove the screens from the HRT core and to patch the hole in the tank was developed. Two tools were designed for detaching the screens from the core wall and passed preliminary tests: a fly-cutter mounted in a folding T-section at the end of a 20-ft shaft, and a remote milling cutter using a flexible-shaft drive. Various tools for maneuvering loose screens were devised. Two methods of removing loose screens were shown to be feasible--electrolytic dissolution in nitric acid and arc cutting. Work is being continued on controlling hydrogen pickup in Zircaloy during the dissolution process. The design and construction of a remote arc-cutter manipulator is in progress.

Better definition of the hole in the core can be obtained with a plastic impression and with dimensionally calibrated photographs. A patch sealed with the use of a toggle bolt was developed, and a model test gave an acceptable leak rate. A tool for remote installation of the patch was tested successfully.

An ultrasonic thickness gauge and positioner for the spherical portion of the core tank was fabricated and tested successfully.

A tool for making a plastic impression of two weld areas in the top tee section of the reactor vessel was designed and built.

A tool was developed for cutting metallurgical specimens from the edge of loose HRT screens.

Several devices, including a parallel-jaw tongs for general use, a revised core specimen removal tool, and a vacuum pickup device, were designed for picking up materials from the cell and core.

4. HRT Component Development

Although four prototype feed and purge pump assemblies have been operated for 16,000 hr or more, four of 12 similar assemblies at the HRT have been replaced after less than 5,000 hr of operation.

Replacement fuel and blanket circulating pumps for the HRT were pretreated and tested. Flushing and vibration were shown to be possible methods of cleaning up heat exchanger plugs caused by corrosion scale.

Operation of the HRT-core model with a transparent conical diffuser indicated that the most satisfactory modification to the present core would be to remove the upper five screens and to reverse the direction of flow. Solids produced during such a maintenance operation were shown to be flushed out of

the core by downward flow. The flow pattern of the replacement core having an annular inlet was made symmetrical by use of a secondary inlet at the opposite pole.

The HRT mockup was operated 811 hr with reversed flow, 694 hr of which was at 1500 psi and 280°C with a fuel composition of 0.045 m UO_2SO_4, 0.036 m $CuSO_4$ and 0.025 m H_2SO_4, in anticipation of reversing the flow through the HRT core. With the conventional stainless steel pressurizer in service, the fuel remained stable at all pressurizer purge rates up to more than 10 gal/hr, a condition which led to uranium precipitation rate of 24 g/day in previous operation with forward flow. There was no noticeable difference in gas separator performance with reversed flow, and the high pressure system liquid level was controlled at a liquid entrainment of 0.21 gal/min in a 13 scfm gas letdown stream. Performance of the system was satisfactory in all respects.

5. HRT Design

The piping on a circulating-pump assembly will be altered to allow a reversal of the direction of flow in the HRT core system.

Temporary equipment, including a basket-type strainer, was designed for both the fuel and blanket systems for removal of solids from the systems during maintenance operations.

The radiolytic-gas concentration was calculated for the HRT as a function of power level and average temperature. The maximum total radiolytic gas, excess oxygen, and D_2O vapor pressure was found to exist at the core and blanket outlets for all average temperatures greater than 250°C.

6. HRT Reactor Analysis

The effect of fuel in the HRT blanket region upon the neutron leakage from the reactor was computed. The addition of blanket fuel increased the neutron leakage and hardened the energy spectrum of the escaping neutrons. With a blanket-to-core concentration ratio of 0.3, the ratio of total neutron leakage relative to that with no fuel in the blanket was about 6; for escaping neutrons having energies above 10^3 ev the corresponding ratio was about 14.

The high-energy flux in the HRT was calculated as a function of position for blanket-to-core fuel-concentration ratios of 0 and 0.33. Only uncollided and once-collided neutrons were considered. The neutron flux above 1 Mev energy at the core-tank wall was about 8×10^{11} neutrons/cm^2.sec at 1 Mw, with no fuel in the blanket. With fuel in the blanket region, the corresponding flux was about 5.6×10^{11} neutrons/cm^2·sec. The integrated fast flux (that above 1 Mev) at the inner surface of the pressure vessel was computed to be $<1.2 \times 10^{15}$ neutrons/cm^2 for HRT run 14, and 3.6×10^{17} neutrons/cm^2 for HRT run 17.

7. HRT Controls and Instrumentation

The presently installed reactor letdown valve has now operated satisfactorily for 3787 hr. A smaller valve tested in the HRT Mockup Loop was operated for 3520 hr and was still leaktight. The smaller valve is considered to be more suitable for the present reactor operating conditions.

A waterproof, gamma-sensitive ionization chamber which utilizes alumina insulators to permit operation in high-temperature environments was satisfac-factory when tested at 150°C.

The miniature television camera designed for resistance to radiation was tested in a 1.5×10^6 r/hr gamma field. The camera operated well, although the lens was quickly browned. A lens made of non-browning glass was ordered and will be similarly tested.

PART II. REACTOR ANALYSIS, RESEARCH, AND DESIGN

8. Research and Analysis

The core-wall temperature in a two-region reactor can be controlled by passing blanket slurry between the wall and a shroud; for a 4 x 12 ft cylindrical core, 400-Mw (thermal) reactor, a fluid flow rate of 19,000 gpm through a 3-in. gap would keep the maximum wall temperature at 250°C if the blanket slurry temperature in the gap were 155°C at the point of maximum heat flux. The wall could also be cooled by using a double-wall core vessel and passing heavy water inside the double wall at the required temperature and velocity (the coolant temperature rise was assumed to be 50°C). For the above reactor the wall temperature would be maintained at 250°C if the coolant flow rate were 690 gpm and the coolant temperature at the midplane were 60°C. If the reactor power were 200 Mw, the required coolant temperature at the midplane would be 157°C.

The effect of temperature distribution upon the maximum power density at the core wall was studied for long cylindrical reactors. Both straight-through flow and reverse flow were considered, and the results obtained compared with those for reactors having a uniform, constant temperature. The maximum power density was essentially independent of temperature distribution for cylinders less than about 15 ft long. In a 20-ft-long core, the maximum power density associated with axially varying nuclear properties was 15 to 20% higher than that obtained with uniform nuclear properties.

The slurry concentration which gives the maximum critical temperature in small slurry reactors was obtained as a function of uranium-to-thorium ratio and moderator composition. For a 3.5-ft bare reactor containing a moderator of 90% D_2O - 10% H_2O and a slurry having a U/Th ratio of 0.075, the slurry concentration which gave the highest critical temperature was about 350 g of Th per liter; this critical temperature was 200°C.

Different two-group models and the harmonics method were used to calculate critical-mass ratios in small, reflected, slurry-core reactors. For reactors 2 ft in diameter surrounded by a 1 1/2-ft reflector, the harmonics method gave critical-mass ratios which were about 20% greater than those obtained by two-group calculations. The addition of resonance fissions increased the thorium concentration at which the minimum critical-mass ratio occurred by about 400 g of Th per liter, and decreased the critical-mass ratio from 20 to 50%, depending on the thorium concentration.

Two machine programs were written; one calculates group-averaged cross sections for use in multigroup programs; the other calculates the energy-group flux associated with uncollided and once-collided neutrons as a function of position in two-region reactors.

Slurry dropout velocities as a function of volume fraction solids were studied in terms of an effective Reynolds number. This "dropout" Reynolds number appears to be ~2100 for volume fraction solids >0.08; below 8% solids, the Reynolds number increased with decreasing slurry concentration. The dropout data were also correlated in terms of the wall-shear velocity and floc settling rate as a function of slurry concentration; at a volume fraction solids of 0.06, the wall-shear velocity required to maintain solids in suspension was about 0.15 fps for a floc settling rate of 6.5×10^{-3} fps.

A 30-gpm-loop slurry run was completed in which thoria was circulated at 275°C and about 450 g of Th per kg of H_2O. The thoria was prepared from oxalate which had been digested for 1 hr prior to filtration; calcination was at 800°C for several hours. The only place a film formed in the loop during 100 hr of circulation was in the 5-fps section. In another 30-gpm loop run, the addition of chromate ion to a normally caking slurry resulted in no cake or sphere formation. The removal of some thoria-cake deposits by circulating a noncaking slurry was demonstrated in other runs.

9. Design of Circulating-Slurry Critical System

Preliminary conceptual design and layout of a 100-kw experimental slurry system were completed.

PART III. ENGINEERING DEVELOPMENT

10. Development of Fuel- and Slurry-System Components

The natural-circulation recombiner operated routinely for 1500 hr at 1500 psi.

The temperature of the steam which could be circulated by the 20-cfm canned-motor blower was increased from 170°C to 225°C. Overheating of the motor by condensation of steam at the interface between the vapor and the cold water in the rotor cavity has prevented operation at higher temperatures. It was decided to terminate the Reliance 6000-gpm-pump contract, because of an expected increase in cost. The 300A pump continued to circulate slurry without difficulty, for a total of 2800 hr; thoria which had dropped out in the pressurizer of the 300A loop was resuspended by using a vibrator.

The three-stage contaminated-service oxygen compressor (Pressure Products Industries) was placed on test and required several adjustments, including replacement of the third-stage diaphragm. Testing of a uranyl sulfate single-stage turbine pump was discontinued following a wear-ring failure and a shaft-seal failure. Satisfactory operation of two diaphragm heads in slurries continued, although output decreased gradually as the result of dropout in the pump suction line.

A set of alumina check-valve trim was still serviceable after 1135 hr of slurry operation. Beryllia seats, operating against alumina balls, indicated deterioration after 200 hr.

Griscom-Russell Company is proceeding with the manufacture of carbon-steel components of their test steam generators; welding tests of stainless steel tube joints were completed.

Measurement of velocity distribution near the wall of the 4-ft re-entrant core model was started. Slurry runs in a 30-in. core vessel were begun; it was shown that variations in sample concentration were introduced by variations in sampling methods.

The thoria concentrations of various slurry settled beds at 200°C averaged 60% of the concentration at room temperature. The hindered-settling rate of a mixed thoria-urania slurry was proportional to the 0.5 power of the acceleration, in the range 1 to 20 g.

11. Development of Reactor Slurry Systems

Three runs were completed in the 200A and B loops, totaling 2957 hr of circulation of a mixed thoria - 8% urania slurry proposed for use in an experimental slurry reactor. The purpose of these runs was to extend the information on handling characteristics, rheological properties, attack rate, heat transfer, settled-bed properties, and stability of this slurry at operating temperature. In the range of approximately 500 to 600 g of Th-U per kg of H_2O the slurry settling rate decreased from 1.1 to 0.25 cm/sec when the temperature was reduced from 200 to 100°C. The rheological constants were τ_y = 0.008 and 0.005 lbf/ft^2 and η = 0.9 and 1.0 centipoise at 150 and 100°C, respectively. On dismantling the 200A pump, the titanium impeller was found to be in good condition. Attack on the titanium scroll liner in the sleeve region was visible in the form of gouge marks about 1/16 in. deep. Heat transfer measurements using the copper-disc heat meter[1] showed that the coefficients for the slurry were not much different from those for water at the same temperature and flow for all concentrations in the range of 0 to 540 g of Th-U per kg of H_2O. Solids that accumulated in a 14-ft vertical stagnant line in loop 200B for several days could be moved under their own static pressure plus a dynamic pressure of 8 psi caused by loop flow, provided that a very small flow (30 cm^3/min) of purge water was introduced in the valve at the bottom. With no purge flow, beds which had settled for as long as 11 days required dynamic heads as high as 21 psi to re-establish flow. The slurry appeared to have a stable uranium content under loop operating conditions at 220°C, and there was no significant particle degradation.

The 30-in.-dia pressure vessel[2] was installed in the 300-SM loop. One run (SM-6) was completed and a second run (SM-7) was started with the mixed thoria-urania slurry, at 500 psi and temperatures covering the range of 150 to 200°C. Both runs are flow tests of a proposed single-region slurry core vessel with re-entrant flow at the bottom. From 93 to 96% of the oxide inventory was maintained in circulation at all conditions, and a substantial part of the missing material could be accounted for by holdup in dead-ended lines and the pressurizer. Slurry samples drawn from within the vessel indicated the possible existence of concentration gradients which were affected by temperature, concentration, and flow rate. There was also evidence that sampler-tube orientation influenced the performance of the samplers, and there was consistent evidence of slightly higher slurry concentrations in the region of the conical wall of the vessel at all flows, which became more pronounced with decreasing flows.

12. Instrument and Valve Development

A differential transformer designed for use at high temperature and in radiation fields exhibited no change in characteristics when cycled from 25 to 350°C. The transformer, which is wound with ceramic-insulated wire, has a sensitivity of 0.1 mv/v per 0.001 in. when used with appropriate exciting and impedance matching circuitry.

Several ceramic coatings tested for possible use as an insulating sleeve in high-temperature magnetic flowmeters decomposed in 300°C oxygenated water in a static autoclave.

An alternate power-control system for pressurizer heaters was built up from static components and satisfactorily tested on a dummy load of Calrod heating elements.

Type 347 stainless steel bellows for use as valve stem seals exhibited a satisfactory life when cycled to failure in thorium oxide slurry at elevated temperature and pressure. A similar bellows assembly fabricated from grade Ti-55 titanium was cycled 11,600 times (1/8-in. strokes) before failing in 280°C uranyl sulfate solution at a pressure differential of 2300 psi.

PART IV. REACTOR MATERIALS RESEARCH

13. Solution Corrosion

Studies concerned with the deposition of salts from simulated fuel solutions under boiling conditions were continued. Deposition of salts did not occur when a heated Zircaloy-2 bypass section was mounted either vertically or horizontally, even when the flow rate was low and the heat flux was high. However, when the bypass was mounted about 10 deg from the horizontal, deposition occurred readily provided the flow rate was low and the solution boiled.

Additional deposition tests were carried out in loop L-2-23 in which the core section was heated. These tests demonstrated that under conditions where deposition took place, increasing the acid concentration of the solution decreased the rate and extent of deposition but did not completely prevent it. Also, it appeared that deposition occurred more readily under boiling conditions when the solution temperature was 225°C than when it was either 250 or 280°C. By use of an apparatus combining a standard x-ray machine, a television camera sensitive to x rays, and a closed-circuit television receiver, it was possible to observe the deposition process. These observations clearly demonstrated the necessity of a heated metal surface above a stable gas phase to obtain salt deposition.

Deoxidine-170 was the most effective of several reagents tested to determine their ability to dissolve stainless steel corrosion products. In a 36-hr loop run at 125°C a Deoxidine-170 solution completely removed the tightly adherent corrosion-product film from the surface of the loop. Zircaloy-2 and stainless steel were not significantly attacked by the reagent, but titanium specimens corroded at a rate in excess of 600 mpy.

A simulated HRT fuel solution was stable with regard to uranium concentration when diluted to 23 ppm at 250°C; however, some copper was lost from solution. In other stability tests solutions containing about 6 g of uranium per liter and equivalent concentrations of copper sulfate and sulfuric acid were not completely stable at 320°C with either H_2O or D_2O as solvent.

Preliminary tests in a uranyl sulfate solution indicate that an 18-8 stainless steel alloyed with either small amounts of platinum or copper is more corrosion resistant at low flow rates than a conventional 18-8 stainless steel; both alloys corroded at the same rate at high flow rates.

A study was made to determine the susceptibility of off-specification type 347 stainless steel to intergranular attack by uranyl sulfate solutions. Sensitized specimens of several heats of the alloy which failed to pass the boiling 65% HNO_3 test in the sensitized condition were subjected to uranyl sulfate solutions at 100, 200, and 300°C. In no case was intergranular attack observed. On the other hand, sensitized specimens of the unstabilized type 310 stainless steel showed mild intergranular attack under the same exposure conditions.

Continued testing with a single heat of cast type 347 stainless steel has confirmed previously reported data to the effect that the cast alloy is more resistant to stress-corrosion cracking than is the wrought alloy. When cracking has been observed in the cast alloy, the cracks appear to be closely related to areas of surface cold work.

Corrosion tests with Uniloy 19-9DL showed that the alloy in the annealed and in the annealed-and-aged condition has corrosion resistance similar to that of type 347 stainless steel in simulated reactor fuel solutions and has less tendency to gall than the austenitic stainless steels. In view of its favorable mechanical properties, it should find use in various HRP applications.

14. Slurry Corrosion

The attack rate, rheological properties, and handling characteristics of a D_2O slurry of mixed ThO_2-UO_3 (0.5% U/Th) containing a Pd-metal recombination catalyst under conditions simulating a proposed in-pile loop experiment were examined in a 100A-loop test of 1036 hr. The test, which was divided into two phases, circulated the slurry at 280°C at ~450 g of Th per kg of D_2O for 508 hr employing an argon atmosphere and for 528 hr using an oxygen atmosphere. Attack rates in mils per year (mpy) under O_2 atmosphere included the following: loop, 1 mpy; pin specimens (at 20 fps) of stainless steels, 1-3 mpy; chromium alloy steels, 1-2 mpy; titanium and Zircaloy-2, <1 mpy; and Inconel, 13 mpy. Under the argon-deuterium atmosphere, attack rates of alloy steels increased severalfold, while rates for the loop and all other materials above decreased (or remained unchanged), the rate of Inconel being lowered to <0.1 mpy. Increase in velocity from 20 to 40 fps resulted, under either atmosphere, in increases in attack rates averaging sixfold.

In another loop test of 553-hr duration using an oxygenated slurry of 3- to 30-μ ThO_2 microspheres at 175°C at an average concentration of 295 g of Th per kg of H_2O, attack rates of specimens of stainless steels, Incoloy, and Croloy 9M exposed at flow velocities of 22 to 32 fps ranged from 0.1 to 0.5 mpy. Specimens of titanium and Zircaloy-2 were not detectably attacked. The mean attack rate on the austenitic stainless steel test loop and circulating pump was 0.4 mpy. The handling and resuspension characteristics of the slurry were satisfactory.

The addition of UO_3 (8% U/Th) to slurries of 1600°C-calcined ThO_2 which were circulated at 200°C at a nominal concentration of 500 g of Th per kg of H_2O generally increased slightly the attack of 300- and 400-series stainless steels, Incoloy, certain Hastelloys, platinum, and gold in both oxygenated and hydrogenated tests. Stainless steels exposed in the velocity range 10 to 50 fps displayed rates about 5 times higher in hydrogenated slurries than in oxygenated slurries. Rates for Inconel and Hastelloy alloys were a factor of 10 lower in the hydrogenated tests. Type 347 stainless steel was least affected by addition of UO_3 or by changing atmospheres. In both atmospheres the attack of alloy steels containing from 0 to 9% chromium decreased as the chromium content of the alloy increased.

In toroid tests conducted at 280°C to compare the attack of a group of alloys in atmospheres of argon, deuterium, and oxygen using slurries of 650°C-calcined ThO_2 containing Pd-metal catalyst and additions of UO_3 at levels of 0.5 and 3% U/total solids, the average ratio of attack rates with 3% U added to those with 0.5% U was 0.7. At a slurry concentration of 450 g of Th-U per kg of D_2O, the normalized rate of type 347 stainless steel in oxygenated slurry, with 0.5% U, was 4 mpy. The susceptibility of the other alloys in O_2 to attack, relative to the normalized reference conditions, was: titanium, 1.4; Zircaloy-2, 0.5; and Inconel, 9; Inconel in D_2 or Ar atmosphere was 0.7. Excluding Inconel, the average effect of D_2 and Ar was to increase corrosion by factors of 2.5 and 1.5, respectively.

Three toroid runs comprised a series of tests with D_2O slurries of Th-8.8% U oxide (urania adsorbed on thoria) to compare the effects of temperature and atmosphere on the attack of a group of selected alloys and on the dissociation of uranium from the thoria-urania. Attack of type 347 stainless steel, titanium, and Inconel was a factor of ~2 higher as a result of increasing the test temperature from 200 to 280°C in runs which circulated 500 g of Th-U per kg of D_2O slurries at 26 fps. Using a deuterium atmosphere, the attack of Inconel was reduced at both temperatures, whereas attack of the other alloys was increased by an average factor of 3. No correlation between uranium dissociation and test temperature or additive (CrO_3) was indicated. Specimens of Zircaloy-2 used in some tests were markedly attacked as a result of deuteriding. Results of a metallurgical examination of the specimens are reported.

Six commercial grades of aluminum oxide were corrosion tested in static slurry environments for possible usefulness as check balls in valves in slurry service. At 100°C five of the six materials corroded at rates of less than 2 mpy; at 300°C only one material, Alox, showed adequate corrosion resistance.

A Zircaloy-2 autoclave experiment (L6Z-129S) containing thoria-urania slurry at a concentration of 1090 g of Th per kg of D_2O, 5 wt % U (coprecipitated) based on thorium, 0.0016 m Pd, and an oxygen atmosphere has been terminated after nine weeks in-pile operation. Following a week of pre-insertion operation at 280°C, it was inserted in LITR beam hole HB-6. It operated there for three weeks at 280°C, followed by one week at 320°C, two weeks at 240°C, and then three additional weeks at 280°C. Short periods of operation at 200°C were made for gas generation and recombination studies.

During the first week of in-pile operation, the corrosion rate was 3 mpy at an average fission power density of 6 w/ml. Values for corrosion at 280°C were fitted by the equation:

$$280°C \text{ corrosion rate, mpy} = \frac{63 + (113 \times \text{w/ml})}{\text{hr at temp.}} .$$

The radiation coefficient was doubled at 320°C. At 0.6 w/ml (av), no corrosion was detected at 240°C. During the first week after returning to 280°C, the incremental corrosion rate was 0.5 mpy at 4 w/ml (av). At 10 w/ml (av) for the final two weeks of operation, the corrosion rate was 0.2 mpy. Radiolytic-gas recombination by the palladium catalyst was studied by means of insertion and retraction experiments. A useful catalyst performance index, both applicable to reactors and observable in experiments, is defined as the power density (w/ml) resulting in an equilibrium pressure of 100 psi radiolytic D_2. It is related to catalyst activity and gas production by the expression:

$$\frac{(w/ml)}{(psi\ D_2)_{eqb/100}} = \frac{(\text{Cat. activity, moles } D_2\text{/liter-hr at 100 psi } D_2)}{0.38\ G_{D_2}}$$

After an original high value, the catalyst performance index appeared to range between 2 and 6 without substantial drift for the duration of the experiment. Lower values were noted at 320°C, 240°C, and 200°C.

Operation of the development model of a 5-gpm loop continued. One run of 500 hr duration at 250°C and with an average slurry concentration of 410 g of Th per kg of H_2O was completed. Unlike previous runs, there was no loss of thorium oxide from the circulating stream. This improved inventory control resulted from the use of continuous water purge to the pump rotor cavity, which appeared to reduce entry and settling of thorium oxide in the pump cavity. The pump purge flow was obtained from the filtrate of a sintered-metal filter unit. A test run is now in operation at 250°C in which the slurry concentration has been approximately 1000 g of Th per kg of H_2O.

15. Radiation Corrosion

In-pile loop L-2-23 has been used in out-of-pile solution-stability tests; it will not be used in a radiation experiment. The first ORR in-pile loop, 0-1-25, was assembled, and out-of-pile testing and pretreatment of the loop began. A final checkout of all equipment and instrumentation was started at the ORR beam-hole HN-1 installation. A mockup loop is being operated as part of this checkout.

The results of two autoclave experiments (L53T-132 and L51Z-137) of Zircaloy-2 corrosion at 280°C are presented and discussed.

Experiment L53T-132 employed a titanium autoclave to expose three Zircaloy-2 coupons (and three titanium coupons) in an experiment designed to provide information on the transport of Zircaloy-2 corrosion product in autoclaves and on the effects, if any, of such transport on the radiation corrosion of Zircaloy-2.

The data indicate that some of the Zircaloy-2 corrosion scales were transferred to the titanium surfaces. The loose scale removed by drying the Zircaloy-2 specimens contained an average amount of uranium of only 1.3 $\mu g/cm^2$, while a larger amount (22 $\mu g/cm^2$) was found in the firmly retained oxide on the surface of a specimen which was examined after the bulk scale was removed by drying and brushing. The Zircaloy-2 corrosion rates at a given solution power density were somewhat higher than those observed in prior Zircaloy-2 tests at 280°C with solutions of similar compositions in light water. The present test employed D_2O as solvent; experimental results for a comparable solution with this solvent are not available for comparison.

In experiment L51Z-137 a solution containing CO_2 was used in order to determine whether CO_2 could displace uranium sorbed on Zircaloy-2 and hence reduce the extent of corrosion. The 3.3% uranium in the loose scale indicated no reduction in the uranium sorption. In the surface-uranium determinations, one value of 34 $\mu g/cm^2$ and another of 3 $\mu g/cm^2$ were reported. The Zircaloy-2 corrosion rates at a given solution power density were somewhat higher than those observed in prior Zircaloy-2 tests at 280°C with solutions containing no CO_2 but which were otherwise similar. It is concluded that the CO_2 did not exercise a beneficial effect on Zircaloy-2 corrosion.

Corrected power-density values for previously reported experiments L52Z-136 and L6Z-133 are reported. The conclusions reached previously from the results of experiment L6Z-133, a test of type 347 stainless steel corrosion with high radiolytic-gas pressure, are altered by the lower power density value. The L6Z-133 data now show a higher corrosion rate for type 347 stainless steel under the influence of the very high radiolytic-gas pressure. No change is indicated for the conclusion drawn previously from the results of experiment L52Z-136 that the separation of the solution into two phases did not alter the corrosion of Zircaloy-2.

Measurements of the adsorptive capacity of hydrous zirconium oxide for uranium from uranyl sulfate solutions at high temperature (250°C) are being made, utilizing a special high-temperature ion-exchange column. These experiments are being carried out with the objective of devising improved methods and technique for such determinations. Previous data of this type were obtained from batch-type experiments and suffer from certain inherent errors connected with the technique. To date, the reproducibility of the results is poor. The apparent capacity of a given oxide preparation for adsorption in a solution of given composition has been shown to change with contact time. Changes have also been observed which cannot be correlated with any recognized change in experimental variables. In general, the results have indicated somewhat higher capacities than those yielded in the batch-type experiments, varying from about 30 mg of uranium per gram of oxide at a concentration of 5 g/liter to about 70 mg of uranium per gram of oxide at a concentration of 50 g/liter. The concentration of the solutions studied has been in the range 5 to 50 g of uranium per liter, with all solutions 0.02 m in H_2SO_4.

16. Metallurgy

The macro- and microexaminations of the specimens removed from the HRT core tank after run 17 have been completed. The specimens were disks cut from five of the top six screens in the core tank, four mechanical-property specimens recovered from the top screen after the run, and the high-flux portion of the A40 titanium specimen-holder inserted in the center of the core tank during the run.

The major conclusions reached were (1) that temperatures above the melting point of Zircaloy and titanium existed in certain restricted regions of the titanium specimen-holder, (2) that these high temperatures were probably caused by uranium concentrating in regions of poor flow or cooling, (3) that the damage to the mechanical property specimens and to the spot on the top screen occurred in a few seconds and was caused by high-temperature events associated with the titanium specimen-holder, (4) that any metal present at the areas of those events would have shown damage, (5) that the pyrophoricity of zirconium and titanium alloys probably contributed to but did not cause the damage or the high-temperature excursions, and (6) that the exfoliation of layers of metal from the Zircaloy-2 screens was caused by corrosion in cracks which were formed in the material during punching of the holes in the screen during manufacture. While the titanium specimen-holder picked up appreciable quantities of deuterium during exposure, no such increase was found in the Zircaloy and titanium specimens nor in the Zircaloy-screen samples.

As a part of the reactor maintenance program, tungsten-arc-melting and cutting procedures have been developed for cutting Zircaloy-2 under water. A cutting torch of a size that might be used in the reactor has been designed and tried. The use of such equipment in cutting the Zircaloy-2 screens into widths that might be removed from the core appears promising.

A study of the effects of fabrication variables on the preferred orientation and anisotropy of mechanical properties of Zircaloy-2 has progressed to the point that some correlations can be made between these properties and fabrication procedures for the variables of cross-rolling, alpha rolling temperatures, and beta quenching as an intermediate step. Pole figures, impact-energy curves, and elliptical index plots for tensile specimens are used in the analyses. A new method of analyzing fractured tensile specimens, called the elliptical index analysis, has shown that considerably more information can be obtained on the anisotropy of mechanical properties, and permits determination of relative ductilities in the thickness direction of plate and sheet. The study has shown (1) that cross-rolling after the intermediate beta quench tends to perfect the preferred orientation in such a manner as to decrease appreciably the ductility in the thickness direction of the sheet, (2) that cross-rolling during ingot breakdown can produce, in certain orientations of specimens, greater ductility in the thickness direction of the sheet than in either the transverse or rolling directions, and (3) that plate material can show little anisotropy during the usual tensile test examination and still possess a considerable degree of perfection of preferred orientation. The study has also shown that the types of examinations and analyses being performed are necessary to establish the effects of fabrication variables to the point that the anisotropy of mechanical properties can be predicted for any proposed fabrication procedure.

It has been shown to be feasible to fabricate 15-in.-dia Zircaloy-2 hemispheres from flat plates with thicknesses of 1/8 to 5/16 in. by power spinning. The variations obtained on diameters and wall thicknesses are slightly greater than could be tolerated for adequate weld fit-up; so, some final machining of the surfaces would still be necessary. The variations were larger with the thicker plates. Such a method would, however, greatly reduce the number of welds required. It has also been shown to be possible to flare Zircaloy-2 shapes to nearly a 100% increase in diameter by warm pressing. Such flaring is accomplished with little difficulty and only a small amount of thinout. These results are very encouraging and indicate that a formed transition, with only a single weld, from a 5-1/2-in.-dia pipe to a 30-in.-dia vessel is quite feasible.

The use of composite Inconel - stainless steel tubing and headers in homogeneous reactor design appears desirable from the standpoint of corrosion resistance. Welding studies on stainless steel tubing clad exteriorly with Inconel, and Inconel tube sheets clad on the primary face with type 347 stainless steel indicate that crack-free welding may be accomplished by using intermediate passes of type 312 stainless steel between the root pass and cover passes. Cover passes in contact with the primary fuel solution may be of type 347, 308L, or 312 stainless steels.

Preliminary welding development on the remote machine-welding of Zircaloy-2 sections, 5/16-in. thick and 2-in. in dia into plate of the same thickness appears feasible, from welding considerations. A motor driven welding torch, mounted on the circular sections and operated remotely, gave welds, which, although not up to new construction standards, would give appreciable service as repair welds to a Zircaloy-2 reactor core vessel. The problem of securing an equivalent degree of control of welding variables in a limited-access vessel and from a remote location will require additional development of apparatus.

In the fabrication of a Zircaloy-2 vessel, automatic, machine-driven welding appears much more desirable than manual or semiautomatic welding. The dimensional tolerances to which the vessel must be fabricated and machined prior to welding may be relaxed, thus increasing the scope of potential methods of

vessel fabrication and reducing prewelding fabrication time and costs. Plate welds made on automatic tungsten-inert-gas equipment have also demonstrated a great saving in welding time with no sacrifice of quality.

PART V. CHEMICAL ENGINEERING DEVELOPMENT

17. Uranyl Sulfate Fuel Processing

The yellow-green solid remaining after a simulated HRT fuel solution containing 1200 ppm of nickel was heated to 335°C and then cooled to 25°C was identified as nickel sulfate containing only trace amounts of copper and uranium.

A 3-in.-dia hydroclone operating at 30 gpm was no more effective for removing solids from a circulating loop than a 0.6-in.-dia hydroclone operating at 1 gpm.

The best method found so far for isolating the small amount of uranium contained in solids taken from the HRT was dissolution of the solids in 10.8 M H_2SO_4 and purification by anion exchange. About 60% of the uranium contained in 100 mg of solids can be recovered by this method.

Scale was successfully removed by three methods from sections of the titanium corrosion-specimen holder which had been in the core of the HRT during run 17. The methods consisted in heating the specimen with chromous sulfate - sulfuric acid solution, Deoxidine 170, or Turco reagents. Scale was not removed from specimens by boiling with dilute or concentrated nitric acid or by dilute oxalic acid at 25°C. Analysis of the scale on the titanium specimens showed it to be chiefly titanium, zirconium, and iron, with only traces of chromium and copper.

Laboratory studies showed that nickel and manganese could be effectively removed from HRT fuel solution electrolytically. A platinum anode and mercury cathode gave best results, reducing to less than 50 ppm the combined concentration of nickel and manganese in the concentrated fuel solution treated in the electrolytic cell.

18. Equipment Decontamination

The gamma activity associated with a pump that had been removed from the HRT chemical plant was decreased from 200 to 10 r/hr by treatment with a chromous sulfate solution. The stability of the chromous ion was increased and the corrosiveness of the solution was decreased by lowering the sulfuric acid concentration in such solutions from 0.5 to 0.1 M. An equal-volume mixture of Deoxidine 170 and water at 104°C was used to descale a specimen of HRT pipe; the gamma decontamination factor was 10^3.

19. Thorium Oxide Slurry Development

A slurry of 650°C-fired thorium oxide (250 g of Th per kg of D_2O; 145 ppm palladium; 0.5 wt % U^{235}, based on thorium) was irradiated for 242 hr at 290°C in the LITR under an O_2 overpressure. No radiolytic-gas pressure was noted at temperature. A second slurry of Th - 8% natural-uranium oxide (no catalyst, 250 g of Th per kg of D_2O) irradiated for 335 hr at 265 to 300°C in the LITR also showed no radiolytic gas. The use of a D_2 overpressure with a slurry of thorium-uranium oxide irradiated in the Graphite Reactor markedly lowered the steady-state radiolytic-gas pressures during the first week's irradiation,

compared with those in similar experiments in the absence of a D_2 overpressure. However, after stirring stopped and was restarted, radiolytic-gas pressure in the latter part of the experiment agreed with that observed in the absence of excess D_2.

Improved methods of cooling in-pile experiments are under development. Heat was removed at a rate of 1800 w from a simulated in-pile autoclave cooled to 300°C by water flowing through stainless steel capillaries wound around the bomb.

The catalytic activity for D_2-O_2 recombination by a thorium-uranium oxide slurry containing a palladium catalyst and pumped at 280°C for 478 hr under an Ar-D_2 atmosphere decreased with increasing pumping time (7.6 moles D_2/liter-hr at 190°C at 47.2 hr; 0.1 mole D_2/liter-hr at 207°C at 478 hr; P_{D_2} = 100 psi). Substitution of O_2 for Ar-D_2 and pumping for an additional 500 hr resulted in only a small further decrease in activity. High recombination rates reported for thorium-uranium oxide slurries containing palladium catalyst and in the temperature range 150-200°C appear to be associated with reduced uranium and/or corrosion products. Oxidation of the uranium in the slurry by treatment at high temperature with oxygen or stoichiometric H_2-O_2 mixtures in autoclaves, or by pumping under an oxygen atmosphere, eliminated the high catalytic activity in this temperature range.

A rolling-ball viscometer is under development for use with small volumes of slurry at room temperature and at elevated temperatures and ultimately for use with irradiated slurries. Yield-stress values obtained for slurries of 650°C-fired oxide at concentrations from 250 to 600 g of Th per kg of H_2O agreed well with those obtained in a capillary-tube viscometer. The rolling-ball viscometer appeared to be limited to slurries containing less than 800 g of Th per kg of H_2O.

One method of keeping a slurry reactor subcritical during startup would be to add to the slurry boric acid, which could be removed when operating conditions were reached. Adsorption-desorption studies indicated that it is feasible for a slurry prepared from 1000°C-fired thorium-uranium oxide.

As shown by electron micrographs of shadow-cast particles, spherical particles were obtained by flame-firing at 1400°C alcoholic solutions of thorium-uranium-aluminum nitrates having a U/Th weight ratio of 0.08 and Al/Th weight ratios of 0.025 and 0.5.

Tests indicated that fluidized-bed techniques probably cannot be used to prepare 50- to 500-μ- dia ThO_2 particles by direct denitration of $Th(NO_3)_4$ solutions. Ten runs were made with aqueous and methanolic solutions of $Th(NO_3)_4$, fluidized-bed materials of ThO_2 and sand, and bed temperatures from 400 to 700°C. The bed caked in nearly every run, and the products contained unacceptably high percentages of fines. A test run with a uranyl nitrate solution indicated that satisfactory uranium oxide particles, unlike the ThO_2, could be readily prepared by fluidized-bed denitration. Agitated-trough denitration is being tried for preparing the 50- to 500-μ particles.

Hydroclone classification was tested as a method for production of thorium oxide containing a high percentage of <0.6-μ material. In a single pass through a 0.5-in.-ID hydroclone, over 60% of the <0.6-μ material and about 6% of the >1-μ material was recovered in the overflow.

Twenty-seven hundred and fifty pounds of slurry oxide, including 2000 lb of thorium-uranium oxide, was prepared for slurry engineering studies. Equipment for thorium oxide production is being relocated in Building 2528.

PART VI. SUPPORTING CHEMICAL RESEARCH

20. Heterogeneous Equilibria in Aqueous Systems

A previously unidentified compound, $CuO \cdot 3UO_3$, has been discovered in the HRT fuel-solution system, the five-component system UO_3-CuO-NiO-SO_3-H_2O (D_2O), at 300°C. X-ray diffraction data have established that this red crystalline solid is identical with solids previously found in the HRT during prepower operation. A new ternary line has been located in the five-component system along which, at different SO_3 concentrations, the three solids, $NiSO_4 \cdot D_2O$, $UO_3 \cdot UO_2SO_4$, and $CuO \cdot 3UO_3$, may co-exist.

Improved methods have been developed for the preparation of appreciable quantities of the new compound $CuO.3UO_3$, and antlerite, $3CuO.SO_3.2H_2O$.

Study of the two-liquid-phase regions of the system, UO_3-SO_3-H_2O, was extended to 350°C and to initial compositions having a SO_3:UO_3 molar ratio of 1.4 and uranium concentrations of 1.5 M.

Recent efforts to find thorium solutions that would be stable at 300°C and suitable for consideration as breeder blankets were unsuccessful. Thorium nitrate - beryllium nitrate, thorium nitrate - lithium nitrate, and thorium fluoride - beryllium fluoride solutions were tested in this study.

Studies of the UO_3-HNO_3-H_2O system were resumed, with improved experimental methods. The solubility of UO_3 was determined in solutions containing 0.05 to 2.0 M NO_3^- from 150 to 300°C. At saturation, $UO_3 \cdot NO_3^-$ molar ratios of 0.4 to 0.7 were obtained.

The solubility of $NiSO_4 \cdot H_2O$ (D_2O) in H_2SO_4-H_2O (D_2SO_4-D_2O) was determined at 250 and 300°C. In contrast with the general behavior of salts at low temperature, the solubility was found to be higher in D_2O systems at 250 and 300°C than in the H_2O systems. There is known to be a corresponding crossover in the vapor pressure of D_2O vs H_2O at 220.7°C, with H_2O having the higher vapor pressure at lower temperatures.

21. Reactions in Aqueous Solutions

Isotopic exchange and tracer studies of the mechanism of the homogeneous catalysis of the oxidation of dissolved hydrogen were continued. Reaction rates were measured for the four combinations of H_2 and D_2 with H_2O and D_2O at 110°C in solutions containing $Cu(ClO_4)_2$ at three different levels of acidity.

The precipitation of uranium peroxide from aqueous uranyl sulfate solutions upon the addition of dilute hydrogen peroxide was found to give two different compounds--$UO_4 \cdot 4H_2O$ below 63.5°C and $UO_4 \cdot 2H_2O$ above 64.5°C. These compounds were, for the first time, differentiated on the basis of mode of preparation, x-ray diffraction pattern, gravimetric analysis, and chemical reactions, all in the same laboratory.

22. Gaseous-Fission-Product Disposal

The number of theoretical plates in charcoal-filled pipes used for adsorbing fission gases from flowing oxygen was observed to be a maximum at a superficial gas velocity of 0.5 ft/min and to be independent of pipe diameter. Krypton holdup times for charcoal decreased by 37% as the oxygen sweep-gas pressure increased from 1 atm to 5 atm. Limits of flammability for deuterium-oxygen mixtures in charcoal were found to be about the same as those obtained earlier with hydrogen-oxygen mixtures.

PART VII. ANALYTICAL CHEMISTRY

23. Analytical Chemistry

A high-frequency titrimetric method was applied successfully to the determination of sulfate and free acid in solutions of uranyl sulfate.

A study was made of the applicability of flame photometry to the determination of rare-earth elements in ThO_2, and a method was devised, utilizing flame photometry, for the estimation of Pd in slurries of ThO_2.

Controlled-potential coulometric titrimetry has been applied to the determination of the U(IV)/U(VI) ratio in thorium oxide-uranium oxide mixtures.

A spectrophotometric method was developed for the determination of Os in both microgram and milligram quantities in solutions of uranyl sulfate.

An effective descaling agent, the trisodium salt of n-hydroxyethylethylenediamine triacetate (Versenol) in an ammonium acetate solution, disintegrated scale composed of the oxides of iron, chromium, and other metals, without damage to stainless steel containers.

CONTENTS

SUMMARY iii

PART I. HOMOGENEOUS REACTOR TEST

1. HRT OPERATIONS 3
   1.1 Reactor Operations 3
      1.1.1 Run 18 Conclusion 3
      1.1.2 Testing and Remote Maintenance 3

2. HRT PROCESSING PLANT 7
   2.1 Hydroclone System 7
      2.1.1 Corrosion-Product Solids Removed 7
      2.1.2 Uranium, Copper, and Nickel Removal 8
      2.1.3 Estimation of Total Zirconium Corrosion 8
      2.1.4 Behavior of the Rare Earths 10
   2.2 High-Capacity Multiple Hydroclone 10
   2.3 Waste-Pond Decontamination 12

3. DESIGN AND DEVELOPMENT OF TOOLS FOR HRT REMOTE OPERATIONS 13
   3.1 Modification of HRT Core 13
      3.1.1 Separation of Diffuser Screens from Core Tank 13
      3.1.2 Loose-Screen Manipulation 16
      3.1.3 Removal of Screens from the Core 16
      3.1.4 Core-Hole Definition 16
      3.1.5 Patching of the Hole in the HRT Core 20
   3.2 Core-Wall Thickness Gauge 20
   3.3 Weld-Impression Device 20
   3.4 Screen-Edge Sample Cutter 24
   3.5 Pickup Tools 24
      3.5.1 Parallel-Jaw Tongs 24
      3.5.2 Core-Specimen Removal Tool 24
      3.5.3 Vacuum Pickup Device 24

4. HRT COMPONENT DEVELOPMENT 27
   4.1 Feed-Pump Endurance Testing 27
   4.2 Test and Pretreatment of the Replacement Circulating Pump for the HRT 27
   4.3 Heat Exchanger Unplugging Studies 27
   4.4 HRT Core Studies 29
      4.4.1 Modification to Present Core 29
      4.4.2 Development of Flush Procedure for Solids Removal 29
      4.4.3 HRT Replacement-Core Model 29
   4.5 HRT Mockup 32

5. HRT DESIGN 33
5.1 Reversed Flow Through Core Tank 33
5.2 HRT Flushing Equipment 33
5.3 Radiolytic-Gas Concentration 33

6. HRT REACTOR ANALYSIS 38
6.1 Effect of Fuel in Blanket of HRT on Neutron Leakage 38
6.2 High-Energy Neutron Flux in the HRT 40

7. HRT CONTROLS AND INSTRUMENTATION 45
7.1 Component Development 45
7.1.1 Letdown Valves 45
7.1.2 Gamma Radiation Detector 45
7.1.3 Remote-Viewing Equipment 47

PART II. REACTOR ANALYSIS, RESEARCH, AND DESIGN

8. RESEARCH AND ANALYSIS 51
8.1 Control of Core-Wall Temperatures in Two-Region Power Reactors 51
8.1.1 Cooling with Blanket Fluid 52
8.1.2 Internal Wall Cooling 52
8.2 Effect of Temperature Distribution upon Maximum Power Density in Cylindrical Reactors 53
8.3 Criticality Conditions for Unreflected Slurry Containers 57
8.4 Criticality Conditions for Small Slurry Reactors Obtained with Different Calculational Models 57
8.5 Machine Programming 59
8.6 Slurry Resuspension and Dropout Studies 63
8.7 Thoria Caking Studies 65
8.7.1 Caking Tendency of Slurries 65
8.7.2 Influence of Chromate Ion on Cake Formation 65
8.7.3 Removal of Thoria Cake Deposits by Erosive Action 65

9. DESIGN OF CIRCULATING-SLURRY CRITICAL SYSTEM 67

PART III. ENGINEERING DEVELOPMENT

10. DEVELOPMENT OF FUEL- AND SLURRY-SYSTEM COMPONENTS 73
10.1 High-Pressure Recombiner Loop 73
10.2 Centrifugal Pumps 73
10.2.1 20-cfm Allis-Chalmers Blower 73
10.2.2 Reliance 6000-gpm Pump 73
10.2.3 300A Slurry Pump and Loop 73
10.2.4 200Z Slurry Pump and Loop 74
10.2.5 Test Program for Slurry-Pump Bearings 74
10.3 Feed Pumps 74
10.3.1 Oxygen Compressors 74
10.3.2 Increased-Capacity Solution Pumps 75
10.3.3 Slurry Feed Pumps 75
10.4 Valve Trim 76
10.4.1 Dump-Valve Trim for Solutions 76
10.4.2 Slurry Valves 76
10.4.3 Slurry Letdown Chokes 76
10.5 Heat Exchanger Test Facility 76

10.6 Core Hydrodynamics 77
10.6.1 Re-entrant Core Model 77
10.6.2 Slurry Core Vessel 77
10.7 Properties of Slurry Settled Beds 77
10.8 Effect of Acceleration Force on Hindered-Settling Rate 77

11. DEVELOPMENT OF REACTOR SLURRY SYSTEMS 80
11.1 Circulating-Slurry Behavior 80
11.1.1 200A-Loop Operation 80
11.1.2 200B-Loop Operation 83
11.2 Blanket System Development 84
11.2.1 300-SM High-Pressure-System Operation 84

12. INSTRUMENT AND VALVE DEVELOPMENT 95
12.1 Instrument Development 95
12.1.1 High-Temperature Radiation-Resistant Differential Transformers 95
12.1.2 Magnetic Flowmeter for Slurry Service 95
12.1.3 Static-Component Power-Control System Evaluation 96
12.2 Valve Development 96
12.2.1 Valve Stem-Sealing Bellows 96

PART IV. REACTOR MATERIALS RESEARCH

13. SOLUTION CORROSION 103
13.1 Dynamic Solution Corrosion 103
13.1.1 Deposition of Salts from Dilute Uranyl Sulfate Solutions on Heated Surfaces 103
13.1.2 Scale Dissolution and Peptization 108
13.1.3 Hydrolytic Stability of Very Dilute Fuel Solutions 109
13.1.4 Corrosion Tests of Various Alloys 112
13.2 Laboratory Corrosion Studies 114
13.2.1 Intergranular Corrosion of Type 347 Stainless Steel 114
13.2.2 Stress-Corrosion Cracking of Cast Type 347 Stainless Steel 117
13.2.3 Corrosion of Uniloy 19-9DL Stainless Steel 118

14. SLURRY CORROSION 121
14.1 Pump Loops 121
14.1.1 Introduction to Pump-Loop Tests 121
14.1.2 Circulation of D_2O Slurries of ThO_2-UO_3 Mixtures Using Atmospheres of Argon and Oxygen 121
14.1.3 Circulation of a Slurry of Thoria Microspheres 126
14.1.4 Materials Evaluation Tests Using ThO_2 and Mixtures with UO_3 at 200°C under D_2 or O_2 128
14.2 Toroids 131
14.2.1 Evaluation of Slurries for the Slurry In-Pile Loop Program 131
14.2.2 Tests with Slurries of Thorium-Uranium Oxides 134
14.2.3 Observation of Hydriding of Zirconium-Base Alloys 134
14.3 Corrosion of Aluminum Oxide by Thoria Slurry 137
14.4 In-Pile Autoclave Slurry Corrosion Tests 139
14.4.1 Introduction to Autoclave Experiments 139
14.4.2 Production and Catalytic Recombination of Radiolytic Gases 140
14.4.3 Correlation of the Time and Radiation Effect on Corrosion 143
14.4.4 Radiation Corrosion of Pin Specimens 145

14.5 In-Pile Slurry Loop 145
14.5.1 Loop Development 145

15. RADIATION CORROSION 152
15.1 In-Pile Loops--Development and Construction 152
15.1.1 LITR HB-2 Loop Package 152
15.1.2 ORR Loop Package 152
15.1.3 ORR Beam Hole HN-1 152
15.2 In-Pile Solution Rocking-Autoclave Tests--LITR 152
15.2.1 Development and Construction 152
15.2.2 Test of Effect on Zircaloy-2 Corrosion of Transport of Bulk Scales from Zircaloy-2 Surfaces to Other Autoclave Surfaces--Experiment L53T-132 153
15.2.3 Test of CO_2 as a Chemical Additive to Deter Zircaloy-2 Corrosion--Experiment L51Z-137 160
15.2.4 Correction of Data Reported in a Previous Quarterly Report 162
15.3 Adsorption of Uranium on Hydrous Zirconium Oxide from UO_2SO_4 Solutions 163

16. METALLURGY 168
16.1 HRT Repair and Examination 168
16.1.1 Examination of Specimens Removed from HRT After Run 17 168
16.1.2 Screen Removal 180
16.1.3 Tungsten-Arc Melting 180
16.1.4 Core-Tank Repair 182
16.2 Zircaloy-2 Fabrication Study 182
16.3 Zircaloy-2 Forming Study 191
16.3.1 Fabrication of a Spherical Vessel 191
16.3.2 Fabrication of Pipe-to-Vessel Transition 192
16.4 Welding Development 195
16.4.1 Composite Welds 195
16.4.2 Zircaloy-2 195
16.5 Combustion of Titanium and Zirconium 197
16.6 Nondestructive Test Development 197
16.6.1 Resonance Measurements of HRT Core Vessel 197
16.6.2 Attenuation of Ultrasonic Energy in Zircaloy-2 197
16.6.3 Measurement of Ultrasonic Velocity in Metals 197
16.7 Effects of Radiation on Structural Metals and Alloys 198

PART V. CHEMICAL ENGINEERING DEVELOPMENT

17. URANYL SULFATE FUEL PROCESSING 201
17.1 Fuel-Solution Behavior 201
17.2 Solids Behavior 201
17.3 HRT Solids 201
17.4 Nickel Removal from Fuel Solution by Electrolysis 202

18. EQUIPMENT DECONTAMINATION 203

19. THORIUM OXIDE SLURRY DEVELOPMENT 204
19.1 Slurry Irradiation Studies 204
19.1.1 Slurry Irradiations in the LITR 204
19.1.2 Postirradiation Examination 204
19.1.3 Slurry Irradiations in the Graphite Reactor 204

19.1.4 Oxygen Solubility in Aqueous Slurries 205
19.1.5 Equipment Development: Capillary Cooling System for Irradiation Bombs 205
19.2 Gas Recombination Studies 208
19.3 Rolling-Ball Viscometer 211
19.4 Boron Adsorption Studies 213
19.5 Development of Oxide Preparation Methods 216
19.5.1 Flame-Calcination Experiments 216
19.5.2 Fluidized-Bed Denitration 216
19.5.3 Agitated-Trough Denitration 220
19.5.4 Hydroclone Classification of ThO_2 220
19.6 Thorium Oxide Production 223

PART VI. SUPPORTING CHEMICAL RESEARCH

20. HETEROGENEOUS EQUILIBRIA IN AQUEOUS SYSTEMS 227
20.1 The System UO_3-CuO-NiO-SO_3-H_2O (D_2O) at 300°C 227
20.2 The Compound $CuO \cdot 3UO_3$ 227
20.3 A New Method of Preparation of Antlerite, $3CuO \cdot SO_3 \cdot 2H_2O$ 230
20.4 The Two-Liquid Phase Regions of the System UO_3-SO_3-H_2O 230
20.5 Investigation of Thorium-Containing Nitrate and Fluoride Solutions for Breeder-Blanket Use 232
20.5.1 Beryllium Nitrate - Thorium Nitrate Solutions 232
20.5.2 Lithium Nitrate - Thorium Nitrate Solutions 232
20.5.3 Beryllium Fluoride - Thorium Fluoride Solutions 233
20.6 The System UO_3-HNO_3-H_2O at 150-300°C 233
20.7 Comparative Solubility of $NiSO_4 \cdot H_2O(D_2O)$ in H_2SO_4-H_2O and D_2SO_4-D_2O Solutions at High Temperature 235

21. REACTIONS IN AQUEOUS SOLUTIONS 239
21.1 Rate of Oxidation of Dissolved H_2 or D_2 Catalyzed by $Cu(ClO_4)_2$ in Light and Heavy Water 239
21.2 Uranium Peroxide Precipitation and Structure 239

22. GASEOUS-FISSION-PRODUCT DISPOSAL 245

PART VII. ANALYTICAL CHEMISTRY

23. ANALYTICAL CHEMISTRY 251
23.1 Determination of Sulfate and Free Acid by High-Frequency Titration: Application to Solutions of Uranyl Sulfate 251
23.2 Flame-Photometric Determination of Rare-Earth Elements in Thorium Oxide 251
23.3 Flame-Photometric Estimation of Palladium in Thorium Oxide Slurries 252
23.4 Determination of U(IV)-U(VI) Ratio in Thorium Oxide - Uranium Oxide Mixtures 252
23.5 Determination of Osmium in Solutions of Uranyl Sulfate 252
23.6 Selection of a Descaling Solution 253

ORGANIZATION CHART 255

Part I

HOMOGENEOUS REACTOR TEST

S. E. Beall

1. HRT OPERATIONS

S. E. Beall P. N. Haubenreich J. W. Hill, Jr.

S. J. Ball
H. F. Bauman
N. C. Bradley
J. R. Buchanan
S. R. Buxton
J. R. Engel
J. D. Flynn
D. F. Frech
R. H. Guymon
R. J. Harvey
J. Hirota[1]
J. O. Kolb
D. M. Richardson
D. Scott
W. Terry
K. W. West

1.1 REACTOR OPERATIONS

1.1.1 Run 18 Conclusion

HRT run 18, which started in December 1958 and had as its purpose an investigation of the relation between reactor power and fuel stability, was concluded on February 2, when the reactor scrammed after a total of 1281 hr of operation. During the run 363 Mw-hr was accumulated, at power levels up to 1.6 Mw, with no indications of power disturbances. The scram, the first in the history of the reactor, occurred when fresh fission gas was trapped in a closed instrument line near the O_2 activity monitors. There was no release of activity from the reactor piping. Shielding was placed around the instrument line and operating procedures were modified to prevent future shutdowns for the same reason.

1.1.2 Testing and Remote Maintenance

Termination of run 18 provided an opportunity to replace or repair equipment in the reactor cells. The east diaphragm head of the fuel feed pump and the diaphragm heads that supply condensate to the fuel circulating pump and to the blanket pressurizer were not functioning properly. They had operated for 2300, 4900, and 4900 hr, respectively. Also there was a large leak in the feed-water line to the fuel heat exchanger. While the reactor high-pressure system was being rinsed with D_2O condensate to prepare the system for remote maintenance, it was found that some additional difficulties had developed following the forced dump. The core circulating pump could not be operated owing to an open electrical lead inside the reactor shield; low power demand of the blanket circulating pump indicated a low flow rate in the blanket circulating system; the blanket dump valve was found to be leaking badly.

The pump heads and the blanket dump valve were replaced under water. A small quantity of light water spilled into the reactor during the replacement of the valve, but it was removed without contaminating the reactor fuel. An O-ring gasket in the feed-water line was replaced and the electrical lead to the pump was repaired by dry-maintenance techniques, with the use of tools

extending through a shielded platform. The electrical lead broke at a junction point several feet from the pump and apparently resulted from overheating of a high-resistance contact.

After completing the maintenance, run 19 was started in an investigation of the core and blanket circulation rates. The reactor is not equipped with flow meters in the high-pressure systems, so the flow rates are inferred from heat-balance and temperature-difference measurements, from the pressure drops across the main heat exchangers, and from heat transfer coefficients determined for the main heat exchangers. Behavior of the core and blanket temperatures when the power was first raised to heat-loss power definitely indicated low flow in both systems.

The low flow in the core system was tentatively traced to operation of the circulating pump in reverse as a result of a change in connections when the wires were repaired in the cell. After it was thought that changes had been made in the wiring in the control room to correct the rotation of the core circulating pump, the reactor power level was raised to 1 Mw to obtain measurements of the flow rates. The blanket flow was indicated as being about 80 gpm, one-fourth normal, and the core flow was approximately 160 gpm, or about one-third normal.

Another pump lead failed inside the shield before the rotation could be checked again. In making repairs the previous arrangement of the electrical leads was lost. The pump rotated in the proper direction after it was reconnected; so it was thought that the low flow in the core, and possibly in the blanket, was caused by partial plugging of the heat exchanger tubes. Plugging was attributed to accumulation of scale flaked off the reactor piping during the dump.

Since there were, however, several possible explanations for the low flows, a systematic study was made to determine whether the difficulty was a result of damage to the pumps, mechanical failure of other components, or plugging by scale accumulation.

The blanket heat exchanger taps, which had been blanked heretofore, were connected to a newly installed differential-pressure cell. Necessary connections were made to enable the same cell to be used for core-loop measurements. The core and blanket high-pressure sample outlets were adapted so that they could serve as pressure taps also. In this way it was possible to measure the pressure drop across several segments in each loop. These tests indicated that the blanket pump was not delivering its required head. However, they indicated essentially normal pressure distribution and normal pump discharge pressure on the core system.

The blanket circulating pump was removed temporarily for recovery of the corrosion-specimen assembly in its discharge flange and installation of a pressure tap at the flange, so that the pump shutoff head could be determined. At the same time the corresponding core corrosion specimens were removed and an orifice plate was installed at the core-pump discharge flange. Both sets of corrosion specimens were covered with films which were several mils thick, and the films had flaked-off in some areas. Tests made after the pumps were reinstalled indicated the blanket-pump shutoff head to be less than 10% of the manufacturer's rating. They also confirmed that the core pump was delivering approximately its design flow at the correct head. A search through logs and other records confirmed that the core pump had been incorrectly wired during the power run, thus explaining the low core flow rate at that time. However, no such explanation could be found for the low blanket flows.

Therefore, the blanket circulating pump was replaced, and the old pump was moved to the hot storage pool for remote disassembly and inspection. The seal weld at the stator flange was cut, and the motor end of the pump was removed from the scroll. A cursory visual inspection revealed that about three-fourths of the titanium impeller and most of the labyrinth seal had been consumed, apparently by combustion. The suction hub and most of the impeller vanes had been destroyed (see Fig. 1.1). The back part of the impeller was still attached to the rotor shaft, and the edges showed evidence of melting and/or burning. The inside of the suction nozzle, to a depth of about 4 in., was covered by a heavy deposit with the appearance of metal slag. Deposits of similar material were also visible inside the scroll.

Although the exact circumstances which resulted in the damaged titanium probably cannot be determined, it is conjectured that the pump became gas bound in a high oxygen atmosphere, and that the protective oxide layer on the titanium was scratched, exposing metal to the oxygen. Newly exposed titanium metal can be expected to burn in an oxygen atmosphere.

During replacement of the blanket pump, other remote operations were performed. The temporary provisions made for differential-pressure and flow measurements were removed. New corrosion-specimen assemblies were installed at the discharge flanges of both circulating pumps. The circulating pump electrical leads were revised, so that mineral-insulated cable now extends to both the pumps and terminates in the pump housing itself. This eliminates 18 connections which had the possibility of burnout because of high-resistance contacts. Hydrostatic pressure tests had established that there was a leak in the intermediate system of the west diaphragm head of the core feed pump. Consequently, the pump head, which had operated for nearly 5000 hr, was replaced.

During the remote-maintenance operations, shield flooding water leaked into the reactor vessel through a plastic O-ring gasket that had relaxed at a blanket circulating-pump flange. The gasket was part of the temporary apparatus used during differential-pressure tests. The fuel solution was protected from contamination since it was isolated in the storage tanks, and the light water was completely removed.

Preliminary startup operations are under way for run 20, in which the investigation of fuel stability will be the primary objective.

REFERENCE

1. Japanese Atomic Energy Research Institute.

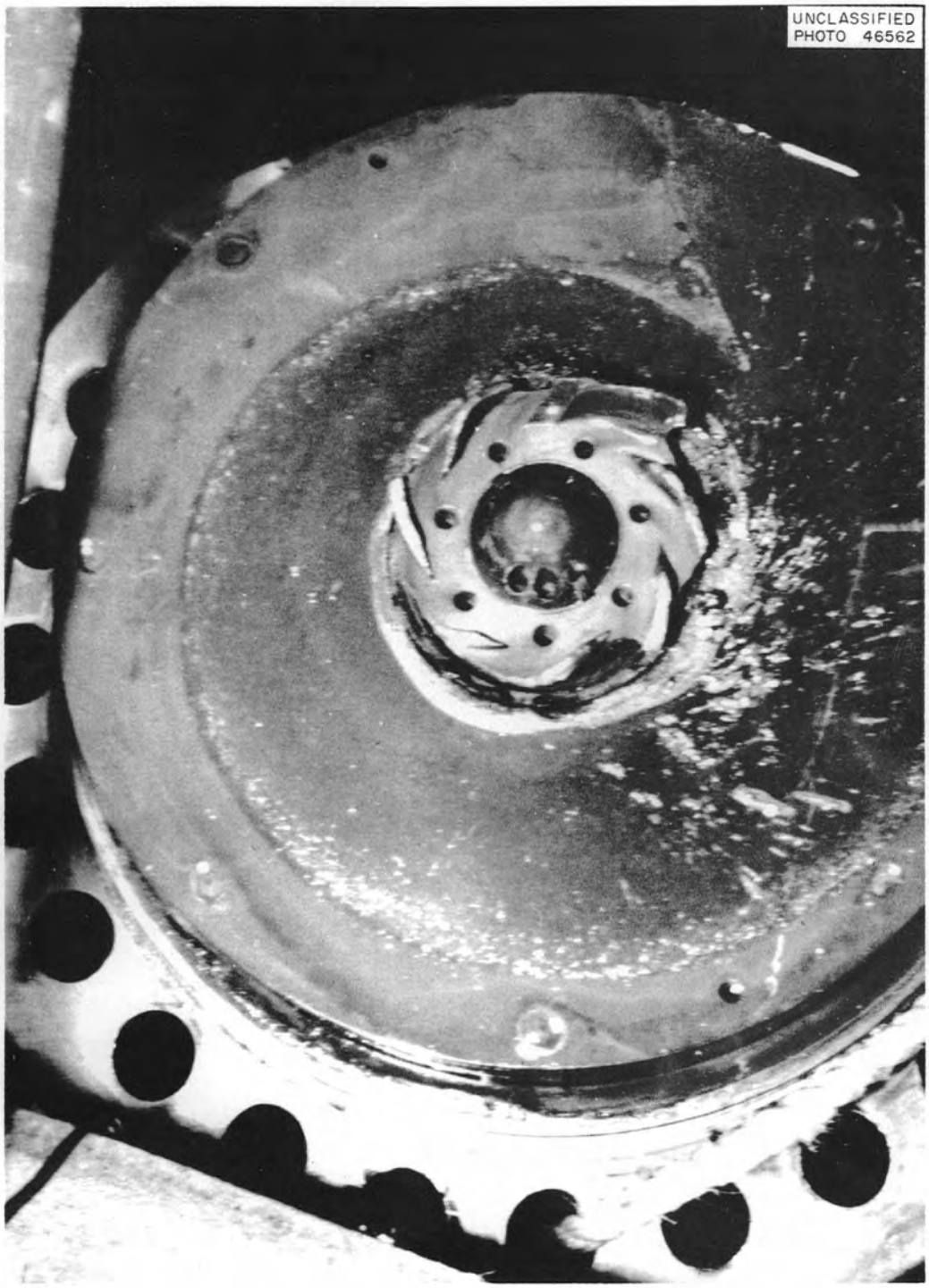

Fig. 1.1. Blanket-Circulating-Pump Titanium Impeller, Showing Suction Hub and Vanes.

2. HRT PROCESSING PLANT

W. D. Burch

L. B. Shappert R. H. Winget O. O. Yarbro

The hydroclone system was operated a total of 964 hr in four different chemical plant runs during reactor run 18. Results of the first two intervals were reported last quarter. The system was also on stream during a four-day period in run 19 when the reactor was operated briefly at power (CP run 19-11).

Decontamination of shield water in the retention pond prior to release by adsorption of activity on a calcium phosphate precipitate continued to prove effective during the reactor maintenance period following run 19.

2.1 HYDROCLONE SYSTEM

2.1.1 Corrosion-Product Solids Removed

The quantities and compositions of corrosion products removed in the last three runs are listed in Table 2.1. Removal rates were typical of similar

Table 2.1. Corrosion-Product Solids Removed

	Chemical Plant Run No.			
	18-9	18-10	(Total Run 18)	19-11
Operating time, hr	341	181	964	106
Total corrosion products, g	106	51	1042	63
Average removal rate, g/hr	0.3	0.3	1.1	0.6
Composition (%)				
Fe	22	24	23	23
Cr	6	6	7	7
Ni	0	0	0.1	0.6
Zr	44	44	41	41
Ti	0.7	0.6	0.7	0.8
Ag	0	0.1	0.1	0.2

periods in runs 16 and 17, dropping off to about 0.3 g/hr after several hundred hours of continuous reactor operation and rising again at the start of a new run. Chemical compositions were also nearly identical to those of the previous runs.

2.1.2 Uranium, Copper, and Nickel Removal

Uranium and copper contents of the solids removed were in the same range as in previous runs. Results in Table 2.2 are based on dissolver samples. The

Table 2.2 Uranium, Copper, and Nickel Removal

	Chemical Plant Run No.			
	18-9	18-10	(Total Run 18)	19-11
Total uranium, g	67.6	66.2	235.5	10.4
Insoluble U, g	4.5	3.9	59.9	8.4
Insoluble U/total solids	0.04	0.08	0.06	0.13
Total copper, g	9.7	9.4	21.15	0.9
Insoluble copper, g	1.4	1.0	15.9	0.6
Insoluble copper/total solids	0.01	0.02	0.02	0.01
Total nickel, g	3.1	3.1	10.4	0.4
Insoluble nickel, g	0.0	0.0	1.1	0.6
Insoluble nickel/total solids	0.0	0.0	0.001	0.01

portion of each constituent known to be dissolved in fuel solution that accompanied the solids as they were discharged from the underflow pot was subtracted from the total to obtain the quantity of insoluble constituent.

2.1.3 Estimation of Total Zirconium Corrosion

Additional calculations, based on results of the last three runs, further refined the estimates of total zirconium corrosion in the reactor to date. The method, which has been explained in detail previously,[1] is based on stainless steel corrosion calculated from nickel buildup in the fuel and the composition of solids removed by the chemical plant. Additional confirmation has been obtained by a similar method whereby the fraction of fission product Zr^{95} removed is assumed to be the same as the fraction of natural zirconium from the core tank which is collected by the hydroclone.

Points calculated for all runs to date are plotted in Fig. 2.1. The scatter appears quite large during run 17, but a trend is apparent and can be explained at least qualitatively. In periods of high zirconium corrosion such as at the beginning of run 17, the zirconium content of solids removed is higher than the average content of all solids present in the reactor. This results in a high estimation of total corrosion. Also at high power levels, the ratio of Zr^{95} to natural zirconium in solids removed is high because of the presence of freshly formed Zr^{95}. This displaces the estimated zirconium corrosion downwards. In the last three runs, when both corrosion and power were low, excellent agreement was obtained.

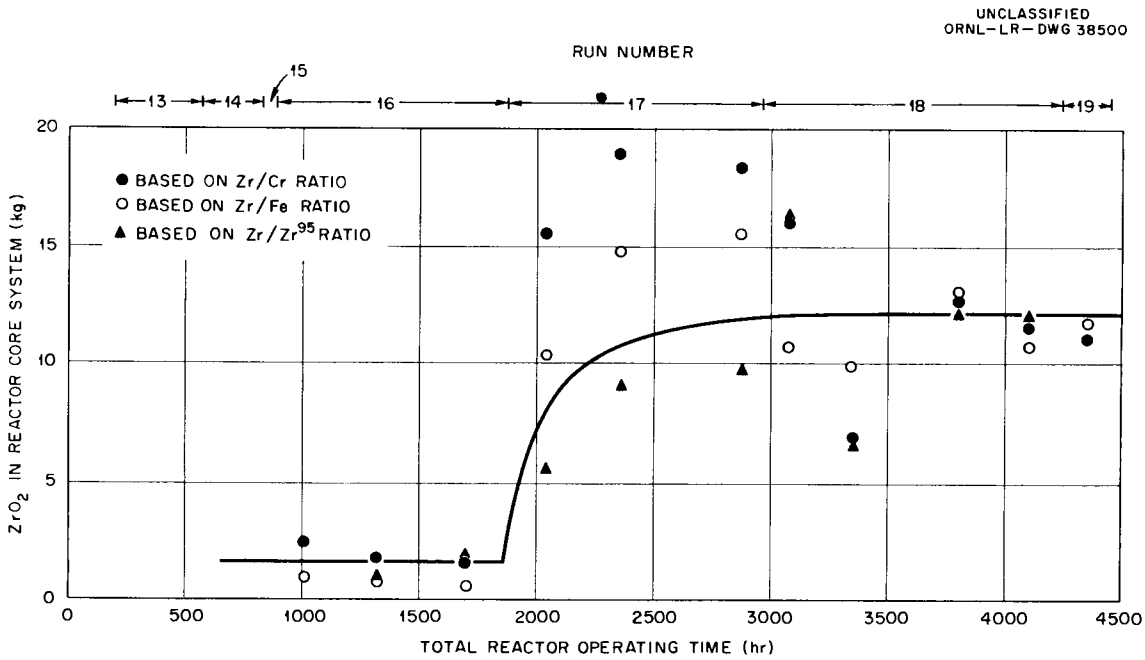

Fig. 2.1. Total ZrO_2 Produced in the Core vs Reactor Operating Time.

Zirconium oxide produced from corrosion in the core system only (12.2 kg) is included in Fig. 2.1. If zirconium corrosion rates were uniform in both core and blanket, total zirconium oxide produced through run 18 is estimated to be 20.8 kg, and the total corrosion-product inventory is 34 kg.

2.1.4 Behavior of the Rare Earths

The present fuel charge in the HRT accumulated 200 Mwd through run 18. Little power was produced in run 19. Rare-earth fission-product concentrations have only built up to the point where they can be detected spectrographically in large, concentrated, dump-tank samples. Rare earths have an inverse solubility, but the specific behavior under reactor conditions is unknown and cannot be determined at present concentration levels. In view of this and the fact that rare earths constitute the major reactor poison, it has been proposed to spike the reactor with a mixed rare-earth charge in proportion to their calculated fission yield at the end of run 18. Table 2.3 presents the amount of rare-earth fission products produced in this fuel charge, both calculated and

Table 2.3. Rare-Earth Concentrations and Proposed Addition

Rare-Earth Fission Product	Analytical (g)	Calc. (g)	Addition (g)	Total (g)	Concentration (ppm)
Nd	17.3	25.8	210	235.8	125
Ce	-	22.8	186	208.8	110
La	5.4	8.1	65	73.1	39
Y	2.5	4.5	39	43.5	23

determined analytically, the first proposed addition, and the approximate operating reactor concentration after the addition.

The quoted analytical detection limit for neodymium is 125 ppm, while the concentrations for the other three will be well above detection limits.

The additional rare earths constitute the equivalent produced if the reactor were run at full power (5 Mw) for 370 days.

2.2 HIGH-CAPACITY MULTIPLE HYDROCLONE

The only means envisioned at present of increasing solids removal rates is by increasing the flow rate through the hydroclone. From results to date, it is clear that the major fraction of corrosion products collected have deposited or settled out and been resuspended at least one time prior to removal in the hydroclone. While there is no clear-cut evidence, it appears that hydroclone operation does not greatly affect circulating solids concentrations. If this is true, solids removal rates will be approximately proportional to flow rates.

Flow rates can be increased effectively while retaining high efficiency only by using small hydroclones in parallel. A unit designed and fabricated for installation in a bypass line across the fuel circulating pump is shown in Fig. 2.2. Thirteen hydroclones of the size presently used in the chemical plant are

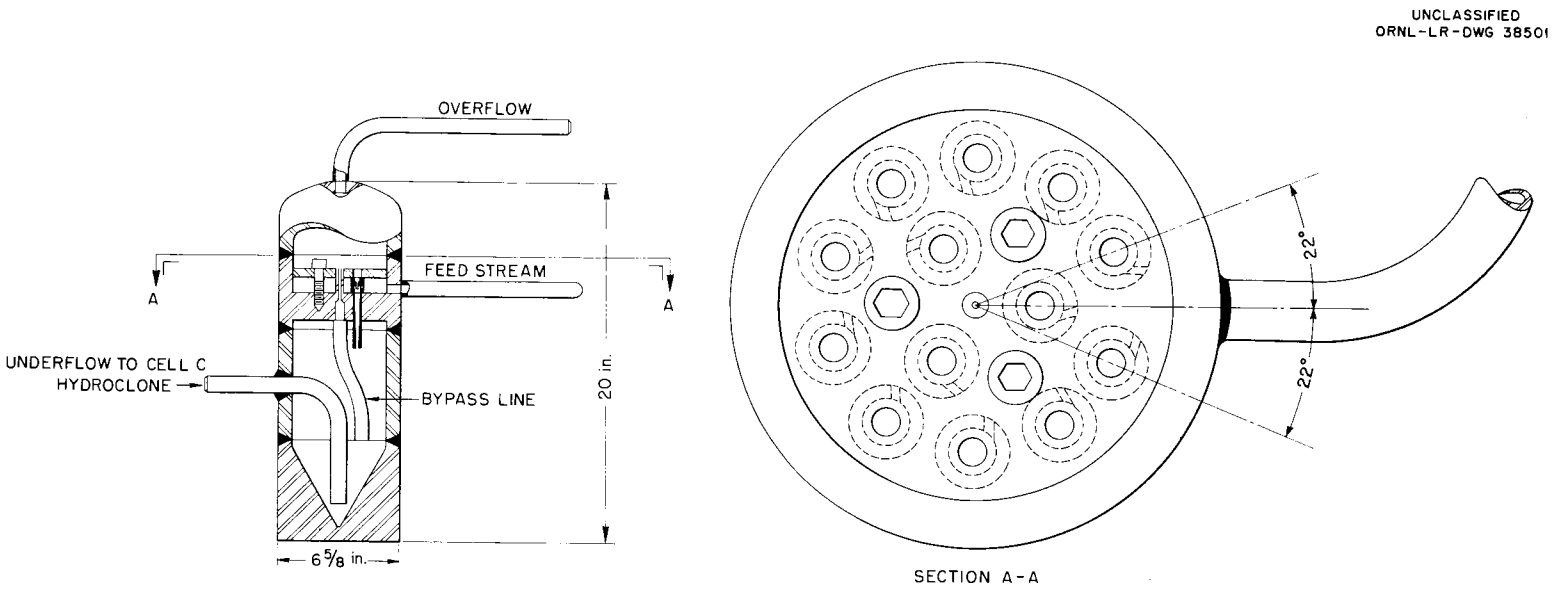

Fig. 2.2. High-Capacity Multiple Hydroclone.

incorporated into one unit. The underflow from this unit will be routed to the present system for final solids collection. A bypass from underflow to overflow was provided to prevent the accumulation of excessive quantities of solids in the multiple-hydroclone underflow pot while the chemical plant is off stream to drain the underflow pot in Cell C.

2.3 WASTE POND DECONTAMINATION

The equivalent of six reactor-cell volumes of contaminated shield water (1,420,000 gal) was pumped to the retention pond and, after decontamination, drained to the environs during this quarter. All except about 20 of the 350 curies of beta activity routed to the pond resulted from spillage during the replacement of one head of the fuel feed pump. Decontamination of the water by adsorption of the activity on a calcium phosphate precipitate continued to be effective, although some of the activity on the bottom of the pond is resuspended or redissolved each time water is pumped to the pond. Total activity released amounted to only 2.2 curies of beta activity, and no more than 0.3 curie was released in any 24-hr period.

REFERENCE

1. W. D. Burch et al., HRP Quar. Prog. Rep. Jan. 31, 1959, ORNL-2696, p 17.

3. DESIGN AND DEVELOPMENT OF TOOLS FOR HRT REMOTE OPERATIONS

I. Spiewak W. R. Gall M. I. Lundin J. R. McWherter

R. Blumberg B. D. Draper
C. A. Burchsted P. P. Holz
C. W. Collins J. E. Jones
J. S. Culver F. C. Zapp

3.1 MODIFICATION OF HRT CORE

Tools are being developed for removing the top six diffuser screens from the HRT core, and plugging the hole in the core tank. The general procedure to be used is:

1. The screen system will be surveyed with periscopes to determine which screens are already loose and to note any special problems.

2. The screens will be cut loose from the wall.

3. By holding the loose screens out of the way, photographs and a cast impression of the hole in the core tank will be made to enable a well-fitting patch to be machined.

4. The loose screens will be sectioned or dissolved and removed.

5. The hole will be plugged.

3.1.1 Separation of Diffuser Screens from Core Tank

Three methods of detaching screens from the core tank are being investigated. Of these, a remote fly cutter and a milling-cutter tool have been designed, fabricated, and tested, with reasonable success. A nibbler operator was also designed.

The remote fly cutter (Fig. 3.1) consists of a folding arm with two hole-saw sectors mounted at the ends. The arm is erected in the core, and cutting is accomplished by rotating the central shaft with an air motor located above the shield and 20 ft away from the cutter. A bearing plate at the lower end of the tool fits into the 3/8-in. holes of the screen. The tool was tested in the Core-Maintenance Mockup, and it cut through a carbon steel screen in 6 hr. Some wear of the cutter teeth was evident. Refinements in cutter design and in centering of the bearing plate appear desirable on the basis of this test.

The milling cutter (Fig. 3.2) is mounted at a 45° angle and is driven by a 3/8-in.-dia flexible shaft coupled to an air motor outside the shield. The

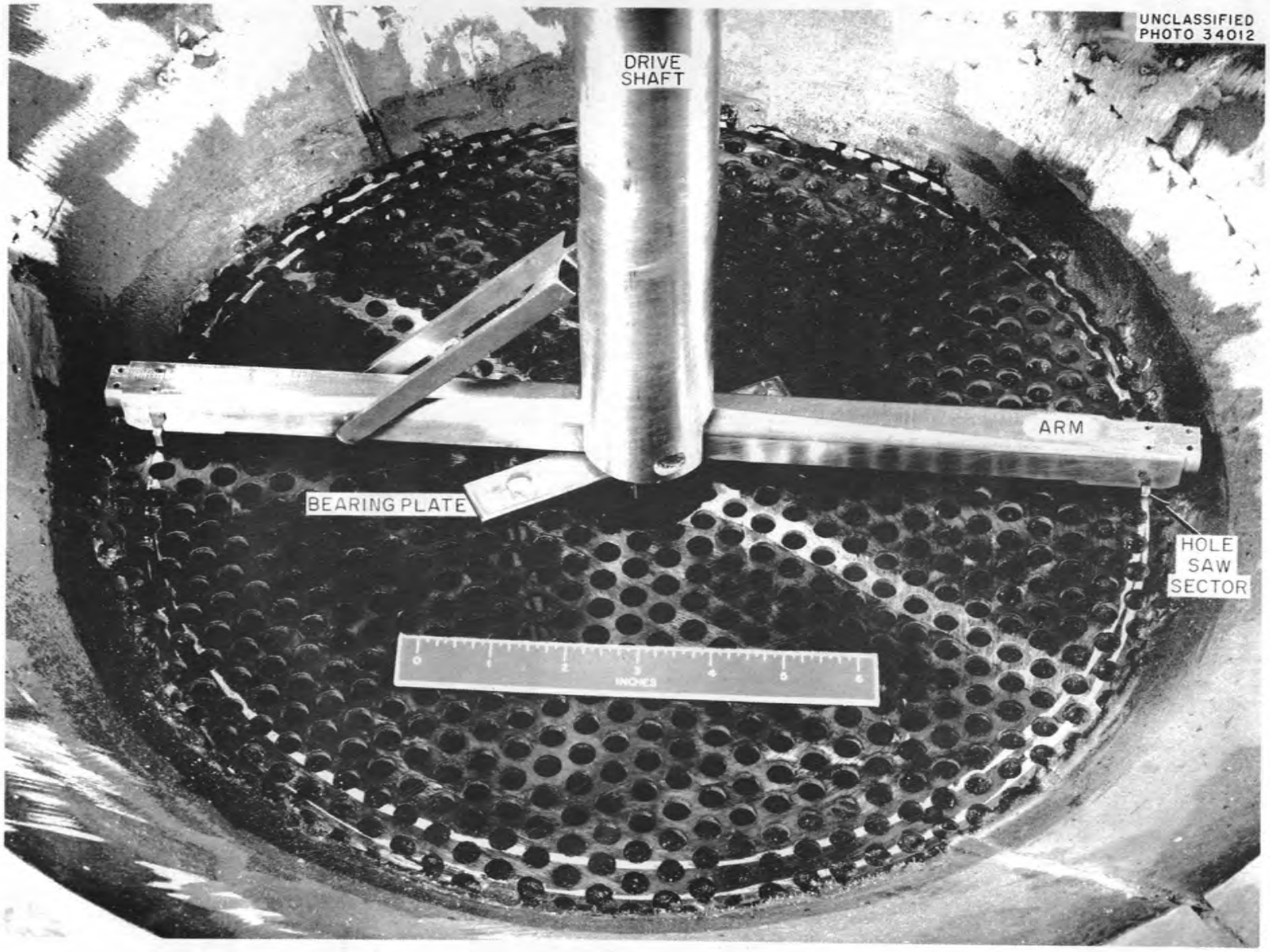

Fig. 3.1. Remote Fly Cutter in Cutting Position.

UNCLASSIFIED
PHOTO 34014

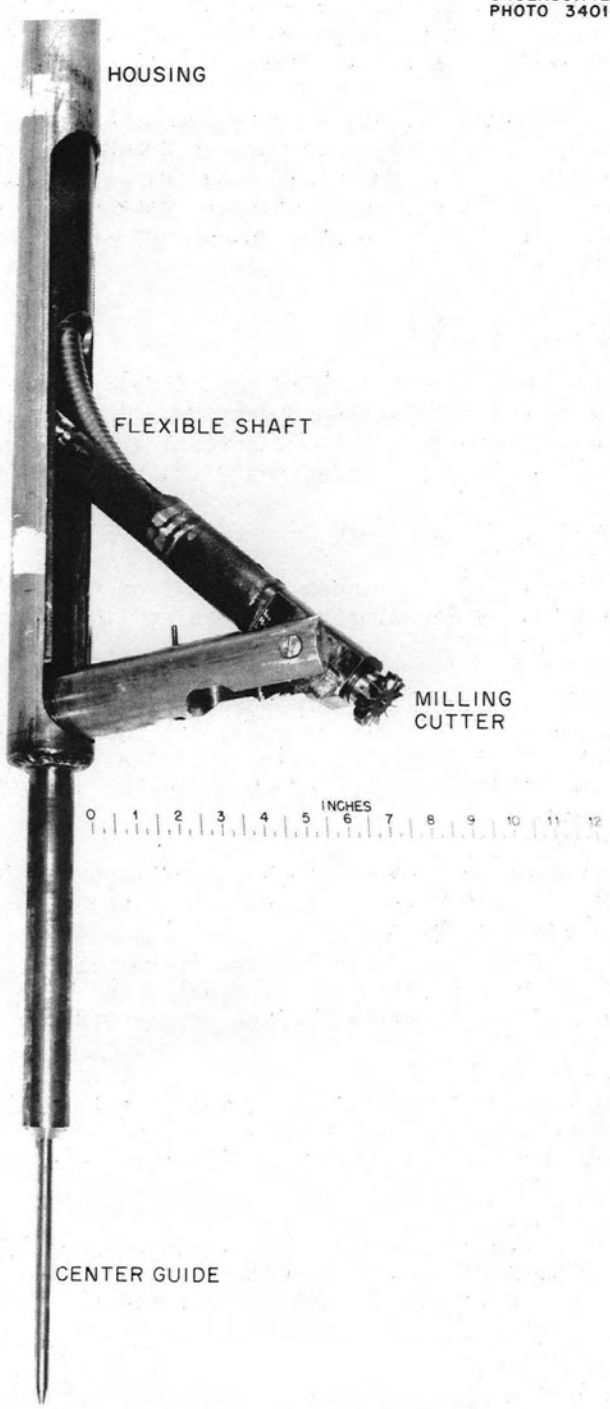

Fig. 3.2. Milling-Cutter Tool.

assembly is slowly rotated by hand around its central mast while the cutter is in use, thereby milling a circular groove in the screen. The milling-cutter tool cut through a carbon steel screen in 3 hr, although the flexible shaft failed following this operation. Further refinements of the cutter are planned, in addition to a torque-limiting device to prevent shaft overloads.

A hydraulic cylinder was designed to accommodate a commercial nibbler head (Fig. 3.3) for screen cutting tests. The unit is capable of fitting through the 2-in.-dia access opening into the HRT core. The hydraulically operated nibbler was able to cut screen in a bench test. However, because of the difficulty of positioning the nibbler and because of the success of other tools, work on this cutting method was stopped.

3.1.2 Loose-Screen Manipulation

Several tools, shown in Fig. 3.4, have been developed to pick up and suspend loose screens during the cutting operation. In addition, a device was designed and is being fabricated to support screens from the core-tank to pressure-vessel joint without restricting the 2-in. access opening.

3.1.3 Removal of Screens from the Core

Two methods of removing the detached screens from the core are being worked out; one uses an electrolytic dissolution process and the other an underwater cutting torch.

In the electrolytic method, it is proposed to partially fill the core with 8 M HNO_3 at 60-80°C, insert a platinum cathode, and then gradually lower the anodic screen into the electrolyte. By using a current density of 0.5 amp/cm^2, it is expected that the largest screen can be dissolved in about 30 hr. The tools have been designed.

The principal problem associated with this approach is the pickup of large amounts of hydrogen in Zircaloy cathode specimens or specimens operating at cathode potential. A specimen biased +0.4 volts with respect to the cathode picked up little or no hydrogen. Further tests of the electrolytic method will attempt to demonstrate the practicability of biasing the potential of mockup core tanks, and to determine the effectiveness of the bias in eliminating hydrogen pickup.

Two experimental cutting-torch heads suitable for insertion into the HRT core were designed--a multiple-electrode torch suitable for operation in gas, and a single-electrode Heliarc cutting head (Fig. 3.5) suitable for underwater operation.

The Heliarc cutting head is used in the design of a manipulator to cut the loose screens into strips less than 2 in. wide. The detail design of the complete assembly has not been completed, but fabrication for test of important subassemblies has been started.

3.1.4 Core-Hole Definition

A core-hole impression device, which is now under construction, was designed after successful operation of a simple prototype. Its function is to provide an impression of the core defect from the inside, from which a contoured patch can be machined. The tool employs an electrically heated cone of Dip Seal,

UNCLASSIFIED
ORNL-LR-DWG 38502

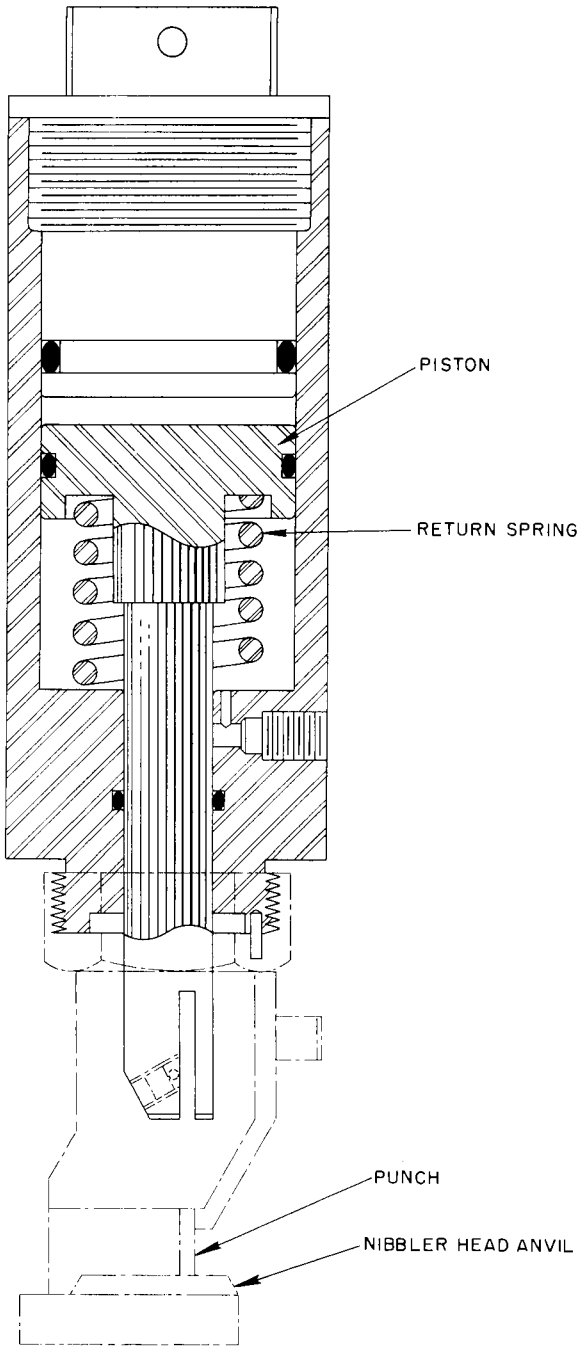

Fig. 3.3. Nibbler Head with Hydraulic Cylinder.

UNCLASSIFIED
PHOTO 34008

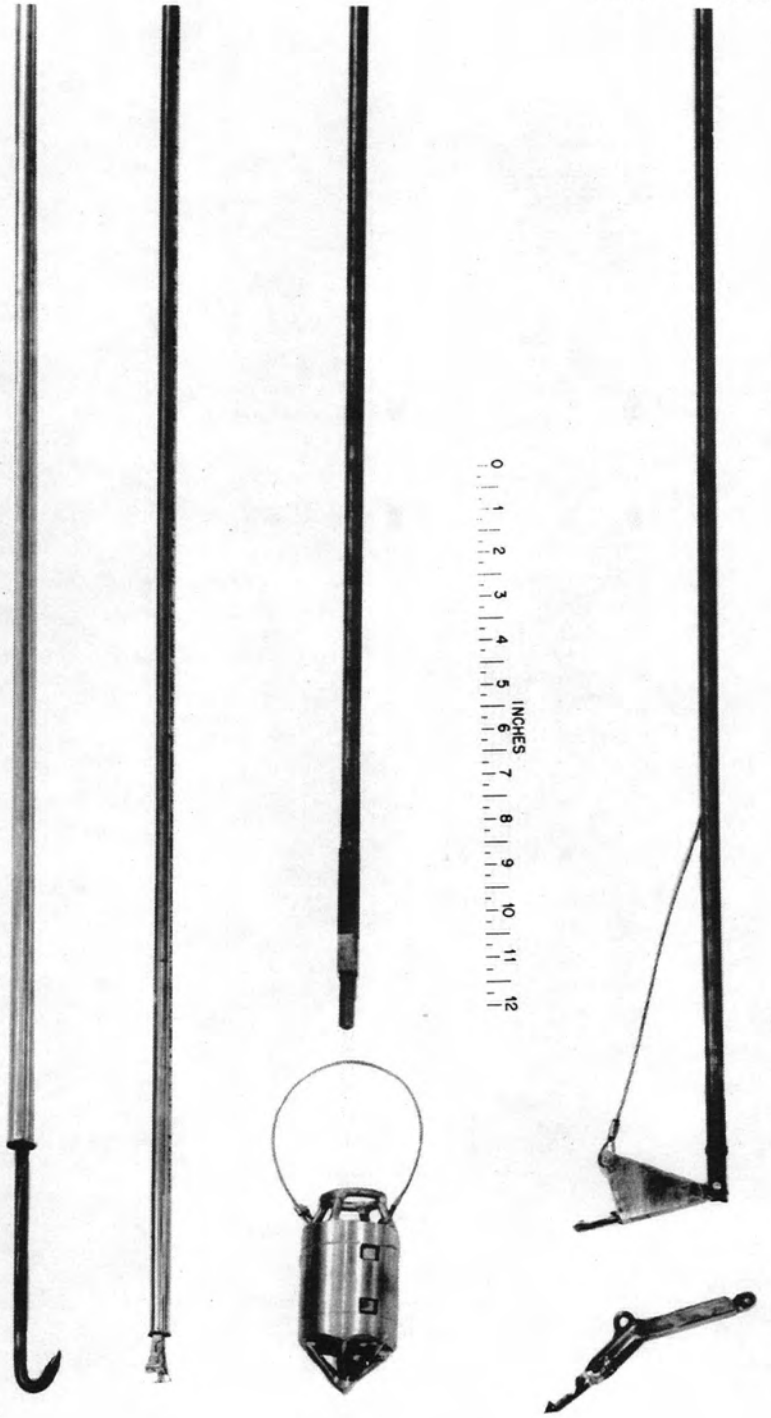

Fig. 3.4. Long-Handle Tools for Screen Manipulation. Left to right: hook; grapple; pawl clamp and key, for holding several screens; pivoted hook.

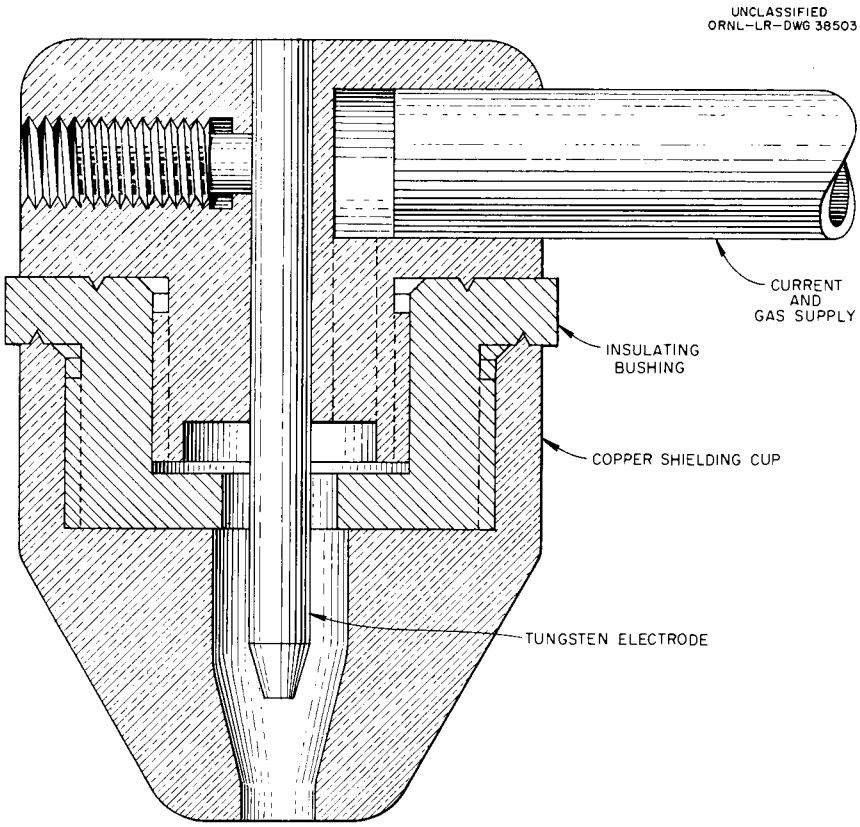

Fig. 3.5. Heliarc Cutting-Torch Head.

a thermoplastic material, which is forced into the hole by means of an air cylinder. After cooling, the formed impression is removed from the core and a plaster mold prepared in a shielded area. After coating the mold to prevent the spread of contamination, an epoxy resin casting is made and then used as a template to machine a properly contoured patch of Zircaloy II.

It is planned to obtain further definition of the hole photographically. Figure 3.6 shows a photograph of the hole taken from the blanket after HRT Run 17. On this is superimposed a scale grid photographed under "identical" conditions in the Maintenance Mockup. A similar photograph will be made from a position inside the core.

3.1.5 Patching of the Hole in the HRT Core

The patch will be machined to duplicate the plastic impression, and a contoured groove will be milled near its edge to receive a hollow gold gasket made of 1/8-in.-OD x 0.005-in.-wall tubing. A 1/4-in. hole will be drilled to receive the toggle bolt assembly shown in Fig. 3.7.

A test patch installed manually in a simulated core hole showed a leak rate of 1 to 2 pounds of water per minute under a head of 17 ft of water from the blanket side. This is several times tighter than the minimum requirement. At 200 psi differential, the gasket failed.

The installation tool, shown in Fig. 3.8, retains the patch for insertion in the core, pushes the toggle bolt through the hole (as viewed from the blanket) and then tightens the toggle bolt. This tool has successfully installed patches in the Maintenance Mockup.

3.2 CORE-WALL THICKNESS GAUGE

An ultrasonic thickness gauge and positioner for measuring the wall thickness of the core tank[1] was fabricated and tested successfully.

3.3 WELD-IMPRESSION DEVICE

A tool (Fig. 3.9) was designed and fabricated to take an impression of two weld areas in the top tee section of the reactor pressure vessel. Two blocks of a thermoplastic material are mounted on a manipulator which is inserted in the 2-in. opening for access to the core. The manipulator is positioned, and an assembly containing the blocks is remotely erected and positioned to lightly press one block of the material against a weld area.

The plastic block is then heated by passing electric current through an embedded grid of Nichrome wire. While the plastic is soft, it is pressed against the weld area and then allowed to cool. The block assembly is then repositioned, thereby removing the first block and positioning the second block in place on the second weld area. The heating and cooling cycle is repeated, the assembly is then retracted into the pipe mast, and finally the entire tool is withdrawn from the reactor. A pipe tap is added to permit the attachment of an air purge during operation.

Satisfactory mechanical operation of the tool has been obtained in mockup tests; further testing of the impression technique is planned.

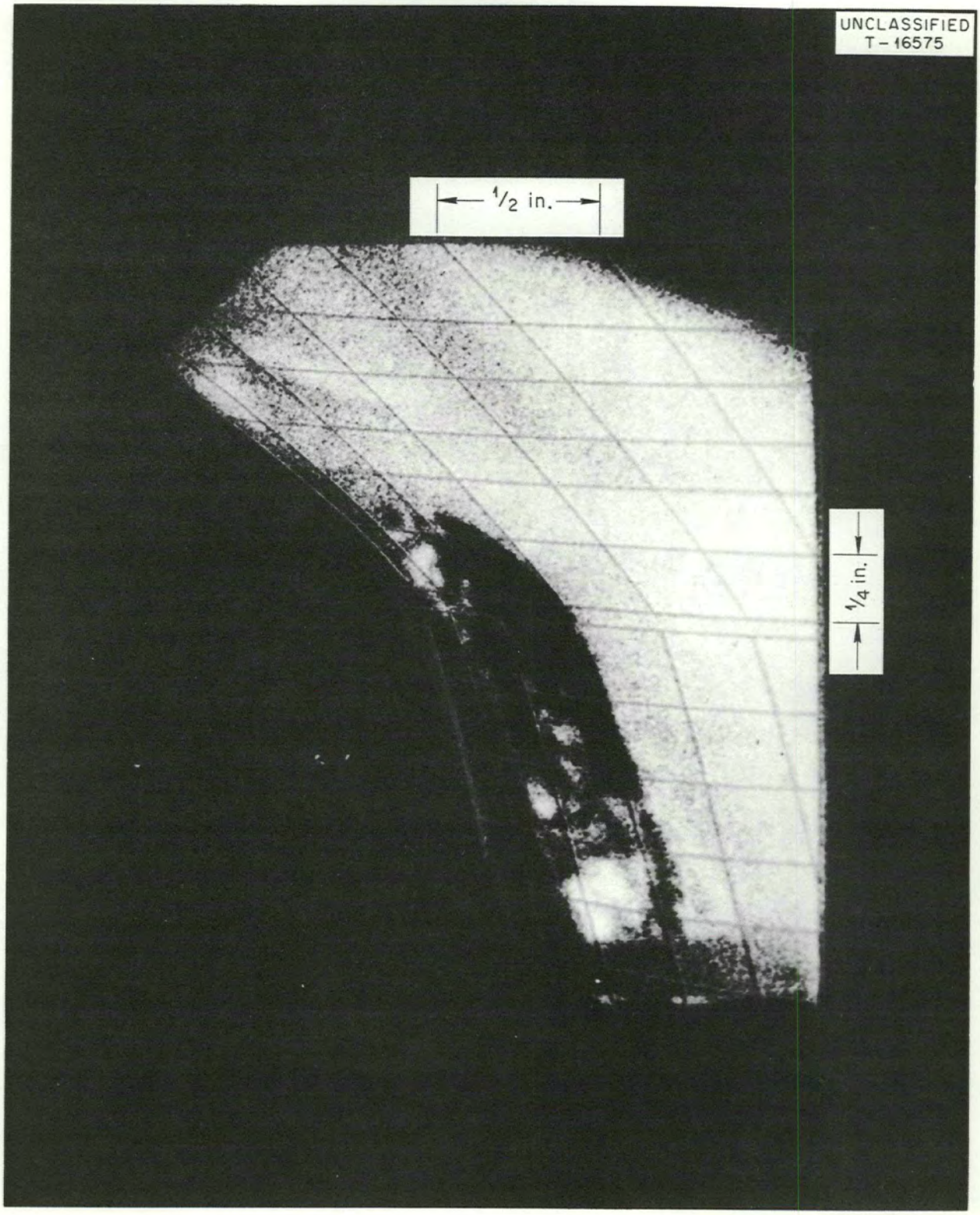

Fig. 3.6. Photograph of Hole in HRT, with Scaling Grid Superimposed in Maintenance Mockup.

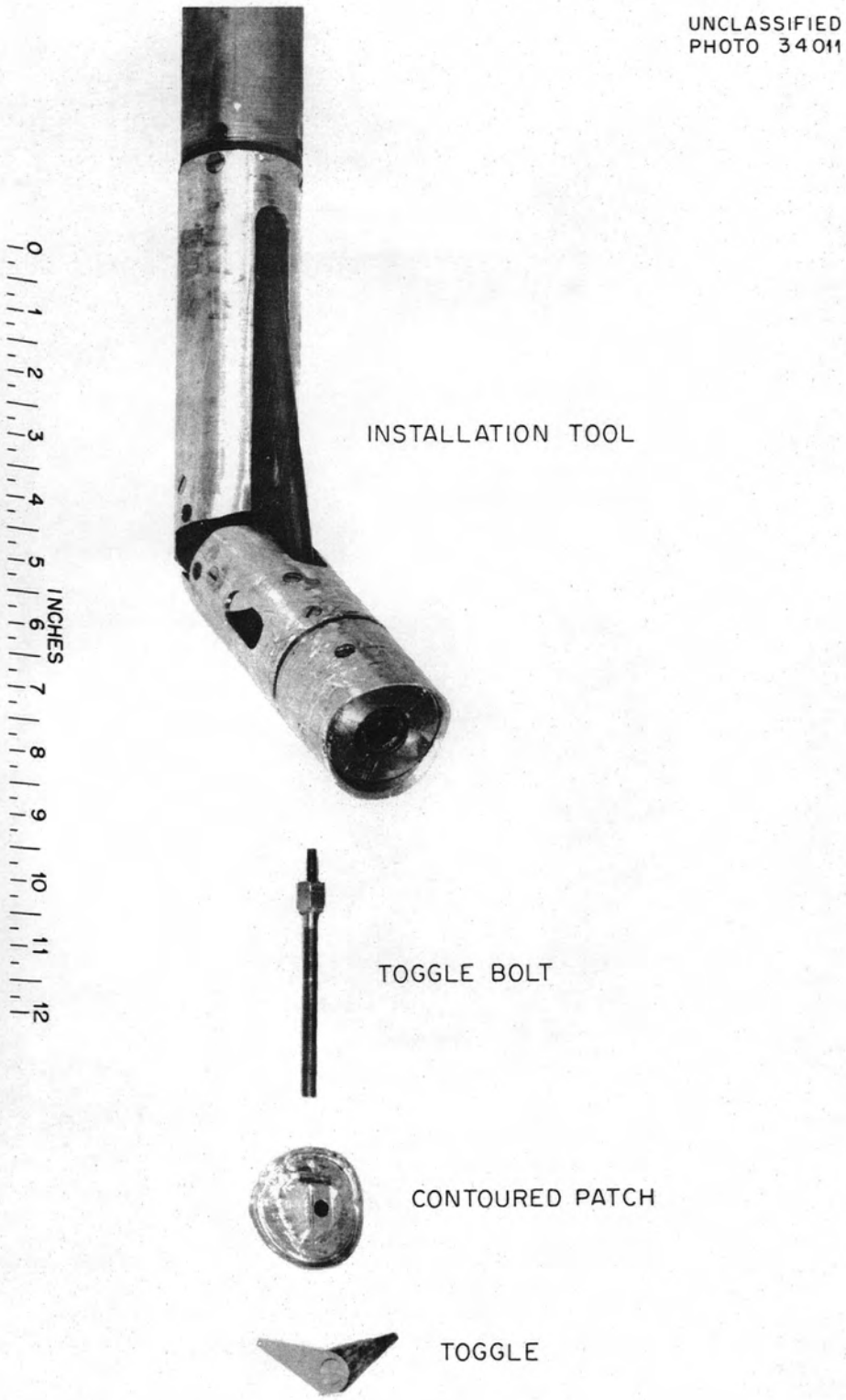

Fig. 3.7. Patch-Installation Tool and Dismantled Patch Assembly.

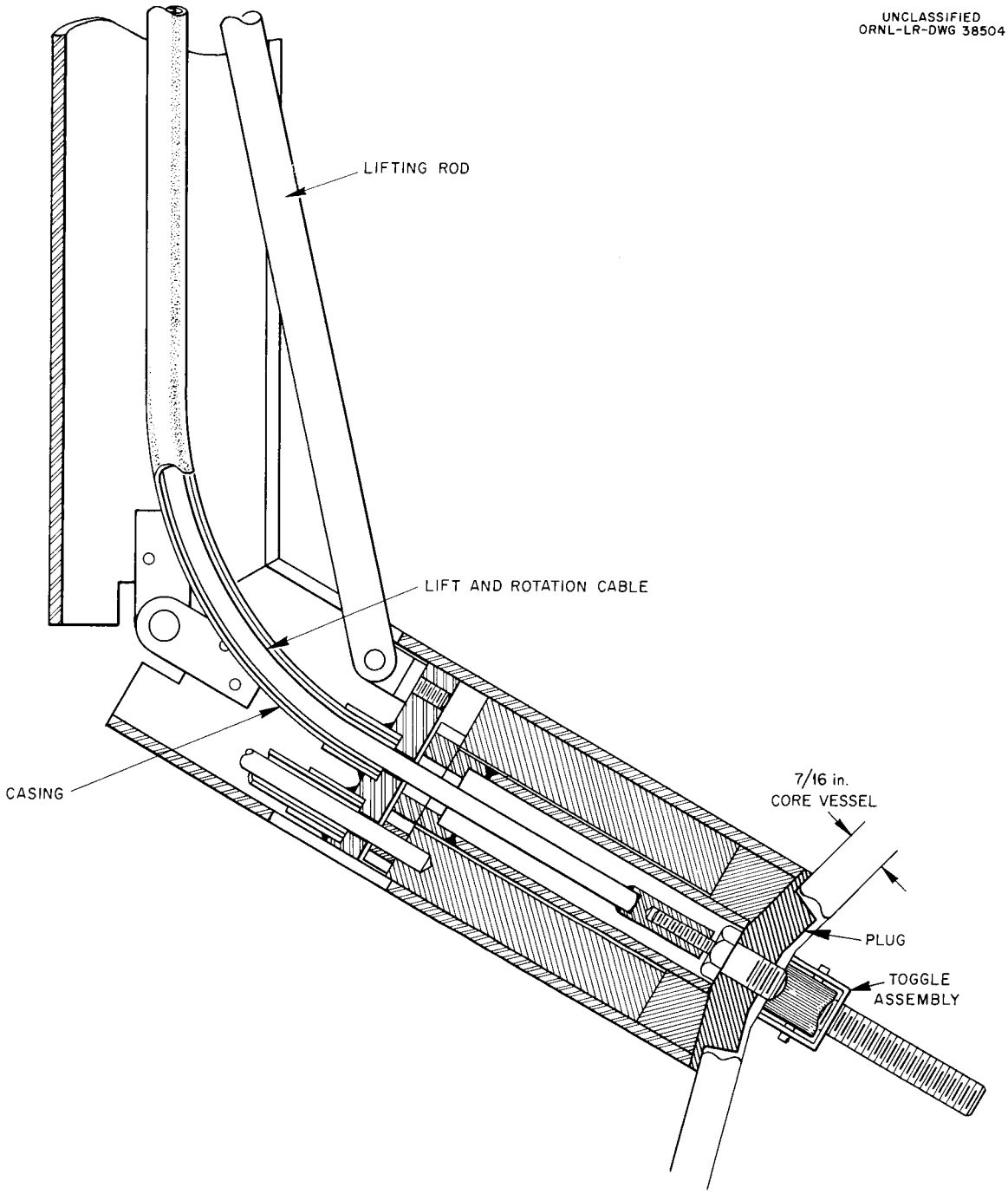

Fig. 3.8. Assembly Drawing of Patch-Installation Tool.

3.4 SCREEN-EDGE SAMPLE CUTTER

This tool, shown in Fig. 3.10 is designed to cut out an edge specimen from a loose screen for metallurgical examination. In operation, the screen is maneuvered into a central holding fixture and the sample is cut with a hole saw. Viewing for the loading operation is accomplished with the external-light-source viewing device[2].

3.5 PICKUP TOOLS

Several devices were designed for use in picking up materials from the cell and core. They are described below.

3.5.1 Parallel-Jaw Tongs

A remote handling tool for general service (Fig. 3.11) was designed for use in retrieving-and-holding operations. The basic action is based on a parallel-jaw gripping head with removable fingers. The jaws are opened by a spring and are closed by a manually operated lever which tightens a cable. A grip-force multiplication of three is provided. The jaws have a 4-in. opening, and the tool is capable of exerting a 100-lb vertical pull.

3.5.2 Core-Specimen Removal Tool

A new tool was designed for removing corrosion specimens that were lost in the core during HRT run 17.[3] This tool uses a torsional coil spring to operate a pair of fingers, rather than the spiral spring previously used. Shopwork on the tool is in progress.

3.5.3 Vacuum Pickup Device

A jet exhauster operating on compressed air was used to provide vacuum to a 1/2-in.-dia tube 19 ft below the jet. Zircaloy droppings weighing up to 2.5 g, such as would be produced in the HRT core if screens were arc cut, were lifted with ease into a filter.

A maneuverable pickup mechanism to remove materials from the HRT core is being designed. An optical system is incorporated to permit viewing of the pickup operation. The capacity of the device is sufficient to remove cutting-torch droppings, screen fragments, and scale which will be left after cutting the screens.

REFERENCES

1. I. Spiewak et al., HRP Quar. Prog. Rep. Jan. 31, 1959, ORNL-2696, p 28.

2. W. R. Gall et al., HRP Quar. Prog. Rep. Jan. 31, 1959, ORNL-2696, p 25.

3. I. Spiewak et al., HRP Quar. Prog. Rep. Oct. 31, 1958, ORNL-2654, p 9.

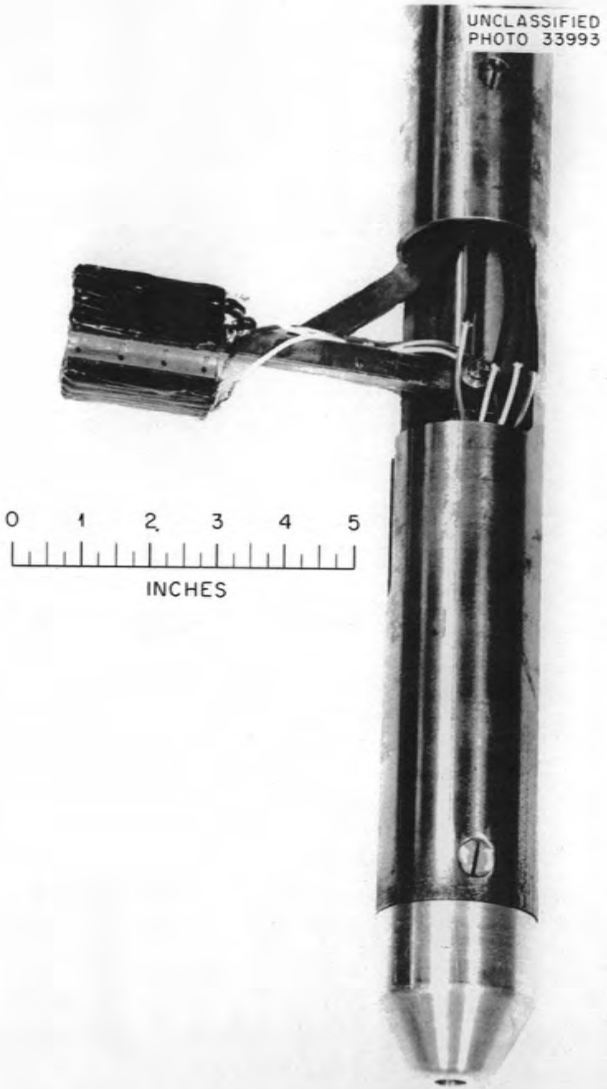

Fig. 3.9. Weld-Impression Device.

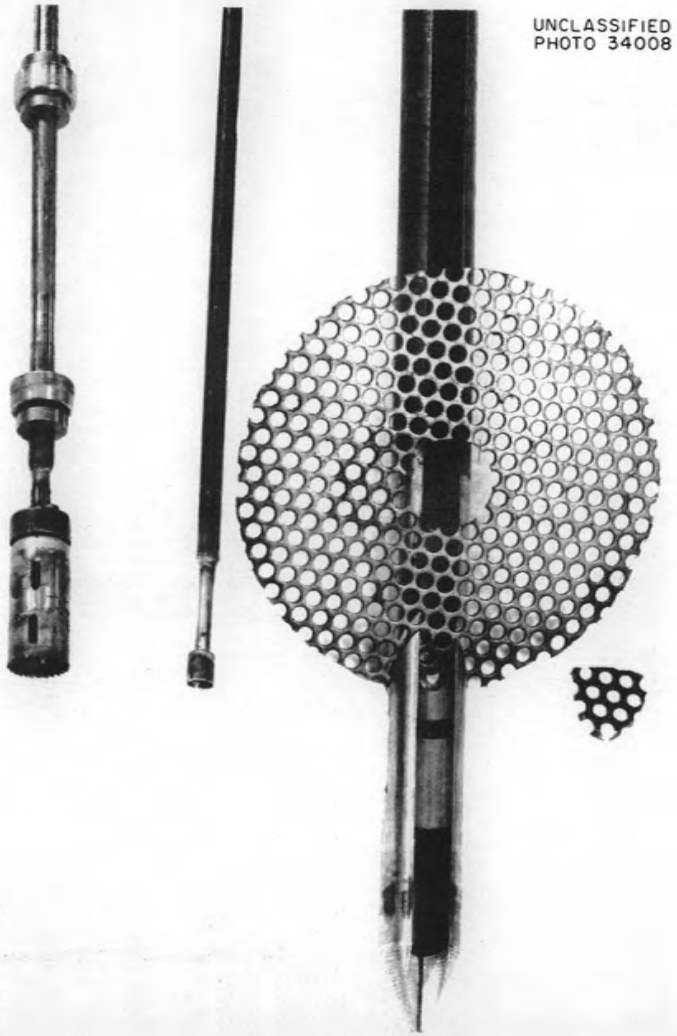

Fig. 3.10. Parts of Screen-Edge Sample Cutter. Left to right: hole saw; wrench for tightening clamp holding screen; mast, showing screen clamped in position for cutting; sample.

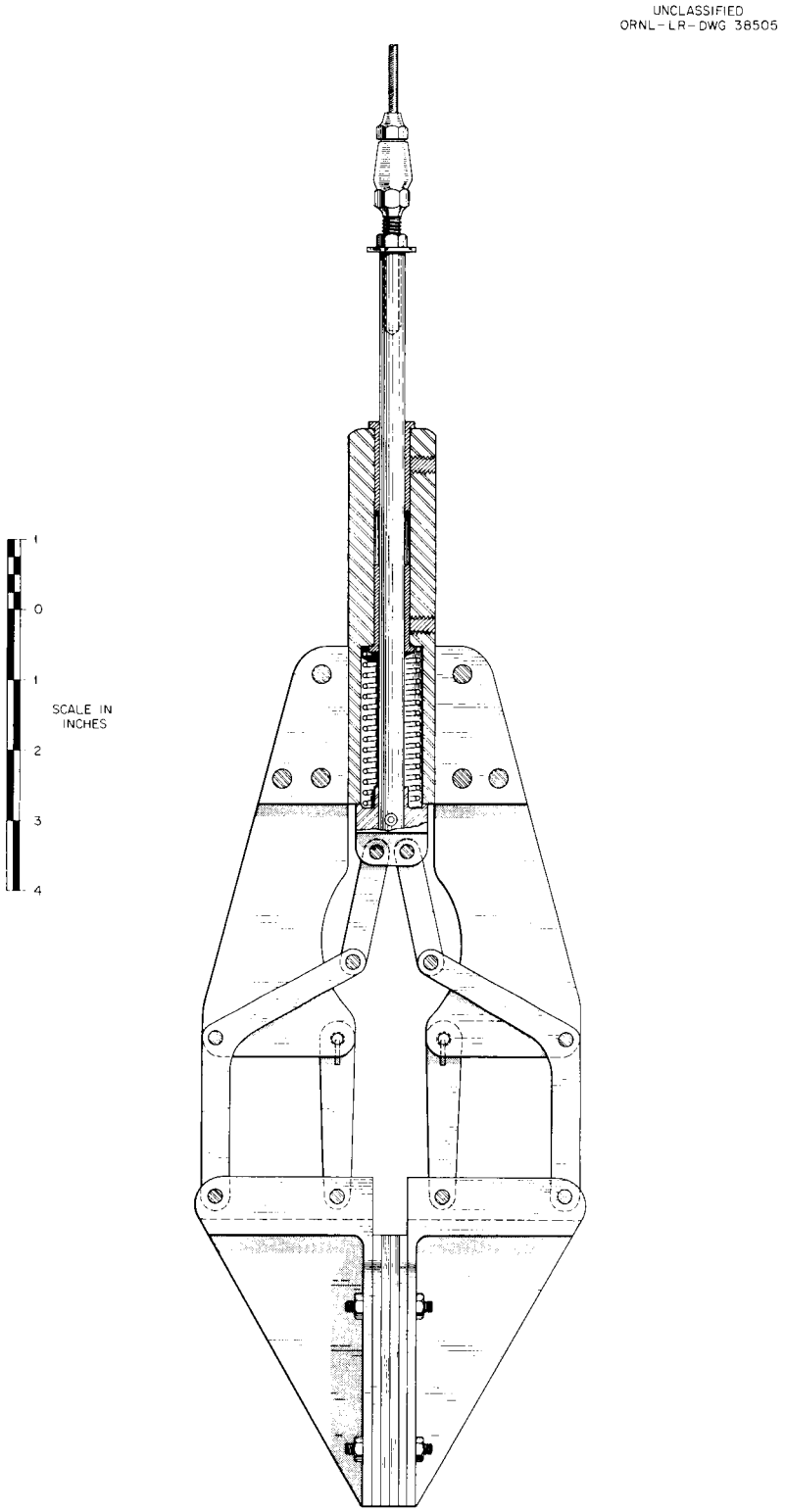

Fig. 3.11. Parallel-Jaw Tongs; 0-to-4-in. Opening, 100-lb Grip.

4. HRT COMPONENT DEVELOPMENT

I. Spiewak

T. G. Chapman
D. M. Eissenberg
C. H. Gabbard
B. A. Hannaford
E. C. Hise
C. G. Lawson
J. C. Moyers
I. K. Namba
H. R. Payne
H. C. Roller
R. P. Wichner

4.1 FEED-PUMP ENDURANCE TESTING

The two HRT prototype feed-pump heads on test have each operated for 16,300 hr. Successful completion of 16,000 test-hours on each of two prototype purge-pump heads was reported previously.

The history of the feed- and purge pumps in the HRT since October 1957 is summarized in Table 4.1. Four of the eight original heads are still in use; however, the service life is below that expected on the basis of prototype tests.

4.2 TEST AND PRETREATMENT OF THE REPLACEMENT CIRCULATING PUMP FOR THE HRT

The replacement for the HRT blanket-circulating pump was fitted with a 230-gpm stainless steel impeller, and complete performance data were taken over its operating range while circulating cold water at low pressure.[1] The pump was then given a rinse with 3% Na_3PO_4, followed by a rinse with 5% HNO_3, and then was operated with oxygenated water at 200 - 262°C for approximately 60 hr to establish a corrosion-resistant film.

The replacement fuel-circulating pump for the HRT was given a similar pretreatment. Performance testing of this pump was delayed due to the urgent need for the replacement blanket pump.

4.3 HEAT EXCHANGER UNPLUGGING STUDIES

In order to evaluate methods of unplugging HRT-type heat exchangers which might become blocked with corrosion products, tests were made by using a full-scale model of an HRT heat exchanger header and a U-tube bundle which had been a spare for the HRE. These items were deliberately plugged with rust particles. In the header mockup test, unplugging was accomplished by back-flushing with water. Vibrators had little or no effect on the unplugging action.

Only a small number of tubes in the spare HRE exchanger were unplugged when 65-psi water was applied to the unit. By vibrating the exchanger with a

Table 4.1. Operating History of HRT Diaphragm Pumps

Head Location	Head No.	Date Installed	Date Removed	Hours of Operation	Remarks
Blanket feed pump, west	14	10-1-57		3688	
Blanket feed pump, east	17	10-25-57		3688	
Fuel feed pump, west	16	10-1-57	4-27-59	4952	Leakage of D_2O from intermediate pipe prevented continuous operation
Fuel feed pump, east	15	10-1-57	7-26-58	2283	Diaphragm rupture suspected from reading of 10 mr/hr on intermediate pipe
Fuel feed pump, east	21	7-26-58	2-13-59	2278	Diaphragm rupture suspected from reading of 10 r/hr on sample of intermediate water
Fuel feed pump, east	23	2-13-59		39	
Blanket-circulating-pump purge pump	17	10-25-57		4656	
Fuel-pressurizer purge pump	18	10-25-57		4754	
Blanket-pressurizer purge pump	19	10-25-57	2-11-59	3654	Leaking suction check valve suspected from reduced output and pressure traces
Blanket-pressurizer purge pump	30	2-11-59		316	
Fuel-circulating-pump purge pump	20	10-25-57	2-13-59	4149	Leaking discharge check valve suspected from reduced output and pressure traces
Fuel-circulating-pump purge pump	31	2-13-59		405	

pneumatic Vibrolator, which exerted a maximum acceleration of approximately 2.5 g, and simultaneously applying water pressure, several more tubes were unplugged. In order to exert more vibrational force, an air hammer with unknown characteristics was then used in conjunction with the Vibrolator and water pressure. After this rather severe treatment, 14 of the 105 tubes were still tightly plugged. The exchanger will be furnace dried, and an attempt will be made to unplug the remaining tubes with dry air or other gas and vibration.

4.4 HRT CORE STUDIES

4.4.1 Modifications to Present Core

Heat transfer measurements at the surface of the full-scale model of the HRT core were completed in both forward and reverse flow, with various numbers of diffuser screens removed from the vessel. Heat transfer coefficients throughout the core were improved over those obtained with the present HRT arrangement by either reversing the flow or removing screens (see Table 4.2).

Table 4.2. HRT Core Heat Transfer Coefficients

	Btu/hr·ft^2·°F at 275 gpm, 10°C		
	Conical Diffuser	Southern Hemisphere	Northern Hemisphere
Forward Flow			
Screens in (present system)	550	179	267
Top four screens removed		349	429
Top seven screens removed		630 max	650 max
All screens removed	750	785 max	1100 max
Reverse Flow			
Screens in	810	701	592
Top four screens removed		716	631
Top seven screens removed		693	633
All screens removed	1050		

The behavior of sand, gravel, metal chips, and CCl_4 were observed in a transparent plastic conical diffuser section attached to the HRT model. Runs were made in forward and reverse flow with (a) all the screens in and tightly bonded to the wall, (b) all the screens in and not bonded to the wall, and (c) with the top five screens removed. The arrangement with the top five screens removed and with the flow entering the top of the vessel was the only one tested that prevented accumulation of solids and CCl_4 on the wall and screens of the model.

The tests performed with the current HRT configuration (where 2-in. holes are cut in the top six screens) and with the top five screens loose indicate that the fifth, fourth, and possibly the third screen from the top tend to be

buoyed up by the hydraulic force of the inlet fluid. However, it is believed that motion of these screens in the reactor is prevented by ligaments welded to the vessel and by corrosion pins which are wedged into the perforated plates in skewed positions.

The amount of fluid bypassing directly from inlet to outlet in reverse flow was determined to be 20% of the inlet flow, on the basis of chemical tracer injections.

As a result of the above investigations, it was concluded that satisfactory hydrodynamic operation of the HRT core could be achieved only by removing the top five or more screens and reversing the direction of flow. The importance of preventing solids deposition in a region of high power density may be appreciated by considering that the power density in corrosion products containing 4% uranium[2] is approximately 20 times that of the fuel solution.

4.4.2 Development of Flush Procedure for Solids Removal

If the screens are removed from the HRT by an electrolytic dissolution process, approximately 3 1/2 liters of ZrO_2 (solid) will be produced. If an arc-cutting method is used to remove screens, about 1/2 liter of droplets is expected. A method is required for removing such material from the high-pressure system. A water flush, combined with a 40-mesh screen filter, has been proposed.

Flushing tests were performed in the HRT core model by using sand and metal chips as the solids in some tests and iron rust in others. The flush procedure that used the least amount of cleaning water consisted in reverse flow at 50 gpm for 1 or 2 min, followed by about 200 gpm for 5 min. The filter in the discharge line collected 90% of the solids added. A purge rate of 1.25 gpm of water through the dump line was required to keep solids from accumulating in the line.

Removal of large flakes of scale from the screen diffuser was accomplished most effectively by alternating flow direction.

4.4.3 HRT Replacement-Core Model

To stabilize the flow pattern in the irrotational, spherical, annular-inlet core model[3], a second inlet was added as a jet at the south pole (Fig. 4.1). Building water at 7°C was fed in at the top annulus while the fluid entering at the south pole was drawn from a 30,000-gal reservoir heated to 55°C. By observing the wall temperatures (T_{1-4} of Fig. 4.1) and making heat balances around various envelopes, some characteristics of the internal flow were deduced.

The amount of hot fluid entrained into the cold boundary stream was a strong function of the polar-inlet velocity, and little affected by the annular-inlet velocity. The minimum amount of hot fluid entrainment achieved to date was 150% of the annular inlet flow. Further reductions of this entrainment as a result of variations in design may permit the vessel wall to be maintained close to inlet temperature.

An annular-inlet velocity greater than 5 fps was required in the model to prevent flow separation near the wall in the southern hemisphere.

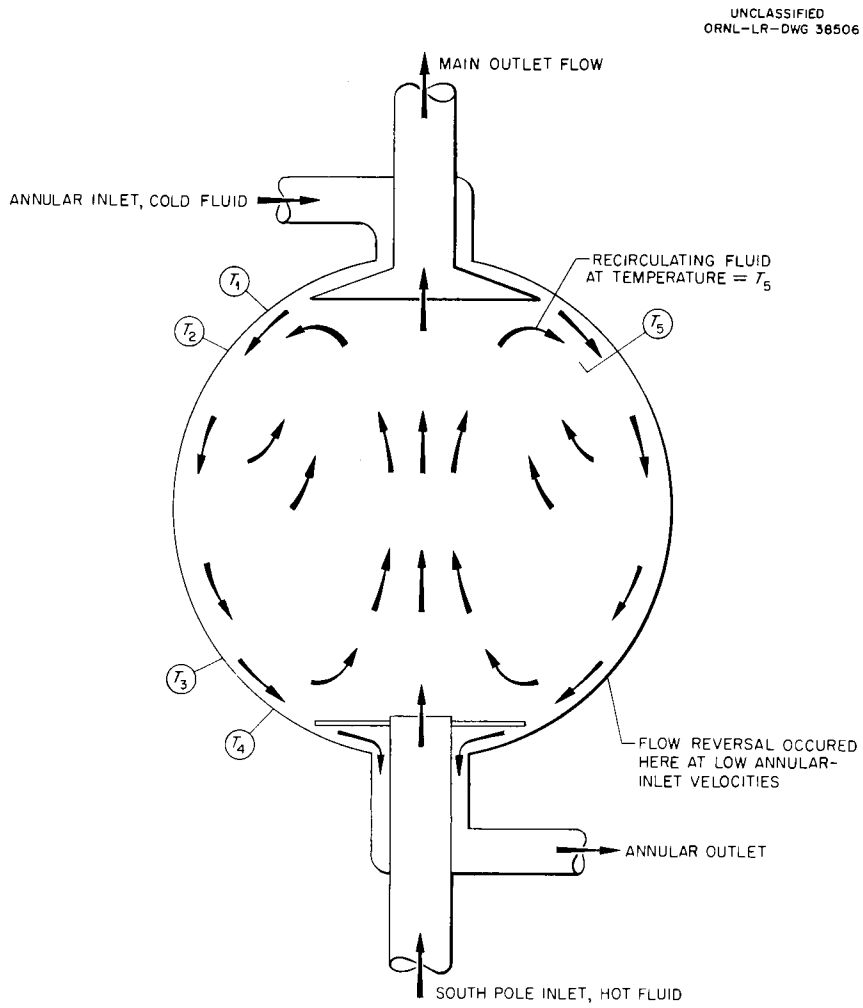

Fig. 4.1. Dual-Entry Core Model.

4.5 HRT MOCKUP

R. B. Korsmeyer P. H. Harley

The HRT mockup was operated for 811 hr during the quarter and was down eight weeks for two revisions and one major inspection. Run CS-24 was completed. It consisted in reversing the direction of flow in the loop in order to observe the effect on the performance of the gas separator and the stainless steel pressurizer in anticipation of reversing the flow through the HRT core.

In run CS-24, 694 hr of operation was at 1500 psi and 280°C with a fuel composition of 0.045 m UO_2SO_4, 0.036 m $CuSO_4$ and 0.025 m H_2SO_4. The fuel was stable at all pressurizer purge rates up to more than 10 gal/hr, in contrast to experience with forward flow under the same conditions. In run CS-22[4] (forward flow), a pressurizer purge rate of 10 gal/hr caused uranium to precipitate at approximately 24 g/day. The reversed flow evidently causes enough mixing in the horizontal line between the main loop and the pressurizer to prevent precipitation in what has heretofore been a sensitive location.

Based on the increase of nickel in solution, the generalized stainless steel corrosion rate was 1.6 mpy. The inspection at the end of the run showed that the loop orifice flanges and O-ring had been badly attacked. The corrosion was caused by leakage around the orifice plate which was bolted to the face of the upstream flange. The O-ring had lost 32 g of stainless steel and the flange approximately 3 g. After correcting the generalized corrosion rate for this local attack, the loop generalized rate was only 0.7 mpy.

The operation of the gas separator was tested with reversed flow by adding oxygen at 13 scfm to the pump discharge. Observation of the loop flow indicator and pump-power recorder indicated that there was no significant amount of gas bypassing the separator. Also, no increase in loop pressure or drop in the pressurizer temperatures indicated that no gas was accumulating in the pressurizer. Level control was maintained with a 0.21-gal/min liquid entrainment rate during this test.

Following Run CS-24, the high pressure system was inspected at the two pairs of flanges in the main loop, the inspection flange below the pressurizer, and the three transition flanges at the hot end of the letdown heat exchanger. The weld caps at both ends of the loop heat exchanger were removed. The system appeared very clean, especially the loop heat exchanger. There were no signs of local attack except at the orifice flange as mentioned above. The loop pipes had a good protective film and a scale of about 10 mg/cm^2.

A hydroclone was installed in a 1/2-in. line across the circulating pump to remove solids during future scale removing tests.

REFERENCES

1. J. C. Moyers and H. R. Payne, "Testing and Cleaning of HRT Replacement Blanket Pump, SN 1-80-F-488," memorandum to S. E. Beall, HRP-59-77 (April 17, 1959).

2. W. D. Burch et al., HRP Quar. Prog. Rep. Jan. 31, 1959, ORNL-2696, p 15.

3. I. Spiewak et al., HRP Quar. Prog. Rep. Jan. 31, 1959, ORNL-2696, p 27.

4. R. B. Korsmeyer et al., HRP Quar. Prog. Rep. July 31, 1958, ORNL-2561, p 38.

5. HRT DESIGN

W. R. Gall M. I. Lundin J. R. McWherter

C. A. Burchsted
R. H. Chapman
C. J. Claffey
E. H. Gift
F. C. Zapp

5.1 REVERSED FLOW THROUGH CORE TANK

Flow experiments[1] in the HRT core model indicate that the hydrodynamics of the core vessel can be improved by reversing the direction of flow with the diffuser plates removed (Sec. 4.4.1). The direction of flow in the HRT core system can be reversed by altering the piping on the fuel-circulating-pump assembly as shown in Fig. 5.1. Consideration is being given to the inclusion of a multiclone station consisting of 13 hydroclones in parallel (Sec. 2.2). About 3% (12 - 15 gpm) of the system flow would pass through the multiclone station. The underflow from the multiclone station, about 1 gpm, would feed to the Chemical Plant for solids removal.

5.2 HRT FLUSHING EQUIPMENT

Equipment was designed to remove scale and other solids from the HRT fuel and blanket systems after the core-vessel modifications are completed. In the concept employed, the circulating pump is raised and temporary cross-over pipes are installed to permit back-flushing. A basket-type strainer is included in the suction cross-over pipe to trap the solids. The strainer, which is removable, is constructed of 40 x 40 mesh screen. A schematic drawing of the equipment for the fuel system is shown in Fig. 5.2. The equipment is designed for 100-psi operation at room temperature.

5.3 RADIOLYTIC-GAS CONCENTRATION

As an aid in the analyses of experimental data and in the determination of operating conditions, the radiolytic-gas concentration in the HRT was calculated as a function of power level and average temperature.[2]

The assumptions used in the calculations for the core system are:

1. Deuterium is produced only in the core.
2. The power density is uniform throughout the core.
3. The net transfer of gas between the core and the blanket system is negligible.
4. Fuel feed occurs at the core outlet.

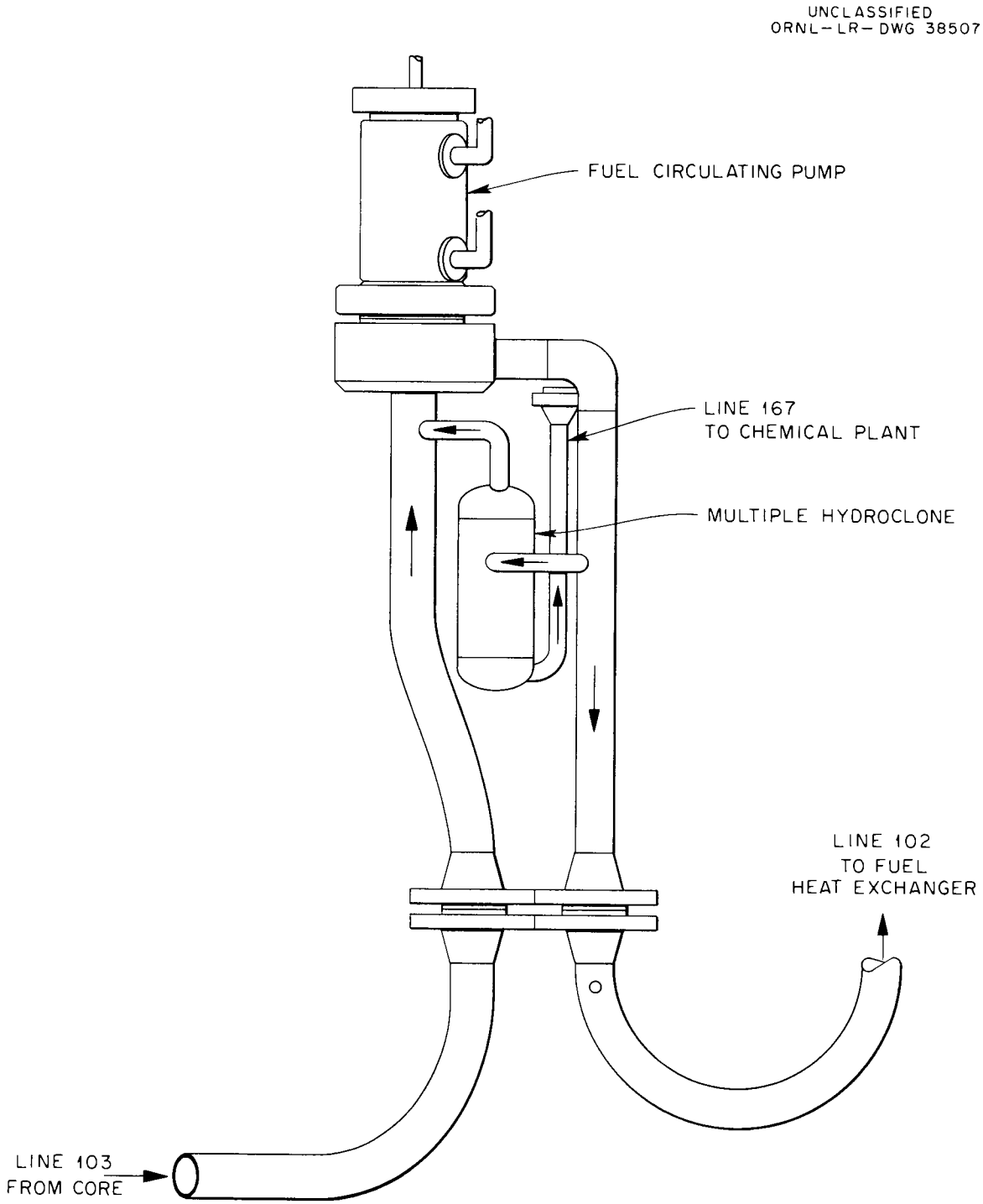

Fig. 5.1. Pump Piping for Reversed Flow in the HRT.

UNCLASSIFIED
ORNL-LR-DWG 38508

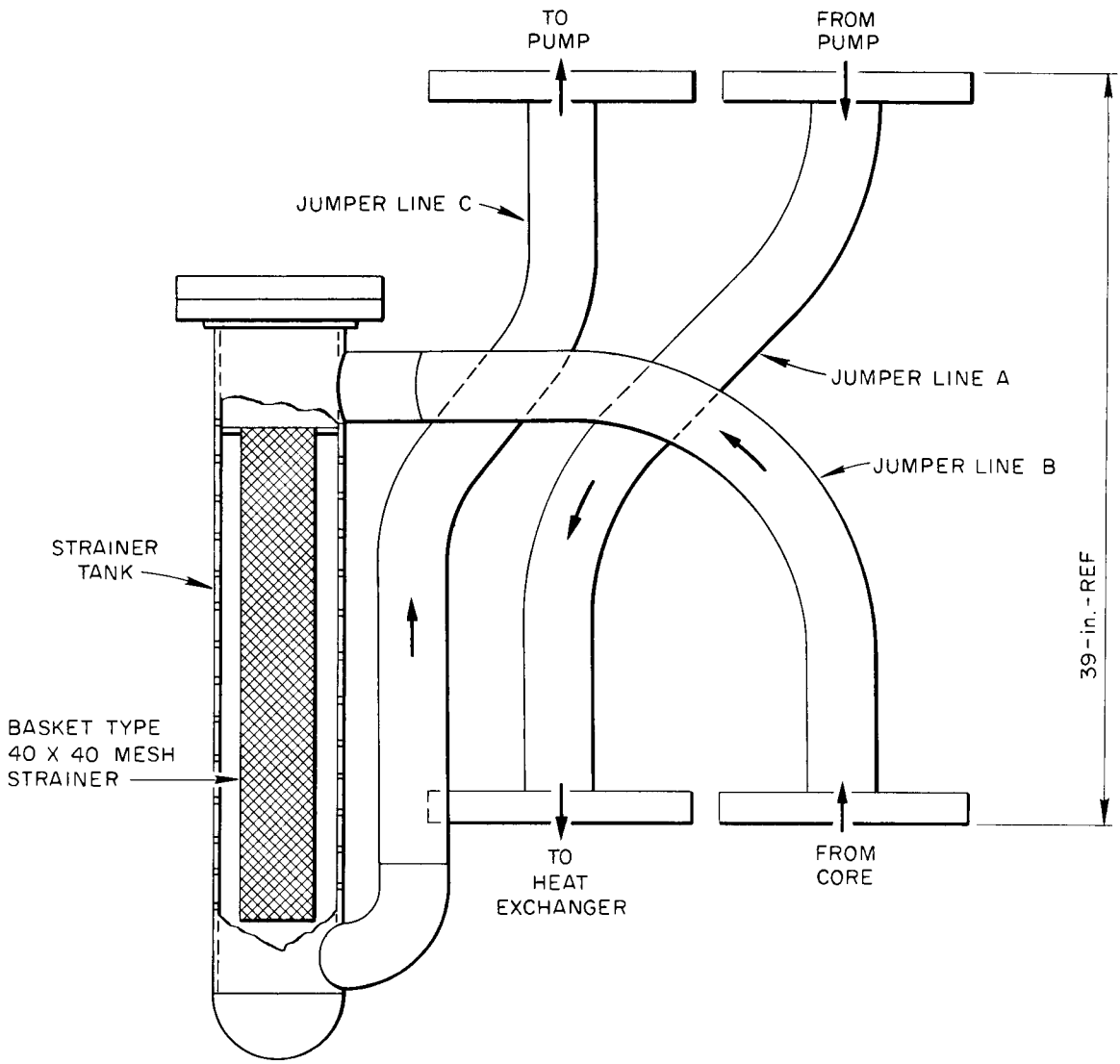

Fig. 5.2. HRT Flushing Equipment.

5. The average recombination-rate constant in the core vessel and heat exchanger is the log mean average of the rate constants at the inlet and outlet conditions.

Similar assumptions were made for the blanket system.

Data from several sources were compared[3] for the determination of the rate constant. The rate constant as given by data from some in-pile loop experiments (D_2O solution) is:

$$k = 3.061 \times 10^8 e^{-10506/T} \text{ (g-moles/liter-sec)},$$

where T is the solution temperature, ^oK.

There is evidence that the rate constant in the HRT is 1.4 times the above constant.[3]

The maximum total vapor pressure (consisting of radiolytic gas and excess-oxygen partial pressure and D_2O vapor pressure) in the circulating stream was found to exist at the core and blanket outlets for all average temperatures greater than 250°C. For average temperatures below 240°C the maximum total vapor pressure was found to exist at either the core and blanket outlet or inlets, depending on both the power level and the recombination-rate constant. This possibility of having the maximum total vapor pressure at the cold side of the system occurs because at temperatures below 240°C the decrease in solubility of the dissolved gas may more than offset the decrease in the vapor pressure of the water. Thus the sum of the two pressures can be greater in the core-inlet side of the system. By using fuel concentration and criticality data from HRT run 18, the predicted total vapor pressure at the core outlet is given as a function of power and temperature in Fig. 5.3, where a rate constant derived from the in-pile-loop recombination data was used, and where the value for the rate constant was 1.4 times that determined from the in-pile loop data.

REFERENCES

1. I. Spiewak et al., HRP Quar. Prog. Rep. Jan. 31, 1959, ORNL-2696, p 26 - 27.

2. E. H. Gift, Predicted Vapor Pressure in the HRT, ORNL CF-59-4-76.

3. J. R. McWherter, A Comparison of Radiolytic Gas Recombination Rate Constants Observed in Several D_2O Solution Experiments, ORNL CF-59-4-67 (to be issued).

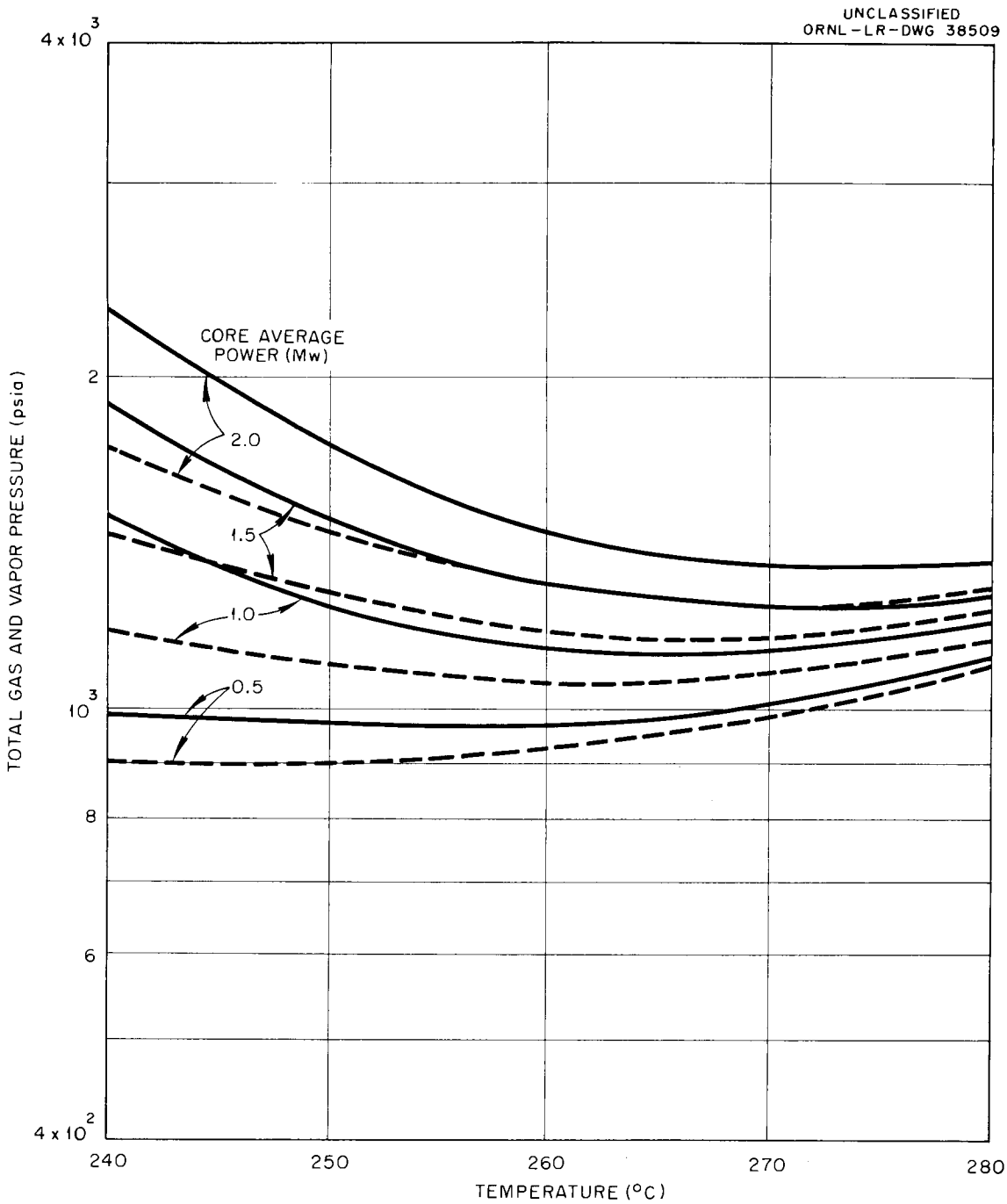

Fig. 5.3. Total Gas and Vapor Pressure in the HRT According to a Recombination-Rate Constant Based on In-Pile Loop Data (Solid Lines) and a Rate Constant 1.4 Times That Based on In-Pile Loop Data (Dashed Lines).

6. HRT REACTOR ANALYSIS

P. R. Kasten

T. B. Fowler
S. Jaye
M. P. Lietzke
B. E. Prince

6.1 EFFECT OF FUEL IN BLANKET OF HRT ON NEUTRON LEAKAGE

The correspondence between the output of the HRT neutron detectors and the fission rate in the reactor depends on the number of neutrons escaping from the pressure vessel and the associated energy spectrum. Addition of fuel solution to the blanket causes significant changes to both the total number escaping and the energy spectrum. To estimate these effects, the neutron leakages were calculated by using a multigroup, multiregion reactor code (CORNPONE) on the Oracle. Table 6.1 gives the number of neutrons, above a specified energy level, which would escape from the pressure vessel per neutron produced in the reactor if there were no fuel in the blanket region.

Table 6.1. Neutron Leakage from Pressure Vessel with No Fuel in Blanket

Energy (ev)	Number of Neutrons Escaping per Neutron Produced	Fraction of Total Leakage
$>1 \times 10^6$	6.66×10^{-4}	0.07
$>1 \times 10^3$	2.35×10^{-3}	0.24
>10.0	5.88×10^{-3}	0.60
>1.0	7.05×10^{-3}	0.72
>0	9.84×10^{-3}	1.0

Figure 6.1 shows the neutron leakage from the pressure vessel with fuel in the blanket region relative to that with no fuel in the blanket; the various curves cover the spectral ranges listed in Table 6.1, and so Table 6.1 and Fig. 6.1 together give the absolute neutron leakage. The divergence of the curves in Fig. 6.1 is due to the change in the energy distribution of the escaping neutrons. For example, the fraction of escaping neutrons which have energies greater than 10 ev is 60% with no fuel in the blanket and 86% if the blanket fuel concentration is 20% that of the core.

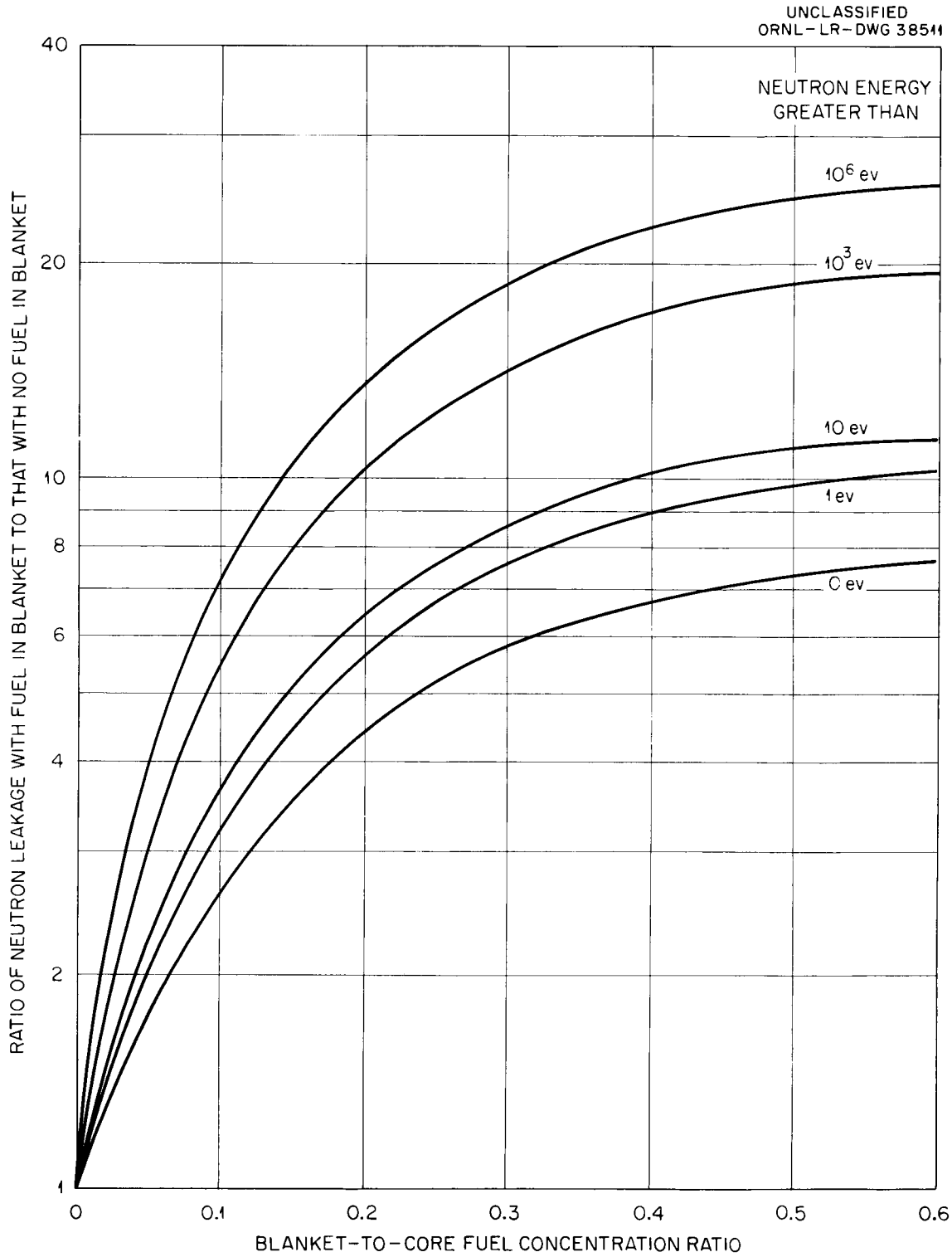

Fig. 6.1. Effect of Blanket Fuel Concentration on Relative Neutron Leakage from Pressure Vessel of HRT at 250°C.

6.2 HIGH-ENERGY NEUTRON FLUX IN THE HRT

The energy distributions of neutron flux for neutrons having energies greater than 0.1 Mev were estimated for HRT runs 14 and 17. At high energies, the primary contributions to the neutron flux are from (1) fission neutrons which have made no collision with moderator atoms and (2) neutrons in flight with reduced energies after having made a single collision with the moderator. These two components were calculated, on the assumption that any scattering collisions were elastic and isotropic in nature (the laboratory system was used in calculating the energy degradation per collision).

In computing the flux, the region from 0.1 to 10 Mev was divided into seven energy groups. Probabilities of neutron transfer from a higher energy group to lower energy groups upon collision were determined from the distribution law associated with energy loss per elastic scattering. The spatial distribution of fission source neutrons in the HRT core and blanket were obtained from multigroup age-diffusion theory, using a 20-group, 4-region version of the Oracle program CORNPONE. In the calculation of the once-collided flux, backscattering from the pressure vessel was neglected. The average moderator temperature during runs 14 and 17 was assumed to be 280°C. There was no fuel in the blanket during run 14; for run 17 the blanket-to-core fuel concentration ratio was assumed to be 0.33.

The computational results are summarized in Figs. 6.2 through 6.4. Figures 6.2 and 6.3 give plots of the cumulative neutron flux above 1 Mev during runs 14 and 17, respectively, showing the uncollided and once-collided components and their sum. The total flux for run 17 is separated into the various energy groups in Fig. 6.4.

For comparative purposes, the volume-averaged neutron fluxes above 1 Mev obtained from the CORNPONE multigroup calculations are listed in Table 6.2. These calculations are based on five energy groups above 1 Mev. In this high-energy region with D_2O moderator, the slowing-down approximations in age-diffusion theory are not strictly applicable. The single-collision model treats the transfer between energy groups during collision more accurately; however, the latter model contains approximations of other types. In the neighborhood of the core tank, the fluxes calculated by using age-diffusion theory are about 50% higher than those obtained from the single-collision technique. The difference is even larger near the pressure-vessel boundary, partially due to neglect of backscattering from the vessel in the single-collision calculation. Other inaccuracies in the single-collision computation result from the assumption of angular isotropy of scattering and the large mesh size used in the numerical calculation (to decrease computation time); these tended to smooth out any rapid changes in flux near the boundaries. In spite of these inaccuracies, the single-collision method gives better values than age-diffusion theory.

Estimates were made of the fast-neutron exposure at the core-tank wall and also at the pressure-vessel wall. By using the values reported for the total thermal power generated during runs 14 and 17,[1,2] estimates of the total nvt values were obtained; these are given in Table 6.3. The values shown are based on the single-scattering model. To date, the exposures given do not constitute any danger insofar as embrittlement of the pressure vessel is concerned. Based on the results here, the HRT could be operated at full power for about two years with a ratio of blanket-to-core fuel concentration of 0.3 before the fast-neutron exposure (>1 Mev) of the pressure vessel exceeds 10^{19} neutrons/cm^2.

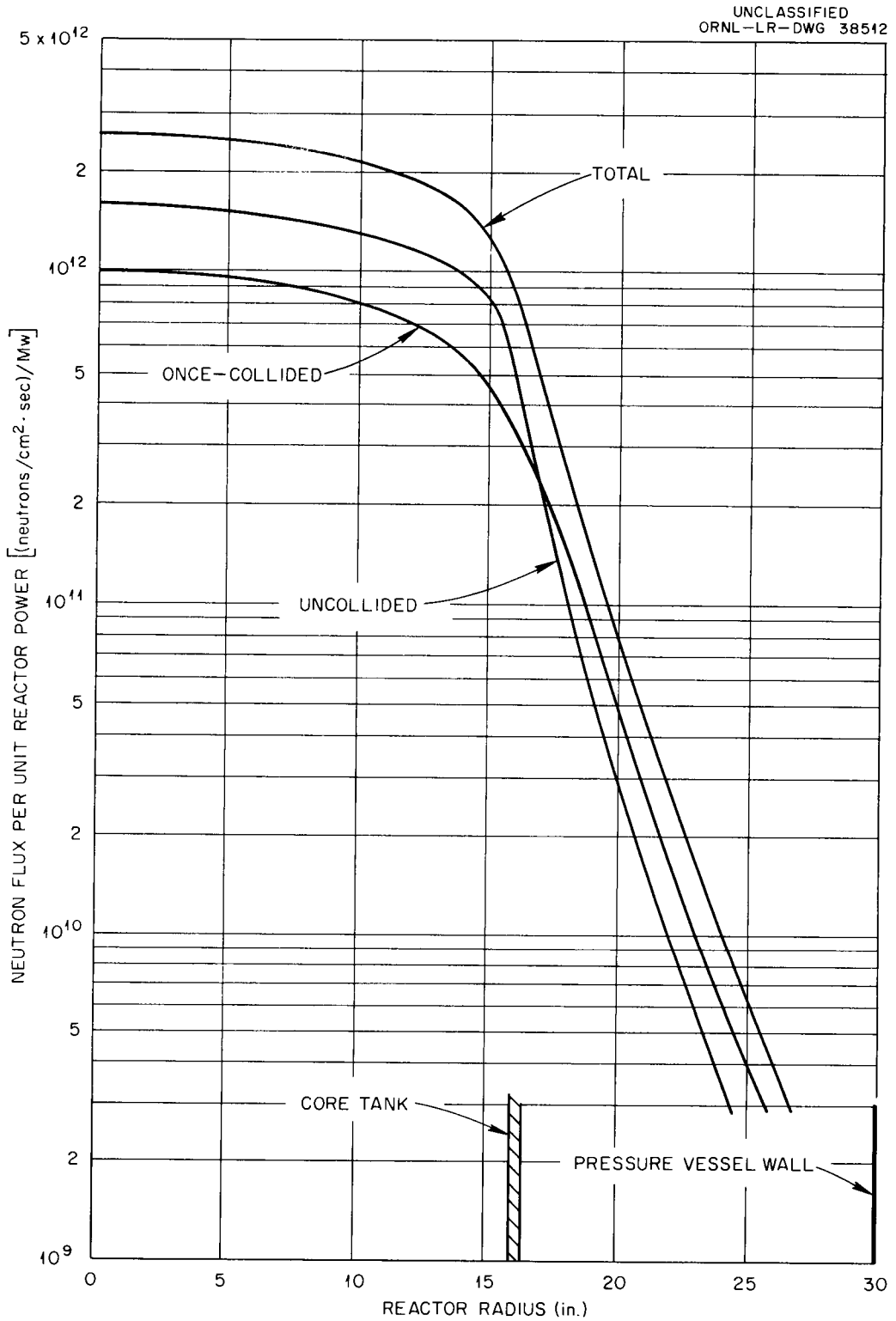

Fig. 6.2. Cumulative Flux of Uncollided and Once-Collided Neutrons Above 1 Mev During HRT Run 14.

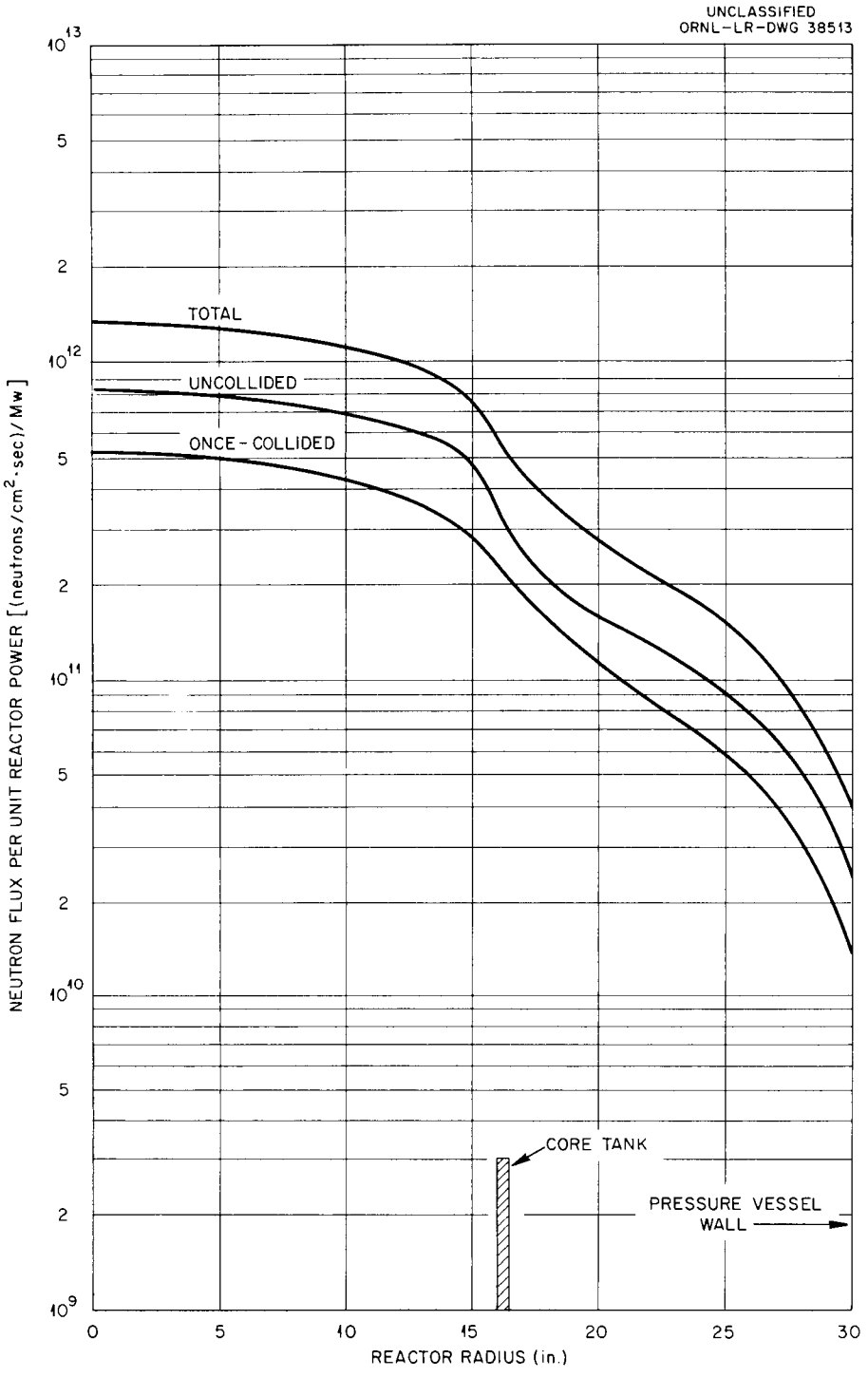

Fig. 6.3. Cumulative Flux of Uncollided and Once-Collided Neutrons Above 1 Mev During HRT Run 17.

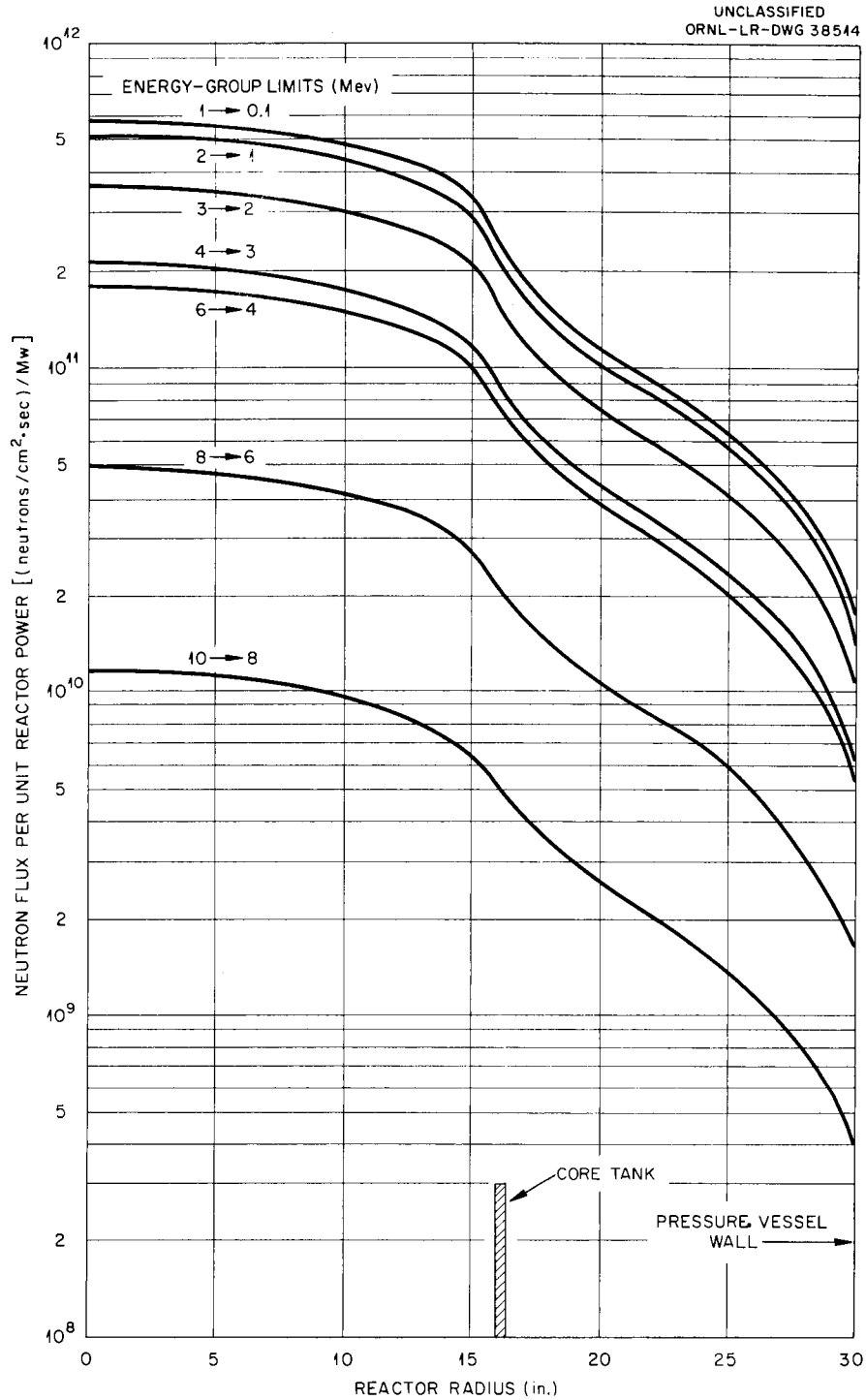

Fig. 6.4. Flux of Uncollided and Once-Collided Neutrons in Various Energy Groups During HRT Run 17.

Table 6.2. Volume-Averaged Neutron Fluxes Above 1 Mev Obtained from Age-Diffusion Calculations (Normalized to 1 Mw)

Region	Average Flux (neutrons/cm^2.sec)	
	Run 14	Run 17
Core	2.33×10^{12}	1.38×10^{12}
Core tank	1.16×10^{12}	8.70×10^{11}
Blanket	1.21×10^{11}	2.79×10^{11}
Pressure vessel	2.89×10^{9}	1.50×10^{11}

Table 6.3. Integrated Fast-Neutron Exposures Above 1 Mev in HRT During Runs 14 and 17 (Based On Single-Scattering Model)

Position	Integrated Flux, nvt (neutrons/cm^2)	
	Run 14*	Run 17**
Inner surface of core tank	1.0×10^{18}	5.1×10^{18}
Inner surface of pressure vessel	$< 1.2 \times 10^{15}$	3.6×10^{17}

*340 Mwhr (ref 1).

**2526 Mwhr (ref 2).

REFERENCES

1. S. E. Beall et al., HRP Quar. Prog. Rep. April 30 and July 31, 1958, ORNL-2561, p 6.

2. S. E. Beall et al., HRP Quar. Prog. Rep. Oct. 31, 1958, ORNL-2564, p 4.

7. HRT CONTROLS AND INSTRUMENTATION

D. S. Toomb

S. J. Ball K. W. West J. R. Brown
A. M. Billings R. L. Moore

7.1 COMPONENT DEVELOPMENT

7.1.1 Letdown Valves

Testing of letdown valves was continued in the HRT mockup loop. This valve is used to throttle about 2 gpm of fuel solution from the high-pressure system of the reactor to the low-pressure dump tank.

The 1/8-in.-dia port valve previously described[1] (No. 22) was removed from the mockup loop after 3520 hr of operation and found to be leak-tight. However, some erosion of the metering portion of the 17-4 PH stainless steel occurred and is illustrated in Fig. 7.1.

A larger valve was needed for subsequent mockup loop tests; so a 1/4-in.-dia port valve (No. 21) of the type and size now in use (17-4 PH stainless steel plug) in the reactor was reinstalled. This valve, which had been used previously, has now operated satisfactorily for 7800 hr.

The 1/4-in.-dia port valve installed in the reactor continues to operate properly after 3787 hr of service. This valve also has a 17-4 PH stainless steel plug.

7.1.2 Gamma Radiation Detector

A gamma-sensitive ionization chamber which utilizes alumina insulators to permit operation in high-temperature environments was acquired for evaluation.

The detector housing is weld sealed, and a threaded cable-connector housing is provided so that the chamber may be operated while completely immersed by threading the detector onto a cable conduit. The chamber which is illustrated in Fig. 7.2 is filled with nitrogen at 10 atm in order to increase sensitivity.

When the detector was cycled from ambient temperature to 150°C, no appreciable change in output signal was observed. Although the manufacturer rated the detector for operation at temperatures to 400°C, the cable connectors now installed have Teflon insulators which would limit the maximum operating temperature to less than 200°C.

UNCLASSIFIED
PHOTO 33530

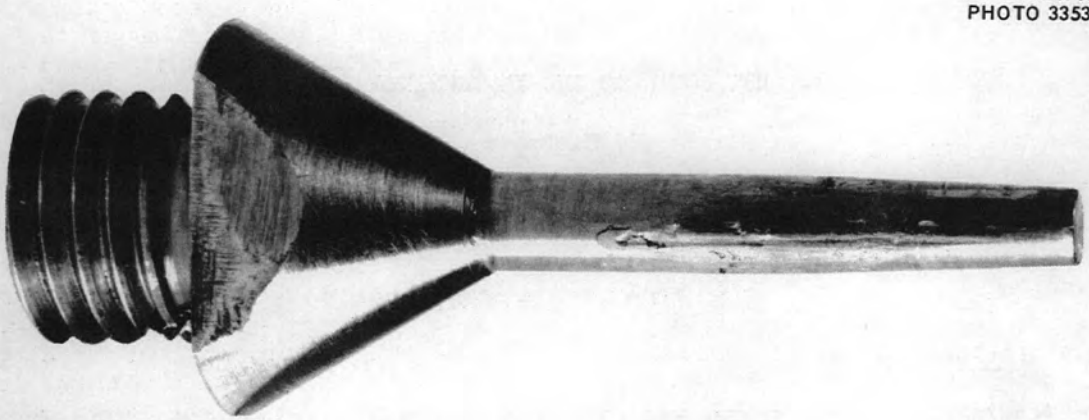

Fig. 7.1. Plug from Letdown Valve No. 22.

UNCLASSIFIED
ORNL-LR-DWG 38515

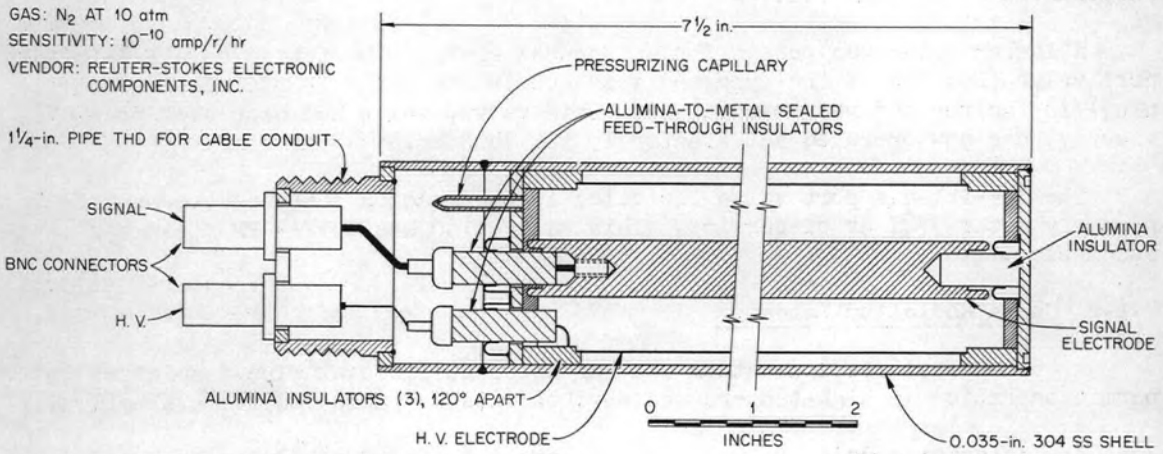

Fig. 7.2. High-Temperature Gamma Radiation Detector.

The detector should be useful as a radiation monitor in reactor steam-valve compartments and other locations where severe environmental conditions exist.

7.1.3 Remote-Viewing Equipment

The miniature television camera designed[2] for resistance to radiation was tested in a high-gamma field. The only electronic components in the camera head are the Vidicon tube, the deflection coils, one ceramic capacitor, and a carbon resistor. The remaining electronic components associated with the camera are in a preamplifier chassis which is connected to the camera by a 10-ft cable. By using this remote preamplifier, most of the electronic components can be kept out of the high-radiation zone by either the use of intermediate shielding from strong sources or physical removal from weaker sources.

There was no observable initial effect on the camera operation when it was lowered into a 1.5×10^6 r/hr field. However, the picture faded rapidly and required maximum target voltage after 20 min. After 1 hr of additional exposure in a reduced field of approximately 5×10^5 r/hr, the picture was not readable. After further exposure for a total dosage of 5×10^6 r, the camera head was removed and the lens was found to be practically opaque. After replacement of the lens, the camera operated satisfactorily with some loss of sensitivity, probably due to browning of the face plate of the Vidicon tube.

The test was performed in the canal of the ORNL Graphite Reactor, and buckets of Co^{60} capsules were used as a source. As the source was underwater, the camera was mounted in the test chamber shown in Fig. 7.3. An air purge for cooling was provided, and the camera temperature was not allowed to exceed 110°F. A photographically reduced standard-television-test-pattern was mounted at the bottom of the watertight chamber. Illumination was provided by two concentric rings of 12 General Electric No. 328 lamps. The intensity of illumination was 50 to 100 foot candles. The glass in some of the lamps which were not energized darkened under irradiation. However, the heat generated by the illuminated lamps was sufficient to keep them clear.

The gamma dosage was monitored by cerium sulfate dosimeters.

A lens made from non-browning glass was ordered from the Wollensak Optical Co. The test will be repeated with this lens at a radiation level of about 10^5 r/hr.

REFERENCES

1. D. S. Toomb, et al, HRP Quar. Prog. Rep. for Periods Ending April 30 and July 31, 1958, ORNL-2561, p 50.

2. Ibid, p 51.

UNCLASSIFIED
PHOTO 33279

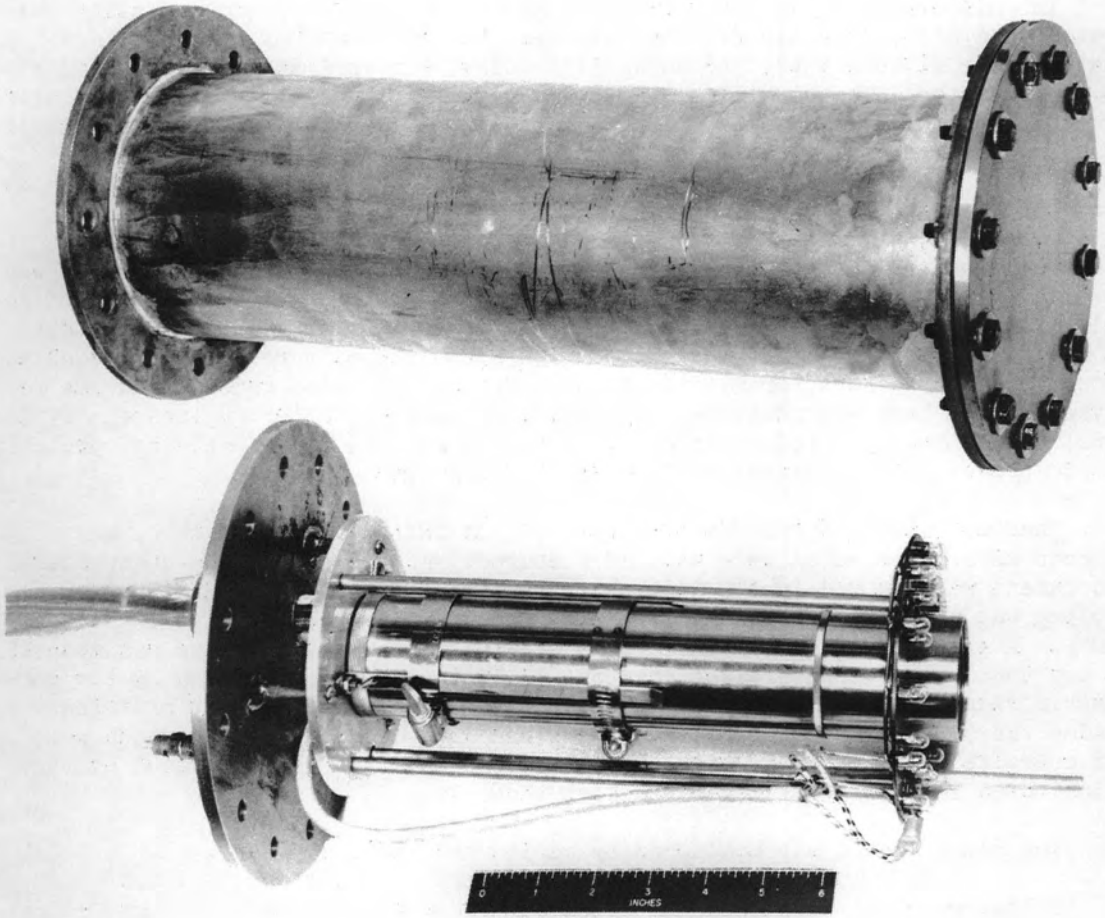

Fig. 7.3. Test Chamber and Miniature Television Camera.

Part II

REACTOR ANALYSIS, RESEARCH, AND DESIGN

R. N. Lyon

8. RESEARCH AND ANALYSIS

P. R. Kasten

H. C. Claiborne
T. B. Fowler
S. Jaye
M. P. Lietzke
C. S. Morgan
B. E. Prince
M. W. Rosenthal
D. G. Thomas
M. Tobias

8.1 CONTROL OF CORE-WALL TEMPERATURES IN TWO-REGION POWER REACTORS

In-pile corrosion studies have indicated that the corrosion rate of a Zircaloy-2 core vessel will increase with increasing wall temperature; therefore, a computational study was made of the temperature which would exist at the surface of the core wall in a large two-region reactor under various fluid-flow conditions.

Three methods of removing heat from the vicinity of the wall to maintain a specified wall temperature were considered:

1. passing the blanket slurry between the wall and a shroud at a temperature low enough to remove heat at the rate required;
2. using a double-wall core vessel and passing heavy water between the two walls at the temperature and velocity required to accomplish the cooling needed;
3. directing the entering stream of core fluid along the wall at a high velocity, so that the wall is in contact with the colder fluid, and the heat transfer conditions are good enough to keep the effect of the volume heat source from being important.

The analysis of the first two methods is discussed below, and some of the results are given. Whether or not the third method would be effective depends on the achievement of the necessary flow condition; an experimental investigation related to this problem is described in Sec. 4.4.3.

Four core systems, whose characteristics are given in Table 8.1, were treated. The sphere diameters were selected to give the same critical concentrations as the corresponding cylinders. For all the reactors the blanket region was 2 ft thick and contained 1000 g of Th per liter and 3 g of U^{233} per kg of Th.

Two energy sources which can contribute significantly to raising the core-wall temperature were considered: (1) power generated in the fluid near the wall and (2) gamma energy absorbed in the wall. A possible third source, energy from fissioning of uranium deposited on the wall surface, was neglected.

The power densities in the blanket and core fluids at the wall were obtained from two-group neutron diffusion calculations for isothermal cores. For long cylinders with axial temperature gradients, the flux distribution can be appreciably distorted from the symmetrical pattern which exists in an isothermal system, and the maximum power density increased. This is discussed in Sec. 8.2. The results given in this section are for the isothermal core.

The gamma heating rate for spheres was estimated by using the Oracle routine[1] of Claiborne and Fowler. The maximum gamma heating rate in the cylinder walls was approximated by adjustment of the sphere results. However, one value was checked by direct calculation, and the agreement was good.

8.1.1 Cooling with Blanket Fluid

In order to cool the core wall from the blanket side, the entering slurry would be directed along the wall by a shroud. Use of eductors to entrain fluid at the shroud inlet would reduce the amount of slurry to be circulated outside the blanket for a specified shroud throughput.

The blanket fluid was assumed to have a yield stress of 0.1 lb/ft^2 and a coefficient of rigidity of 1.0 cp. At a Reynolds number several times greater than the critical value (associated with the onset of turbulence), the heat transfer behavior of this material can be estimated satisfactorily by using the relationships for Newtonian fluids. For a Bingham plastic having the properties assumed, the critical velocity through a 3-in. gap would be 3.4 fps. The heat transfer coefficient would be 4000 $Btu/hr.ft^2.°F$ for a velocity four times the critical velocity.

The values given in Table 8.1 are based on the assumption that all the heat generated in a $\frac{1}{2}$-in.-thick Zircaloy core wall is removed by the blanket fluid (the temperature differences would be greater if some of the heat released in the core fluid were also transferred to the blanket fluid).

8.1.2 Internal Wall Cooling

For the case of internal cooling of the wall, it was assumed that two $\frac{1}{4}$-in. thicknesses of Zircaloy are separated by a $\frac{1}{2}$-in. gap through which heavy water flows. Results of heat transfer calculations are given in Table 8.2 for the case of axial flow of fuel through the core with a temperature rise from 250 to 300°C; the coolant temperatures at the points of maximum wall power density that would be required to reduce the wall temperature either to 275 or to 250°C are given. The flow of fuel fluid was assumed to be fully developed at the mid-plane. The coolant temperature rise was taken as 50°C; fluid flow was assumed to be directed about the cylinder in a spiral path so that the velocity was always 10 fps.

If in the two examples of case 1 (Table 8.2) the power were 200 Mw instead of 400, the corresponding coolant temperatures required at the mid-plane to remove the energy generated would be 157 and 216°C. Increasing the coolant velocity would have little effect on the required coolant temperature, since most of the temperature drop takes place across the metal wall.

The change in power density in the fuel solution at the inner surface of the core wall which would result from the coolant acting as a reflector was also estimated. For the cylinder of case 1, the maximum wall power density with a $\frac{1}{2}$-in. coolant gap was 7% greater than that associated with no coolant gap. A more exact treatment of the wall cooling problem would require inclusion of this effect; however, for the $\frac{1}{2}$-in. gap only a small change in temperature would result.

Table 8.1. Results for Wall Cooling by Blanket Slurry

Case Core Geometry	Case 1, Cylinder	Case 2, Sphere	Case 3, Cylinder	Case 4, Sphere
Core-vessel dimensions, ft	4 x 12	5.34 ID	7 x 18	9.08 ID
Core Th conc., g/liter	0	0	200	200
Total power, Mw	400	400	1000	1000
Max. heat generation rate in core wall, w/ml	19	30	6	9
Max. power density in blanket slurry at core wall, kw/liter	59	63	9	9
Shroud flow rate, gpm	19,000	25,000	34,000	43,000
ΔT, core-side of wall to blanket fluid, °C	95	147	32	49
ΔT across core wall, °C	89	138	29	44
ΔT wall-to-slurry for wall gamma heat, °C	5	8	3	5
Adiabatic wall* ΔT, °C	0.8	0.9	0.2	0.3

*Difference between surface temperature and mean slurry temperature due to heat generation within the slurry.

The results given in Table 8.2 are essentially based on straight-through, fully developed flow conditions. Some wall-cooling advantage may be gained by changing the core flow pattern so that the entering fuel fluid is directed along the wall. If a favorable flow pattern can be achieved, simultaneous use of internal wall cooling would permit the wall temperature to be kept at the specified value with higher coolant temperatures than those given in Table 8.2.

8.2 EFFECT OF TEMPERATURE DISTRIBUTION UPON MAXIMUM POWER DENSITY IN CYLINDRICAL REACTORS

In a long cylindrical reactor in which fuel solution enters at one end and leaves at the other, the nuclear properties of the reactor will vary continuously along the axis due to the rise in temperature experienced by the fluid. It may be expected, therefore, that the power-density distribution will differ from that obtained on the basis of a uniform reactor temperature. However, a study of the power distribution of particular 12- and 18-ft-long cylindrical reactors showed that the power distribution for straight-through flow is not unduly different from that obtained under the uniform-temperature assumption. This conclusion is supported by the computations performed by an MIT Practice School group. Figure 8.1 shows their results[2] for maximum core power density obtained for cylindrical

Table 8.2. Results for Internally Cooled Core Walls

	Case 1		Case 3*	
Mean fuel temp. at mid-plane, °C	275		275	
Max. power density in fuel fluid at core wall, kw/liter	48		26	
Adiabatic wall** ΔT, °C	37		65	
Max. core-wall temp. at mid-plane, °C	250	275	250	275
q/A removed from core fuel x 10^{-3}, Btu/hr.ft^2	109	67	88	63
Coolant temp. at mid-plane, °C	60	143	119	178
Total heat removed by coolant, Mw	9	5	21	14
Coolant flow rate, gpm	690	390	1900	1200
Coolant pressure drop, psi	4.6	8.1	2.7	4.2

*See Table 8.1.

**Difference between surface temperature and mean fuel temperature due to heat generation within the fuel.

reactors varying in length between 10 and 40 ft and operating at 400 Mw thermal power. The assumed temperature rise in all their cases was 40°C. These results were obtained by use of the one-dimensional IBM code WANDA. Each point was obtained after a succession of iterations in which the previously computed flux was used to determine a new temperature distribution and a new set of nuclear properties.

In the work reported here, a two-dimensional IBM-704 code, PDQ, was employed to take radial reflection into account more adequately than is possible with the WANDA code. However, because of the relative slowness of the PDQ code, iteration to revise initial temperature-distribution estimates was not attempted. (Prior experience indicated that the changes which would be computed by continuing the calculation are small.)

The characteristics of the reactors studied are listed in Table 8.3. Four cases were run in which flow was involved. In the "straight-through" case, slug flow was assumed, so that radial temperature variations were neglected. In the "reversed-flow" cases, the fluid was assumed to enter the reactor core tangentially at one end, flow along the outside wall until it reached the other end, where it would turn around and flow down the middle of the core, leaving the reactor at the same end at which it entered. This flow pattern is shown schematically in Fig. 8.2. For these reverse-flow cases, the core was divided into two concentric cylindrical zones. In the outer zone, the fluid was assumed to rotate around the cylinder axis with an axial velocity of either 5 or 10 fps.

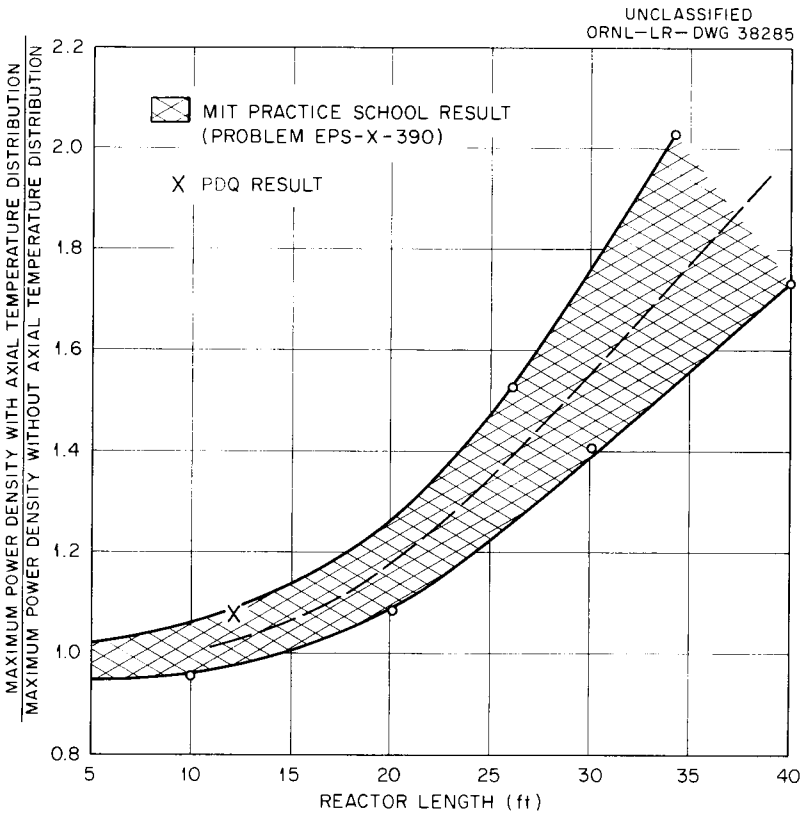

Fig. 8.1. Effect of Temperature Distribution upon Maximum Power Density as a Function of Reactor Length for Cylindrical Reactors (Core Diameter, 4 ft; Thermal Power, 400 Mw). (Results taken from MIT Engineering Practice School Problem EPS-X-390.)

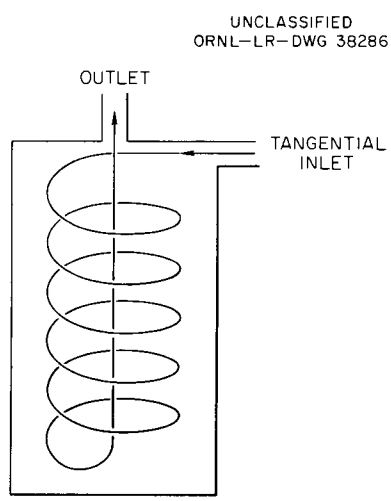

Fig. 8.2. Schematic Drawing of Reversed-Flow Pattern in a Cylindrical Reactor.

Table 8.3. Nuclear Characteristics of "Reverse-Flow," "Straight-Through-Flow," and Uniform-Temperature Cylindrical Reactors (Blanket Thorium Concentration, 1000 g/liter; Blanket U^{233} Concentration 4 g/kg Th; Blanket Thickness, 2 ft; Blanket Temperature 230°C; Core Tank, $\frac{1}{2}$-in. Zircaloy. Ends unreflected. Extrapolation distance, 6 in.)

Case No.	Flow Type	Core Temp. Range (°C)	Core Dia. (ft)	Reactor Length (ft)	Core Th Conc. (g/liter)	Assumed Core Critical Concentration (g U^{233}/liter at 275°C)	Total Reactor Power (Mw of Heat)	Axial Velocity, Outer Core Zone (fps)	Dia. of Central Core Zone (ft)	Ratio of Power Densities*
1	-	Uniform temp., 275	4	12	0	2	-	-	-	0.61
2	Straight through	250-300	4	12	0	2	Any	-	-	0.66
3	Reversed	250-300	4	12	0	2	400	10	3.0	0.64
4	-	Uniform temp., 275	7	18	200	6.8	-	-	-	0.46
5	Reversed	250-300	7	18	200	6.8	1000	5	3.14	0.46
6	Reversed	250-300	7	18	200	6.8	1000	10	5.42	0.47

* Ratio of maximum core wall power density to average core power density

As can be seen from the last column of Table 8.3, the maximum core wall power density is only a few per cent different from that associated with a uniform temperature distribution independent of the type of flow.

8.3 CRITICALITY CONDITIONS FOR UNREFLECTED SLURRY CONTAINERS

A computational study was made of the critical uranium-to-thorium ratios required for specified temperatures in unreflected spheres containing urania-thoria in D_2O-H_2O mixtures; moderator mixtures containing up to 20 mole % H_2O were studied; the sphere diameters were varied between $2\frac{1}{2}$ and $3\frac{1}{2}$ ft; critical temperatures considered were 20 and 200°C. Various slurry concentrations were considered; the concentration desired was that associated with the highest critical temperature for a specified U/Th ratio. The calculations were performed on the IBM-704, by using a modified Fermi-age single-region reactor model with an approximate correction for resonance fissions in fuel. The fast leakage was calculated by using an Age-Yukawa kernel; the ages in D_2O-H_2O mixtures were those given by Tobias.[3] A detailed description of the criticality model is given in ref. 4.

Results of these computations are summarized in Fig. 8.3, where the uranium-to-thorium ratio for the specified maximum critical temperature is plotted vs the moderator composition; the numbers opposite the circled points are the approximate slurry concentrations at which the maximum critical temperature occurs.

In applying these results to physical systems, a small distance should be subtracted from the diameter of the bare sphere to account for the reflectivity of the containment vessel. The results may also be applied to unreflected cylinders by equating the bucklings of the cylinders and spheres. For infinite cylinders, the critical diameter is about three-fourths that of the sphere.

8.4 CRITICALITY CONDITIONS FOR SMALL SLURRY REACTORS OBTAINED WITH DIFFERENT CALCULATIONAL MODELS

In obtaining criticality information for reactors whose fuel concentration, size, and geometry are dependent upon criticality relations, a large number of parameter values are considered. Under such circumstances, preliminary results based on a relatively simple reactor model are obtained so as to reduce computing cost. The study here concerns criticality results obtained from two-group two-region, two-group four-region, and harmonics-type calculations; fast-fission effects were considered in some of the two-group calculations. The reactors considered were small, reflected slurry-core systems containing D_2O-H_2O moderator; ratios of U^{235} to thorium required for criticality were calculated with the various models.

Comparisons were first made between results from two-group two-region and harmonics calculations; no core tank was considered in these calculations. Two sets of two group - two region results were obtained, one considering resonance fissions in fuel and the other neglecting such fissions. No resonance fissions were considered in the harmonics calculations; however, this model considers an Age-Yukawa slowing-down kernel for fast neutrons, rather than the Yukawa kernel used in two-group calculations. In these computations, the moderator composition was varied between practically pure D_2O and 90% D_2O - 10% H_2O, and the thorium concentration was varied between 100 and 800 g/liter. The core diameters studied

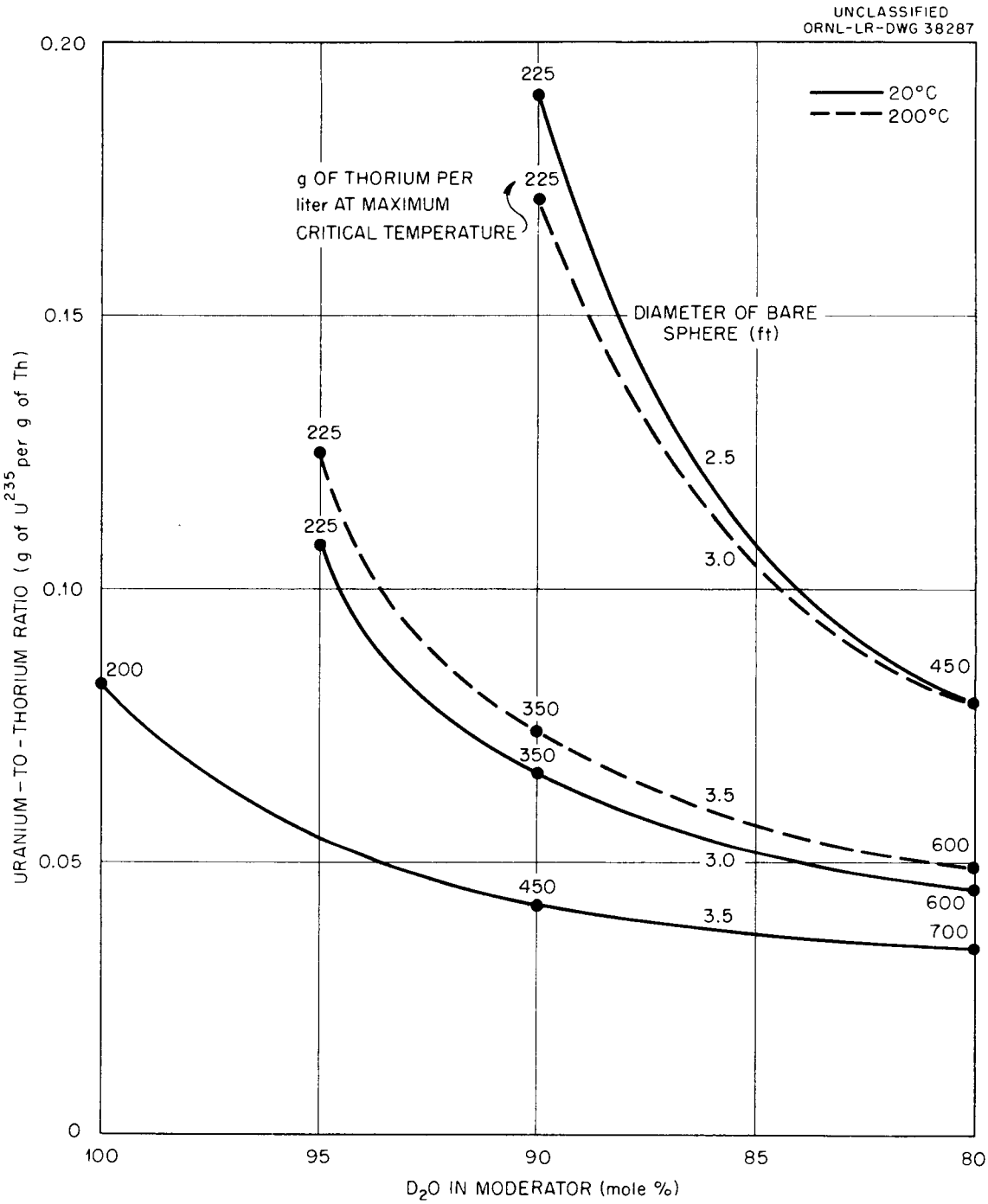

Fig. 8.3. Critical Uranium-to-Thorium Ratios for Optimum Slurry Concentrations in Unreflected Spheres at 20 and 200°C as a Function of Moderator Composition.

were 2 and $2\frac{1}{2}$ ft, the blanket diameter was 5 ft, and the temperatures were 20 and 200°C. Some results of these computations are shown in Fig. 8.4 (moderator 90% D_2O - 10% H_2O, temperature 200°C) and in Fig. 8.5 (99.8% D_2O, 200°C).

Sets of calculations were also made by using various two-group models in which a $\frac{1}{2}$-in.-thick stainless steel core tank and a 1-in.-thick steel pressure shell were considered. The reactor had a core diameter of $2\frac{1}{2}$ ft, a blanket thickness of 1 ft, and a temperature of 200°C; the moderator contained either 90 or 95% D_2O. In one calculation the two-region model was employed, and a "thin shell" approximation was used to obtain the nuclear effect of the core tank; an "extrapolation distance" correction was used to account for the pressure shell. Figure 8.6 gives the results for this case; curve a refers to results which do not consider resonance fissions, and curve b gives results in which resonance fissions were considered. A third set of calculations was made by using a two-group four-region model in which resonance fissions were neglected. The resulting critical-mass ratios are plotted as curve c in Fig. 8.6.

In the reactors studied in which no core tank was present, the strong coupling between the core and blanket is evidenced by the relative "flatness" of the critical-mass-ratio curves at the higher slurry concentrations. Neutrons produced in the core escape resonance capture in the thorium by slowing down in the blanket and returning to the core as thermal neutrons. The fact that the critical-mass ratios are controlled by resonance capture in the thorium and the fuel is obtained by comparing curves b and c in Figs. 8.4 and 8.5. In curve b, the reactor is critical on thermal fissions alone; in curve c resonance fissions contribute in an increasing amount to the chain reaction as the slurry concentration is increased.

The improvement in the calculation of fast-neutron leakage by use of the harmonics method does not significantly affect the shape of the criticality curves; however, the critical-mass ratio obtained with the harmonics method was significantly greater than that given by two-group calculations.

Introduction of a stainless steel core tank reduced the coupling between the core and blanket due to neutron absorptions in the tank; thus a higher critical-mass ratio was required to offset the increased leakage associated with the core. It is evident from comparison of curves a and c in Fig. 8.6 that the thin-shell approximation overestimates the absorptions in a $\frac{1}{2}$-in.-thick stainless steel shell.

8.5 MACHINE PROGRAMMING

Multigroup cross sections have been prepared for materials of interest in homogeneous reactors for use in GNU (IBM-704 multigroup program) and CORNPONE (Oracle multigroup program); 34 energy groups were considered. The structure consists of 32 "fast" groups of fixed energy width, one epithermal group from 0.60 ev down to the 1/E cutoff energy (~5.5 kT), and one thermal group having a Maxwell-Boltzmann energy distribution.

A program was written for the IBM-704 to calculate the uncollided flux and the once-collided flux in a reactor, given an initial source distribution. The program will handle one to ten energy groups, and up to forty space points. The reactor may have one or two regions, and the source may be discontinuous at the core wall in the two-region case.

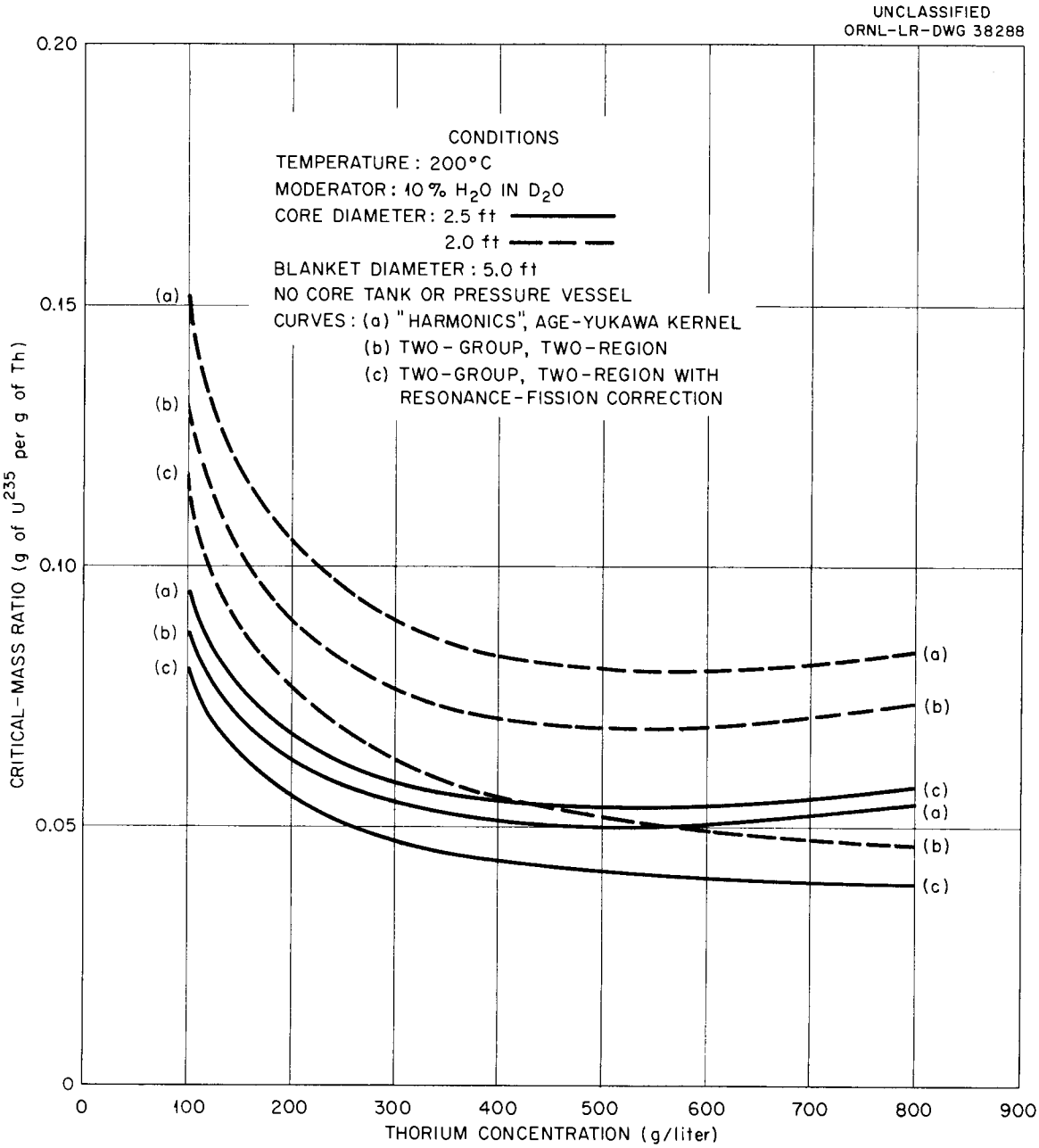

Fig. 8.4. Critical Uranium-to-Thorium Ratios in Small Reflected Slurry-Core Reactors, Calculated by Different Criticality Models; Moderator is 90% D_2O–10% H_2O.

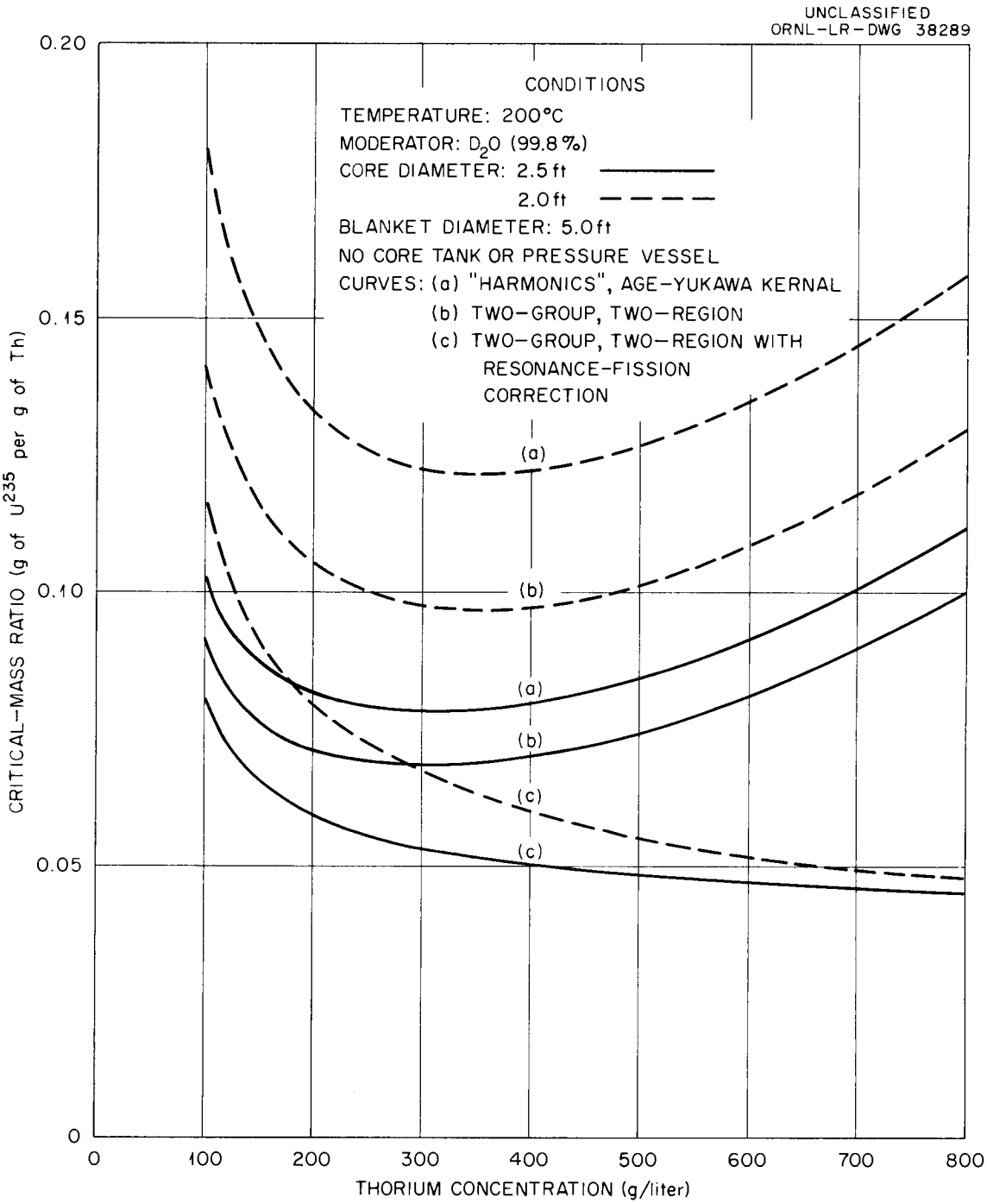

Fig. 8.5. Critical Uranium-to-Thorium Ratios in Small Reflected Slurry-Core Reactors, Calculated by Different Criticality Models; Moderator is 99.8% D_2O.

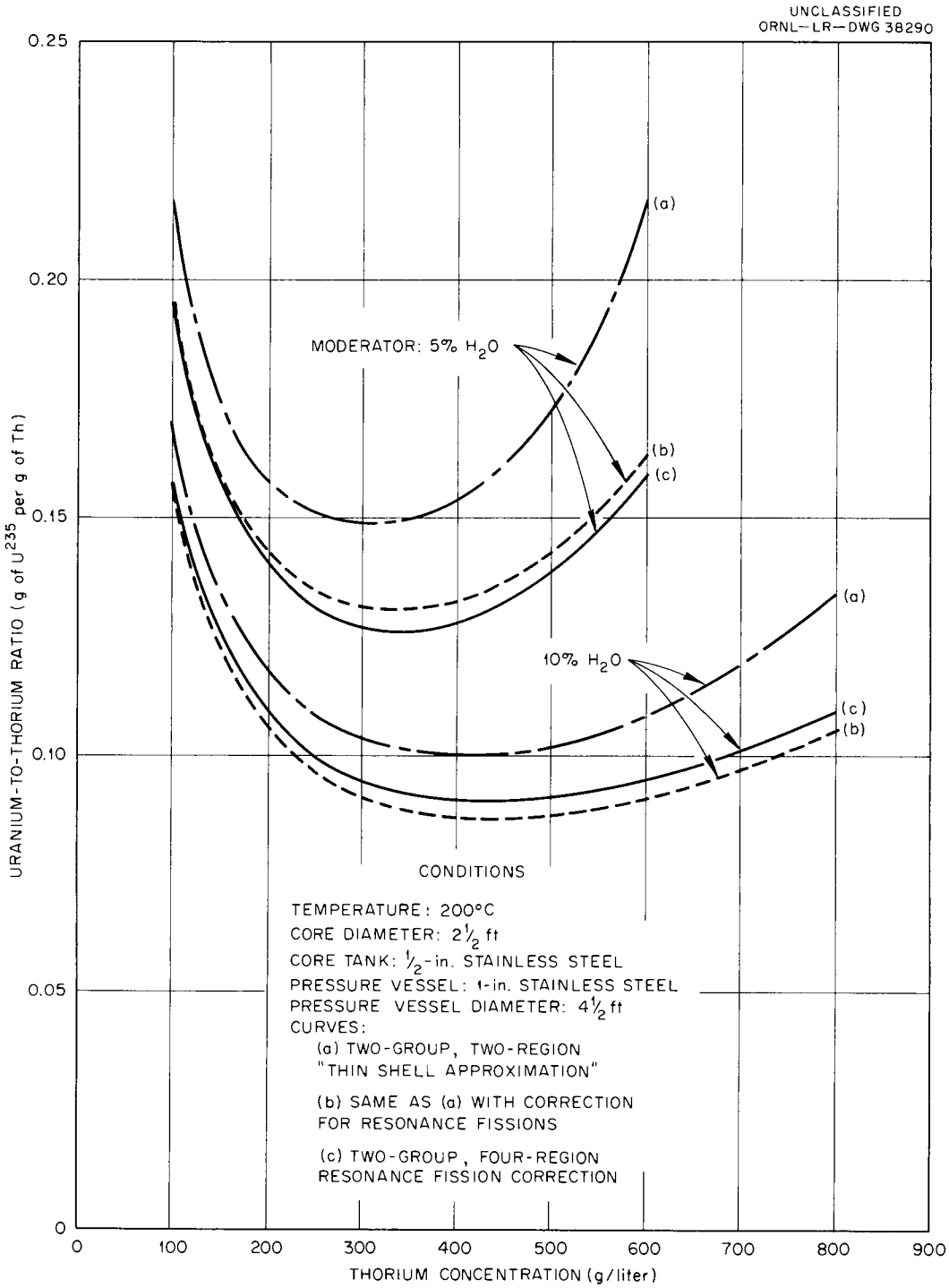

Fig. 8.6. Comparison of Results Obtained with Various Two-Group Diffusion Models, for a Reflected Slurry-Core Reactor with a Core Tank.

8.6 SLURRY RESUSPENSION AND DROPOUT STUDIES

Several tests in the last several years have shown that fluid velocities between 2 and 8 fps are required to maintain ThO_2 in suspension over a wide range of operating conditions;[5-7] the range of conditions covered temperatures from 30 to 280°C, average particle sizes from 1 to 20 microns, concentrations from 400 to 1500 g of Th per kg of H_2O, and pipe diameters from 3/4 to 3 in. A program was initiated[8] to determine the relationship between these variables in order to be able to accurately determine thoria dropout velocities.

The problem of slurry dropout may be further broken down into (1) the conditions under which spacial concentration gradients occur in flowing streams and (2) the maximum concentration of solids that can be transported at any given mean flow rate.

In an attempt to study possible concentration gradients, eight evenly spaced sampling stations were installed around the periphery of 2- and 4-in. pipes in the resuspension-velocity loops.[8] Samples were withdrawn from these flush-mounted sampling ports; the sample concentration appeared to be independent of sampling flow rate for the flow rates studied. For mean stream velocities of 1.1 and 2 times the dropout velocity, there was less than 5% difference in concentration between samples taken at the top and bottom of the pipes. This result is in accord with theoretical predictions[9,10] based on considerations of the rate of mass transfer downward by the action of gravity and the rate of transfer in the vertical direction due to turbulent mixing.

Preliminary results of load-carrying-capacity studies indicate two regions of flow. In the first region the suspension is apparently sufficiently concentrated to be in the compaction zone, and hence has an extremely slow settling rate. The second region is observed with more dilute suspensions which are in the hindered-settling region and settle about 10 to 100 times faster than slurries which are in compaction.

Data taken over a wide concentration range are shown in Fig. 8.7. The results assume that for slurries in compaction, all the material in the pipe is transported uniformly once turbulent flow is achieved. Using the Bingham-plastic model to fit the laminar-flow shear diagram, the onset of turbulence may be estimated from the relation

$$\frac{DV_c\rho}{\mu_e} = \frac{DV_c\,\rho}{\eta\left[1 + \dfrac{g_c\,D\,\tau_y}{6\,\eta\,V_c}\right]} \approx 2100\,, \qquad (1)$$

where, for these dropout studies,

V_c = minimum velocity at which all material in the pipe is moving, fps,

D = tube diameter, ft,

ρ = slurry density, lb/ft^3

η = coefficient of rigidity, lb/(ft)(sec),

τ_y = yield stress, lb/ft^2,

$g_c = \dfrac{\text{lb mass}}{\text{lb force}}\,\dfrac{\text{ft}}{(\text{sec})^2}$.

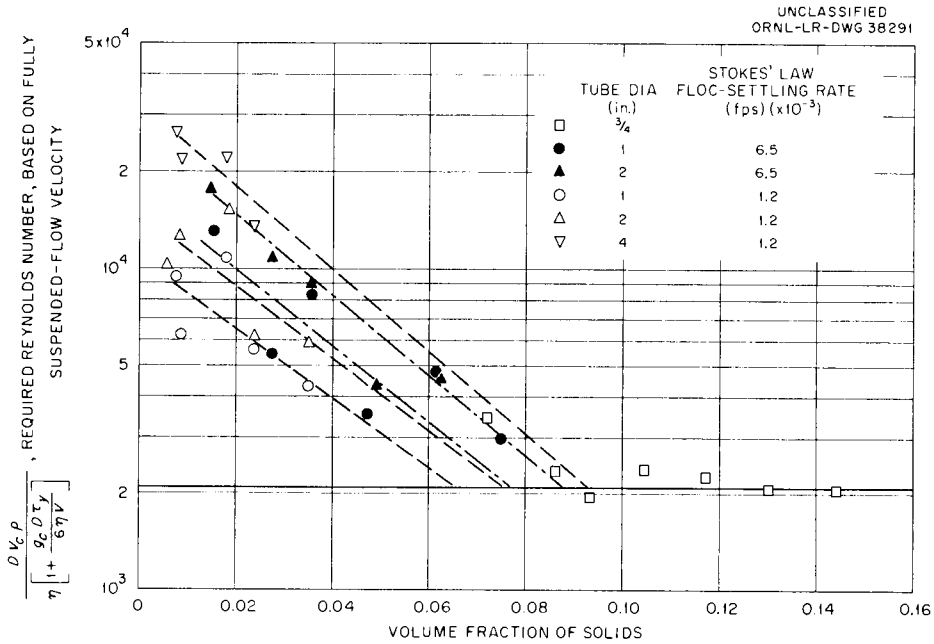

Fig. 8.7. Effect of Volume Fractian Solids on Effective Reynolds Number Required to Maintain Thoria in Suspension.

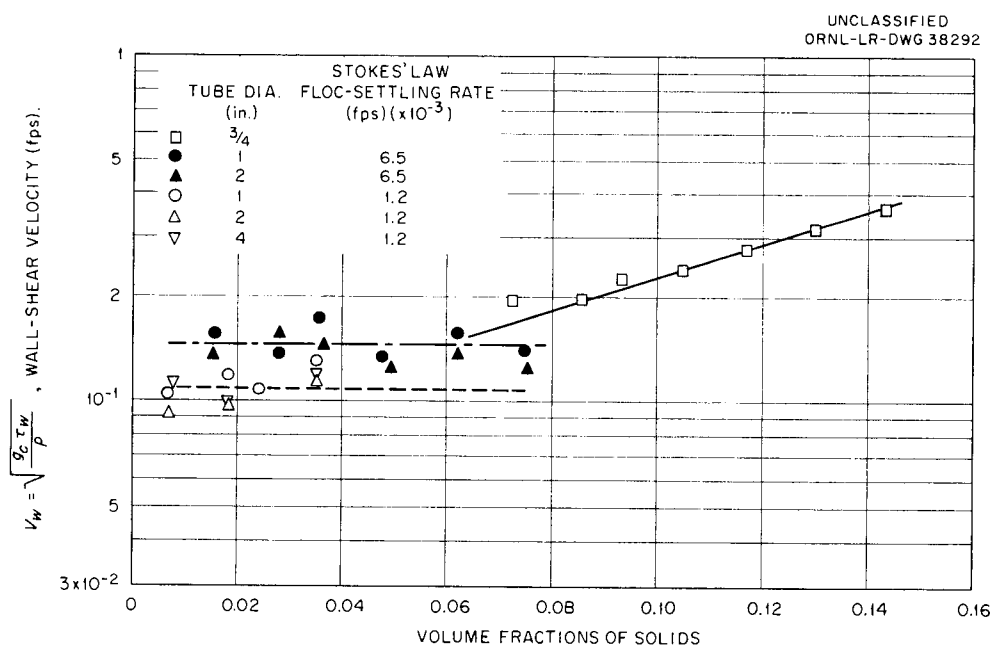

Fig. 8.8. Effect of Volume Fraction Solids on Wall-Shear Velocity Required to Maintain Solids in Suspension.

Figure 8.7 gives the experimentally determined relation between $DV_c\rho/\mu_e$ as a function of volume fraction solids. At low concentrations there appears to be a tube-diameter effect; however, the value of $DV_c\rho/\mu_e$ approaches 2100 at the higher concentrations. In Fig. 8.8 the data are shown in terms of the wall-shear velocity as a function of volume fraction solids (the wall-shear velocity is defined as $\sqrt{\tau_w g_c/\rho}$, where τ_w is the shear stress at the wall. The wall-shear velocity has been found to be roughly proportional to the turbulent-velocity fluctuations in the radial direction).[11] Plotted in this manner, the required wall-shear rate associated with dilute slurries appears to be a function of the floc settling rate.

8.7 THORIA CAKING STUDIES

8.7.1 Caking Tendency of Slurries

One measure of slurry caking tendency is the value of the CRI (cake re-suspension index); slurries which have a high CRI value tend to cake more readily than those having a low value.[12] Normally, slurries made fom thoria which has been digested for less than an hour during preparation will have high CRI values. To obtain additional data, two runs were made in the 30-gpm loop with thoria prepared by oxalate precipitation at 70°C followed by 1 hr of digestion before filtration. The thoria used in one run was calcined at 800°C for 2 hr; that in the other run was calcined at 800°C for 4 hr. The CRI of the 2-hr-fired batch was 6; that of the 4-hr-fired batch was 4.

Circulation was at 275°C and a concentration of about 450 g of Th per kg of H_2O. The two slurries exhibited similar caking behavior; a thin oxide film formed in the 5-fps section of the multidiameter sample barrel, but did not form in the sections where the velocities were 20 and 10 fps, nor in the pump impeller. Small spheres formed within about 2 hr of the start of circulation, but they did not appear to grow during the remainder of the run (~100 hr for each run).

8.7.2 Influence of Chromate Ion on Cake Formation

Small quantities of surface-active agents such as $NaAlO_2$, MoO_3, and UO_3 appear to inhibit slurry cake formation.[13] Since chromate ions are normally produced when oxygenated slurry is circulated in a stainless steel system, a test was made of their influence on cake formation. CrO_3 equivalent to 350 ppm (based on ThO_2) was added to thoria from batch LO-20 (slurry made from this thoria usually results in cake and sphere formation), and the slurry was circulated in the 30-gpm loop at a concentration averaging 460 g of Th per kg of H_2O. Cake formation did not occur and spheres did not develop.

In another run, thoria spheres produced in the 200A loop were circulated in the presence of CrO_3; the CrO_3 concentration was 500 ppm based on ThO_2. Although cakes formed, the quantity of ThO_2 deposited was less than in two runs identical to the above except that chromate was not added.

8.7.3 Removal of Thoria Cake Deposits by Erosive Action

The removal of thoria cakes deposited within reactor-type systems by the usual mechanical methods involves considerable time and effort; a preferable method would be the circulation of a noncaking slurry which would remove thoria deposits by erosive action. As a test of this method, a caking slurry was

circulated in the 30-gpm loop until cakes were deposited in the impeller and in the 5-, 10-, and 20-fps sections of the sample barrel; then a noncaking slurry (1600°C-calcined thoria) was circulated for 23.3 hr. Subsequent examination disclosed that the amount of cake in the impeller vanes had been significantly reduced, about 75% of the cake in the impeller weep holes had been removed, and film deposits in the 10- and 20-fps sections of the sample barrel were entirely removed. In the 5-fps section most of the old film remained; deposits of 1600°C-fired thoria appeared to have been "brushed on" over part of the original film.

REFERENCES

1. H. C. Claiborne, T. B. Fowler, Heat Generation Rate in Core Tank of HRE-3, ORNL CF-57-12-45 (Dec. 12, 1957).

2. Private communication, to M. Tobias from Robert T. Morgan, April 1959.

3. M. Tobias, HRP Quar. Prog. Rep. Oct. 31, 1958, ORNL-2654, pp 66-67.

4. B. E. Prince and M. P. Lietzke, Survey of the Static Nuclear Characteristics of Small One-Region Slurry Reactors: Part III, ORNL CF-58-12-15 (Dec. 8, 1958).

5. J. D. Perrett, HRP Quar. Prog. Rep. Oct. 31, 1955, ORNL-2004, p 71.

6. R. B. Korsmeyer et al., HRP Quar. Prog. Rep. Oct. 31, 1958, ORNL-2654, p 93.

7. E. L. Compere et al., HRP Quar. Prog. Rep. Jan. 31, 1959, ORNL-2696, pp 105, 110.

8. D. G. Thomas, Atmospheric Pressure System for Determining Resuspension Velocity of Thorium Oxide Slurries in Round Horizontal Pipes, ORNL CF-56-10-136 (Oct. 10, 1956); see also ORNL-2331, pp 64-67.

9. V. A. Vanoni, "Transportation of Suspended Sediment by Water," Trans. Am. Soc. Civil Eng. 111, p 67 (1946).

10. A. W. Marris, "Fluid Turbulence and Suspended Sediment," Canadian J. Tech., 33, pp 470-493 (1955).

11. John Laufer, The Structure of Turbulence in Fully Developed Pipe Flow, NACA Report 1174 (1954).

12. C. S. Morgan, Status Report on ThO_2 Caking Studies, ORNL CF-57-9-102 (Sept. 26, 1957).

13. R. B. Korsmeyer et al., HRP Quar. Prog. Rep. April 30 and July 31, 1958, ORNL-2561, p 109.

9. DESIGN OF CIRCULATING-SLURRY CRITICAL SYSTEM

J. R. McWherter
R. B. Korsmeyer
R. B. Schappel
B. E. Prince
T. B. Fowler

A preliminary design of a 100-kw slurry-core critical system was completed. The flowsheet is shown in Fig. 9.1. The system is designed for operation at 200°C with slurry containing about 500 g of ThO_2 per liter and a U^{235}-to-Th ratio of about 0.08 in a mixture of about 80% D_2O - 20% H_2O. A blanket of water with the same isotopic concentration is required for criticality at any temperature from room temperature to 200°C, and advantage is taken of this fact to provide for a positive shutdown. With a mixed thoria-fuel concentration of 400 to 500 g/liter the critical temperature is a maximum--either an increase or a decrease in concentration results in a lowering of the critical temperature. It had been proposed that such an experimental system be built and operated to aid in developing techniques for handling radioactive slurry, to test the behavior of slurries and suspended recombination catalysts in a fissioning system, and to study control of the nuclear reactivity in slurry-fueled reactors.

The proposed layout in the reactor pit in Building 7503 is shown in Fig. 9.2. Some modifications would be required for the building to provide satisfactory housing for the reactor experiment.

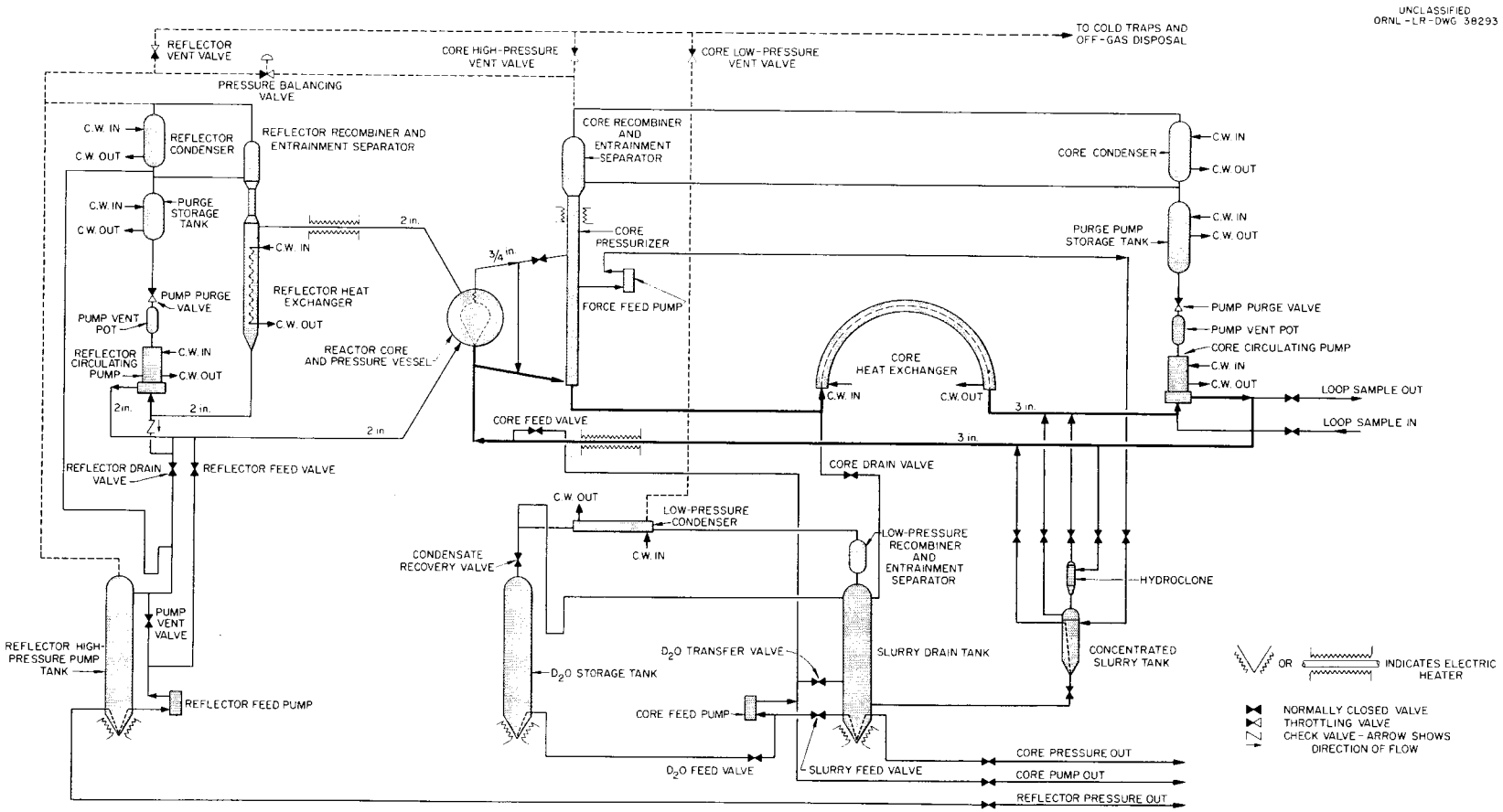

Fig. 9.1. Conceptual Flowsheet of a Circulating-Slurry Critical System.

UNCLASSIFIED
ORNL-LR-DWG 38294

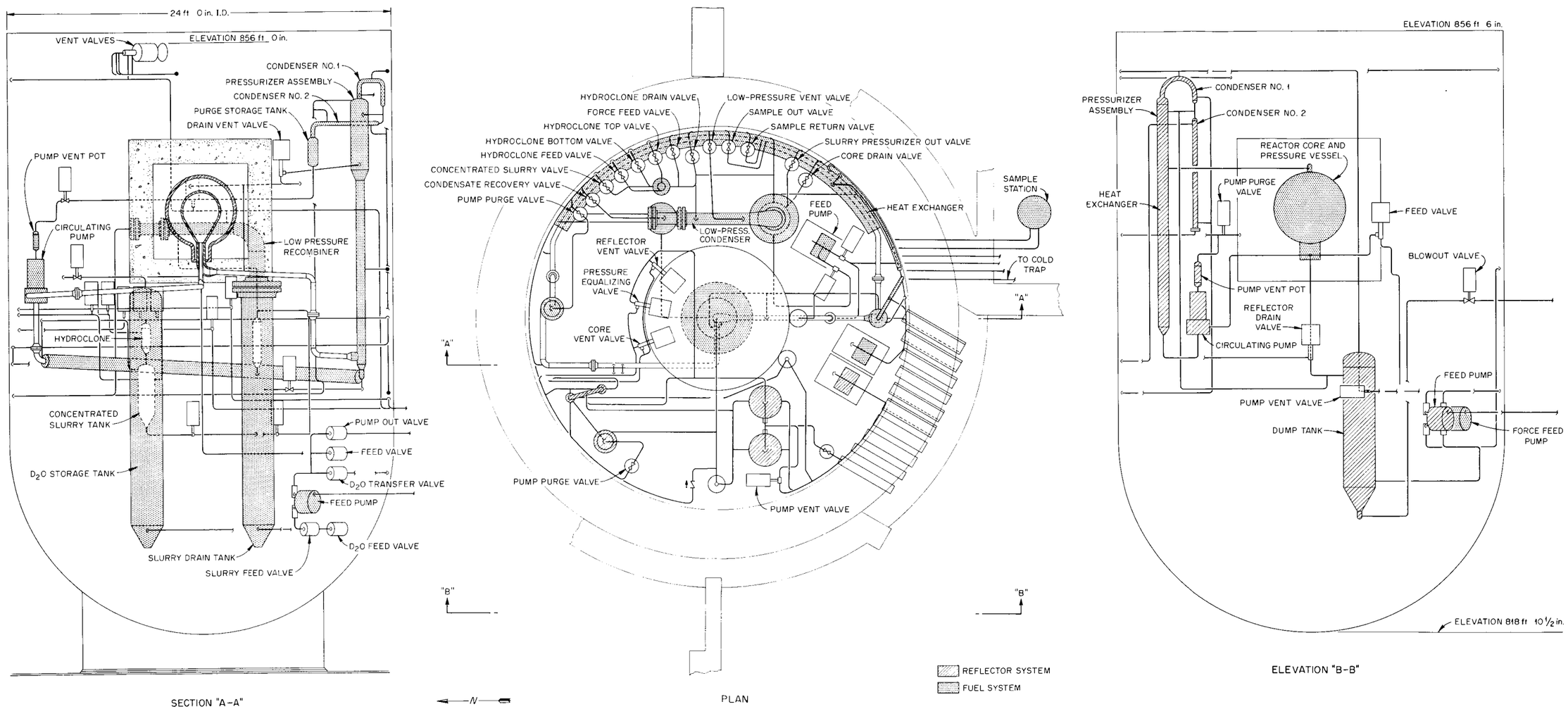

Fig. 9.2. Conceptual Layout of a Circulating-Slurry Critical System.

Part III

ENGINEERING DEVELOPMENT

R. N. Lyon

10. DEVELOPMENT OF FUEL- AND SLURRY-SYSTEM COMPONENTS

I. Spiewak

T. G. Chapman
D. M. Eissenberg
C. H. Gabbard
B. A. Hannaford
E. C. Hise
C. G. Lawson
J. C. Moyers
I. K. Namba
H. R. Payne
H. C. Roller
R. P. Wichner

10.1 HIGH-PRESSURE RECOMBINER LOOP

The natural-circulation recombiner operated routinely for 1500 hr at 1500 psi and an average stoichiometric-gas input of 0.60 scfm.

10.2 CENTRIFUGAL PUMPS

10.2.1 20-cfm Allis-Chalmers Blower

The 170°C, 1400-psi run of the 20-cfm canned-motor blower was terminated after 7300 hr of trouble-free circulation of a steam-nitrogen mixture. The loop heater capacity was then increased to 18.5 kw in order to permit operation at higher temperatures; the highest temperature achievable with the new heaters was only 225°C. The major heat loss is the result of steam condensing at the interface between the vapor and the cold water in the rotor cavity. Heat losses to the motor cooling water were 8 and 16 kw at 170 and 225°C, respectively.

10.2.2 Reliance 6000-gpm Pump

It was decided to terminate the Reliance 6000-gpm pump contract, because of an expected large increase in price of the prototype pump.

The insulation-test stator being irradiated in a Co^{60} source has received approximately 3.7×10^9 rad to date. Recent measurements indicate that, at approximately 2000 v, the insulation resistance has begun to decrease. Gas generation as a result of insulation breakdown was approximately 0.37 scc per cubic centimeter of insulating resin; analysis of a gas sample showed much of the production to be H_2 and CH_4.

10.2.3 300A Slurry Pump and Loop

The 300A slurry pump has operated for approximately 2800 hr at 280°C and 1500 psi since the pump closure was seal-welded. The average circulating slurry concentration has been approximately 460 g of Th per kg of H_2O during the run. Difficulty has been experienced in maintaining the desired circulating concentration, however, since there is a tendency for thoria to collect in the lower

end of the pressurizer. This material could be recovered temporarily by vibrating the pressurizer support, but an attempt to correct the situation permanently by increasing the bypass flow through the bottom of the pressurizer was unsuccessful.

10.2.4 200Z Slurry Pump and Loop

The 200Z pump-motor is undergoing repairs, following a short circuit between phases and to ground. The bypass line between the main loop and the pressurizer was redesigned to incorporate an air-operated, bellows-sealed Hammer-Dahl control valve with Zircaloy-2 trim.

10.2.5 Test Program for Slurry-Pump Bearings

The Franklin Institute has acquired the aluminum oxide test-bearing parts, and testing is now scheduled to start early in May.

The aluminum oxide bearings mounted mechanically in the 300A pump have operated satisfactorily for 2800 hr to date. Bearings flame-plated with aluminum oxide were purchased and will be installed in the pump at the end of the present run. Completion of the solid-shoe thrust bearing was delayed by part spoilage during annealing.

10.3 FEED PUMPS

10.3.1 Oxygen Compressors

The Pressure Products Industries single-stage diaphragm compressor with the Scott & Williams P1 drive unit has been in use for 4240 hr of HRT-mockup operating time. The diaphragm head, in intermittent service, operated for 1760 hr over this period. After 850 hr of operation a diaphragm failed at the rubber O-ring seal and was replaced. There was no evidence of damage to the operating portion of the diaphragm. The diaphragm of a reactor compressor would be seal-welded; the head would not contain an O-ring groove. The P1 drive unit suffered a bearing failure, which was repaired.

The Pressure Products Industries three-stage contaminated-service oxygen compressor has been placed on test compressing approximately 3 scfm of atmospheric air to 2500 psi. The diaphragm-head designs of the compressor are summarized in Table 10.1. After 49 hr, the third-stage diaphragm (0.016 in. thick, type 304 stainless steel, 106,000- to 127,000-psi yield strength) failed,

Table 10.1. Diaphragm Heads of Three-Stage Compressor

Stage No.	Contour Dia. (in.)	Stroke Volume ($in.^3$)	Discharge Pressure (psi)	Manufacturer's Calculated Stress in 0.016-in.-Thick Diaphragm (psi)
1	16.5	40.4	75	31,686
2	9.5	7.37	400	36,891
3	6.5	1.68	2500	27,815

at a small dent apparently caused by a metal filing. It was replaced with a 0.019-in.-thick, annealed, type 347 stainless steel diaphragm. After 200 hr, the second-stage suction check valve occasionally stuck for one to several cycles, permitting the first-stage pressure to rise 25 psi or more and creating a loud noise. The valve spring loading was increased, which seemed to eliminate the trouble. A regular check of the water-drive plunger-packing leak rate is being made. It is quite variable, ranging from 2 drops/min to 600 cc/min and has required the installation of a constant-supply tank for the drive-water makeup system. Only the third-stage packing gland has required tightening, and that only once. At 240 hr the third stage stopped operating, due to a failure of the water makeup valve. This difficulty is being corrected.

10.3.2 Increased-Capacity Solution Pumps

The double-diaphragm 10-3/4-in. head and the single-diaphragm 12-in. head have continued in operation for 7791 and 3169 hr, respectively, at an average of 60 strokes/min. They have been tested up to 80 strokes/min and 2.9 and 2.6 gpm, respectively.

The test of single-stage turbine pump is being discontinued, since there is no immediate need for solution feed pumps in the range above 10 gpm. A 2000-psi reactor pump would require eight or more stages and a canned motor; both features are outside of normal commercial practice.

The single-stage unit operated satisfactorily with Al_2O_3 wear rings and an Electrolyzed type 316 stainless steel impeller for 3740 hr, pumping 10 gpm of fuel solution to 300 psi. At that time the operation became noisy and the pump was dismantled. The outboard wear ring was found to be chipped at the suction inlet, the suction lip of the outboard flange was broken, and the impeller was damaged. A type 316 stainless steel impeller was installed, and the pump operated for an additional 200 hr before excessive seal leakage caused a shutdown.

10.3.3 Slurry Feed Pumps

The remote-leg and single-contour diaphragm pumps have operated for 4000 hr, pumping various 1600°C-fired thoria slurries of specific gravities of 1.5 to 2.1 to an average of 1500 psi. No diaphragm failures have occurred.

During the report period, LO-33 and -34 1600°C-fired thoria, which had been pumped in a high-temperature loop, was circulated in the feed-pump loop. Particle size degradation was again observed:

	Particle Size (μ)						
	<5	<3	<2	<1.5	<1.0	<0.7	<0.5
% as charged into feed-pump loop	99	90	69	45	18	4	-
% after 427 hr	100	100	95	82	40	13	3

The 5-gpm Vanton Flexiliner pump used to prime the slurry feed pumps suffered a liner failure after 2500 hr of operation and 25 hr in the LO 33-34 slurry. Two new liners and a new pump failed in rapid succession thereafter.

The feed-pump system was operated for 686 hr thereafter without a low-pressure circulating pump. The feed-pump output dropped steadily from 0.8 gpm to almost zero over a period of 450 hr. At that time as much slurry as possible was drained from the system, and it was operated for an hour with flush water. After the slurry was recharged to the system, the pump output was 0.65 gpm but dropped to zero over the next 236 hr. The loop was dismantled and examined. The horizontal 3/4-in. suction line contained a settled bed of thoria with the consistency of cream cheese; there was about a 1/4-in. passage at the top.

10.4 VALVE TRIM

10.4.1 Dump-Valve Trim for Solutions

Solution dump-valve testing has been discontinued.

10.4.2 Slurry Valves

A second set of Al_2O_3 feed-pump check-valve trim was removed for examination after 1135 hr of operation. The 1-in. balls had lost an average of 1.5 mil in diameter. The seats were worn uniformly from an original seating-cone width of 0.015 in. to an average of 0.065 in. They will be returned to service and operated to failure.

Beryllia seats were operated against Al_2O_3 balls in the slurry check-valve-material test loop for 1390 hr. Their performance indicated leakage after 200 hr, and at the end of the test period the seats were severely eroded.

10.4.3 Slurry Letdown Chokes

Both the 0.063-in.-ID and the 0.125-in.-ID tubes are still intact after 4990 and 3060 hr, respectively, of service.

10.5 HEAT EXCHANGER TEST FACILITY

Design of the heat exchanger test facility is 80% complete. The pressurizer will be a full-flow type with the flow entering just above the conical bottom in a downward-directed nozzle.

Manufacturing release has been given Griscom-Russell Company to proceed with fabrication of carbon-steel components of their test steam generator units.[1] The welding of tube-joint test blocks containing types 304 and 347 stainless steel tubes has been completed, and work on the tube bundles will be started.

As a result of manufacturing defects, lots of composite tubing of both type 347 - carbon steel and type 347 - Inconel combinations were rejected. Production procedures are being modified by the tube mill in an effort to correct the difficulties.

10.6 CORE HYDRODYNAMICS

10.6.1 Re-entrant Core Model

Probes for measuring water velocities to within 0.1 in. of the core wall were procured and applied to the 4-ft re-entrant spherical core model. Components included total-head Kiel probes and directional Wedge probes (manufactured by Aerotech Instrument Company) coupled to Taylor force-balance D/P cells of 2.5 and 25 in. of water range.

Calibrations in a stream flowing in a 3-in. pipe agreed with literature velocities to within 3%. Preliminary runs in the core model confirmed the existence of a high-velocity stream near the core wall. Measurements in progress are intended to fully define the velocity distribution of this stream as a function of position.

10.6.2 Slurry Core Vessel

Tests of the 30-in. slurry core vessel were begun at a nominal concentration of 500 g of Th per kg of H_2O. This model is a low-pressure facsimile of the 300-SM loop core (see Sec. 11.2). There is provision for wall heat transfer measurements and extensive sampling of the core interior.

Sampling techniques for ThO_2 slurries are being studied to determine to what extent apparent concentration variations found in the high-pressure slurry core may be attributed to sampling errors. These tests are being carried out in a pipeline, and results to date are shown in Fig. 10.1.

The maximum difference in the concentrations of samples taken by the four methods illustrated in Fig. 10.1 is only 4%, compared with the 25% difference found in the high-temperature core samples of the SM loop. However, sampling errors probably increase with temperature due to decreasing fluid viscosity and increasing settling rate. It is not yet possible to conclude whether gradients observed in the high-temperature core are due to sampling error.

10.7 PROPERTIES OF SLURRY SETTLED BEDS

The settled-bed concentrations of various thoria slurries were determined at room temperature and at 200°C in 6-mm quartz tubes. The results, summarized in Table 10.2, show that the ThO_2 concentration at 200°C is close to 60% of that at room temperature for all slurries investigated.

10.8 EFFECT OF ACCELERATION FORCE ON HINDERED-SETTLING RATE

The hindered-settling rate of a Th-U mixed oxide, which had previously been circulated in the 300-SM loop, was obtained as a function of acceleration forces imposed. For this purpose the low-speed centrifuge[2] was modified for use with a standard 10-ml graduate. The rate of settling was obtained for the linear portion of the settling curve.

For an initial concentration of 533 g of oxide per liter, the settling rate was proportional to the 0.5 power of the acceleration, in the range 1 to 20 g. The increase in settling rate is less than that predicted by Stokes' law.

UNCLASSIFIED
ORNL-LR-DWG 38295

PIPE SIZE: 3-in. SCHED-40

SAMPLER SIZE: 1/4-in.-OD TUBE, 0.083-in. WALL

AVERAGE SLURRY VELOCITY IN PIPE: 11.9 fps

GEOMETRY	NO. OF SAMPLES	SAMPLE WITHDRAWAL RATE (ml/sec) (APPROX. EQUAL TO VELOCITY IN SAMPLING TUBE IN FEET PER SECOND)	ThO_2 CONCENTRATION AND STANDARD DEVIATION (g OF ThO_2 PER kg OF H_2O)
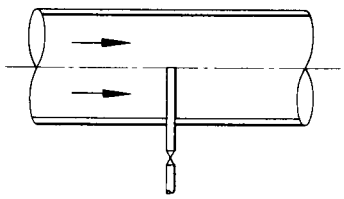	10	~ 10	603.53 ± 1.62
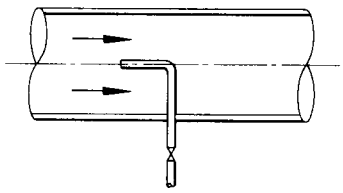	10	~ 10	618.95 ± 2.90
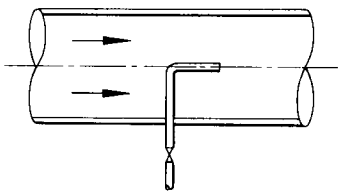	10	~ 10	607.69 ± 1.19
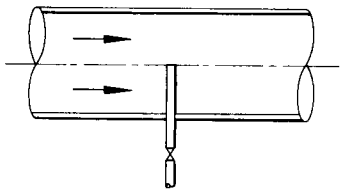	10	~ 3	594.36 ± 1.78

Fig. 10.1. Room-Temperature Slurry Sampling Test.

Table 10.2. Slurry Settled-Bed Concentrations

Slurry Designation	Average Particle Size (μ)	Initial Conc. (g of ThO_2 per liter) at 18°C	Settled-Bed Conc. (g of ThO_2 per liter) at 18°C	Settled-Bed Conc. (g of ThO_2 per liter) at 200°C	Ratio ($C_{200°}/C_{18°}$)
MO-1 unpumped	1.3	225	1035	700	0.68
MO-1 pumped	1.3	320	1525	870	0.57
DT-1 pumped	1.1	645	2610	1770	0.68
200A-14	1.8	660	2560	1590	0.62
DT-6 unpumped	2.5	390	1250	752	0.60
DT-6 pumped 100 hr	2.5	420	1440	920	0.64
DT-6 pumped 1500 hr	2.5	550	1860	1050	0.54

REFERENCES

1. I. Spiewak et al., HRP Quar. Prog. Rep. April 30 and July 31, 1958, ORNL-2561, p 105.

2. I. Spiewak et al., HRP Quar. Prog. Rep. April 30 and July 31, 1958, ORNL-2561, p 106.

11. DEVELOPMENT OF REACTOR SLURRY SYSTEMS

R. B. Korsmeyer F. N. Peebles

R. D. Bundy L. F. Parsly M. Richardson
D. G. Davis H. B. Piper A. N. Smith
R. J. Kedl R. Van Winkle

11.1 CIRCULATING-SLURRY BEHAVIOR

Three runs were completed in the 200A and B loops totaling 2957 hr of circulation of a mixed thoria-urania slurry proposed for use in an experimental slurry reactor. The purpose of these runs was to extend the information on handling characteristics, rheological properties, attack rate, heat transfer, settled-bed properties, and stability of this slurry at operating temperature, beyond that obtained in run 200A-18. The oxide for these runs was prepared in the manner previously described.[1]

11.1.1 200A Loop Operation

Run 19A was operated 965 hr at 100 to 225°C, 750 psi, with mixed thoria-urania at a concentration of 403 to 613 g of Th-U per kg of H_2O. Attack rates, slurry particle stability, system and pump performance data are summarized in Table 11.1. Prior to termination of the run the loop temperature was reduced in 25°C decrements to 100°C, and at these reduced temperatures the slurry level in the pressurizer, settling rate in the pressurizer, and rheologic properties of the slurry were measured. There was an increase in the pressurizer slurry-interface height of 8 in. in going from 200 to 100°C, and the slurry settling rate decreased from 1.1 to 0.25 cm/sec over the same temperature range. The rheologic constants were τ_y = 0.008 and 0.005 lbf/ft^2 (±0.005) and η = 0.9 and 1.0 centipoise (±0.1) at 150 and 100°C, respectively. Measurements of the rheologic properties at room temperature, which show the effect of pumping time, are summarized in Table 11.2.

The slurry was removed from the circulating stream by withdrawal at the lower sampling point with simultaneous addition of distilled water on the suction side of the pump. Approximately six loop volumes of slurry were withdrawn, which contained 27.15 kg of oxide. An additional 1.29 kg of oxide was recovered from the supernate siphoned off the settled slurry removed from the loop and from the pump thermal cavity. These amounts of oxide indicated a recovery of 102.5% of the initial load to the loop.

On dismantling the pump, the titanium impeller was found to be in good condition (weight loss of 1.8 g). Attack on the titanium scroll liner, in the form of gouge marks approximately 1/16 in. deep and inclined with respect to

Table 11.1. 200-gpm-Loop Run Summary

	Run No.		
	19A	1B	2B
Duration, hr	965	1030	962
Loop	200A	200B	200B
Circulating volume, liters	50	96	96
Slurry	MO-41	MO-41	MO-41
Temperature, °C	100-225	220	220
Th fraction in oxide (mean, all samples)	0.779 ± 0.018	0.793 ± 0.038	0.793 ± 0.029
U fraction in oxide (mean, all samples)	0.0605 ± 0.0033	0.0613 ± 0.0058	0.0626 ± 0.0019
Initial oxide book inventory, kg	34.6	23.4	50.4
Final oxide book inventory, kg	28.1	20.0	45.1
Total oxide recovered at shutdown	28.4	-----	45.1
Approx. fraction of inventory in circ.	0.82-0.78	0.89	0.95
Mean slurry concentration, g Th-U/kg H_2O	570	223	538-477 (390 for 60% of the run)
Comparative Attack Data			
Fe (Total accumulated, g	3.58	7	18
Fe (Equiv. generalized attack rate, mpy	0.045	0.06	0.16
Cr (Total accumulated, g	1.53	2	3.8
Cr (Equiv. generalized attack rate, mpy	0.111	0.06	0.14
Ni (Total accumulated, g	0.32	3	3.1
Ni (Equiv. generalized attack rate, mpy	0.046	0.13	0.20
Impeller weight loss, g	1.8 (Ti)	← 8 (SS) →	
1-1/8-in. SS orifice weight loss, g	2.7	-----	-----
1-1/2-in. SS orifice weight loss, g	0.18	← 0.416 →	
Initial mean particle size, μ	2.80	2.25-2.5	2.12
Final mean particle size, μ	2.38	2.25	2.2
Oxygen concentration, ppm	400-700	170-480	180-300

Table 11.2. Rheological Properties of Mixed-Oxide Slurry from Run 19A

Viscometer Run No.	Temp. (°C)	Yield Stress, τ_y (lbf/ft^2)	Coefficient of Rigidity, η (centipoises)	Mean Particle Size (μ)	Volume Fraction Solids $1 - \epsilon$	Pumping Time (hr)
			ρ = 1.50 g/cc			
39	22	0.048	1.62	2.80	0.056	Unpumped
40	24.5	0.021	1.25	2.20	0.056	293
46	26.5	0.019	1.23	2.13	0.056	462
42	22.5	0.016	1.33	2.21	0.056	528
48	27.0	0.019	1.31	2.11	0.056	624
			ρ = 1.42 g/cc			
44	22.3	0.005	1.25	2.38	0.048	965
			ρ = 1.35 g/cc			
38	22.0	0.027	1.32	2.80	0.040	Unpumped
41	25.0	0.006	1.15	2.20	0.040	293
47	26.3	0.005	1.10	2.13	0.040	462
43	22.7	0.007	1.15	2.21	0.040	528
49	27.0	0.008	1.12	2.11	0.040	624
45	22.5	0.005	1.15	2.38	0.040	965

the horizontal by about 30°, was visible in the straight sleeve-seal region. On the basis of the titanium content of the slurry it is estimated that the scroll liner lost about 3 g during the run.

11.1.2 200B-Loop Operation

Two 1000-hr runs were completed with two different concentrations of MO-41 oxide at 220°C in the 200B loop. In reality, these runs were one continuous run, in which run 1B was arbitrarily defined as being completed after 1030 hr of operation at a slurry concentration of 220 g of Th-U per kg of H_2O, when the addition of 30.4 kg of MO-41 oxide recovered from run 19A was begun. The addition increased the concentration to 540 g of Th-U per kg of H_2O and marked the beginning of run 2B.

In addition to the usual attack-rate and particle-degradation information obtained in previous loop runs, slurry heat transfer tests at high temperature and settled bed flow tests in a 14-ft high, 1-in. vertical pipe were performed.

Heat transfer data were obtained, by using the copper-disc heat meter described previously,[1] which indicated that MO-41 slurry heat transfer coefficients were not much different from those for water at the same temperature and volumetric flow rate for all slurry concentrations in the range of 0 to 540 g of Th-U per kg of H_2O. The heat meter also showed no indication of the formation of a thoria scale throughout nearly 2000 hr of operation with slurry. The slurry velocity was 15.4 fps through the 1-1/2-in.-dia flow passage of the copper disc, which was initially plated with a 0.002-in. thickness of nickel. At the completion of the run, its diameter had increased by 0.023 in.; the heat transfer surface was blackish in color and roughened to a somewhat sandpaper-like appearance, but there appeared to be no exceptional slurry attack (no grooves or striations were present). After the solids had been removed from the loop without cooling down, measurements of the over-all heat transfer coefficient with water appeared to be approximately identical with measurements made prior to charging the loop with slurry.

Advantage was taken of the provision of three parallel flow lines on 200B loop to study the behavior of a deep settled bed in a 14-ft vertical line. Solids were accumulated in the line from the flowing stream by closing the 1-in. valve at the bottom. According to the change in loop concentration, 10 kg of solids were lost from circulation when the valve was closed. With a 30-cc/min flow of purge water into the bellows region of the valve, and finally upward through the 1-in. vertical line, the settled bed, after standing for periods of 1 day and 4 days, respectively, flowed under the static pressure of its own head plus a dynamic pressure of 8 psi caused by flow through the parallel 1-1/2-in. and 2-in. lines. With no purge flow to the 1-in. line, pressure differences of 10 to 15 psi and 18 to 21 psi were required to cause the settled bed to flow after standing 2 and 11 days, respectively.

For the first 600 hr of operation in run 1B, uranium appeared to accumulate in the pressurizer at a linear rate, which implied a uranium dissolution rate of about 0.07 mg of U per hr per kg of Th+U. However, the uranium accumulation rate appeared to go to zero after reaching a concentration of ~100 ppm U in the pressurizer, for the rest of run 1B and for all of run 2B. Thus the slurry appeared to have a stable uranium content under loop operation conditions.

There was no significant degradation of particles; their mean diameter remained near 2.2 μ throughout runs 1B and 2B.

The stainless steel impeller lost 8 g; the 1-1/2-in.-dia orifice plate, which is located about 4 ft directly downstream of the pump discharge, lost 0.418 g and was gouged in a manner which indicated possible rotational flow in this section of pipe.

According to the volume and weight measurement method of estimating mass of solids in a slurry, more than 100% of the book inventory was recovered when the loop was drained and flushed. Yet, it is known that a few hundred grams still remained in the many crevices (between flanges, etc.) of the loop. During operation, less than 3 kg of the 50-kg charge of oxide was out of circulation, except when the 1-in. valve was closed.

The 2-in. Hancock valve began leaking at the bonnet during run 1B, and this leak grew progressively worse, until a leak rate of ~4 liters of water per day existed at the end of the run. There did not appear to be any thoria leakage.

The instrument lines and slurry traps to at least one d/p cell became plugged with slurry, resulting in false readings.

11.2 BLANKET SYSTEM DEVELOPMENT

11.2.1 300-SM High-Pressure-System Operation

Installation of the 30-in.-dia experimental pressure vessel[2] in the 300-SM blanket system was completed during the quarter. After a hydrostatic test at 1000 psi, the system was rinsed with water and cleaned chemically with trisodium phosphate and nitric acid solutions. A brief water run at 200°C was made to check out controls and instrumentation.

One slurry run consisting of 880 hr of slurry operation, designated run SM-6, was completed, and after shutting down the system to install additional sampling facilities, slurry run SM-7 was started. Both runs are flow tests at 500 psi of a proposed single-region slurry core vessel in which slurry is introduced at the bottom through a 2-in. inlet nozzle and flows from the vessel through an annulus concentric with the inlet nozzle. Approximately 5% of the flow leaves through a 3/4-in. bypass line at the top of the vessel. The slurry used in the tests was prepared from a thorium - 8% uranium mixed oxide. The initial charge concentration was near 530 g of Th-U per kg of H_2O; oxygen was added to a concentration of 350 ppm.

Slurry concentration within the vessel and the external piping was determined by sampling. Six sample stations were on the pressure vessel, as shown in Fig. 11.1; one was on the 3-in. pipe; one was on the 3/4-in. bypass line; and two were on the pressurizer (one was 17 in. above the slurry inlet and the other was approximately 17 in. below the liquid level). All sample lines were 0.250-in.-OD, 0.083-in.-ID tubing, with 0.10-in.-OD, 0.060-in.-ID capillary-tube chokes 15 ft long. Continuous gamma-transmission densitometers[3] were provided to monitor the slurry flowing in the main 3-in. pipe and in the 3/4-in. bypass line. The gamma-transmission path was normal to the 3-in. pipe and along a 6-in. offset length of the 3/4-in. pipe.

(a) Slurry Distribution Studies.--During run SM-6, slurry distribution within the pressure vessel and the piping system at 200 and 150°C was determined over a flow-rate range of 130 to 380 gpm at three concentration

UNCLASSIFIED
ORNL-LR-DWG 38296

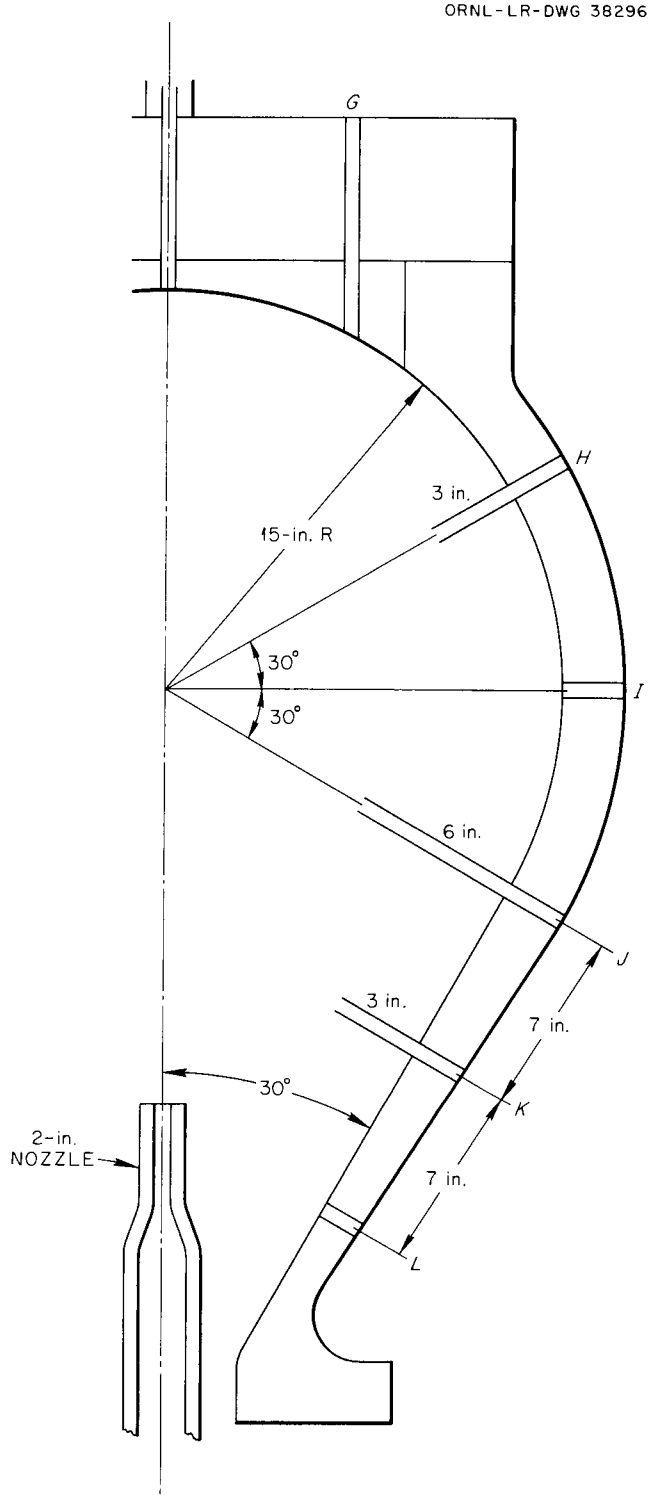

Fig. 11.1. Vessel Sample-Point Locations, Run SM-6.

levels: 530, 375, and 240 g of Th-U per kg of H_2O. At the lowest concentration, data were taken at 200°C only. Flow was controlled by regulating the frequency of the pump power supply. Samples were drawn after steady flow had been maintained at a specified test condition for at least 12 hr. In each sampling, four samples were withdrawn from the loop through each sample point, the first being discarded and the others analyzed for oxide content by specific-gravity determination. Approximately 1% of the loop inventory was removed in each sampling.

Figure 11.2 summarizes the test conditions during run SM-6. As indicated, the circulating loop concentrations were 93 to 96% of the "book" concentration at all conditions. A substantial part of the discrepancy can be accounted for by holdup in "dead" lines. There was a volume of approximately 2 liters in small lines connected to the bottom of the loop piping, and this volume, filled with settled slurry, accounted for 2 to 5 kg (1 to 2.5% of the initial charge). Holdup in the pressurizer is believed to have accounted for the remaining inventory variation.

Table 11.3 presents the ratio of local concentration to circulating concentration found at the six pressure-vessel sample points and the 3/4-in. bypass from the top of the vessel. Statistical analyses of these slurry distribution data consistently showed less than 1% probability that the observed differences could have resulted from the random errors of the sampling and analytical procedures.

Figure 11.3 shows typical concentration patterns within the vessel during run SM-6 and illustrates the effects of flow rate, slurry concentration, and temperature on the slurry distribution. The measured concentrations at the wall were approximately equal to the circulating loop concentration and were perhaps even slightly higher than the circulating concentration for the lowest sample point on the wall in the conical section. The concentrations observed from the three points in the interior of the vessel were lower than the circulating concentration and were consistently lowest for the 6-in. penetration into the vessel. For the regions of low concentration within the vessel, the concentration ratio tended to decrease with increasing flow rate and temperature, and to increase with concentration. The latter two effects were the result of the increased slurry settling rate at the higher temperature and lower concentrations.

The slurry distribution patterns observed in run SM-6 indicated the existence of a toroidal eddy between the inlet jet and the region near the wall. The centrifugal forces associated with such an eddy could cause the concentration gradient. While this theory was plausible, the data available did not exclude the possibility that the observed concentration gradient was the result of sample bias caused by the fluid and particle dynamics at the sampler-tube inlet. In an attempt to resolve these questions, run SM-6 was terminated for the installation of additional sampling facilities.

Since the low-pressure system was not ready and therefore no convenient means of unloading the slurry from the high-pressure loop was available, the solids were left in the loop during the shutdown. The solids were allowed to settle out, and the liquid level was reduced to well below the equator of the vessel sample lines. The new samplers were placed in existing sample bosses at and above the vessel equator.

Figure 11.4 shows the modified vessel sampler installations. Six additional samplers, designated "M" through "R", were added to the vessel. All

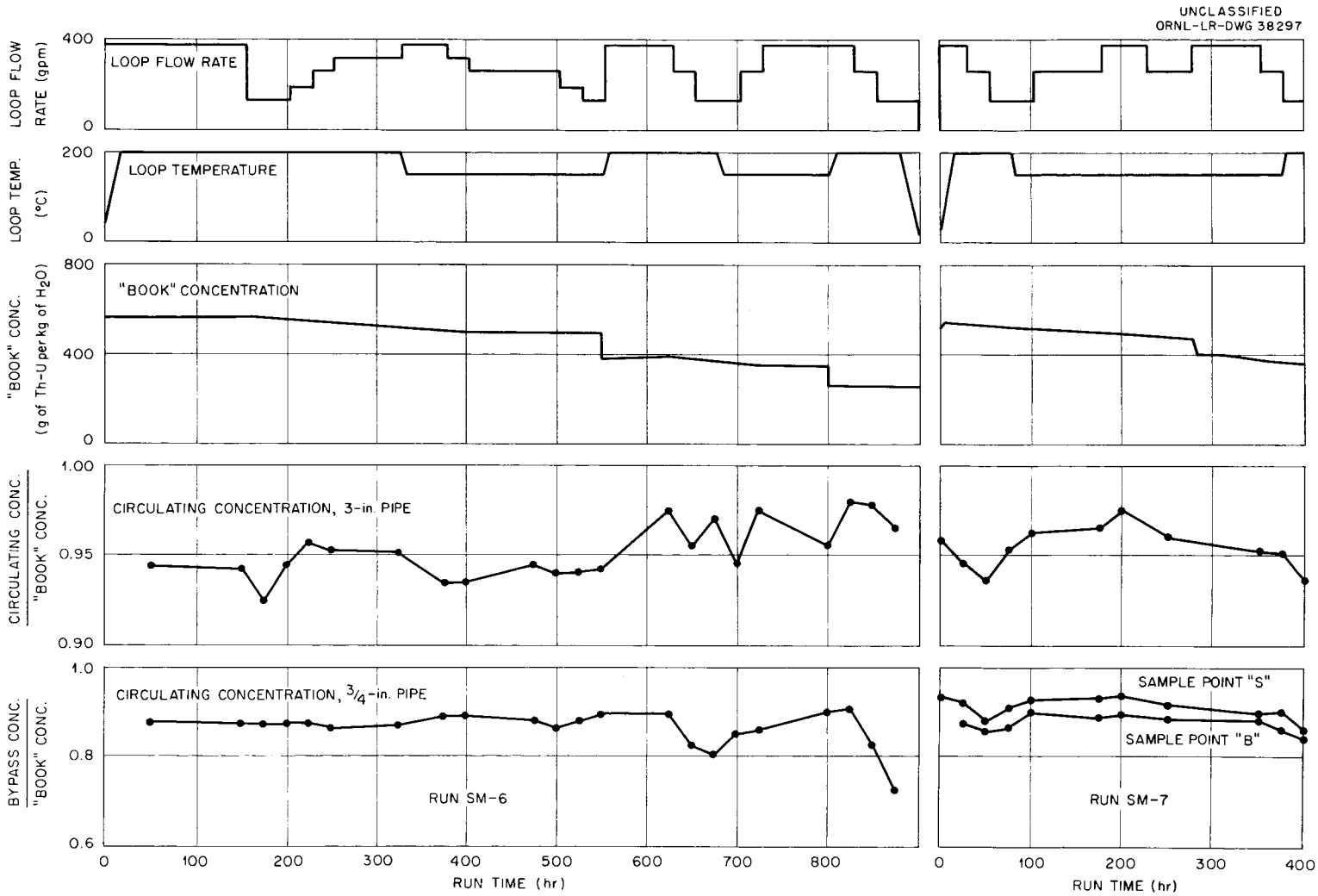

Fig. 11.2. 300-SM Operating Conditions for Single-Region-Vessel Flow Tests.

Table 11.3. Ratio of Local Concentration to Circulating Loop Concentration, Run SM-6

Flow rate, gpm	130			190	260			320	380		
Conc., g Th-U/kg H_2O	530	375	240	530	530	375	240	530	530	375	240
				150°C							
G*	1.000	0.978		0.987	0.999	0.973		0.999	0.994	0.960	
H	0.990	0.969		0.980	0.972	0.930		0.968	0.951	0.943	
I	0.990	0.980		0.995	0.996	0.954		0.996	1.010	0.995	
J	0.970	0.964		0.945	0.930	0.885		0.919	0.861	0.848	
K	0.994	0.971		0.961	0.951	0.916		0.945	0.908	0.880	
L	1.006	1.025		0.995	1.002	0.977		1.018	1.003	1.018	
B**	0.947	0.900		0.936	0.928	0.890		0.950	0.944	0.940	
				200°C							
G	0.988	0.960	0.930	0.996	1.004	0.951	0.965		1.008	1.009	0.978
H	0.995	0.962	0.892	0.991	0.971	0.930	0.891		0.955	0.910	0.901
I	0.989	0.985	0.925	0.994	0.993	0.990	0.971		0.995	1.007	1.012
J	0.981	0.925	0.850	0.949	0.924	0.864	0.789		0.911	0.837	0.735
K	0.990	0.950	0.901	0.968	0.991	0.899	0.840		0.910	0.890	0.793
L	1.039	1.069	1.170	1.003	1.000	1.035	1.048	1.000	1.003	1.020	1.012
B	0.936	0.831	0.751	0.996	0.908	0.866	0.847	0.914	0.934	0.918	0.927

*Letters refer to sample-point designation of Fig. 11.1.

**Sample point B is on the 3/4-in. bypass from the top of the vessel.

UNCLASSIFIED
ORNL-LR-DWG 38298

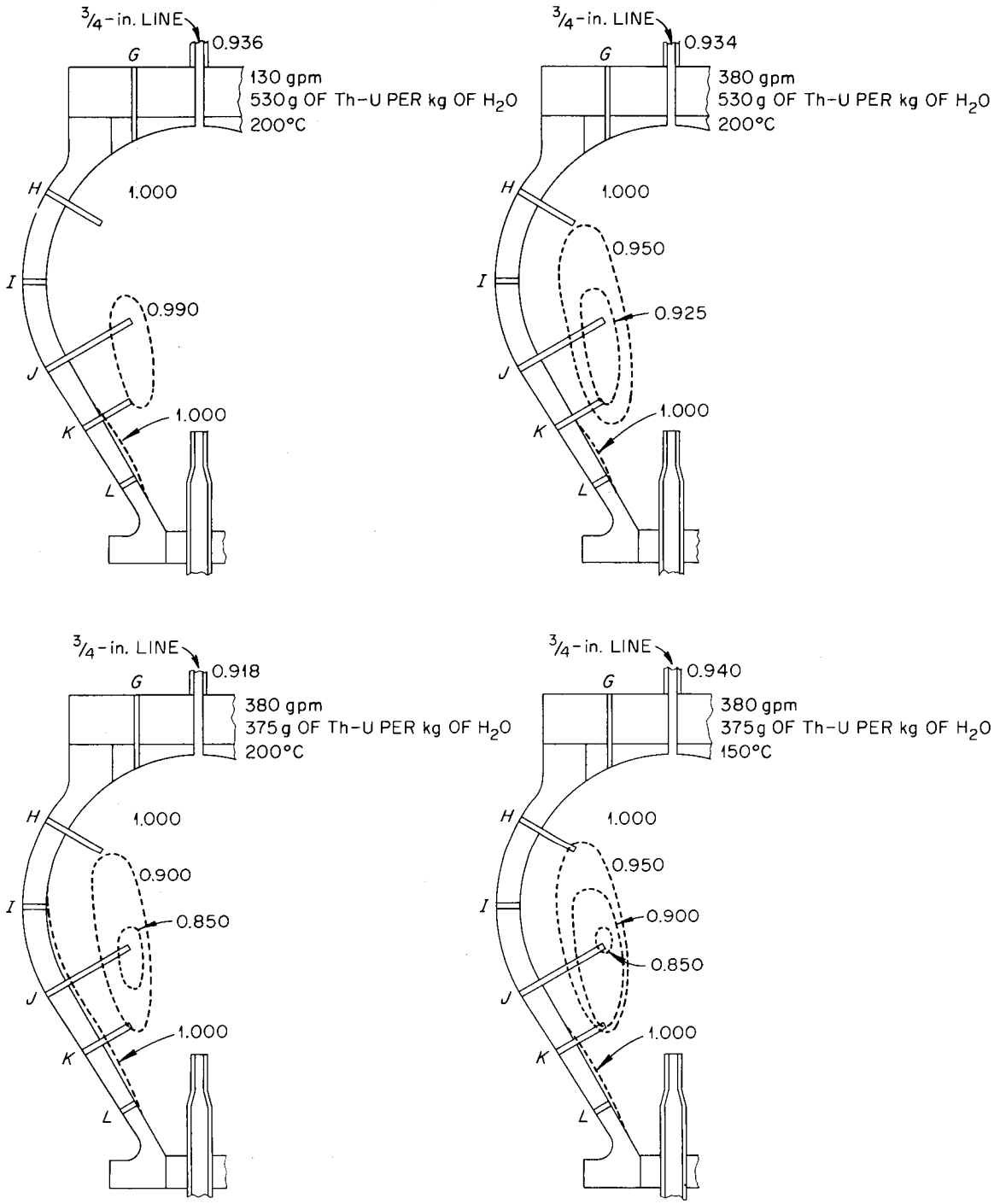

Fig. 11.3. Slurry Concentration Patterns, Run SM-6.

UNCLASSIFIED
ORNL-LR-DWG 38299

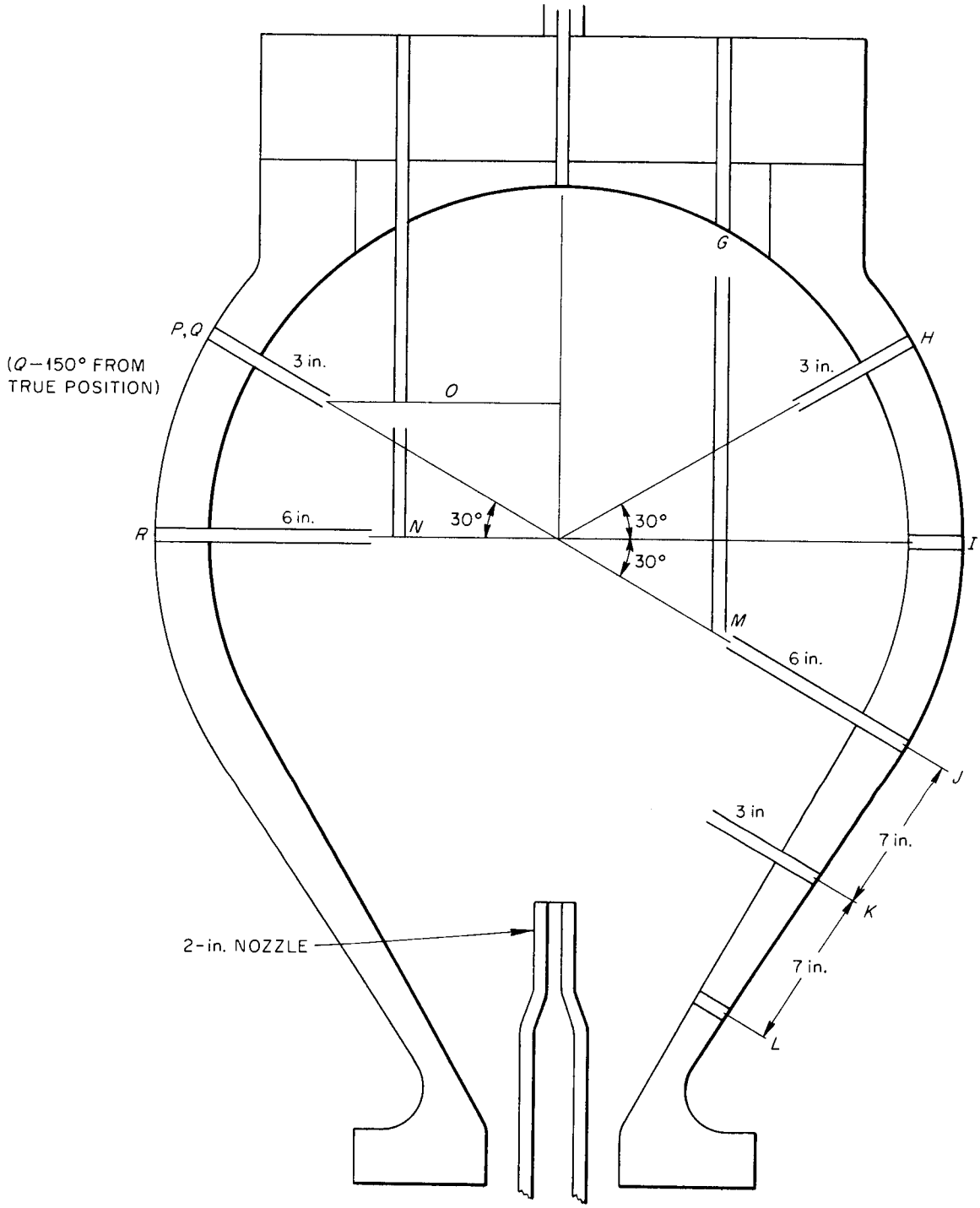

Fig. 11.4. Vessel Sample-Point Locations, Run SM-7.

the additional samplers except Q were 0.250-in.-OD, 0.083-in.-ID tubes with the end cut square and the outisde diameter reduced to 0.125-in. for a 1-in. length at the end. Sampler Q was installed to feed a continuous gamma densitometer, and since relatively high flow was desired to minimize slurry dropout, the sample tube projecting into the vessel was 0.250-in.-OD, 0.180-in.-ID. Outside the pressure vessel the line size was increased to 0.375-in.-OD, 0.250-in.-ID. An additional sampler, designated "S", was installed in a vertical run of the 3/4-in. bypass line. The sampler-tube end was 0.125-in.-OD, 0.083-in.-ID, cut off at 45° with the beveled side directed toward the flow and extended to the center line of the pipe.

After the additional samplers were installed, slurry distribution studies were continued and were designated as run SM-7. The system operating conditions to date are summarized in Fig. 11.2, along with those of the previous run. Values for the main-circulating-stream concentration continued to be 93 to 96% of the "book" concentration values. The concentration in the 3/4-in. bypass line also remained below that of the main circulating stream, with a somewhat higher concentration being indicated at point S than at point B. Because of the more favorable sampler geometry the data from S are considered more reliable.

The slurry distribution data for 530 and 375 g of Th-U per kg of H_2O at 150 and 200°C are summarized in Table 11.4, along with comparative values from run SM-6.

The samples from runs SM-6 and SM-7 taken from the same sample points for the same operating condition did not differ significantly. However, results from sample points M, N, and R relative to J, all of which sampled the low-concentration region in the interior of the vessel, indicated either that there was a marked radial concentration gradient as pictured in Fig. 11.5, or that sampler-tube orientation within the vessel biased the samples. There was evidence for azimuthal concentration symmetry within the vessel as shown by the results from sample points H and P. The concentration indicated by Q was consistently lower than that indicated by H, P, and O, which sampled approximately the same region, and the low results were probably the result of sampler geometry. Slurry flowed from Q to the continuous densitometer, and samples were withdrawn from a tee section in this line.

Conclusions from the two runs regarding slurry distribution are:

(a) The major fraction (0.93 to 0.96) of the slurry charged to the system was suspended and accounted for in the main circulating stream. Slurry holdup in the pressurizer accounted for the principal variation in the circulating concentration, and the amount held up varied with temperature, slurry concentration, and flow rate within the limits indicated.

(b) Slurry samples drawn from within the vessel indicated the possible existence of concentration gradients which were affected by temperature, slurry concentration, and flow rate. There was also evidence that sampler-tube orientation influenced the performance of the samplers. Further development of slurry sampling equipment will be required to determine whether a significant concentration gradient existed within the vessel at the test conditions.

(c) There was consistent evidence of slightly higher slurry concentrations on the conical wall of the vessel at all flow rates, which became more pronounced with decreasing flow rate.

Table 11.4. Ratio of Local Concentration to Circulating Loop Concentration, Run SM-7

Flow rate, gpm	150°C						200°C					
	130		260		380		130		260		380	
Conc., g Th-U/kg H_2O	530	375	530	375	530	375	530	375	530	375	530	375
H*	0.980	0.982	0.971	0.955	0.950	0.947	0.992	0.945	0.975	0.936	0.965	0.984
H (SM-6)	0.990	0.969	0.972	0.930	0.951	0.943	0.994	0.962	0.971	0.930	0.955	0.910
P	0.979	0.958	0.951	0.935	0.936	0.918	0.963	0.927	0.975	0.899	0.966	0.880
Q	0.899	0.933	0.929	0.914	0.899	0.900	0.936	0.899	0.936	0.869	0.955	0.862
O	0.970	0.956	0.950	0.921	0.938	0.920	0.963	0.919	0.947	0.901	0.975	0.885
J	0.982	0.982	0.928	0.912	0.884	0.854	0.972	0.936	0.896	0.852	0.892	0.798
J (SM-6)	0.970	0.964	0.930	0.885	0.861	0.848	0.981	0.925	0.924	0.864	0.910	0.837
M	0.982	0.965	0.952	0.939	0.944	0.916	0.969	0.936	0.974	0.905	0.970	0.889
R	0.972	0.954	0.948	0.932	0.926	0.900	0.972	0.921	0.950	0.879	0.927	0.865
N	0.967	0.963	0.952	0.944	0.944	0.911	0.963	0.921	0.958	0.901	0.966	0.905
G	0.982	0.982	0.984	0.984	0.982	0.986	0.992	0.960	0.997	0.978	0.998	0.980
G (SM-6)	1.000	0.978	0.999	0.973	0.994	0.960	0.988	0.960	1.004	0.951	1.008	1.009
I	0.982	0.982	0.987	0.986	0.995	0.994	0.982	0.954	1.000	0.984	1.009	0.987
I (SM-6)	0.990	0.980	0.996	0.954	1.010	0.995	0.989	0.985	0.993	0.990	0.995	1.007
L	1.011	1.051	0.991	1.018	1.002	1.005	1.018	1.084	1.009	1.015	1.024	1.018
L (SM-6)	1.020	1.025	1.002	0.997	1.003	1.018	1.039	1.069	1.000	1.035	1.003	1.020
K	0.988	0.984	0.946	0.921	0.920	0.880	0.965	0.949	0.922	0.905	0.920	0.860
K (SM-6)	0.994	0.971	0.952	0.916	0.908	0.880	0.990	0.950	0.991	0.899	0.910	0.890
B**	0.936	0.898	0.919	0.905	0.916	0.927	0.906	0.825	0.918	0.874	0.927	0.907
B (SM-6)	0.947	0.900	0.928	0.890	0.944	0.918	0.936	0.831	0.908	0.866	0.934	0.918
S**	0.962	0.921	0.958	0.946	0.955	0.940	0.954	0.883	0.941	0.918	0.988	0.916

*Letters refer to sample-point designations of Figs. 11.1 and 11.4.

**Sample points B and S are on the 3/4-in. bypass from the top of the vessel.

UNCLASSIFIED
ORNL-LR-DWG 38300

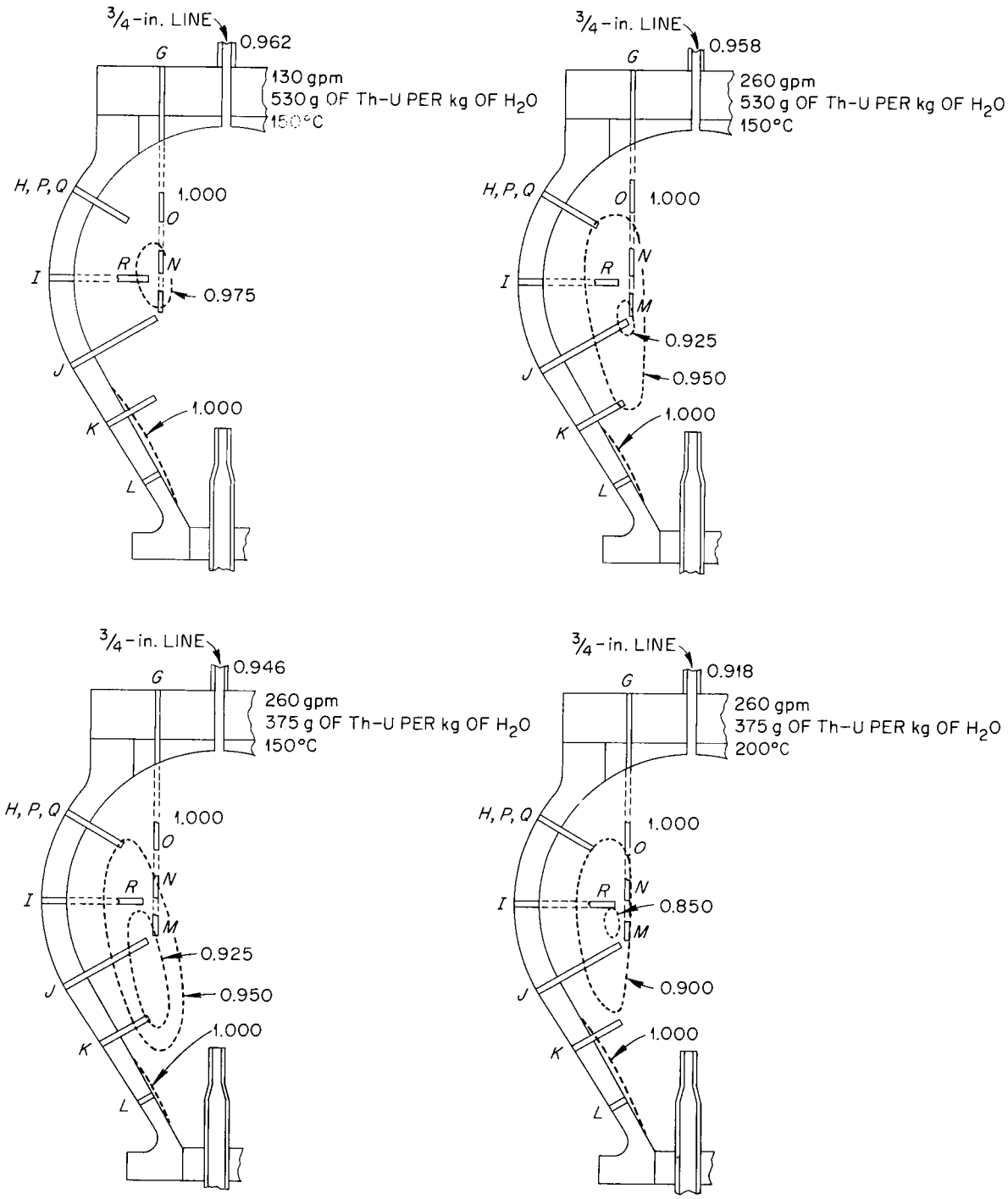

Fig. 11.5. Slurry Concentration Patterns, Run SM-7.

(b) System Performance and Slurry Behavior.--The continuous densitometers on the main 3-in. pipe and on the 3/4-in. bypass indicated steady concentrations within ±15 g of Th-U per kg of H_2O except during system upsets due to temperature changes and some flow-rate changes. Significant exchanges of solids between the pressurizer and the circulating stream were usually indicated by the densitometer on the 3-in. pipe. Other indicated changes in circulating density in the main piping and the 3/4-in. bypass were traced to the effect of sunlight heating the high impedance cables used to transmit the ionization-chamber signal to the densitometer readout instruments.

On two occasions, during run SM-6, the pump was shut off to observe the settled-bed concentration. In the first test, at 200°C, a maximum concentration of 1560 g of Th-U per kg of H_2O was reached in 20 min, but the concentration had not leveled off. In the second, at 150°C, the settled-bed concentration leveled off at 1550 g/kg after 50 min. While the second test was going on, the supernate from the pressurizer was displaced from the loop with demineralized water, and samples were taken at intervals to determine the chromium and uranium distribution. It was found that the concentration gradient was fairly close to the exponential distribution anticipated as a result of uniform convectional transport upward and diffusion downward. It was also found that the arithmetic mean concentration of samples drawn from the top and bottom of the pressurizer was within 10% of the true mean and thus could be used to estimate the holdup of soluble ions in the pressurizer.

While attempting to trace the cause of the unaccountable densitometer excursions, 176 std liters of oxygen were fed into the circulating stream through the loop sample point, at a rate of 5 std liters/min, for the purpose of generating a system disturbance. The first 132 liters dissolved immediately. The pressurizer level increased 4 in. as the final 44 liters were added; the rise was equal to 25.5 std liters of undissolved gas, which either dissolved or escaped to the pressurizer 30 min after oxygen feeding was stopped. The final oxygen concentration represented 80% of saturation at operation conditions. The power and flow instrumentation indicated no disturbances as a result of the addition, even though the addition point was 6 ft upstream of the pump suction.

The corrosion rate during run SM-6 was 0.109 mpy based on iron accumulation on the slurry, and 0.085 mpy based on chromium accumulation in the pressurizer. Uranium transfer from the loop to the pressurizer occurred at a rate of 0.0146 mg per hr per kg of Th+U; however, the change in the U/Th ratio in the circulating slurry was not statistically significant. No detectable particle degradation occurred.

REFERENCES

1. R. B. Korsmeyer et al., HRP Quar. Prog. Rep. Jan. 31, 1959, ORNL-2696, p 60-67.

2. R. B. Korsmeyer et al., HRP Prog. Rep. for Quarters Ending April 30 and July 31, 1958, ORNL-2561, p 126-27.

3. R. B. Korsmeyer et al., HRP Quar. Prog. Rep. Oct. 31, 1958, ORNL-2654, p 100-101.

12. INSTRUMENT AND VALVE DEVELOPMENT

D. S. Toomb

A. M. Billings
E. H. Bell
R. L. Moore
J. L. Redford

12.1 INSTRUMENT DEVELOPMENT

12.1.1 High-Temperature Radiation-Resistant Differential Transformers

The development of differential transformers for sensing the primary-element motions of instruments and capable of operating for long periods at high temperatures and in radiation fields was continued.

The transformer described previously[1] was tested at temperatures from 25 to 350°C with a span setting of 0.025 in. and exhibited no changes of characteristics other than negligible zero shifts due to differential expansion in the test jig. During these tests the 1000-cps primary excitation current was maintained constant, and all conducting materials in the field of the transformer were Inconel. The substitution of austenetic stainless steel for Inconel in parts located in the transformer field resulted in temperature-induced shifts in the phase and magnitude of the signal voltage. If austenetic stainless steel is necessary in this application, because of corrosion considerations, these shifts could be reduced by splitting or laminating the parts, where possible, to reduce eddy currents.

The 1-1/8-in.-long movable transformer core was Armco iron.

The sensitivity of the transformer and its associated circuit was found to be approximately 0.1 mv/v per 0.001 in.

Nickel-plated, ceramic-coated No. 24 AWG wire (Secon Metals Corporation) was used for the windings in the transformer. The two secondary windings were wound on the Inconel form and were separated by a Lava spacer. The primary winding was wound over both secondaries.

The windings were impregnated with Allen PBX ceramic cement, and the entire transformer was enclosed in a cyclindrical Inconel housing, 2-1/2 in. in diameter and 3 in. long, which was weld-sealed. A 5/8-in.-dia bore was provided for the instrument pressure housing. The lead wires were brought out through 1/4-in.-OD tubing.

12.1.2 Magnetic Flowmeter for Slurry Service

As magnetic flowmeters have worked very well in nonradioactive low-temperature slurry test loops, several inorganic insulating materials were corrosion tested to determine whether they would be satisfactory as liners for

the metering section of meters for 300°C slurry systems. The Foxboro Company E-M flowmeters now in use have a Teflon insulating liner to prevent the stainless steel pipe in the metering section from shorting-out the millivolt signal produced at the electrodes and across the relatively low-conductivity fluid. Teflon is not satisfactory in this application at temperatures above 365°F (ref. 2) and decomposes under irradiation.

The ceramic coatings were deposited on one side of type 347 stainless steel coupons by the Norton Company and were tested by the Materials Research Section in a static autoclave filled with oxygenated deionized water at 280°C. The coating materials, which all tested unsatisfactorily, were as follows:

Rokide A	Aluminum oxide
Rokide A+	As above plus Linde R64 silicone resin binder
Rokide ZS	65% zirconium oxide, 34% silicon dioxide
Rokide ZS+	As above plus Linde R64 silicone resin binder
Rokide C	Chrominum oxide
Rokide C+	As above plus Linde R64 silicone resin binder

12.1.3 Static-Component Power-Control System Evaluation

The electric-resistance elements used in HRP systems for supplying heat to the pressurizer vessels are controlled by a time-duration off-on mode. This control method functions by turning off and on the electric current to the heaters, the percentage on-time being varied in a fixed period. This system is inexpensive in the use of control equipment but suffers from the disadvantages of causing the temperature to cycle and requires that the relays and contactors be preventively maintained to ensure reliable operation. The temperature cycle is minimized by increasing the cycling rate of the control mode.

An alternate supply-voltage proportioning system utilizing static control components was investigated[3] to determine the control-characteristic curves obtainable with available magnetic amplifiers and saturable reactors.

The test setup shown schematically in Fig. 12.1 consisted of a 0- to 10-ma current source, a magnetic amplifier connected as a self-saturating doubler with bridge rectifier output, and three saturable reactors. The reactors were connected with their inputs in parallel and their outputs wye-connected to a 30-kw resistive load. The load was conveniently supplied by connecting Calrod heating elements in parallel.

The over-all control-characteristic curve for the test system is shown in Fig. 12.2. The curve is nonlinear, and neither zero nor full power output was obtained. However, the reliability to be gained from a system without moving parts and off-on contacts makes the scheme attractive for future applications.

12.2 VALVE DEVELOPMENT

12.2.1 Valve Stem-Sealing Bellows

Two three-ply type 347 stainless steel valve stem-sealing bellows of the type used in the HRT (Fulton Sylphon Division No. 10716-R3) were cycled to failure in slurry containing 400 g of Th per kg of H_2O at 285°C and with a 2300-psi differential. The first bellows failed at 63,716 strokes and the

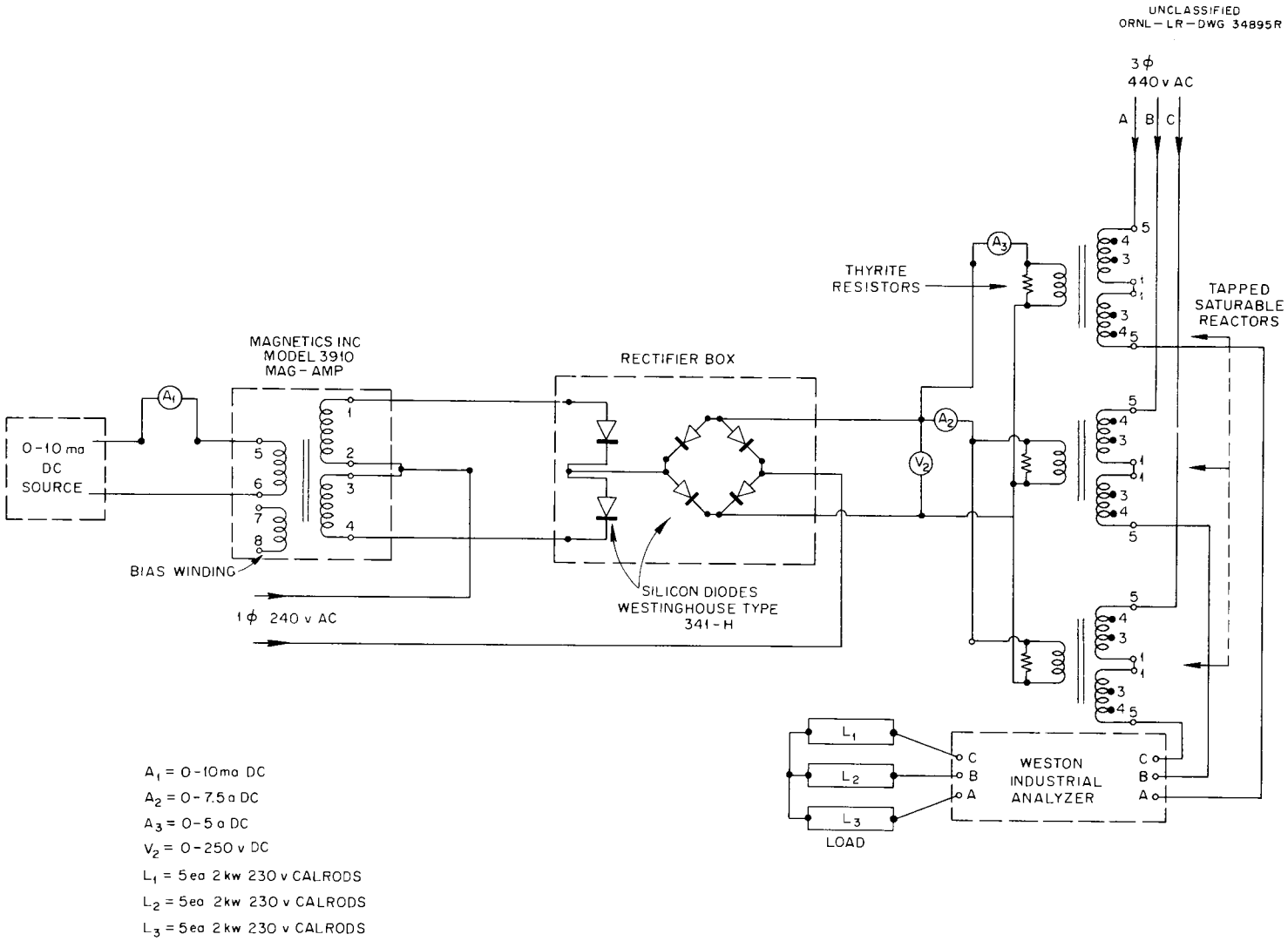

Fig. 12.1. Schematic Diagram of Static-Component Power-Control System Test.

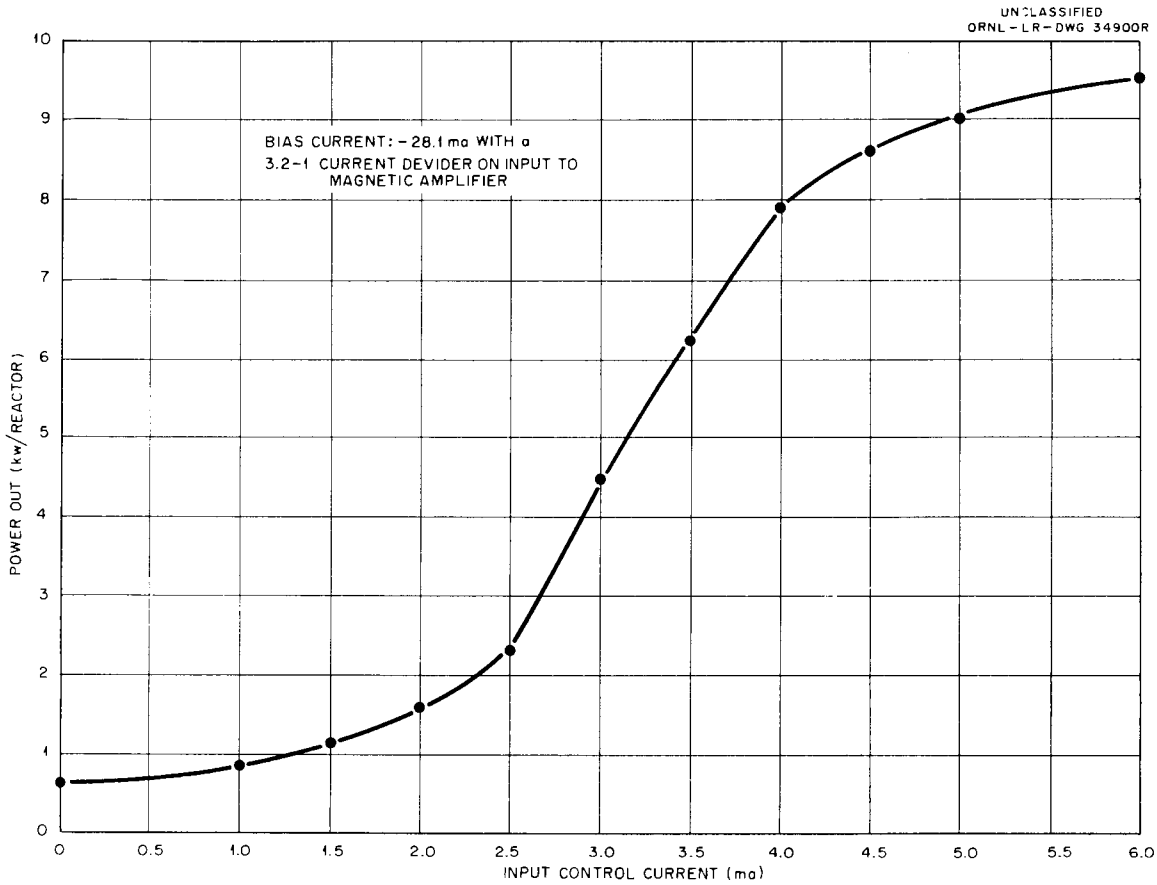

Fig. 12.2. Control-Characteristic Curve – Static-Component Power-Control System Test.

second at 71,607. The stroke length was 1/8 in. in both cases. These bellows have an inside diameter of 0.875 in. and a length of 3-3/4 in. The indicated life from these two tests makes these bellows entirely satisfactory for use as stem seals for small valves in high-temperature slurry systems.

A grade TI-55 titanium bellows assembly was cycled 11,600 times, with a 1/8-in. stroke length, in uranyl sulfate at 280°C and with a 2300-psi differential before failure occurred at a convolution. The bellows assembly, illustrated in Fig. 12.3, was supplied by the Fulton Sylphon Division as a prototype for acceptance testing on an ORNL developmental order. The bellows, which are made up from three 0.010-in. plys, have an ID of approximately 13/16 in. and a spring rate of 300 lb/in. As the prototype was considered satisfactory, additional bellows will be procured and tested.

REFERENCES

1. D. S. Toomb et al., HRP Quar. Prog. Rep. Jan. 31, 1959, ORNL-2696, p 59.

2. The Foxboro Company, Magnetic Flow Transmitters, Bulletin 16-146 (November 1956).

3. J. L. Redford, Static-Component Electric Power Control System Evaluation, ORNL CF-58-12-99 (Dec. 16, 1958).

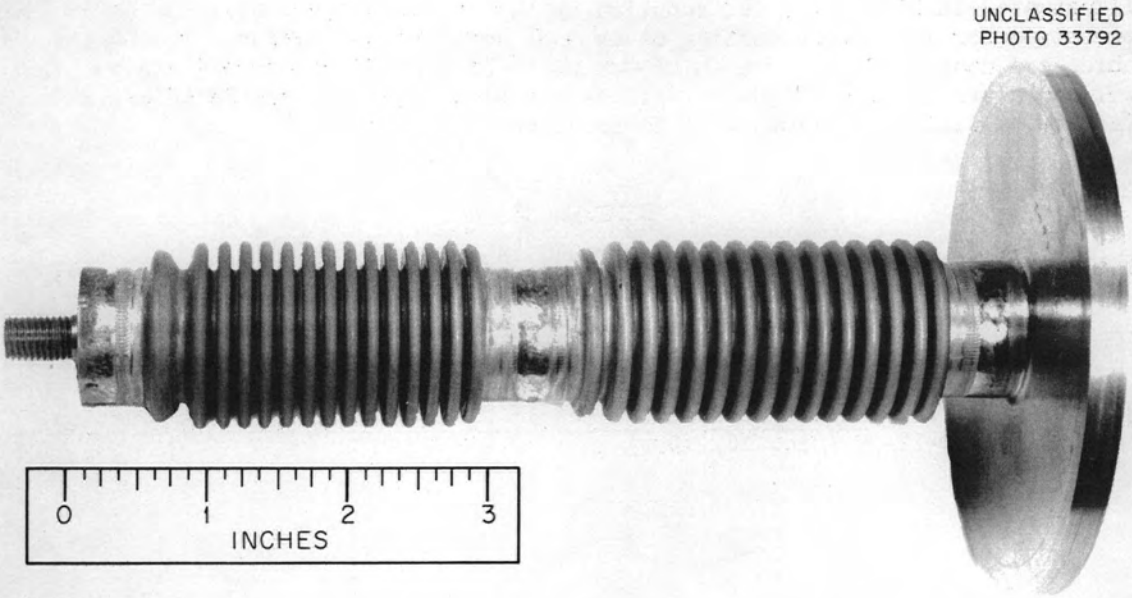

Fig. 12.3. Titanium Bellows Assembly After Testing.

Part IV

REACTOR MATERIALS RESEARCH

E. G. Bohlmann

13. SOLUTION CORROSION[1]

J. C. Griess H. C. Savage

S. E. Bolt P. D. Neumann
J. L. English A. J. Shor
R. S. Greeley E. S. Snavely
D. N. Hess W. C. Ulrich

13.1 DYNAMIC SOLUTION CORROSION

13.1.1 Deposition of Salts from Dilute Uranyl Sulfate Solutions on Heated Surfaces

A number of tests were conducted during the past quarter to investigate the effect of heated metal surfaces on the stability of uranyl sulfate solution. The equipment used was a heated Zircaloy-2 bypass line in 100A loop H and a 5-gpm in-pile pump loop in which the core section was externally heated. These tests are described below.

(a) Heated Zircaloy-2 Bypass.--Experimentation has continued with the heated Zircaloy-2 bypass installed in 100A loop H. Table 13.1 lists the general conditions of runs H-124A, B, and C, which were made during the report period, and of run H-124, which was described previously.[2] These four runs were made to investigate the effects of flow rate, bypass orientation, and pressurization on salt deposition and heat-transfer properties. In all cases D_2O solutions containing 0.025 *m* UO_2SO_4, 0.014 *m* D_2SO_4, 0.011 *m* $CuSO_4$, and 200 ppm of nickel as nickel sulfate were used.

As noted in Table 13.1, deposition of salts did not occur with horizontal or vertical orientation of the bypass even at flow rates as low as 0.1 fps and relatively high heat fluxes, up to 58,000 Btu/hr·ft^2. It appeared that this was because a stable vapor region was not maintained under these conditions, and hence any salts that deposited rapidly redissolved. Similarly no evidence of deposition was observed with the bypass mounted in a position 10 deg from the horizontal with the temperature of the solution entering the bypass at 150°C, even though the calculated inner-wall temperature indicated that boiling should have occurred at the total pressure on the system. However, when the inlet temperature of the solution was raised to 250 or 280°C and the inner-wall temperature was sufficiently high for the solution to boil, all salts began depositing in the bypass in a manner similar to that observed in run H-121.[3]

The effect of gas (oxygen) concentration in solution on boiling and salt deposition was investigated by pressurizing with oxygen or by hydraulic pressurization. Partial gas pressurization resulted in oxygen concentrations as high as 2000 ppm, while hydraulic pressurization gave an oxygen concentration

Table 13.1. Summary of Tests in Heated Zircaloy-2 Pipe Section with Uranyl Sulfate Solution

Run Number	Bypass Position	Flow Direction	Pressure (psia)	Loop Temp. (°C)	Press. Temp. (°C)	Flow Rate (fps)	Max. Heat Flux (Btu/hr·ft^2)	Max. Calc. Wall Temp. (°C)	Maximum h (Btu/hr·ft^2·°F)	Salt Deposition
H-124	Vertical	Top to Bottom	1150*	280	280	0.10-0.65	58,000	430	400	No
H-124A	Vertical	Bottom to Top	1300-1350*	280	280	0.10-0.20	40,000	351	460	No
			1800**	250	250	0.20-0.80	46,000	415	430	No
			1800**	280	280	0.20	39,500	372	360	No
H-124B	Horizontal		1115-1450*	280	285	0.10-0.20	39,000	391	300	No
			1800**	280	280	0.10-0.70	50,500	444	440	No
H-124C	Inclined ~10 deg	Top to Bottom	200-250*	150	150	0.15-0.20	16,300	226	270	No***
			650*	200	205	0.15	16,000	298	200	Yes
			1000-1050*	250	255	0.08-0.30	16,000	327	215	Yes
			840-1690*	280	285	0.15	15,700	362	340	Yes

* Steam + O_2.

** Hydraulic.

*** Not conclusive; solution sample from the bypass showed increased uranium concentration, but a continuous loss from the loop solution was not observed.

of ~20 ppm. The total system pressure was also varied as shown in Table 13.1 and as reported previously.[2]

With hydraulic pressurization (~20 ppm oxygen) and the bypass mounted about 10 deg from horizontal, deposition could be achieved only under conditions of maximum heat flux (58,000 Btu/hr·ft^2) and minimum flow rate as was indicated in the last quarterly report.[2] Only 20% of the salts were lost from solution and presumably deposited in the bypass. With gas pressurization (~2000 ppm oxygen) essentially all salts were lost from solution, even at a low heat flux (16,000 Btu/hr·ft^2).

The type of boiling, as indicated by the fluid-film heat transfer coefficients shown in Table 13.1, was not affected by the orientation of the bypass, the dissolved-gas concentration (from 20 to 2000 ppm), or the total system pressure. All values, including those previously reported for run H-123,[2] were between 200 and 460 Btu/hr·ft^2·°F, values indicative of film-type boiling. Considering that the experiment was not designed to obtain exact data, it is concluded that there is no real difference between the two numbers and that the boiling regime was the same in all cases.

(b) Heated Core Section, Loop L-2-23.--Additional out-of-pile solution stability tests have been made in loop L-2-23 with an externally heated titanium core as previously described.[4,5] A series of runs was also performed after the titanium core was replaced with a stainless steel core with an improved heater which gives higher heat fluxes. More complete temperature measurements of the core wall can also be obtained.

(1) Titanium Core, Loop L-2-23.--The series of runs with a titanium core was an extension of previous studies, both in-pile[6] and out-of-pile,[7] of the loss of uranium from solutions in contact with a heated metal surface at temperatures below the second-liquid-phase temperature but sufficient to produce boiling. The present runs, nominally at 225°C, represent a continuation of a study of the effect of solution temperature on the deposition of salts from solution. Runs made at temperatures higher than 225°C have been reported.[7]

Table 13.2 is a summary of the operating conditions which resulted in loss of uranyl sulfate, copper sulfate, and sulfuric acid by deposition from solution in the titanium core section. It was observed that deposition was initiated more readily at 225°C than at 280 or 250°C. It was also found that the acid concentration influenced the deposition. Loss of salts from solution was at a lower rate, and the total amount of loss was less, at an acid concentration of 0.050 *m* than at 0.014 *m*. However, even with the 0.05 *m* acid, deposition of uranium and copper sulfates could not be completely prevented.

When the salts were lost from solution by deposition, they could be rapidly recovered by any of the following procedures: (1) removal of core heat, (2) increase in steam overpressure, or (3) increase in the solution flow rate. However, increasing the acid concentration from 0.014 *m* to 0.025 *m* by injecting acid after deposition had occurred effected no apparent re-solution of the deposited salts.

At the conclusion of these tests the titanium core was sectioned for examination of the interior surfaces. Corrosion damage was found on the upper section of the core where deposition of salts had occurred. Figure 13.1 is a photograph of this surface. The interface between liquid and vapor is clearly visible; attack on the surface in contact with liquid was negligible. The location and type of attack was similar to the severe attack found on the surface of the heated Zircaloy-2 bypass exposed under comparable conditions.[8]

Table 13.2. Summary of Operating Conditions, Loop L-2-23, Titanium Core

Loop temperature, 225°C
Pressurizer temperature, 227°C
Core flow rate, 0.3 fps
Core heat, 8,000 Btu/hr·ft^2

Run Number	UO_2SO_4 Conc. (*m*)	D_2SO_4 Conc. (*m*)	$CuSO_4$ Conc. (*m*)	O_2 (psi)	Total Press. (psia)	Deposition Half-Time (hr)	% U Deposited After 60 hr
15	0.025	0.014	0.011	165	550	7	96
15	0.025	0.014	0.011	146	518	8	96
18	0.025	0.025	0.011	147	558	18	65
19	0.025	0.050	0.011	200	594	18	68

(2) Stainless Steel Core, Loop L-2-23.--The titanium core of loop L-2-23 was replaced with a stainless steel core. Core heating was with Calrod-type electric heating elements cast in aluminum on the outside surface of the core. An initial series of runs was made to duplicate previous tests. Generally the results indicated the same behavior that had been observed in the titanium core; i.e., deposition depended on whether or not boiling occurred and on the flow rate of the solution. The actual deposition process was observed by means of an apparatus combining a standard x-ray machine, a television camera sensitive to x rays, and a closed-circuit television receiver. With this machine it was possible to witness the formation of a gas space and the subsequent buildup of a deposit on the upper, heated surface of the core. A photograph of a television image of the core during operation of the loop with a 1.3 *m* UO_2SO_4 solution (under boiling conditions) is presented in Fig. 13.2 and shows the solid (attached to the upper wall), the gas, and the liquid phases. This highly concentrated solution was used to magnify contrast between vapor, liquid, and solid phases. However, later runs using a uranyl sulfate solution of 0.025 *m* uranium, 0.025 *m* $CuSO_4$, and 0.025 *m* H_2SO_4 gave adequate contrast for observation of the various phases.

It was observed that when the core was heated sufficiently to produce a distinct vapor phase under conditions of low flow and low system overpressure, a substance, probably crystallized salts, deposited on the upper core surface. When the bulk solution flow rate was increased from ~0.3 to ~0.4 fps, some of the deposited material returned to the solution as liquid, as evidenced by drops falling through the vapor or by small rivulets running down the core wall. Increasing the flow rate to 0.6 fps resulted in increased turbulence of the solution; this resulted in disappearance of the vapor space followed by rapid and complete dissolution of the salt.

Attempts to deposit salts at a flow rate of 0.6 fps with maximum available heat input through the core wall of 20,000 Btu/hr·ft^2 were unsuccessful.

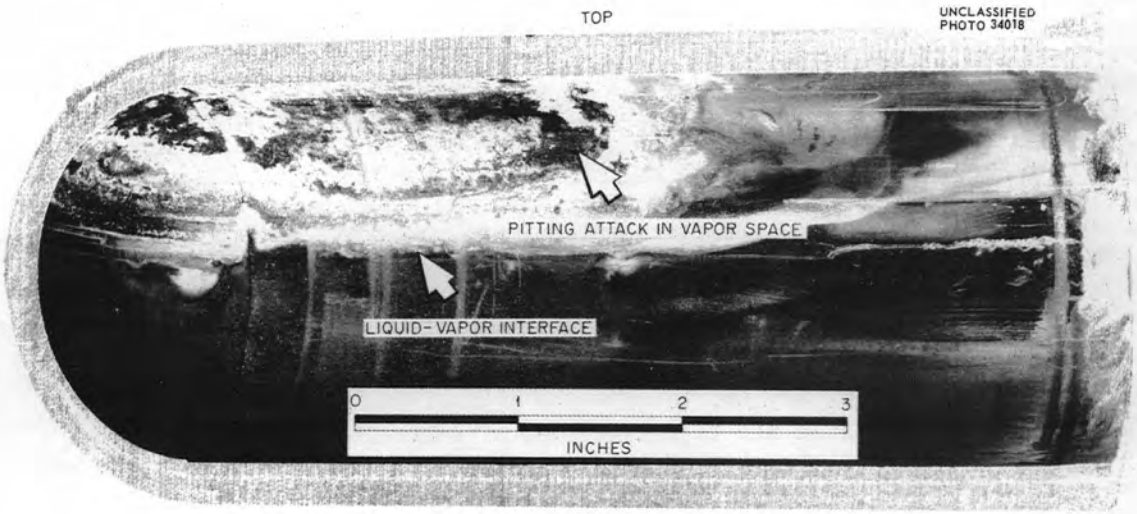

Fig. 13.1. Sectioned View of Titanium Core of Loop L-2-23.

Fig. 13.2. X-Radiograph of L-2-23 Core at Boiling Conditions.

To observe the second-liquid phase in the 1.3 *m* UO_2SO_4 solution, the loop was operated slightly above the second-liquid-phase temperature (~285°C) and sufficient heat was applied to the core to produce boiling and salt deposition. The formation of the dense second-liquid phase was confirmed by momentarily stopping the flow. The four-phase system of deposited salt, vapor, light- and heavy-liquid phases was clearly visible. After observing the heavy-liquid phase the pump was started at 20 cps to produce a bulk flow rate through the core of 0.2 fps. The temperature of the solution was then gradually lowered below the second-liquid-phase temperature, and the disappearance of the dense solution (in the bottom of the core section) was observed. It was interesting to note that even after the solution temperature was lowered below 285°C, 5 to 10 min were required at the low flow rate to remove the concentrated solution from the core.

Other test runs were made with a 0.025 *m* UO_2SO_4 solution containing 0.025 *m* $CuSO_4$ and 0.025 *m* H_2SO_4 in H_2O, and observation with the x-ray - television unit confirmed the fact that loss of salts from solution occurred by deposition on the upper part of the heated core wall when a vapor space was formed as a result of boiling.

(c) Discussion of Results.--Test results with the heated Zircaloy-2 bypass and heated core section of loop L-2-23 were in agreement with previous hypotheses concerning the deposition of salts from uranyl sulfate solutions;[2] i.e., deposition occurs on a heated surface when it is separated from the bulk solution by a stable vapor-phase pocket formed by boiling. Boiling and the formation of a stable vapor pocket are functions of heat flux, system geometry (orientation), solution flow rate, total system pressure, gas concentration in solution, and solution temperature.

Increasing the acid concentration in solution appeared to decrease the rate and extent of salt deposition, but did not completely prevent the deposition.

13.1.2 Scale Dissolution and Peptization

Several reagents were tested for use as descaling agents in stainless steel systems. The reagents included Deoxidine-170 (inhibited phosphoric acid), 20% Versenol-120 (trisodium-N-hydroxyethylethylenediaminetriacetate) buffered with 25% ammonium acetate, 20% nitric acid plus 3% hydrogen peroxide, and 0.05% oxalic acid.

The tests were conducted in 100A loops in which specimens of titanium, Zircaloy-2, type 347 stainless steel, and Stellite were exposed. In some cases, specimen holders were packed with oxide scale. Type 347 stainless steel coupon specimens included new samples and some which had been prefilmed by previous corrosion tests.

Of all reagents tested, only Deoxidine-170, used under the conditions recommended by members of the Chemical Technology Division, was a satisfactory solvent for the corrosion-product scale. In a run in which Deoxidine-170 was circulated at 125°C for 36 hr in a stainless steel loop coated with a tightly adherent layer of corrosion products, essentially all the oxide was dissolved, leaving a surface free of heavy scale. The attack on film-free stainless steel and Zircaloy-2 specimens was trivial, but titanium specimens corroded at rates in excess of 600 mpy. The effectiveness of the solvent for removing a plug of corrosion products was not tested, but in view of the slow rate of dissolution of the oxide scale it is doubtful that a heavy plug would have been dissolved in any reasonable length of time.

The Versenol-120 - ammonium acetate solution seemed to be somewhat effective as a solvent and dispersant for oxide scale; however, an 80-hr run failed to unplug a specimen holder packed with corrosion products. During this operation the solution accumulated 9.7 g of iron per liter, much of which was in suspension. The rate at which adherent scale was dissolved from prefilmed type 347 stainless steel coupons was about 0.01 $mg/cm^2/hr$ without any significant effect on the base metal.

The 20% HNO_3 - 3% H_2O_2 solution appeared promising as a peptizing agent for scale in static laboratory tests. However, in subsequent loop tests, the mixture failed to remove a scale-plug from a sample holder and did not appear effective otherwise as a scale dissolver. The 0.05% oxalic acid solution had little, if any, effect on corrosion scale. Neither of these reagents was particularly aggressive toward any of the corrosion specimens.

The possibility of removing a tightly packed plug from a heat-exchanger tube by chemical dissolution or dispersion seems very remote. The difficulty of getting fresh reagent to the plug and the slowness with which even Deoxidine-170 dissolved the scale indicate that mechanical means would be necessary to dislodge thick plugs of corrosion products. On the other hand, solutions capable of dissolving thin, tightly adherent scales would be extremely useful for decontaminating reactor systems and thereby reducing the shielding necessary for remote maintenance.

13.1.3 Hydrolytic Stability of Very Dilute Fuel Solutions

(a) Fuel Dilution.--It is possible that a patch on the hole in the HRT core tank would allow a small flow of fuel solution from the core to the blanket, where a sudden dilution would occur. If dilution caused hydrolytic deposition of uranium on the core in a localized region, a hot spot would result. To determine the stability of dilute fuel solutions, consecutive additions of 20, 40, 80, and 500 ml of a solution containing 0.04 *m* UO_2SO_4, 0.025 *m* H_2SO_4, 0.02 *m* $CuSO_4$, and 0.005 *m* $NiSO_4$ were made to 12 liters of distilled water circulating in a loop at 250°C. After each addition several samples of solution were taken for analysis.

Figure 13.3 shows how the analytically determined uranium concentration compared with that calculated from the amount of uranium added. From the figure it is apparent that the resulting solutions were stable within experimental error with respect to uranium concentration, except for the 500-ml addition where there was a large, unexplained discrepancy between calculated and observed concentrations. The copper was the least stable species in solution; less than 80% of the added copper was present in solution at all dilutions. Nickel concentration data were erratic, but in general fair agreement was obtained between observed and calculated values.

Although the uranium concentration appeared constant, the present results cannot be extrapolated directly to the HRT. Appreciable amounts of chromium(VI) and acid formed from the corrosion products present in the loop, and it is possible that this acid helped stabilize the solutions. Presumably this source of hydrogen ions would not be present in the blanket of the HRT. Consequently the above experiment will be repeated in a titanium loop free of chromium.

(b) Stability and Corrosiveness of Potential Fuel Solutions.--The corrosiveness of two possible fuel solutions to several alloys was determined at 250°C, and the chemical stability of the same solutions was determined at 320°C. The solutions were: (1) 0.025 *m* UO_2SO_4 containing 0.025 *m* D_2SO_4, 0.025 *m* $CuSO_4$,

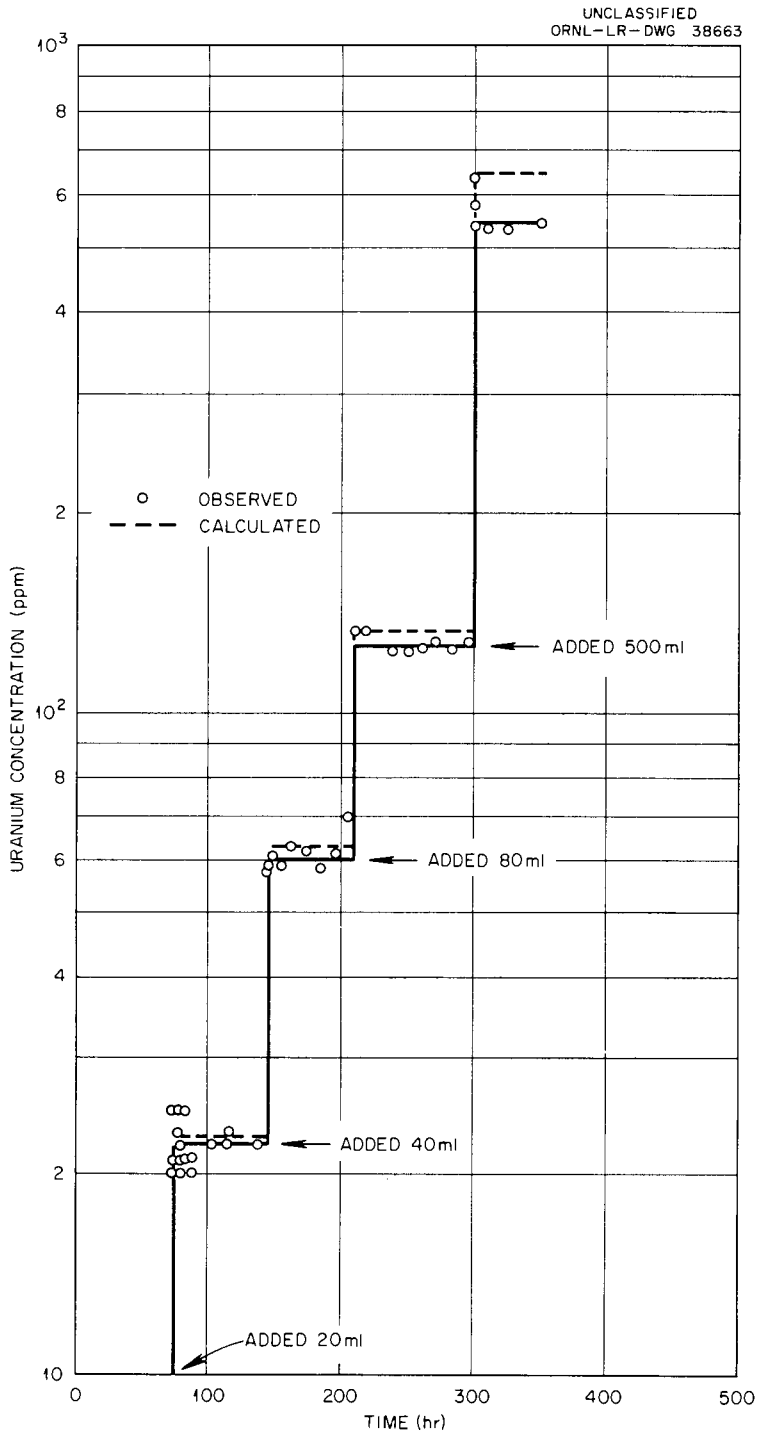

Fig. 13.3. Comparison Between Calculated and Determined Uranium Concentrations at 250°C.

and 0.005 *m* $NiSO_4$ in D_2O; and (2) 0.03 *m* UO_2SO_4 containing 0.03 *m* H_2SO_4, 0.025 *m* $CuSO_4$, and 0.005 *m* $NiSO_4$ in H_2O. It should be noted that on a volume basis these two solutions were essentially of the same concentration. In each case the solution was circulated in a stainless steel loop containing corrosion specimens at 250°C for 200 hr; then the corrosion specimens were removed and the same solution was circulated at 320°C for an additional period.

Table 13.3 lists average corrosion rates for pin specimens exposed to the solutions for the 200-hr period. The values were similar to those obtained previously. Corrosion rates for the new nickel-base alloy, Incoloy 804, were as high as those for the stainless steels.

Table 13.3. Average Corrosion Rates of Various Alloys Exposed to Light- and Heavy-Water Fuel Solutions for 200 hr at 250°C and a Solution Velocity of 17 fps

D_2O Solution: 0.025 *m* UO_2SO_4, 0.025 *m* D_2SO_4, 0.025 *m* $CuSO_4$, 0.005 *m* $NiSO_4$
H_2O Solution: 0.03 *m* UO_2SO_4, 0.03 *m* H_2SO_4, 0.025 *m* $CuSO_4$, 0.005 *m* $NiSO_4$

Alloy	Corrosion Rate (mpy)	
	D_2O	H_2O
Ti-55A	0.0	0.0
347, cast	10.6	12.5
347, wrought	9.6	12.0
347, wrought	8.8	13.6
347, wrought	9.7	12.9
309SCb	10.2	12.0
309SCb	9.7	12.7
CD4MCu	9.5	10.7
CD4MCu	8.9	10.2
Incoloy 804	13.1	12.5
Zircaloy-2	0.7*	1.4*

* Calculated from weight gains.

The critical velocity of type 347 stainless steel coupons was found to be 32 fps in the D_2O solution and 46 fps in the H_2O solution. These values are higher than those observed previously.[9] It should not be construed from these results that the D_2O solution is more corrosive than the H_2O solution, because of several factors which must be considered. The two runs were made in different loops, and corrosion rates have been found to be sensitive to loop history.[10]

Neither solution was chemically stable at 320°C. The concentration of uranium decreased during both runs as shown in Fig. 13.4. Copper was apparently stable in the H_2O but not in the D_2O solution.

13.1.4 Corrosion Tests of Various Alloys

Small amounts of impurities introduced into a metal sometimes increase the corrosion resistance of the metal.[11] In some cases the impurity acts as a cathodic site, and the increased corrosion resistance can be attributed to a lowered hydrogen overvoltage which allows the anodic sites to achieve potentials where the metal is passive.

Several alloys made by the ORNL Metallurgy Division were tested to determine whether small additions of platinum or copper would increase the corrosion resistance of type 304 stainless steel in uranyl sulfate solutions. Results for a part of this program are shown in Table 13.4, where the corrosion resistance of the platinum and copper alloys is compared with that of types 304 and 347 stainless steel. The 0.5% Pt and 1.2% Cu alloys had lower corrosion rates than the unalloyed material at low solution velocity but showed no significant improvement at high velocity. (Corrosion rates for the stainless steels at low velocities were much higher than usually encountered; however, they are reported here as an indication of the relative rates of corrosion of the various alloys.) Future tests will be designed to determine the performance of the platinum and copper alloys, both cast and wrought, particularly with regard to velocity effects.

Table 13.4. Corrosion Rates of Various Alloys for 200 hr in 0.04 *m* UO_2SO_4, 0.025 *m* D_2SO_4, 0.02 *m* $CuSO_4$ at 250°C

Alloy	Corrosion Rate (mpy)	
	17 fps	68 fps
Ti-45A	0.1	1.2
304 stainless steel (wrought)	35.0	97.0
	36.0	99.0
304 + 0.1% Pt (cast)	40.0	102.0
304 + 0.5% Pt (wrought)	15.0	88.0
	15.0	96.0
304 + 1.2% Cu (wrought)	23.0	91.0
	22.0	94.0
347 stainless steel (wrought)	62.0	107.0
347 stainless steel (cast)	74.0	125.0
	72.0	104.0
Incoloy 804	66.0	145.0

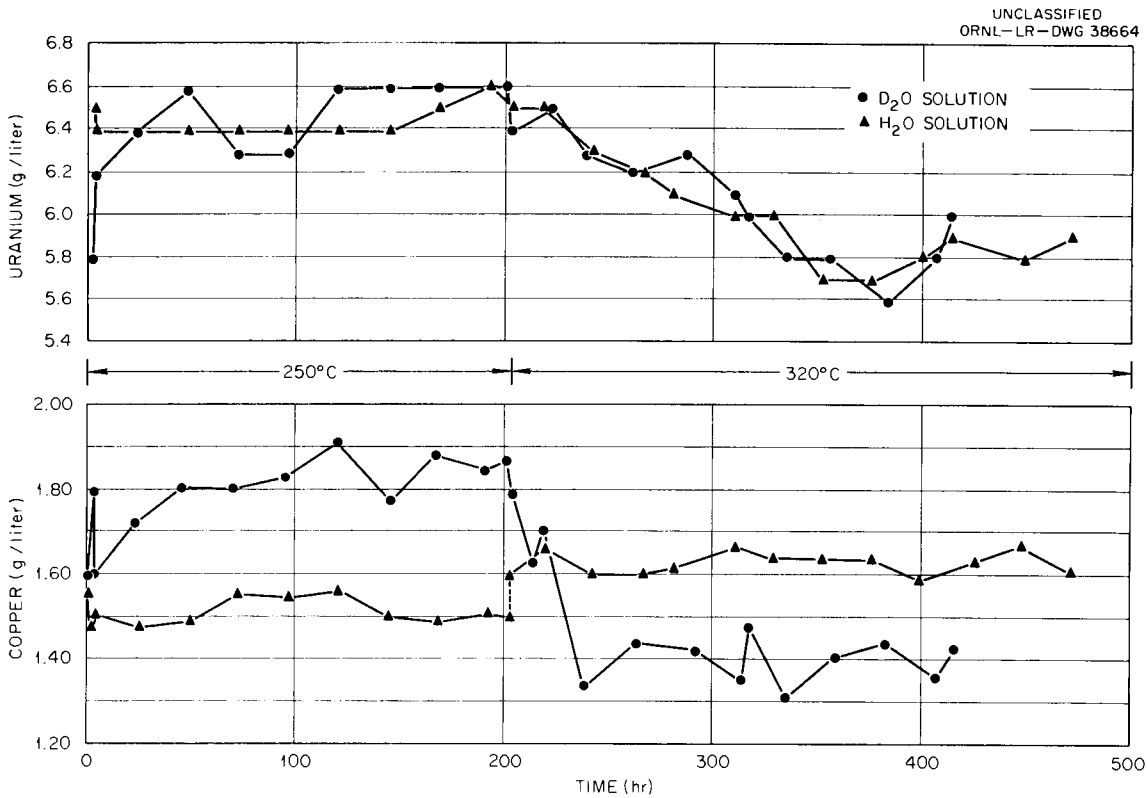

Fig. 13.4. Concentrations of Uranium and Copper as a Function of Time.

13.2 LABORATORY CORROSION STUDIES

13.2.1 Intergranular Corrosion of Type 347 Stainless Steel

A test program has been completed in which the objective was to determine whether any correlation existed between the corrosion behavior of type 347 stainless steel in the boiling 65% HNO_3 test[12] and in uranyl sulfate solutions. The boiling nitric acid test is required by material specifications for type 347 stainless steel used in the HRP and related programs. The criterion for acceptance is that corrosion rates of specimens of the alloy in a sensitized condition (1 hr at 1250°F) shall not exceed a value of 0.002 in. per month during five 48-hr exposure periods.[13]

From hundreds of nitric acid tests that have been performed, a number of type 347 stainless steel heats that showed penetration rates ranging from 1.3 to 39.2 mils per month were selected for test. In addition, an unstabilized grade of austenitic stainless steel, type 310, was included among the tests for comparative purposes. Table 13.5 presents a summary of the nitric acid results for the sensitized test materials. The severity of intergranular attack was related directly to the magnitude of the penetration rates. For example, the material which corroded at a rate of 1.3 mils per month did not undergo intergranular attack, but that which corroded at an average rate of 39.2 mils per month exhibited intergranular attack, more than 10 mils deep, and intense pitting as well.

Table 13.5. Results of Boiling 65% HNO_3 Test on Sensitized* Stainless Steel Test Materials

48-hr Periods	Penetration Rate (mils per month per 48-hr period)					
	310 SS** (Lot 2)	347 SS** (Lot 13)	347 SS** (Lot 24)	347 SS** (487/c)	347 SS** (No. 34)	347 SS (No. 431/A)
1st	1.7 1.8	1.1 1.0	5.8 6.2	12.3 11.2	2.2 2.5	1.3
2nd	59.0 57.8	1.1 0.8	25.5 28.5	6.6 6.3	3.8 3.9	1.7
3rd	72.2 76.5	1.2 1.1	48.1 53.4	5.1 5.0	8.2 8.4	4.4
4th		1.7 1.4	52.7 58.7	3.8 3.8		7.7
5th		1.8 1.6	51.5 60.0	3.6 3.7		9.0
Average	44.3 45.4	1.4 1.2	36.7 41.8	6.3 6.0	4.7 4.8	5.0

* Heated 1 hr at 649°C (1200°F) followed by air cooling.

** Duplicate specimens.

The test environments selected for the intergranular study included a simulated HRT reactor fuel solution and a 1.33 *m* UO_2SO_4 solution. The fuel solution contained 0.04 *m* UO_2SO_4, 0.02 *m* H_2SO_4, and 0.005 *m* $CuSO_4$. Tests were run at temperatures of 100, 200, 250, and 300°C. The tests at 200, 250, and 300°C were run with an oxygen overpressure of approximately 150 psi; at 100°C air was bubbled through a boiling solution. A few tests were run also at 300°C in an oxygen-deficient fuel solution to simulate conditions in a crevice.

Most of the tests were conducted with two heats of type 347 stainless steel (lot Nos. 13 and 24 in Table 13.5), which corroded at average rates of 1.3 and 39.2 mils per month, respectively, in the boiling 65% HNO_3 test. These two materials will hereinafter be designated as the "control" and the "off-specification" materials. All materials were within the required AISI chemical composition limits except that the carbon content of the off-specification material was 0.10%, 0.02% above the specified limit. Both the control and the type 310 stainless steel contained 0.07% carbon.

Test results for the sensitized control, off-specification, and type 310 stainless steel materials are given in Table 13.6. In no case was any indication found of intergranular corrosion attack on the control and off-specification specimens. Although the data are not included in Table 13.6, the same was true in tests with the other type 347 stainless steel heats listed in Table 13.5. On the other hand, the type 310 stainless steel specimens underwent intergranular attack in every environment tested, the maximum depth of penetration being 6 mils in the oxygenated fuel solution at 200°C.

The highest corrosion rates for type 347 stainless steels were encountered, as was expected, in the oxygen-deficient fuel solution at 300°C. Actually the rates would have been considerably higher than the rates reported in Table 13.6 had the solution been maintained; in the absence of oxygen uranyl ions are reduced, ferrous and nickelous ions are formed, and acid is consumed, after which corrosion essentially ceases. Average rates of 1.3 mpy during a 2500-hr test were experienced with the alloy in the 1.33 *m* UO_2SO_4 solution at 250°C. The rates for both the control and the off-specification specimens in the other environments were 0.3 mpy or less. Type 310 stainless steel specimens corroded at similar rates. In all cases, corrosion rates decreased with increased exposure time.

The following conclusions were suggested by the results of the laboratory tests:

1. There is no relation between the intergranular corrosion behavior of sensitized type 347 stainless steel in the boiling 65% HNO_3 test and its behavior in aqueous uranyl sulfate solutions at temperatures up to 300°C. Steels subject to intergranular penetration and exhibiting corrosion rates as high as 39.2 mils per month in the boiling nitric acid test were not prone to intergranular attack in the uranyl sulfate environments.

2. Sensitized, unstabilized type 310 stainless steel which was highly subject to intergranular corrosion in the boiling nitric acid test was also subject to intergranular attack in uranyl sulfate solutions at 100°C and above. Presumably a similar behavior would be exhibited by other grades of unstabilized stainless steels, exclusive of the extra-low-carbon types.

Table 13.6. Intergranular Corrosion Behavior of Sensitized[a] Stainless Steels in Uranyl Sulfate Solutions

Material Type	Medium	Temp. (°C)	Total Time (hr)	Corrosion Rate (mpy)	Intergranular Penetration
347 SS (control)[c]	Fuel solution[b]	100	5000	<0.1	None observed
347 SS (off-spec)[d]			5000	<0.1	None observed
310 SS[e]			5000	<0.1	Present; 3 mils deep
347 SS (control)	Fuel solution	200	5000	0.1	None observed
347 SS (off-spec)			5000	0.2	None observed
310 SS			5000	0.2	Present; 6 mils deep
347 SS (control)	Fuel solution	300	2000	0.3	None observed
347 SS (off-spec)			2000	0.3	None observed
310 SS			5000	<0.1	Present; 0.5 mil deep
347 SS (control)	Fuel solution	300	200	3.3[f]	None observed
347 SS (control)	(O_2-deficient)		1000	3.0[f]	None observed
347 SS (off-spec)			200	1.6[f]	None observed
347 SS (off-spec)			1000	1.3[f]	None observed
347 SS (control)	1.33 *m* UO_2SO_4	100	5000	<0.1	None observed
347 SS (off-spec)			5000	<0.1	None observed
310 SS			5000	<0.1	Present; 4 mils deep
347 SS (control)	1.33 *m* UO_2SO_4	250	2500	1.3	None observed
347 SS (off-spec)			2500	1.3	None observed

(a) Heated 1 hr in air at 1250°F.
(b) 0.04 *m* UO_2SO_4 - 0.02 *m* H_2SO_4 - 0.005 *m* $CuSO_4$.
(c) Penetration rate (sensitized) in 65% HNO_3, 1.3 mils per month.
(d) Penetration rate (sensitized) in 65% HNO_3, 39.2 mils per month.
(e) Penetration rate (sensitized) in 65% HNO_3, 44.9 mils per month.
(f) Low rates due to the fact that acid concentration was low after initial corrosion.

13.2.2 Stress-Corrosion Cracking of Cast Type 347 Stainless Steel

Preliminary tests with a single heat of cast type 347 stainless steel showed it to possess unusually good resistance to stress-corrosion cracking in boiling 42% $MgCl_2$ solution and in chloride-containing water at elevated temperatures.[14,15] Results of tests with specimens of the same heat of cast material in both the $MgCl_2$ solution and in chloride-containing water at 300°C are presented in Tables 13.7 and 13.8. Only one case of possible cracking occurred in the chloride-containing water. A shallow crack (4 mils deep and reported previously[15]) was found in a simple-beam specimen. Wrought type 347 stainless steel specimens crack in 500 hr or less in the same environments.

Table 13.7. Stress-Corrosion Cracking Behavior of Cast Type 347 Stainless Steel* at 300°C in Chloride-Containing Water

Chloride Concentration (ppm)	Initial Solution pH	Applied Stress (psi)	Total Time (hr)	Remarks
0	6.5	20,000	1800	No cracks
			2000	No cracks
100	2.8	30,000	2000	No cracks
	6.5	20,000	1500	One shallow crack
			1600	No cracks
	10.5	30,000	2000	No cracks

* Simple-beam, mechanically abraded specimens.

An interesting fact was disclosed by metallographic examination of the specimens exposed in the boiling magnesium chloride solution. The sensitivity of the cast specimens to cracking appeared to be associated directly with areas of cold work. Metallographic examination of the mechanically abraded specimen stressed at 20,000 psi disclosed no evidence of a cold-worked surface; this specimen did not crack. Similarly, electropolished specimens showed no surface cold-working effect; these specimens did not crack except for the areas around stamped identification numbers where metallographic examination of the region showed a highly deformed crystal structure. Machined specimens, particularly the U-bends, had severely cold-worked structures at the surface; these specimens were highly susceptible to cracking during short periods of exposure. In the case of the U-bend specimens, the cold-work effect in the stressed area extended to a depth of approximately 15 mils below the surface. Additional tests will be run to examine the effect of cold working in greater detail.

Table 13.8. Stress-Corrosion Cracking Behavior of Cast Type 347 Stainless Steel in Boiling 42% $MgCl_2$ Solution at 154°C

Specimen Type	Surface Condition	Applied Stress (psi)	Surface Cold Work	Total Time (hr)	Remarks
Simple beam	Abraded	20,000	None	30	No cracks
Simple beam	Machined	15,000	*	50	Cracks in stamped identification numbers
		30,000	*	50	No cracks
		30,000	Yes	5	Cracks
U-bend	Machined	>40,000	Severe	1	Cracks
U-bend**	Machined	<40,000	Severe	2	Cracks
Simple beam	Electro-polished	15,000	None	50	Cracks in stamped identification numbers only
		30,000	None	50	No cracks

* Submitted for metallographic examination; results unavailable.

** Annealed 1 hr at 1950°F after bending.

13.2.3 Corrosion of Uniloy 19-9DL Stainless Steel

Uniloy 19-9DL is an austenitic stainless steel that has been modified by the addition of small amounts of molybdenum, tungsten, titanium, and niobium. The nominal chemical composition of the alloy in weight per cent is: 0.28-0.35 C, 18-20 Cr, 8-11 Ni, 0.75-1.50 Mn, 1.00-1.75 Mo, 1.00-1.75 W, 0.10-0.35 Ti, 0.25-0.60 Nb + Ta, and balance iron. The mechanical properties of the alloy in the annealed and in the annealed-and-aged condition are compared with those of type 347 stainless steel in Table 13.9. It has been used with marked success at elevated temperatures for bolt material and valve trim, particularly in oil refineries and steam generation plants. Because of its favorable properties at high temperatures, the material was considered as one of potential interest for similar applications in the homogeneous reactor program.

Extensive corrosion testing with the alloy in a wide variety of heat-treated conditions was carried out in a simulated reactor fuel solution containing 0.04 *m* UO_2SO_4, 0.02 *m* H_2SO_4, and 0.005 *m* $CuSO_4$ and in other reactor-related environments. The corrosion resistance of as-received material (condition unknown) was quite erratic in all environments tested in the temperature range between 100 and 300°C. At 300°C the observed defilmed corrosion rates were 2 mpy or less during 1000-hr tests. However, 50- to 100-hr tests in the same environment at atmospheric boiling resulted in corrosion rates as high as 250 mpy. Both annealing (1/2 hr at 1800°F followed by water quench)

and age-hardening (50 hr at 1350°F) treatments greatly improved the corrosion resistance of the alloy. In the oxygenated simulated core solution at 100 and 300°C and in 5% HNO_3 solution at 100°C, the 1000-hr corrosion rates were 0.5 mpy or less. An aging treatment on annealed material at 1200°F for periods from 0 to 48 hr produced no deleterious effect on the corrosion resistance of a heat of the alloy in the simulated reactor fuel solution at atmospheric boiling. All observed rates were 0.3 mpy or less for exposure periods of 1000 and 1100 hr.

Table 13.9. Comparison of Mechanical Properties of Types 19-9DL and 347 Stainless Steels

Material	Condition	Tensile Strength (psi)	Yield Strength (psi)	Hardness (Rockwell)
347 SS	Annealed	90,000	40,000	B75-80
19-9DL	Annealed	108,000	61,000	B92
	Annealed; aged at 1200°F	130,500	88,500	C23

Stress-corrosion cracking studies were made with the alloy in (1) reactor fuel solution with 50 ppm of chloride at atmospheric boiling; (2) chloride-free reactor fuel solution at 300°C; (3) deionized water at 300°C; and (4) 42% $MgCl_2$ solution at 154°C. Simple-beam and U-bend specimens were used. In specimens annealed before bending, cracking occurred within 50 to 250 hr in the boiling, chloride-containing fuel solution. However, when the annealed specimens were aged (1200°F, 16 hr) prior to bending, no cracking took place in 300 hr, the length of the test. Cracking did occur in the boiling magnesium chloride test. No cracking has been observed in annealed and in annealed-and-aged specimens after periods of 2000 hr at 300°C in deionized water or in the chloride-free reactor fuel solution.

Final experiments consisted of determining the antigalling properties of the alloy. Tests were run at 300°C with 3/8-16 cap screws of Uniloy 19-9DL stressed to approximately 20 ft-lb in reactor fuel solution and in deionized water. The cap screws were dismantled and reassembled frequently during the test. No tendencies toward galling were observed during 1500 hr. Under the same conditions, a similar cap screw fabricated from type 304 stainless steel galled in less than 500 hr in the deionized water environment.

In conclusion, it is believed that in a properly heat-treated condition, annealed or annealed-and-aged, the satisfactory corrosion resistance of 19-9DL stainless steel and its superior mechanical properties (as compared with those of type 347 stainless steel) would make the alloy suitable for a number of applications within the homogeneous reactor program. Actually, its general corrosion behavior in the above conditions compares favorably with that of type 347 stainless steel in similar reactor-related environments. Its susceptibility to stress-corrosion cracking, however, in chloride-containing reactor fuel solution appears to be analogous to that of type 347 stainless steel. Preliminary tests indicate also that the alloy possesses good antigalling properties.

REFERENCES

1. Reported in greater detail by J. C. Griess et al., Quar. Rep. of the Solution Corrosion Section for the Period Ending April 30, 1959, ORNL CF-59-4-44.

2. J. C. Griess et al., HRP Quar. Prog. Rep. Jan. 31, 1959, ORNL-2696, pp 81-83.

3. J. C. Griess et al., HRP Quar. Prog. Rep. Oct. 31, 1958, ORNL-2654, p 116.

4. J. C. Griess et al., HRP Quar. Prog. Rep. Jan. 31, 1959, ORNL-2696, p 84.

5. G. H. Jenks et al., HRP Quar. Prog. Rep. Oct. 31, 1953, ORNL-1658, p 71.

6. G. H. Jenks et al., HRP Quar. Prog. Rep. Jan. 31, 1959, ORNL-2696, pp 133-143.

7. J. C. Griess et al., HRP Quar. Prog. Rep. Jan. 31, 1959, ORNL-2696, pp 84-86.

8. J. C. Griess et al., Quar. Rep. of the Solution Materials Section, Jan. 31, 1959, ORNL CF-59-1-79, p 12.

9. J. C. Griess et al., HRP Quar. Prog. Rep. July 31, 1954, ORNL-1772, p 79.

10. J. C. Griess et al., HRP Quar. Prog. Rep. April 30, 1957, ORNL-2331, p 89.

11. N. D. Tomashoff, Corrosion 14, 229t-236t (1958).

12. Boiling Nitric Acid Test for Corrosion-Resisting Steels, ASTM Designation A262-55T, ASTM Standards, Part I, Ferrous Metals, 1955, pp 1108-1112.

13. Modified Type 347 Austenitic Stainless Steel Material, HRP Specification No. 200a, Mar. 21, 1957, p 3.

14. J. C. Griess et al., HRP Quar. Prog. Rep. Oct. 31, 1958, ORNL-2654, pp 120-121.

15. J. C. Griess et al., HRP Quar. Prog. Rep. Jan. 31, 1959, ORNL-2696, pp 90-91.

14. SLURRY CORROSION

E. L. Compere H. C. Savage

J. M. Baker D. T. Jones S. A. Reed
S. E. Bolt R. A. Lorenz L. Rice
V. A. DeCarlo A. R. Olsen W. C. Ulrich
R. B. Gallaher L. F. Woo

14.1 PUMP LOOPS

14.1.1 Introduction to Pump-Loop Tests

Three 100A-loop tests were completed during the report period to determine the corrosion-erosion attack and handling properties of slurries of ThO_2 and mixed ThO_2-UO_3. One test was made at 280°C with a D_2O slurry of a 650°C-calcined, 0.8-μ thoria preparation, with additions of $UO_3 \cdot H_2O$ and Pd-metal recombination catalyst, which was proposed for use in the slurry in-pile loop program. The other two tests were made at 200°C with hydrogenated slurries of 1600°C-calcined, 1.8-μ thoria, and admixed $UO_3 \cdot H_2O$ to determine the effect of the addition of UO_3 on the attack of a group of selected alloys.

A fourth test was made at 175°C with an oxygenated slurry of thoria microspheres.

14.1.2 Circulation of D_2O Slurries of ThO_2-UO_3 Mixtures Using Atmospheres of Argon and Oxygen

Run BS-25.--Run BS-25, which was initiated during the previous quarter,[1] was conducted to evaluate a D_2O slurry of mixed ThO_2-UO_3 that was proposed for possible use in the slurry in-pile loop program. The test employed a slurry of 650°C-calcined thoria of 0.8-μ mean particle size to which was added approximately 0.5% U/Th (as $UO_3 \cdot H_2O$) and 0.001 *m* Pd-metal recombination catalyst. The thoria and catalyst preparations were furnished by the PAR Project.[1-3]

The run, which was made at 280°C, consisted of an initial operational period of 508 hr with an argon atmosphere in the test loop, followed by a second 528-hr period of circulation with an oxygen overpressure. Data for the test are summarized in Table 14.1.

Catalyst activities of samples withdrawn from the loop during the run were determined in the Chemical Technology Division laboratory. Results of these tests are reported in Sec. 19.2 of this report.

A description of the slurry preparation and of the operational variables during the first phase of the test was reported last quarter.[1,2]

Table 14.1. Synopsis of Run BS-25

Test temperature: 280°C
Pipeline flow velocity: 4.5 fps
Batch LCC-29108 ThO_2, 650°C-calcined, 0.8 μ (σ = 1.42)

	First Phase		Second Phase		Total Run	
Circulation time (hr)	508		528		1036	
Atmosphere (std cc per liter of slurry)	Ar (D_2, 35)[a]		O_2 (446)			
Average concentration (g of Th per kg of D_2O)						
Inventory	454		425		439	
Circulating	427		378		402	
Additives ($m \times 10^3$)						
Uranium	9.3 - 10.5		9.0 - 10.2		9.8	
Palladium	0.6 - 1.0		0.4 - 0.6		0.6	
Yield stress, τ_y (lb/ft^2, room temperature)	0.12[b]		0.06[b]			
Modulus of rigidity, η (centipoise, room temp.)	1.77[b]		1.72[b]			
pH of slurry (room temperature)	4.3 - 8.3		6.3 - 7.4			
Specimen attack rates, mpy	20 fps[c]	40 fps[c]	20 fps[c]	40 fps[c]	20 fps[d]	40 fps[d]
Type 347 stainless steel	0.6	3.2	1.2	7.2	1.1	5.4
CD4MCu stainless steel (cast)	0.5	4.8	1.3	8.5	1.0	6.8
Type 430 stainless steel	2.2	11	2.7	10	2.8	11
Croloy 2 1/4	14	140	1.1	22	9.7	96
Croloy 5	5.6	47	1.6	19	5.3	40
Incoloy	0.2	1.7	1.1	6.5	0.7	4.3
Inconel	<0.1	0.6	13	22	7.8	14
Ti-RC55	0.3	0.3	0.7	4.3	0.5	2.4
Zircaloy-2	0.5	2.3	0.2	1.6	0.3	2.0
Platinum	<0.1	<0.1	0.1	2.0	<0.1	1.0

(a) Generated during run.
(b) At 500 g of Th per kg of D_2O, room temperature, unpumped slurry, τ_y = 0.20 lb/ft^2, η = 1.48 centipoise.
(c) Undefilmed.
(d) Defilmed.

Based on analytical chemical data for samples withdrawn from the test loop during the first phase of the run, the mean 508-hr circulating slurry concentration was 427 g of Th per kg of D_2O, and average U and Pd concentrations were 0.01 *m* and 0.0008 *m*, respectively. During the second phase of the run, the mean circulating concentration was 378 g of Th per kg of D_2O, with 0.01 *m* U and 0.0005 *m* Pd.

(a) Uranium Redox.--During circulation of the slurry in the first phase of the test (argon atmosphere), deuterium was generated as a by-product of corrosion of the austenitic stainless steel loop system. Gas analyses of samples taken periodically from the loop were used as a means of following the increase of D_2 in the slurry as the run progressed. At the conclusion of the 508-hr test period, the D_2 concentration in the slurry was 35 std cc of D_2 per liter of slurry. The slurry charged to the system contained 42.3 g of U^{+6} (54 g of $UO_3 \cdot H_2O$); at the end of the 508-hr period the uranium was determined by chemical analysis to have been completely reduced to U^{+4}. It was attempted to follow the U^{+4}/U^{+6} ratios during the test to establish a reduction rate for the uranium; however, reliable analytical methods for the determination of U^{+4} in the slurry were not available until late in the run. Also, the reduced uranium was readily reoxidized to U^{+6} when the slurry was exposed to the atmosphere at room temperature. Using chemical data selected as most reliable, the uranium appeared to have been completely reduced after ~175 hr of circulation.

The slurry removed from the loop at the conclusion of the first period of the run was stored in a container exposed to the atmosphere for 12 days before it was recharged in the second phase of the test. The U^{+4} was completely oxidized to U^{+6} during this period.

(b) Slurry Properties.--With the exception of the periods during which dropout tests were being conducted, the flow velocity in the 1 1/2-in. piping of the test loop was maintained at 4.5 fps. The system was initially charged to a concentration of 454 g of Th per kg of D_2O for the first phase of the run. A gradual loss of circulating solids was observed during the course of the 500-hr circulation period. The concentration of a sample taken just before dropout tests were begun was 402 g of Th per kg of D_2O. Based on that value, 0.8 kg of Th out of a total of 7.3 kg was not being circulated. After the dropout tests, the circulating solids were removed from the loop with a 0.4-in. hydroclone using induced underflow while the system was operated at 280°C and approximately 1100 psi pressure. The loop was subsequently drained and rinsed four times, after which no deposits were noted in the system.

The material balance on the system was reported earlier[1] to have been 90% after the hydroclone operation; this was essentially the case after the hydrocloning and rinsing were completed. Based on weight and volume measurements on slurry, the material balance on the system was as follows: loaded, 8.3 kg of Th; removed as samples, 1.9 kg; removed by hydroclone, 3.6 kg; removed by rinses, 2.0 kg; residual-and-error, 0.8 kg. Half or more of the residual-and-error may be attributed to volumetric errors due to gas bubbles in the slurry. This would not affect the loading quantities, but would affect the removal values. A variation averaging 4% has been regularly observed between concentrations determined on the same samples by weight-volume measurements and by chemical analysis and would serve to increase all removal values in proportion.

For the second phase of the run the loop was charged in two steps to a concentration of 425 g of Th per kg of D_2O. The first charge, which was made in a routine manner, contained 5.5 kg of solids which had been recovered from the loop after the first phase of the run. The second charge was a mixture of

unpumped ThO_2, $UO_3 \cdot H_2O$, and Pd catalyst. As had been experienced during the initial loading of the system,[1] the 3/8-in. tubing connecting the system addition tank to the loop was plugged intermittently with solids. As a result, the target concentration was not attained until 95 hr of pumping time had elapsed.

A gradual loss of circulating solids was also noted during the second phase of the run, in which an oxygen atmosphere was used. The concentration of the final sample taken from the loop prior to dropout tests was 354 g of Th per kg of D_2O, which indicated a loss of 1.5 kg of ThO_2 from the circulating stream. By hydrocloning, 83% of the charged solids was removed from the stream. A total of 99.5% of the solids was recovered by additional rinses with water at room temperature. When the loop was opened, a uniform, solid cake up to ~1/8 in. thick was found in the pump discharge line, and a small amount of lumpy sludge remained in the pump suction line. The pump cavity and impeller were free of solids. The deposit was removed by circulating a 5% solution of HNO_3 in the system for 2 hr at room temperature; this dissolved the uranium and resuspended the thoria. The U/Th ratio in the deposits was approximately the same as that of the slurry.

(c) Dropout Tests.--Results of the dropout tests with the oxygenated slurry essentially duplicated those reported[1] for the first phase of the test using an argon atmosphere.

The slurry velocity in the loop was reduced from 4.5 fps by 1-fps increments by means of a motor-generator set to control the pump speed to determine the minimum flow velocity required to keep the solids in suspension. At a velocity of 2.5 fps, ~15% of the solids were lost from the circulating stream in 1 hr. After the velocity was again increased to 4.5 fps, 2 hr of circulation was required to completely resuspend them, based on half-hour samples.

(d) Slurry Rheological Properties and Settling Rates.--Data are presented in Table 14.1 which show the changes in rheological properties of the slurry as a result of circulation during the two phases of the test. The values were computed from data obtained at room temperature with a capillary-tube viscometer. A plot of the settling rates of the slurry as a function of temperature is shown in Fig. 14.1.

At a concentration of 500 g of Th per kg of D_2O the yield stress of a slurry of the unpumped ThO_2-$UO_3 \cdot H_2O$-Pd catalyst mixture was 0.20 lb/ft^2. After the first phase of the run the yield stress of the slurry at this concentration was found to be 0.12 lb/ft^2, and after the second phase it had diminished to 0.06 lb/ft^2.

A normal decrease in settling rates occurred after the slurry was pumped in the initial phase of the test, but no significant changes in rates occurred as a result of circulation in the oxygen atmosphere.

As noted previously, the uranium in the slurry was readily oxidized on exposure to air. Both viscometer and settling-rate measurements were made in the laboratory under ambient conditions. It is not known whether the valence state of uranium changed during some of the above measurements and, if so, what effect the valence state would have on the rheological properties of the slurry.

(e) Corrosion-Erosion: Loop.--Attack rates of the type 347 stainless steel loop components and of the titanium pump scroll and thermal barrier were calculated during run BS-25 from the corrosion products detected by chemical analysis

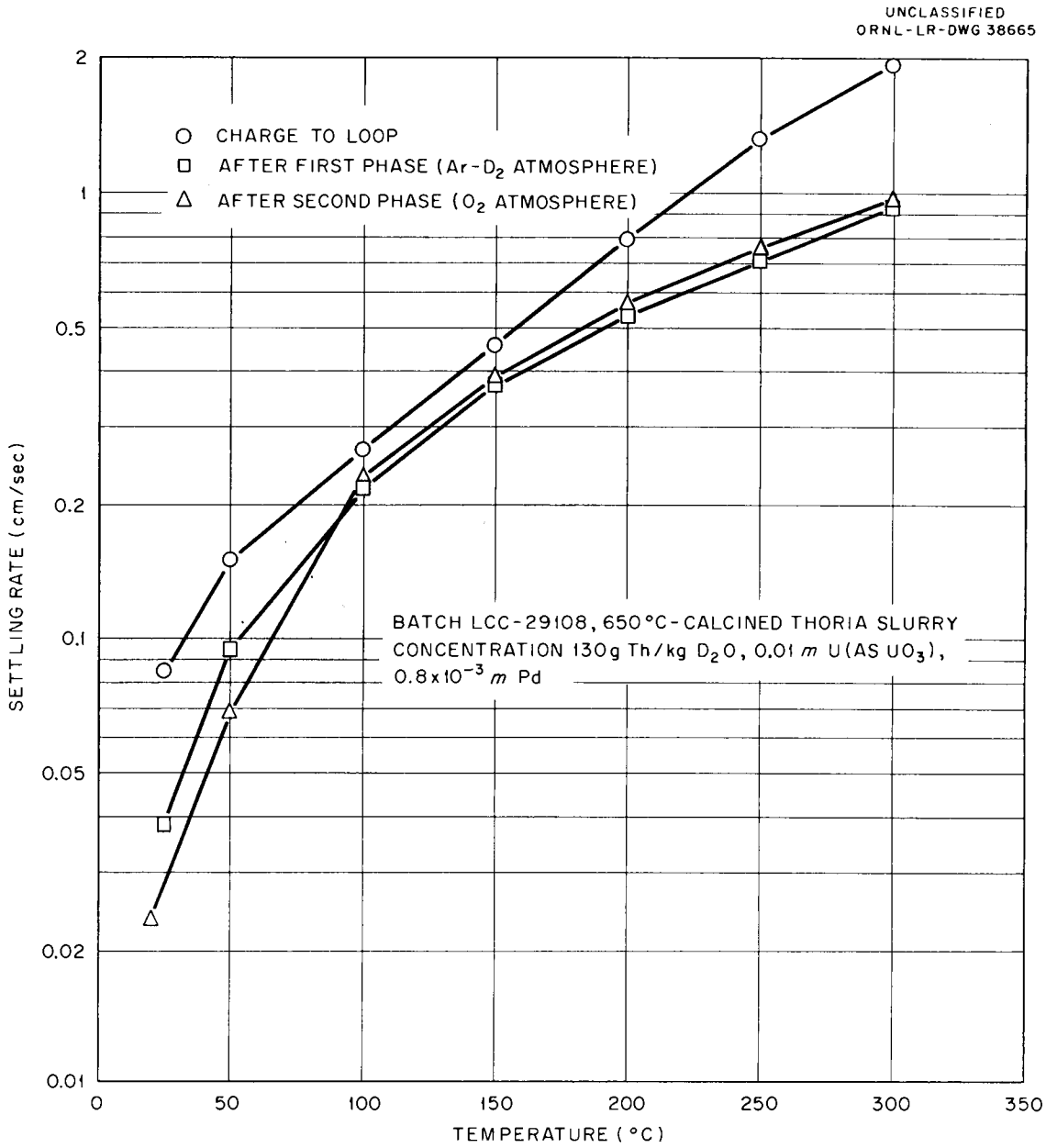

Fig. 14.1. Settling Rates of Slurry Circulated in Loop Test BS-25.

in slurry samples withdrawn from the system. The mean stainless steel corrosion rate for the 528-hr period with an oxygen atmosphere was 1.7 mpy, compared with 0.9 mpy for the 508-hr period with Ar-D_2 atmosphere. The type 347 stainless steel impeller in the circulating pump lost 17 g during the entire test (1036 hr), which accounted for 55% of the corrosion products in the slurry. This was prorated between the two test periods on the basis of specimen attack data in them and was subtracted from gross corrosion-product pickup in the slurry. On this basis, the estimated attack rates on the loop piping during the first and second phases of the run were 0.4 and 0.8 mpy, respectively.

The scroll and thermal barrier of the circulating pump used in run BS-25 were fabricated of titanium. No titanium was detected by chemical analysis during the first portion of the run (argon atmosphere) nor during the first 334-hr period of the second phase of the test (oxygen atmosphere). However, during the last 194 hr of the run, titanium was detected in the slurry. The computed attack rate of titanium in the pump during the 528-hr test was 8.5 mpy.

(f) Corrosion-Erosion: Specimens.--Attack rates of pin-type corrosion specimens exposed during run BS-25 are shown in Table 14.1. The majority of specimens were carried through both phases of the run. One specimen of type 347 stainless steel was removed from each array after the first test period and a new specimen of the same material was exposed in each array during the second test period. The attack rates of these pins, computed from defilmed weight losses, were at 20 and 40 fps, respectively, 0.8 and 4 mpy during the first test period, and 1.3 and 8.5 mpy during the second period.

The other specimens in the arrays were weighed without defilming after the first test period and then reinserted into the loop for additional exposure. Mean 1036-hr attack rates were computed from defilmed weight changes of the specimens.

Type 347 and cast CD4MCu stainless steels, Incoloy, Inconel, and titanium-RC55 were more severely attacked by oxygenated slurry (the second phase of the test). In contrast, Croloys 2 1/4 and 5 and Zircaloy-2 displayed lower rates in the oxygenated slurry. Type 430 stainless steel was attacked at about the same rate in both atmospheres. Except for Inconel and the Croloy alloys, the mean 1036-hr attack rates of the specimens ranged from <0.1 to 2.8 mpy at 20 fps, and from 1 to 11 mpy at 40 fps. Titanium and Zircaloy-2 were the least severely attacked of the alloys exposed.

A number of the effects noted above indicate less severe attack under hydrogen atmosphere, which is not in these cases consistent with results in various other tests. No explanation is asserted; however, the above tests were unique in that the slurry contained some Pd recombination catalyst and are the only loop tests which used PAR, 650°C-calcined, long-digested thoria.

14.1.3 Circulation of a Slurry of Thoria Microspheres

Run CS-47.--A second loop test completed during the quarter circulated an oxygenated slurry of an experimental preparation of thoria microspheres. The spheres, obtained through the Chemical Technology Division from the Houdry Process Corporation, were prepared from a quick-setting thoria gel by programmed drying and final calcination at 1000°C.[4] The original lot of microspheres ranged in size from 3 to 150 μ. A portion of the spheres, in the size range 3 to 30 μ, was separated from the original preparation by gravitational sedimentation. The separated fraction was not closely sized, and no effort at classification according to shape was made. The mean size of the spheres was 12 μ; however, 20% by weight of the batch was less than 7 μ, and 8% of the material was less than 3 μ and was not spherical in shape.

(a) Slurry Properties During Loading and Operation.--Because the material settled rapidly and subsequently formed a highly compacted bed (~2000 g of ThO_2 per liter) in the equipment which is used to charge the loop while it circulates water at temperature and pressure, a slurry of the microspheres was injected into the test loop at room temperature. After charging oxygen to the loop the system was preheated to approximately 175°C, and the circulating pump was turned on. The spheres, which had been allowed to settle in the loop during the 30-min preheating period, were easily suspended.

The loop inventory concentration was 320 g of Th per kg of H_2O. The loop was operated under steam pressurization with a static water leg in the pressurizer. The circulating slurry concentration in the loop was followed during the course of the run from chemical analyses of samples withdrawn from the loop in the usual manner.

After the slurry had been circulated satisfactorily for 96 hr, the pump was stopped for 30 min. When circulation was resumed, all but approximately 10% of the spheres were resuspended. By means of a motor-generator set the pump was then run at a higher speed to increase the flow velocity in the loop piping (1 1/2-in. ID) from 6.5 to 9 fps. After 72 hr of circulation at the higher velocity, the solids were completely resuspended.

As pumping continued, the slurry became more flocculated as indicated by more pronounced hindered-settling properties, and the interface of the slurry solids, which was detected by G-M survey meter scans, slowly rose in the static, vertical loop pressurizer. As a result, the circulating slurry concentration in the loop slowly diminished to 196 g of Th per kg of H_2O.

The test was terminated after 553 hr of circulation at 175°C and ~1000 psi pressure by removing the spheres from the loop with a 0.4-in. hydroclone. Ninety-eight per cent of the thoria was recovered from the system. The mean circulating slurry concentration during the test was 295 g of Th per kg of H_2O. The pH of the slurry, measured at room temperature, varied without trend from 6.7 to 8.2.

A portion of each sample was submitted for particle-size distribution analysis and was also examined by using an optical microscope to determine the integrity of the microspheres. Little change in particle-size distribution was observed. However, due to the high percentage of nonspherical fines in the original charge to the loop, mild attrition of the spheres would not have been detected. By microscopic examination the spheres appeared to have been little affected by the pumping. An occasional chipped or broken sphere was seen, but apparently in no greater number than in the original charge material.

When the system was opened, thin films of thoria were found on the walls of the loop piping, and about 2 to 5 g of material was caked on each of two of the vanes of the impeller in the circulating pump.

The deposits were attributed to the fine particle fraction of the charge material rather than to degradation of the spheres. It is known that the fine fraction of the preparation was contaminated by nitrogen-containing impurities.[5] The spherical material in the batch had a very low specific surface area, 0.3 m^2/g, and none of the corrosion products from the loop adhered to them. All the corrosion products were associated with the fines of the slurry. The corrosion ion concentration in the deposits, inferred to have been composed of nonspherical material, was a factor of 10 higher than in the circulating slurry.

(b) Corrosion-Erosion.--The type 347 stainless steel impeller used during the 553-hr test lost 1 g. At the pump speeds used, the peripheral velocity of the impeller was 71 to 102 fps. The total corrosion-product pickup during the run was 5 g. The generalized attack rate of the stainless steel components in the loop, including the impeller, was 0.4 mpy.

One set each of coupon- and pin-type corrosion specimens was exposed in the main line of the loop during run CS-47. As a result of changing the pump speed, flow velocities past the coupons varied from 26 to 37 fps and past the pins from 18 to 26 fps; respective mean velocities were 32 and 22 fps. At 32 fps the following attack rates for coupon specimens were observed:

	mpy		mpy
Stainless steel		Alloy steel	
Type 347	0.2	Croloy 5	2.0-2.2
Cast CD4MCu*	0.1	Croloy 9M	0.2
USS Corex*	0.2	Incoloy	0.3
Type 431	0.2	Titanium-75A	0.0
Type 446	0.2	Zircaloy-2	0.0

* CD4MCu: 5 Ni, 25 Cr, 2 Mo, 3 Cu, bal. Fe
USS Corex: 25 Ni, 17 Cr, 1.2 Mo, 1.5 Mn, bal. Fe

At 22 fps, rates of pin specimens, which were exposed to more turbulent flow, were as follows:

	mpy		mpy
Stainless steel		Incoloy	0.5
Type 347	0.2-0.3	Inconel	5.0
17-4 PH	0.3	Gold	8.0
Type 414	0.5	Pt - 5% Ir	0.3
Type 440C	1.1	Titanium-RC55	0.0
Alloy steel		Zircaloy-2	0-0.1
Croloy 5	3.5		

In general, the levels of attack indicated above are comparatively mild. Noteworthy, however, are increased rates of attack on pin specimens which, although at the lower velocity, were of a geometry permitting impingement and considerably greater turbulence. Thus with such slurries geometry effects appear to be as important as pure velocity effects.

14.1.4 Materials Evaluation Tests Using ThO_2 and Mixtures with UO_3 at 200°C Under D_2 or O_2

Two additional runs were completed during the report period which were part of a series of tests being conducted to study the effects of hydrogen and oxygen atmospheres and of the addition of UO_3 on the corrosion-erosion attack of materials by circulating aqueous ThO_2 slurries. The test series, which was initiated during the previous quarter,[6] is being made at 200°C with a prepumped slurry of 1600°C-calcined, 1.8-μ thoria at a nominal circulating concentration of 500 g of Th per kg of H_2O.

In two tests (ES-7 and -8) which were reported[6] last quarter, slurries of ThO_2 and ThO_2-UO_3 (7.8% U/Th) were circulated using oxygen atmospheres. Similar tests, runs ES-9 and -10, using hydrogen atmospheres were made during the current quarter. Data for the four runs are summarized in Table 14.2.

Table 14.2. Summary of Materials Evaluation Tests

Batch DT-9 ThO_2, 1600°C-Calcined, 1.8-μ Mean Particle Size, Prepumped
Test Temperature: 200°C

Run Number	ES-7				ES-8				ES-9				ES-10			
Circulation hours	334				306				310				338			
Avg circulating conc, g Th/kg H_2O	505				522				581				510			
U (as $UO_3 \cdot H_2O$), *m*	None				0.15				0.20				None			
Atmosphere (std cc/liter slurry)	O_2 (1085)				O_2 (1634)				H_2 (288)				H_2 (496)			
pH of slurry[a]	5 - 6				5 - 6				7 - 10				9 - 10			
Loop attack rate, mpy	0.7				0.8				5.1				0.6			
Flow velocity, fps	10	20	30	50	10	20	30	50	10	20	30	50	10	20	30	50
Specimen attack rate, mpy																
Type 347 SS, pins	0.1	0.1	0.1	1.3	0.1	0.1	0.4	0.6	0.1	0.2	0.9	43	0.1	0.1	0.1	1.6
Type 430 SS, pins	<0.1	0.1	0.1	0.3	<0.1	0.2	0.4	1.2	0.2	0.5	0.9	18	0.3	0.5	0.6	1.2
Type 431 SS, pins	0.1	<0.1	0.1	0.6	0.3	0.3	0.5	1.6	0.2	0.4	1.0	44	0.4	0.6	0.6	4.7
Type 440C SS, pins	0.4	0.4	0.3	0.7	0.5	0.8	0.9	2.0	0.6	1.1	1.8	37	1.2	1.4	1.5	3.0
Type 446 SS, pins	0.2	0.2	0.5	1.7	0.1	0.3	0.7	2.9	0	0.2	0.7	8	<0.1	0.1	0.2	3.7
17-4 PH SS, pins	0.1	0.1	0.1	0.5	0.1	0.1	0.5	1.7	0.2	0.4	1.5	85	0.1	0.1	0.7	9.0
Incoloy, pins	0.1	0.1	0.4	1.9	0.2	0.2	0.9	5.5	0.1	0.1	1.0	37	0	<0.1	<0.1	0.7
Inconel, pins	11	7.8	7.6	9.9	1.1	1.3	1.5	7.1	<0.1	0.1	1.9	43	0.2	0.1	0.2	0.3
Hastelloy B, pins	4.6	0.3	5.8	30	13	16	164	596	65	188	962	>1600	8.5	9.2	19	14
Hastelloy C, pins	13	7.6	5.9	15	1.9	2.1	3.6	18	0.3	0.6	5.6	55	<0.1	0.2	<0.1	0.5
Haynes Alloy 25,[b] pins	13	9.0	6.9	15	2.0	2.0	3.2	11	0.2	0.4	2.5	33	0.1	0.2	0.3	1.0
Platinum, pins	<0.1	0.1	0.1	1.8	<0.1	0.2	0.8	8.2	<0.1	0	0	0	0	<0.1	<0.1	0.2
Gold, pins	<0.1	<0.1	0.1	0.7	<0.1	0.1	2.9	19	0	0	0	0	0	0	0	0
Croloy 1/2, coupons	0.7				2.7				1.4				10			
Croloy 1, coupons	0.6				2.2				1.2				10			
Croloy 2, coupons	0.4				1.5				1.1				8.6			
Croloy 3M, coupons	0.3				1.5				1.0				8.1			
Croloy 5, coupons	0.2				0.7				0.9				7.1			
Croloy 5 Si, coupons	0.2				1.0				1.2				7.1			
Croloy 7, coupons	0.1				0.5				0.9				4.5			
Croloy 9M, coupons	0.1				0.4				0.7				1.2			

(a) Measured at room temperature.
(b) Haynes alloy 25: Co, 15 W, 10 Ni, 20 Cr, 2.5 Fe, 1 Si, 1.5 Mn.

Run ES-9

(a) Operation.--For run ES-9 the test loop was charged to a concentration of 527 g of Th per kg of H_2O with the addition of a sufficient quantity of $UO_3 \cdot H_2O$ (rods) to provide 8.5% U/Th. Hydrogen was injected into the system to provide a concentration of 400 std cc of H_2 per liter of slurry.

In general, conditions of operation of the test were very erratic. A building power outage stopped the circulating pump after 18.2 hr of circulation. After that time, analyses for determining the hydrogen concentration in the slurry varied markedly. At slurry circulation hour 118, analyses indicated that there was no hydrogen in the system, although loop pressure instruments did not corroborate this. Because gas concentrations were uncertain at this time and in order to assure an adequate hydrogen atmosphere, two additional injections of hydrogen were made during the run.

The run was terminated as scheduled after a total of 310.4 hr of slurry circulation at an average slurry concentration of 581 g of Th per kg of H_2O. The test was concluded by removing solids from the system with a hydroclone. Approximately 58% of the solids inventory was removed from the loop during two 1-hr periods of hydrocloning. The residual slurry, up to a total of 94% of the solids inventory, was recovered from the loop by circulating rinses before the loop was opened.

(b) Deposits and Removal.--Postrun inspection of the system showed thin, hard films of solids coating most of the loop piping, and cakes 1/4 in. thick were found immediately downstream of the specimen holders in both sections of the loop. A lumpy sludge lay in the bottom of the loop piping. The pump thermal barrier was coated with a hard, glossy black film. Chemical analyses of the sludge and deposits from the loop (not including the thermal barrier) indicated that, other than iron, the ratios (by weight) of U and corrosion products (Ni, Al, Zr, and Cr ions) to thorium were the same as had been determined in slurry drained from the loop. The Fe/Th ratio was a factor of 2 higher. However, the U/Th ratio of the deposit from the thermal barrier was 0.92, and the Fe/Th ratio was 0.84. X-ray diffraction analyses of that deposit have not been completed. In order to remove the deposits, 5% HNO_3 was circulated for 2 hr at room temperature. This removed residues in the piping and a portion of the deposit on the pump thermal barrier. The remainder of the material on the thermal barrier was chipped off.

Run ES-10

(a) Operation.--In run ES-10, the comparison test to run ES-9, thoria slurry without UO_3 was circulated in a routine manner. The 338-hr test was made at an average circulating concentration of 510 g of Th per kg of H_2O and 496 std cc of H_2 per liter of slurry.

(b) Corrosion-Erosion, ES-9 and ES-10.--The cast Zircaloy-2 impeller lost 2 g during run ES-9 and 1 g during run ES-10; the generalized attack rates of the stainless steel components of the loop were 5 and 0.6 mpy for the respective runs.

Runs ES-9 and ES-10 compare the effect under hydrogen atmospheres of $UO_3 \cdot H_2O$ addition to thoria slurries. Some erratic operational behavior in run ES-9 has been noted above. However, except for higher attack rates on alloy steels in run ES-10, without added uranium, attack rates were generally slightly lower than in run ES-9, to which uranium was added. At 50 fps rates were generally considerably increased in run ES-9.

With oxygen atmospheres no significant difference in attack rates was noted between run ES-8 (slurry containing $UO_3 \cdot H_2O$) and run ES-7 (no uranium).

It is noteworthy, despite the high attack rates in run ES-9, that the alloy steels responded in a like manner in the four runs of this series. Regardless of atmosphere, pH, or uranium additive, their relative resistance to corrosion generally increases with increasing chromium content of the alloy, in a fashion given by:

$$\log R/R_o = - k\ Cr^{1/2}.$$

In this expression, R is the corrosion rate of a given alloy in the test in question. However, as is shown in Fig. 14.2, the dependence of attack rate on chromium content is much less pronounced under hydrogen atmosphere than under oxygen atmosphere.

A comparison of the attack data shown in Table 14.2 reveals that the stainless steel alloys, with the exception of type 347, generally displayed a normal dependence on flow velocity over the range 10 to 50 fps and were attacked at rates approximately 5 to 6 times higher under hydrogen atmosphere than under oxygen atmosphere. A mild increase in attack by the inclusion of UO_3 in the slurry is indicated. The attack of type 347 stainless steel was least affected by changes in atmosphere or velocity, or by the addition of uranium. Incoloy displayed a normal velocity dependence but was attacked less severely under hydrogen atmosphere.

Rates of Inconel and Hastelloy alloys were about a factor of 10 lower in the hydrogenated slurries. Of the nickel-base alloys tested, Hastelloy B was the most severely attacked at all test conditions.

14.2 TOROIDS

14.2.1 Evaluation of Slurries for the Slurry In-Pile Loop Program

As part of the program to evaluate slurries for possible use in an in-pile slurry loop, six toroid tests were completed recently with a 650°C-calcined, 0.8-μ thoria preparation furnished by the PAR Project.[1] Slurries to which were added $UO_3 \cdot H_2O$ rods at levels of 0.5 and 3% U/total solids and 0.001 *m* Pd were circulated at 26 fps and 280°C, at a concentration of 450 g of Th-U per kg of D_2O, in 300-hr tests using atmospheres of deuterium, oxygen, and argon.

A summary of the tests and the results of an examination of the attack data by a factor analysis method are presented in Table 14.3.

There was a substantial difference in the response of the various metals, but the factors for the metals are generally consistent with those previously reported for oxygen and deuterium systems.[7] The normalized rate for type 347 stainless steel pins under reference test conditions (oxygen, with the 0.5% added U) was 4 mpy. This value is slightly lower than ordinary and indicates that this thoria preparation is not particularly aggressive. The average susceptibility of the various metals to attack, relative to type 347 stainless steel pins under the reference condition, was: type 347 stainless steel pins, 1.0; 347 stainless steel toroid piping, 0.2; Ti-75A, 1.4; Zircaloy-2, 0.5; and Inconel under oxygen, 9; while Inconel under D_2 or Ar was 0.7. Not including the Inconel data, the effects of D_2 or Ar on the metals were to increase corrosion by average factors of 2.5 and 1.5, respectively, relative to tests with oxygen atmosphere. On the average, increasing the uranium content to 3% U/Th reduced the rate to 70% of the value for the 0.5% U/Th tests.

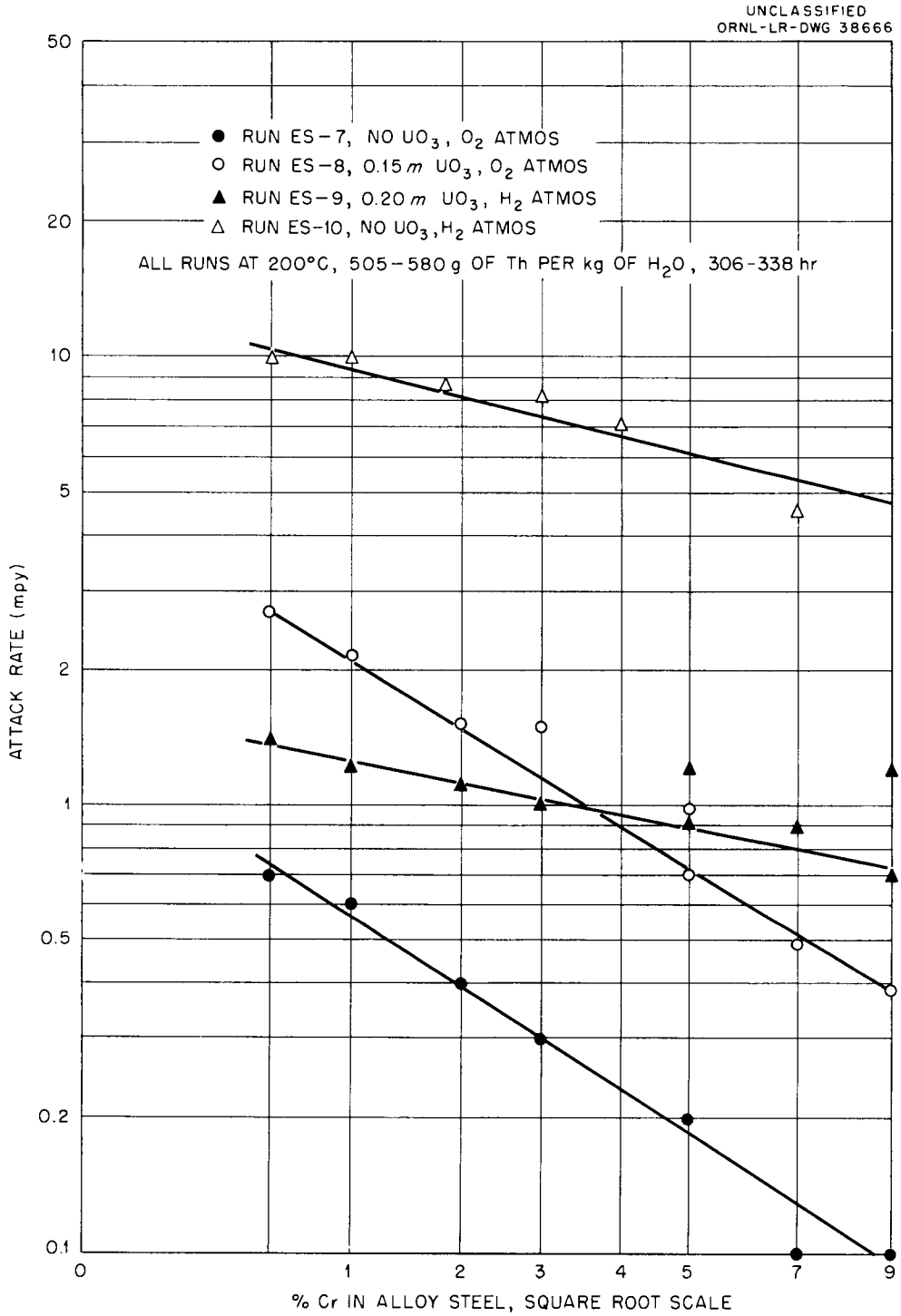

Fig. 14.2. Effect of Chromium Content of Alloy Steel on Slurry Corrosion at 200°C.

Table 14.3. Results of Toroid Tests of Material Obtained from the PAR Project

Time: 300 hr
Velocity: 26 fps
Concentration: 450 g of Th-U per kg of D_2O
Temperature: 280°C
Calcination Temperature: 650°C
Additive, Pd: 0.001 *m*

Per Cent U/Th Added as $UO_3 \cdot H_2O$	Atmosphere	Attack Rate* (mpy)					Slurry pH, Postrun	Average Particle Size (μ)	
		Toroid (347 SS)	347 SS	Ti-75A	Inconel	Zircaloy-2		Prerun	Postrun
0.5	O_2	0.6	4.3	5.7	36	2.2	7.4	0.8	0.7
0.5	D_2	0.5	30	21	2.4	5.3	-	0.8	0.7
0.5	Ar	1.6	11	8.6	1.7	2.0	7.8	0.8	1.1
3.0	O_2	0.8	2.6	3.9	25	1.3	6.6	0.8	1.0
3.0	D_2	1.9	8.0	4.6	1.8	0.9	7.7	0.8	1.1
3.0	Ar	0.8	5.6	5.9	3.5	1.1	7.2	0.8	1.5

Statistical Analysis into Multiplicative Factors
(The normalized rate of type 347 stainless steel pins under oxygen, with the 0.5% added U slurry, was 4 mpy.)

Average Effect of Major Variables

Metal	Relative Factor	% U	Relative Factor	Atmosphere	Relative Factors for Given Metal				
					347 SS	347 SS (piping)	Ti-75A	Zircaloy-2	Inconel
347 SS piping	0.2	0.5	1.0	O_2	1	1	1	1	1
347 SS	1.0	3.0	0.7	D_2	5	1.5	2	1.5	0.1
Ti-75A	1.4			Ar	2	1.5	1.5	0.9	0.1
Zircaloy-2	0.5								
Inconel	9.0								
Inconel (under D_2 and Ar)	0.7								

* Corrected for slug flow.

14.2.2 Tests with Slurries of Thorium-Uranium Oxide

Data for the initial series of tests with mixed Th-U oxide fuel slurries were reported last quarter.[7] The test series has been continued with slurries of batch MO-39 mixed oxide (8.8% U/Th, calcined at 1050°C), which was produced in the Chemical Technology Division pilot plant. Recent conditions and results of the test series are presented in Table 14.4.

It has been reported[8] that one factor contributing to the dissociation of uranium from mixed Th-U oxide preparations at elevated temperature might be the concentration of Cr^{+6} ions in the slurry. Therefore CrO_3 was added to several of the tests included in this series to determine its effect.

As shown in Table 14.5, the attack data of the series were resolved[9] into a table of the effects of different variables expressed as ratios relative to rates in a reference condition. This condition was selected as 280°C, 25 psi O_2, with no added CrO_3. The normalized rate for type 347 stainless steel pin specimens in this condition was 10 mpy, which is an ordinary value for many pure thoria slurries. However, normalized rates of Ti-75A and Zircaloy-2 were lower than ordinary. A general reduction in rate at 200°C was noted, the reference rates averaging about 40% of values at 280°C. Except for Inconel, rates for all materials increased substantially at 280°C under D_2 atmosphere, and higher D_2 pressures further increased the effect. Rates for Inconel were generally reduced under D_2. The effect of CrO_3 additive generally was to reduce the rates slightly, even under D_2 atmosphere.

No correlation between CrO_3 concentration and uranium dissolved in the supernatant was evidenced. No effect of temperature on the uranium content of the supernatant was indicated.

As indicated in Table 14.4, specimens of Zircaloy-2 exposed in two of the tests using deuterium underwent some deuteriding. The topic is discussed further in Sec. 14.2.3, which follows.

In general the attack by slurries of batch MO-39 pilot-plant oxide was higher than had been observed in previous tests[7] with experimental laboratory preparations of 650°C-calcined mixed oxides containing 5 to 33% U/Th which, however, had exhibited comparatively unaggressive properties.

14.2.3 Observation of Hydriding of Zirconium-Base Alloys

During the routine postrun microscopic examination of the pin corrosion specimens used in the tests with Th-U oxide fuel slurries (see Sec. 14.2.2), large longitudinal fissures or cracks were observed in and adjacent to the region of maximum attack on the upstream surface of one specimen of Zircaloy-2. The specimen had been exposed in a 300-hr test made at 280°C employing a deuterium atmosphere at 65 psia (room temperature) with a D_2O slurry of Th-8.8% U oxide (batch MO-39) containing 0.0017 *m* CrO_3. In a test at 200°C a second pin of the same heat of Zircaloy-2, which was exposed with a slurry of the same composition using the same overpressure of D_2, did not appear to be similarly attacked. The two specimens, along with an unexposed control specimen of the same heat of alloy, were submitted for detailed metallographic examination.

The examination[10] disclosed that the structure of the specimen exposed at 280°C had been grossly changed as a result of the formation of zirconium hydride or deuteride (the two are reported to be metallurgically identical).

Table 14.4. Attack by Slurries of Mixed Th-U Oxide

Time: 300 hr
Velocity: 26 fps
Concentration: 500 g of Th-U per kg of D_2O
Calcination Temperature: 1050°C (in air)
Batch MO-39: 8.8% U/Th

Temp. (°C)	Atmosphere (psia)	CrO_3 Molality	Attack Rate* (mpy)					Slurry pH, Postrun	Concentration of Ions in Supernatant Liquid (ppm)		Average Particle Size (μ)	
			Toroid (347 SS)	347 SS	Ti-75A	Inconel	Zr-2		Cr^{+6}	U	Prerun	Postrun
200	O_2 (50)	None	0.5	9.4	0.8	2.8	0.7	(a)	(a)	<8	3.7	2.7
200	O_2 (65)	None	0.5	3.3	0.8	6.6	0.7	(a)	(a)	<8	3.7	2.9
200	O_2 (65)	0.0017	0.1	2.5	1.0	6.3	0.5	(a)	(a)	<15	3.7	2.5
200	D_2 (65)	0.0017	0.5	12.0	0.6	0.5	0.4	(a)	(a)	<8	3.7	2.9
280	O_2 (65)	None	1.5	9.4	2.2	22	0.4	5.7	11 (c)	<2	3.7	3.5
280	O_2 (65)	0.0017	1.2	7.7	0.8	24	1.0	6.2	14 (c)	<2	3.7	3.1
280	O_2 (115)	0.015	1.5	6.1	4.6	29	WG	5.1	82 (c)	12	3.7	2.7
280	O_2 (25)	0.015	0.7	6.7	0.9	24	WG	9.9	<1	12	3.7	7.2
280	D_2 (65)	0.0017	7.3	150	50	20	9.2 (b)	10.4	(a)	(a)	3.7	10.7
280	D_2 (115)	0.015	3.3	57	38	11	5.3 (b)	5.7	36 (c)	6	3.7	2.5
280	D_2 (25)	0.015	0.7	28	3.8	3.4	3.8	8.2	<1	4	3.7	3.7

* Corrected for slug flow.

(a) Insufficient sample for determination.
(b) Pins hydrided (see Sec. 14.2.3).
(c) 0.001 *m* = 52 ppm Cr.

Table 14.5. Factors in Attack by Mixed Thoria-Urania Slurries

Average Effects of Major Variables Expressed as Ratios Relative to Rate in Reference Condition Based on Data from Table 14.4

Reference condition: 280°C, 25 psi O_2, no added Cr

Metal	347 SS Piping	347 SS Pin	Ti-75A Pin	Inconel Pin	Zircaloy-2 Pin	Geometric Mean Effect
Rate (normalized) in reference condition, mpy	1.3	1.0	1.2	25	0.4	-
Effect of variable expressed as ratio relative to rate in reference condition:						
Metal (347 SS pin)	0.12	1.0	0.11	2	0.03	-
Temperature (200/280)	0.14	0.4	0.7	0.2	1.8	0.4
Atmosphere D_2/O_2 at 280°C	2	9	13	0.4	25	5
at 200°C	2	5	0.6	0.08	0.8	0.8
Effect of Cr with O_2, 280°C	0.5	0.8	1.3	1.0	0.7	0.8
Effect of high Cr with O_2, 280°C	0.7	0.7	0.9	1.2	0.3	0.7
Effect of Cr with O_2, 200°C	0.8	0.8	0.4	1.1	3	0.9
Effect of high/low Cr with D_2, 280°C	0.2	0.3	0.2	0.3	0.5	0.3
O_2 pressure 280°C, 115/25 psi	2	0.8	5	1.2	1.0	1.6
D_2 pressure 280°C, 115/25 psi	5	2	10	3	1.4	3

Photographs of the specimen and of a transverse section of the specimen are shown in Figs. 14.3 and 14.4. The outer region, shown to the right in Fig. 14.4, was due to the conversion of the Zircaloy-2 base metal to the deuteride and showed a gradient of precipitated deuteride beneath it which decreased toward the interior of the pin. The region of maximum penetration (30 mils) occurred on the upstream side of the pin. Conversion of the base metal to deuteride tapered off to nil on the downstream side of the pin. It was postulated that the fissures resulted from a volume change which accompanies a conversion of the alloy to deuteride, rather than being the result of pitting or stress-corrosion cracking in the usual sense.

The specimen exposed in the 200°C test showed little or no increase in deuteride content over the control. Examination of the control specimen indicated that the H_2 content of the heat of Zircaloy-2 used was 100 ppm as estimated on the basis of visual comparison with a standard, and contained no unusual levels of other impurities.

Based on these findings, ten specimens from the same heat of Zircaloy-2 which were exposed in a previous series of similar tests[7] were re-examined for evidence of hydriding. The pins had been exposed to D_2O slurries of 650°C-calcined Th-U oxide preparations that contained from 5 to 33% U/Th which were also circulated in 300-hr tests at 280°C using overpressures of 1 atm of deuterium or 25 to 115 psia of oxygen. Hydriding was not detected on those specimens.

Since the hydriding of Zircaloy-2 in the present test was coincidental to the major study, a number of variables conceivably could have contributed to the phenomenon. Therefore a separate series of tests has now been initiated to ascertain the relative effects of temperature, deuterium overpressure, and oxide preparation on the hydriding of a number of zirconium alloy compositions. Preliminary microscopic examinations of specimens from the same heat and from one other heat of Zircaloy-2 which have been exposed in subsequent tests using six different preparations of Th-U oxides and atmospheres of D_2 ranging from 15 to 115 psia have indicated similar instances of hydriding. Currently the specimens are undergoing metallographic examinations.

14.3 CORROSION OF ALUMINUM OXIDE BY THORIA SLURRY*

Six commercial grades of aluminum oxide were corrosion tested in static, oxygenated thorium oxide slurry at 100 and 300°C. The materials are under consideration for use as check balls in valves for slurry service. The slurry used for the tests consisted of 300 g of ThO_2 (LO-37-1400) per 100 ml of water. Observed corrosion rates for 100- to 1000-hr periods are included in Table 14.6.

Five of the six oxides exhibited satisfactory corrosion resistance at 100°C; the 1000-hr rates were 1.2 mpy or less. The sixth material, P-3142, produced by the Diamonite Corporation, exhibited a 1000-hr corrosion rate of 7 mpy. In all cases, the rates remained constant or decreased with increased exposure periods.

Only one of the six materials, Alox, produced by the Thermal Refractory Company, showed promising corrosion resistance at 300°C. With one exception, observed corrosion rates for duplicate specimens after 100- and 300-hr intervals were 0.5 mpy. One of the specimens, however, showed a rate of 2 mpy after 300 hr. The 300-hr rates for the other five materials ranged from 7 to 23 mpy.

---

* This section contributed by J. C. Griess and P. D. Neumann.

UNCLASSIFIED
T-16690

Fig. 14.3. Fissures on Upstream Surface of Zircaloy-2 Toroid Specimen Exposed in Th-U Oxide Slurry Using D_2 Atmosphere. 10X

UNCLASSIFIED
T-16691

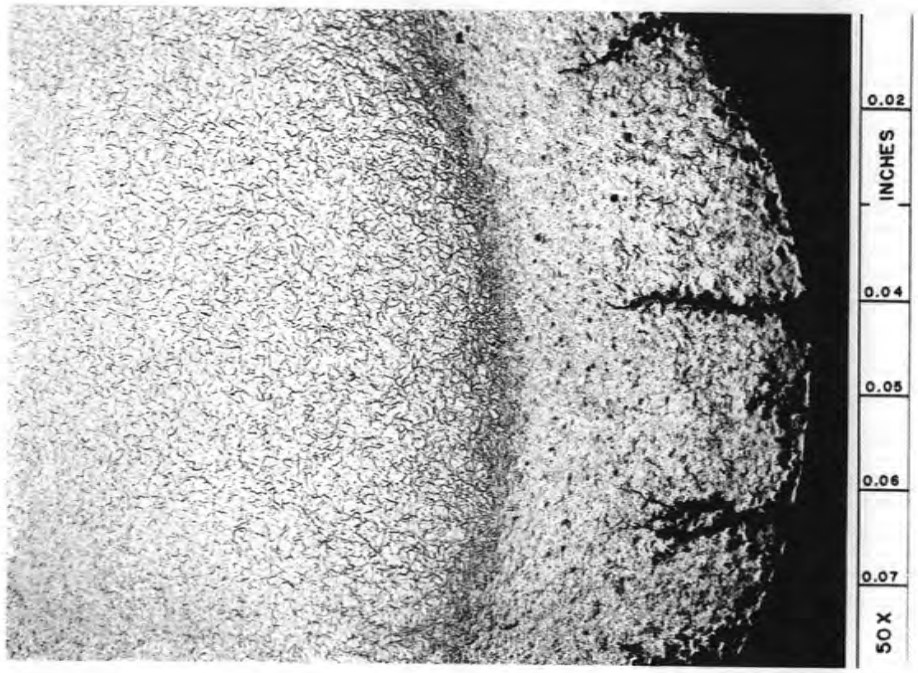

Fig. 14.4. Transverse Section of Zircaloy-2 Toroid Pin Showing Fissures and Deuteride Gradient. Bright field; etch: 46 HNO_3, 46 glycerin, and 8 HF. 50X

Three of the five materials showed increasing rates with time; the rates for the other two oxides either remained constant or decreased slightly with increased exposure time.

Table 14.6. Corrosion of Sintered Aluminum Oxide by Oxygenated Thoria Slurry* at 100 and 300°C

Supplier	Trade Name	% Al_2O_3	Corrosion Rate (mpy)			
			100°C		300°C	
			500 hr	1000 hr	100 hr	300 hr
American Lava Corporation	Alsimag 614	95	1.1	0.7	16	13
Centralab Corporation	4-948	85	1.9	1.2	5	7
Diamonite Corporation	P-3142	94.7	12	7	20, 30	23, 23
Frenchtown Corporation	95% Body	95	0.5	0.3	10	10
Thermal Refractory Company	Alox	99.6	0.2	0.2	0.5, 0.5	0.5, 2.0
Norton Company	LA-687	99	1.0	0.6	5, 20	10, 20

* 300 g of ThO_2 per 100 ml of H_2O.

In both the 100 and 300°C tests, there was no direct relation between the purity of the aluminum oxides and their observed corrosion behavior. Although the material produced by the Thermal Refractory Company, which showed the best over-all corrosion resistance, was the highest-purity product tested, there was no apparent correlation between purity and corrosion rate for the other materials.

14.4 IN-PILE AUTOCLAVE SLURRY CORROSION TESTS

14.4.1 Introduction to Autoclave Experiments

Operating results from in-pile Zircaloy-2 autoclave slurry corrosion experiment L6Z-129S are presented below. The experiment, which was operated in the HB-6 facility of the LITR, contained 1090 g of Th per kg of D_2O with 5 wt % enriched uranium, based on thorium, and an excess oxygen atmosphere. Instead of the molybdenum trioxide used in previous experiments,[11] 0.0016 *m* Pd was added as a catalyst for the recombination of the radiolytic gases. Assuming a flux of 1×10^{13} neutron/cm^2·sec, the fission power density generated in the autoclave in the fully inserted position was estimated to be 12.4 w/ml. Except for one week at 320°C and two weeks at 240°C, the autoclave

was generally operated at 280°C. Studies of the production and the catalytic recombination of radiolytic gases were made during the in-pile operation.

The autoclaves from experiments L6Z-126S and -127S were opened this quarter, and the pin-corrosion results were obtained.

14.4.2 Production and Catalytic Recombination of Radiolytic Gases

Flux Map.--In order to study the production rate and the catalytic recombination of radiolytic gases, and to maintain safe levels of radiolytic gas, the L6Z-129S autoclave was often moved from the fully inserted or retracted positions to intermediate positions of insertion. Consequently a good knowledge of the thermal-neutron fluxes in these intermediate positions was necessary to estimate the power density for a particular degree of insertion. Figure 14.5 presents the relative thermal-neutron fluxes in HB-6 for different positions of insertion based on the average of two activation analyses of Co-Al flux monitors just prior to the operation of experiment L6Z-129S and one analysis just afterward.

Although the several flux-mapping experiments agreed closely in terms of the relative variation in flux with position of insertion, only slightly better than order-of-magnitude agreement was achieved in these experiments in evaluating the absolute flux level at a given position. Consequently a valid representative value of the empty-beam-hole flux for a particular autoclave experiment has not been obtained with certainty from these experiments, and the best estimate would appear to be that obtained by activation of materials from the autoclave experiment itself. Values of 8.3×10^{12} neutron/cm^2·sec were obtained by activation of materials from experiment L6Z-127S. Between experiments L6Z-127S and L6Z-129S, a half-fuel element in the LITR lattice position nearest the beam hole was replaced by a full fuel element. Until activation analyses from experiment L6Z-129S have been reported, a flux of 1×10^{13} neutrons/cm^2·sec will be assumed for this experiment, which leads to an estimated fission power density in the fully inserted position of 12.4 w/ml. This estimate is used in all values reported below.

Catalyst Performance Index.--Forty-seven insertion and retraction experiments were performed during irradiation of experiment L6Z-129S to measure the equilibrium pressure of radiolytic gas generated. Attempts were also made to measure the production rate of the radiolytic gases and catalytic activity of the palladium catalyst. To facilitate the discussion below, a catalyst performance index which is directly applicable to reactors and directly observable in experiments, is defined as power density (w/ml) maintaining an equilibrium pressure of 100 psi of radiolytic D_2. It is related to catalyst activity and gas production rate by the following expression:

$$\frac{(\text{w/ml})}{(P_{\text{eqb.}}\ D_2/100)} = \frac{(\text{Cat. activity, moles } D_2\text{/liter-hr at 100 psi } D_2)}{0.38\ G_{D_2}} .$$

Figure 14.6 presents the performance indices which were obtained in experiment L6Z-129S from insertion and retraction experiments. The original value was quite high, with a resultant low equilibrium pressure. When the autoclave was first fully inserted, any increase in gas pressure resulting from the formation of small quantities of radiolytic gases was masked by a decrease in pressure caused by adjustment of the temperature control system to (normal) gamma heating of the thermocouple located in a thermowell in the center of the autoclave. From a rough approximation of the effect of the gamma

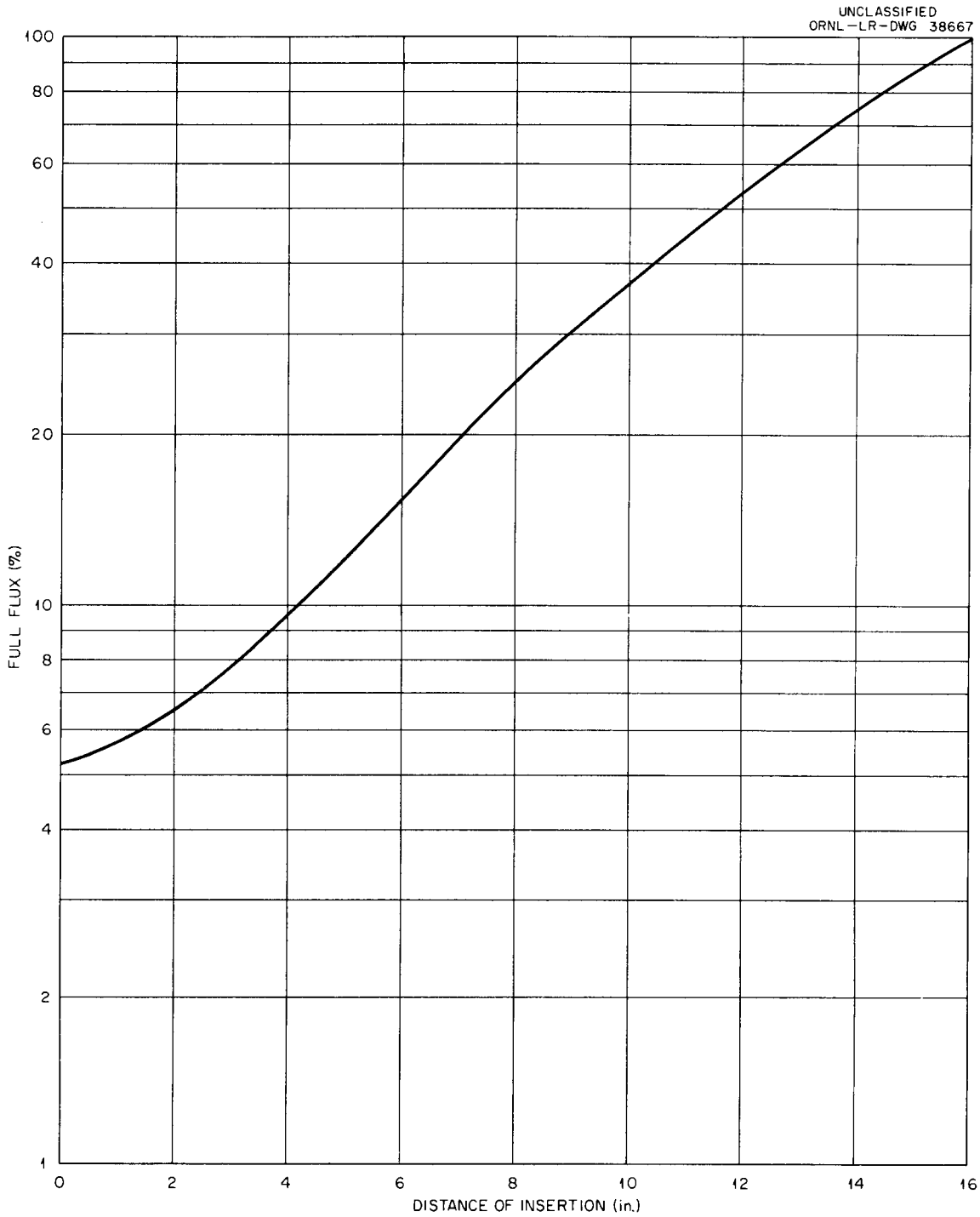

Fig. 14.5. Relative Flux in the HB-6 Facility Before Experiment L6Z-129S.

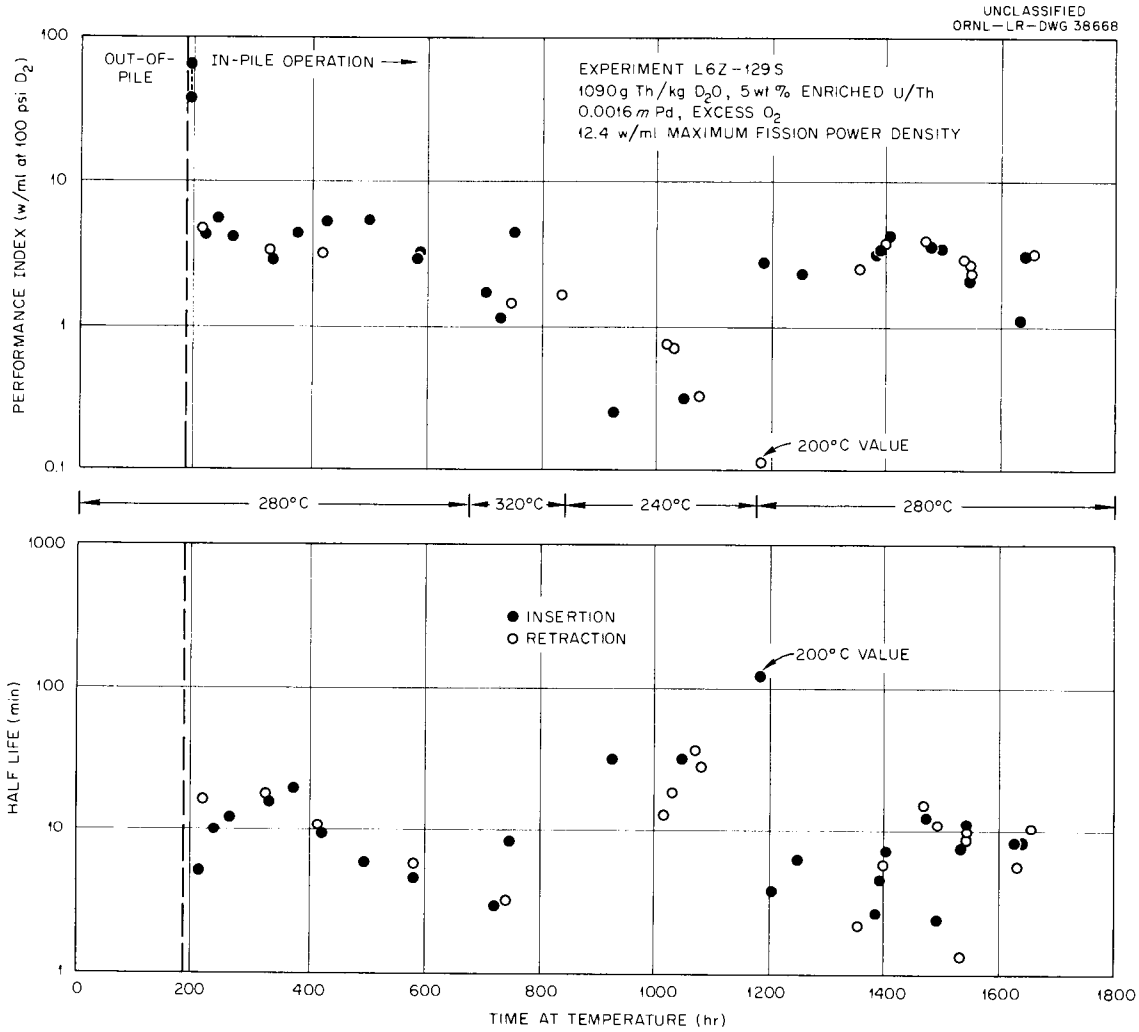

Fig. 14.6. Radiolytic-Gas Phenomena, Experiment L6Z-129S.

heating, the radiolytic gas was estimated to be less than 50 psi and the performance index to be greater than 38 w/ml at 100 psi radiolytic D_2. After 13 hr irradiation a retraction experiment indicated an equilibrium pressure of 255 psi D_2 at a power density of 12.4 w/ml, which corresponded to a performance index value of 4.9 w/ml at 100 psi D_2. For the following 460 hr, in retraction and insertion experiments at fission power densities of between 4.6 and 12.4 w/ml, the performance index remained at this level, ranging between 3.1 and 6 w/ml at 100 psi D_2. The experiment was operated in positions less than fully inserted in order to prevent the accumulation of more than 250 psi radiolytic gas as a safety limit.

When the temperature was raised to 320°C, the performance indices, with the exception of a value of 4.7 in one experiment, were all lowered to 1.2 to 1.8 w/ml at 100 psi D_2. Performance indices of 0.3 to 0.8 were observed at 240°C. One value of 0.1 w/ml at 100 psi D_2 was observed at 200°C. Upon return to 280°C, performance indices of 2.1 to 4.3 w/ml were measured.

Half-Life and G_{D_2}.--The apparent catalytic activities of the palladium, expressed as half-lives of the reaction, are presented in Fig. 14.6. The shorter half-life values are believed to be the more reliable. Inconsistencies in the observed half-lives appear to have been due to a partial plugging of the capillary tubing leading to the pressure-sensing cell. Evidence of partial plugging was noted first 14 hr after irradiation of the autoclave was begun. Original pressure oscillations of 23 psi/°C which resulted from temperature oscillations became greatly dampened. Later, when retraction experiments were performed, instead of a fairly rapid decrease in pressure resulting from the recombination of the radiolytic gases, the pressure would often decrease slowly in the range of 1 psi/min and then in a few minutes suddenly drop between 50 and several hundred psi. Unduly slow decreases in pressure were also observed when the autoclave was rapidly cooled to room temperature. After the temperature had decreased about 50 degrees, the pressure frequently would then very quickly drop several hundred psi to its anticipated level for that particular temperature and follow the temperature down. The relative increase in the observed half-lives of each experiment would depend on the extent of plugging at the time of the experiment.

Since no complete plugging of the capillary tubing was experienced, it has been presumed safe to accept the equilibrium values of radiolytic gases, and thereby the performance indices, as valid. In arbitrarily using an average half-life of 2.6 min obtained from two insertion experiments following reactor shutdown and cooling of the autoclave to room temperature, a G_{D_2} value was computed. Assuming a neutron flux of 1×10^{13} neutrons/cm^2·sec^2 and using a mean value for the performance index at 280°C of 3.63 w/ml at 100 psi D_2 (excluding the performance index of 38 w/ml at 100 psi D_2 observed initially), a value for G_{D_2} of 0.7 was obtained.

14.4.3 Correlation of the Time and Radiation Effect on Corrosion

Corrosion was followed in the usual way from the decrease in oxygen pressure as determined from measurements during reactor shutdowns.[12,13] Figure 14.7 presents the incremental corrosion rate and the average fission power density in experiment L6Z-129S. In the first 23 hr of preirradiation operation, the autoclave exhibited a fairly high corrosion rate, typical of the initial corrosion rate of Zircaloy-2. The corrosion rate diminished fairly rapidly so that after 70 hr it was 0.5 mpy. Upon exposure of the autoclave in-pile, the corrosion rate was increased. However, the effect of a given fission power density appeared to diminish substantially as the experiment proceeded.

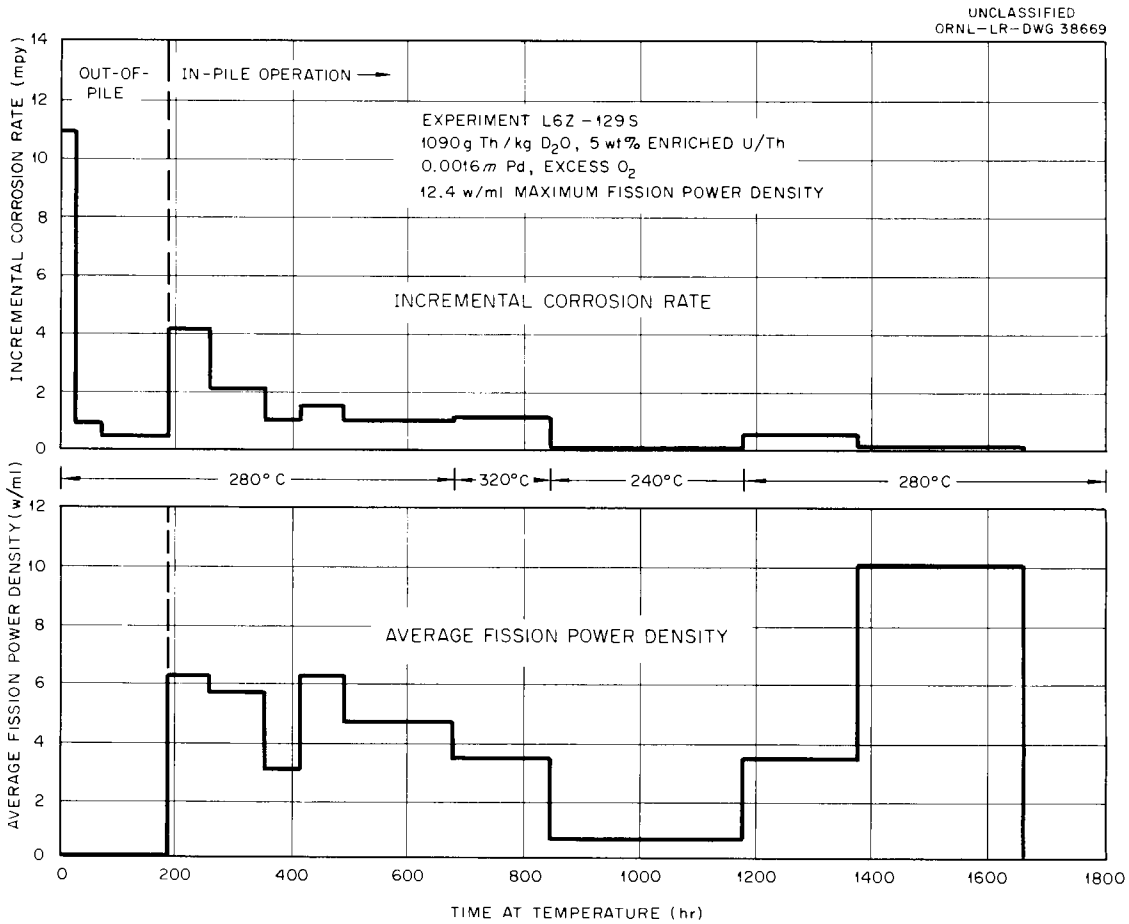

Fig. 14.7. Incremental Corrosion Rates and Fission Power Density in Experiment L6Z-129S.

Figure 14.8 presents a correlation of the effect of time and radiation on the corrosion in experiment L6Z-129S. The data shown represent the actual experiment results, and the lines represent a correlation of the corrosion data obtained by successive approximations. Except for the last 12 days of operation, the relationship

$$280°C \text{ corrosion rate, mpy} = \frac{63 + (113 \times \text{w/ml})}{\text{hr at temp.}}$$

fits the corrosion results at 280°C fairly well. Based on one week of operation at 320°C, the observed corrosion rate of 1.2 mpy at an average fission power density of 3.5 w/ml fits the equation:

$$320°C \text{ corrosion rate, mpy} = \frac{63 + (230 \times \text{w/ml})}{\text{hr at 280°C or above}} .$$

The corrosion rate observed at 240°C was 0.02 mpy at an average fission power density of 0.6 w/ml. A corrosion rate of 0.17 mpy was observed for the last 12 days of operation in-pile at 280°C and 10 w/ml (average), considerably below the values predicted by the above equation.

14.4.4 Radiation Corrosion of Pin Specimens

Operating results of experiments L6Z-126S and -127S have been reported previously.[14,15] The autoclaves from the experiments have now been opened, and the defilmed weight changes of the different alloy pins have been determined. Tables 14.7 and 14.8 contain the comparisons of corrosion from pin-weight changes with the corrosion as measured by changes in D_2 and O_2 pressures, respectively, in experiments L6Z-126S and L6Z-127S. Pin-weight changes of about 1 mg were observed. In experiment L6Z-126S the agreement of corrosion results between pin-weight data and gas measurements was unusually good. The corrosion rate of the two Zircaloy-2 pins in experiment L6Z-127S was in fair agreement with the rate obtained from gas data. The corrosion rates of the Inconel and the type 347 stainless steel pins were slightly less than the rate of the Zircaloy-2 pins.

14.5 IN-PILE SLURRY LOOP

14.5.1 Loop Development

(a) Slurry Filtration.--During the quarter several sintered-metal (stainless steel) filters with specified mean pore diameters of 3-5 μ (but found to contain pore openings as large as 12-20 μ) were evaluated for their effectiveness in filtering thorium oxide slurry. These tests were carried out at room temperature in a glass loop so that the slurry and filtrate streams could be observed. In order to obtain satisfactory filtration of the slurry with these filter units, it was found necessary to install an inner liner containing a number of 0.002-in. perforations, which provided an annular space for the formation of a filter cake.[16] A similar unit has operated satisfactorily in tests with thorium oxide at elevated temperature and pressure. In addition to the filter units described above, a sintered-metal (nickel) filter of 1.2-μ mean pore size, with maximum pore openings of 2 μ, is now under test with thorium oxide slurry. Continuous and satisfactory filtration at room temperature with a slurry of 300 g of Th per kg of H_2O concentration has been demonstrated in 200 hr of operation to date. Thus it appears that a filter with sufficiently small pore size would eliminate the need for an inner liner and

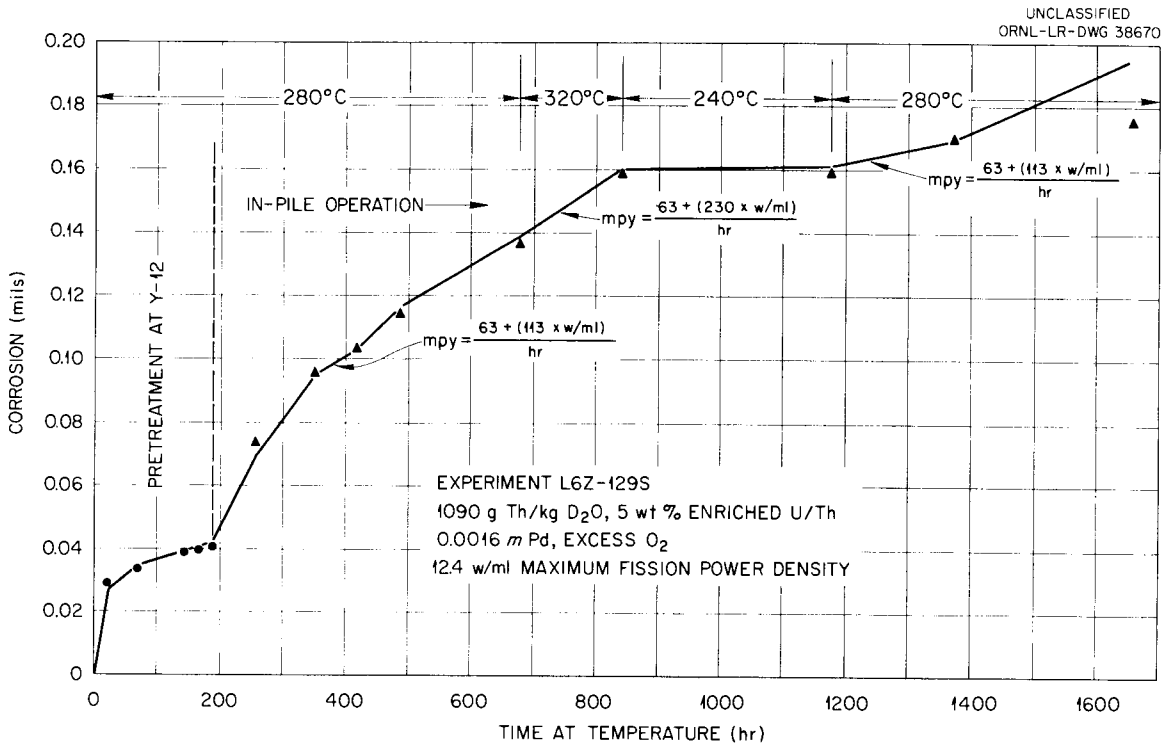

Fig. 14.8. Effect of Time, Radiation, and Temperature on Zircaloy Corrosion Under Oxygen Atmosphere in Experiment L6Z-129S.

Table 14.7. Radiation Corrosion of Pin Specimens

Experiment L6Z-126S

280°C, 980 g of Th per kg of D_2O, 5 wt % U/Th, 0.04 *m* MoO_3, Excess D_2, Zircaloy-2 Autoclave

Hours at temperature	313.7
Hours irradiated :	140.1
Effective fraction of full irradiation time, fully inserted flux	0.251
Flux from specimen activation, neutrons/cm^2·sec (corrected to fully inserted position)	5.5×10^{12}
Average power density while irradiated, w/ml	1.6
Autoclave generalized corrosion rate, mpy* (313.7 hr)	1.5

Pin Material	Pin Corrosion Rate, mpy** (313.7 hr)
Zircaloy-2	1.5
Zr - 15 Nb, 550°C - 2 weeks	1.3
Zr - 15 Nb, beta-quenched	1.3
Zr - 15 Nb, 5 Mo	1.4

* Based on increase in D_2 pressure.

** Based on weight gain.

Table 14.8. Radiation Corrosion of Pin Specimens

Experiment L6Z-127S

280°C, 400 g of Th per kg of D_2O, 5 wt % U/Th, 0.01 *m* MoO_3, Excess O_2, Zircaloy-2 Autoclave

Hours at temperature	1122.5
Hours irradiated	731.5
Effective fraction of full irradiation time, fully inserted flux	0.179
Flux from specimen activation, neutrons/cm^2·sec (corrected to fully inserted position)	8.3×10^{12}
Average power density while irradiated, w/ml slurry	0.8
Autoclave generalized corrosion rate, mpy* (1122.5 hr)	0.8

Pin Material	Pin Corrosion Rate, mpy** (1122.5 hr)
Zircaloy-2	0.2, 0.8
Inconel	0.4
347 stainless steel	0.3, 0.2

* Based on decrease in O_2 pressure.

** Zircaloy-2 corrosion based on weight gain; Inconel and 347 stainless steel corrosion based on weight loss.

filter cake. However, the installation of the liner does not appear to be a problem, and this arrangement will continue to be used if smaller pore-size filters cannot be easily obtained.

(b) Circulating Pump.--The 5-gpm canned-rotor pump with aluminum oxide bearings and journal bushings was removed from the glass test loop and dismantled for inspection. There was no measurable wear (<0.0005 in.) of the bearings and journal bushings. The pump had circulated thorium oxide slurries for approximately 2000 hr at room temperature. The pump bearings were not purged during this period.[17]

(c) Loop Test at Elevated Temperature.--Subsequent to run 14, previously reported,[16] the 5-gpm in-pile type test loop was modified to provide purge to the pump-rotor cavity to prevent the loss of slurry from the main circulating stream through accumulation of thoria in the pump-rotor cavity. This modification involved routing part of the filtrate flow from the filter unit to the rear of the pump as shown diagramatically in Fig. 14.9.

Run 15, which followed, was of 550-hr duration at temperatures up to 250°C and with a slurry concentration of ~410 g of Th per kg of H_2O. The filtrate from the filter unit was divided to provide a flow rate of 1.6 cc/sec to the pressurizer and 0.3 cc/sec purge flow to the pump. Thorium oxide from batch LO-40 calcined at 1600°C with a mean particle size of 1.2 μ was used. The thorium oxide concentration remained practically constant throughout the run. This improvement over previous runs[16] in the control of the concentration is attributed to the pump purge flow.

During run 15 a closed-circuit television camera and x-ray unit were used to observe the slurry flow in the loop core section during operation at temperature and pressure. Settling of thorium oxide could be clearly seen when the flow was stopped by shutting off the circulating pump, and in addition, concentration gradients in the core were observed under certain operating conditions.

Run 16, now in progress, is operating at 250°C with a thorium oxide concentration of approximately 1000 g of Th per kg of H_2O. The thoria being used is from batch DT-46-1600°C-fired with a mean particle size of 2.3 μ. No loss of thoria from the circulating stream has been observed, based on analyses of slurry samples removed from the loop, in the 200 hr of operation to date. The sintered-metal filter unit has provided adequate filtrate for the pressurizer flow and pump purge. Over-all loop operation has been very satisfactory.

REFERENCES

1. E. L. Compere et al., HRP Quar. Prog. Rep. Jan. 31, 1959, ORNL-2696, p 106.

2. J. P. McBride et al., HRP Quar. Prog. Rep. Jan. 31, 1959, ORNL-2696, p 184.

3. D. E. Byrnes and W. O. Fletcher, PAR Quar. Prog. Rep. May 31, 1958, WCAP-900, p 51 (cf. also S. A. Reed and J. P. McBride, HRP-58-461).

4. R. L. Pearson et al., HRP Quar. Prog. Rep. Jan. 31, 1958, ORNL-2493, p 175.

5. E. L. Compere et al., HRP Quar. Prog. Rep. for Periods Ending April 30 and July 30, 1958, ORNL-2561, pp 184-189.

6. E. L. Compere et al., HRP Quar. Prog. Rep. Jan. 31, 1959, ORNL-2696, p 111.

7. Ibid., p 114.

8. J. P. McBride et al., HRP Quar. Prog. Rep. Jan. 31, 1959, ORNL-2696, p 186.

9. E. L. Compere, Factor Analysis of Corrosion Data Using Logarithmic Transformation, ORNL CF-58-9-3.

10. Private communication; memorandum from E. S. Bomar to S. A. Reed, Interim Report on Metallographic Examination of Zircaloy-2 Pins Exposed to Slurry in Toroids with Deuterium Overpressure, March 23, 1959.

11. E. L. Compere et al., HRP Quar. Prog. Rep. Jan. 31, 1959, ORNL-2696, p 120.

12. E. L. Compere et al., HRP Quar. Prog. Rep. Jan. 31, 1958, ORNL-2493, p 113.

13. K. S. Warren and R. J. Davis, In-Reactor Autoclave Corrosion Studies - LITR I - Outlines of Methods and Procedures, ORNL CF-57-5-110.

14. E. L. Compere et al., HRP Quar. Prog. Rep. Oct. 31, 1958, ORNL-2654, pp 133-139.

15. E. L. Compere et al., HRP Quar. Prog. Rep. Jan. 31, 1959, ORNL-2696, pp 120-124.

16. H. C. Savage et al., HRP Quar. Prog. Rep. Jan. 31, 1959, ORNL-2696, pp 124-126.

17. D. W. Hubbard and H. C. Savage, Operation of ORNL In-Pile Slurry Pump with Thorium Oxide Slurry, ORNL CF-58-4-39, April 15, 1958.

UNCLASSIFIED
ORNL-LR-DWG 38671

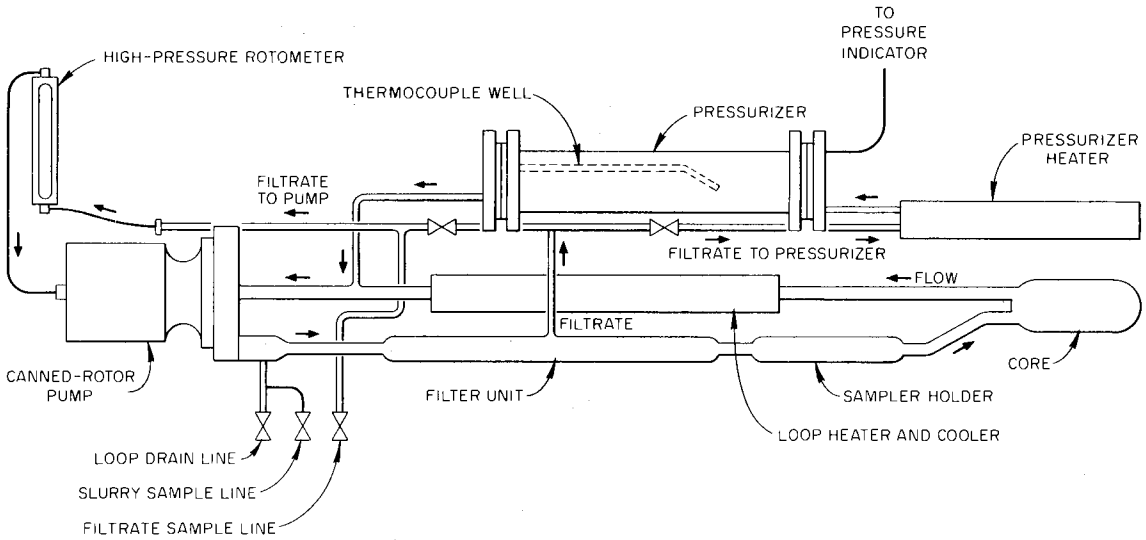

Fig. 14.9. Loop L-4-24S, Modified to Permit Filtrate Purge Flow to Circulating Pump.

15. RADIATION CORROSION

G. H. Jenks H. C. Savage

A. L. Bacarella
J. E. Baker
S. J. Ball
J. C. Banter
S. E. Bolt
R. J. Davis
V. A. DeCarlo
D. T. Jones
R. A. Lorenz
A. R. Olsen
A. J. Shor
M. D. Silverman
W. C. Ulrich
K. S. Warren
S. H. Wheeler
W. C. Yee

15.1 IN-PILE LOOPS--DEVELOPMENT AND CONSTRUCTION

15.1.1 LITR HB-2 Loop Package

Loop L-2-23 is being used in out-of-pile solution-stability experiments and will not be used in a radiation experiment. There are no plans to construct and operate solution loops in the LITR in the near future.

15.1.2 ORR Loop Package

Assembly of the first ORR in-pile loop, designated O-1-25, was completed. Operational tests and pretreatment at operating temperature and pressure are in progress. The core section of this loop includes two tapered-channel coupon holders and three low-velocity coupon holders containing corrosion test specimens of zirconium alloys (with various heat treatments and surface preparations), type 347 stainless steel, crystal-bar zirconium, CD4MCu, and cast type 347 stainless steel. A cobalt-aluminum flux monitor encased in type 347 stainless steel tubing is also installed in the core. One tapered-channel holder and two low-velocity holders in the line position external to the core contain duplicates of the alloys in the core section. Tensile specimens of Zircaloy-2 are also located in the line position. The ORR loop package has been described in previous reports.[1,2]

15.1.3 ORR Beam Hole HN-1

Final changes and additions to the auxiliary equipment at beam hole HN-1 of the ORR, including charcoal traps to hold up gaseous fission-product activity, were completed. A systematic checkout of all equipment and test operation with a mockup loop are in progress.

15.2 IN-PILE SOLUTION ROCKING-AUTOCLAVE TESTS--LITR

15.2.1 Development and Construction

Because of the recent difficulties with the three-hole HB-5 beam-hole

facility[3,4] of the LITR, experimentation in this facility has been curtailed, and no HB-5 type rocking-autoclave experiments were constructed during the period covered by this report. The facility has been in use for 21 months, during which time 21 rocking-autoclave experiments were operated to obtain radiation-corrosion information for the HRP.

Two experiments, L6Z-143 and L6Z-139, were assembled and were operated in beam hold HB-6 of the LITR. Autoclave L6Z-143 contained Ag_2SO_4 additive in a uranyl sulfate fuel solution to study the effect of the silver additive on the corrosion behavior of Zircaloy-2 and on the radiolytic-gas recombination under irradiation. Autoclave L6Z-139 contained a solution of 1.3 m UO_2SO_4 (300 g of U per liter), 0.04 m $CuSO_4$, and 0.04 m D_2SO_4 in D_2O, and was designed to obtain radiation-corrosion data at a relatively high fission power density on a Zr - 1% Cr alloy. The uranium in solution was enriched to 66% U^{235}.

15.2.2 Test of Effect on Zircaloy-2 Corrosion of Transport of Bulk Scales from Zircaloy-2 Surfaces to Other Autoclave Surfaces--Experiment L53T-132

(a) Results.--Previously reported analyses of autoclave data have indicated that differences between Zircaloy-2 corrosion rates in in-pile autoclaves and in in-pile loops are related to the amounts of uranium found in the heavy zirconium oxide scales present on Zircaloy-2 exposed in autoclaves.[5] Subsequent data analyses have indicated that the quantity of uranium found adsorbed on the surfaces of loop specimens (and probably on autoclave specimens after the loose, heavy scale has been removed) is another significant parameter.[6] Reduction of the quantity of this surface uranium, perhaps by solution additives or by use of alloying elements, is a promising means of reducing Zircaloy-2 corrosion in a dynamic reactor system. However, the study of surface-sorbed uranium and its effect on corrosion in autoclaves is hampered by the heavy scale usually observed in Zircaloy-2 autoclaves and the uranium contained by the scale.

As mentioned, the heavy, brass-colored, loose scale is found on Zircaloy-2 surfaces exposed in autoclaves; it has also been found on specimens of other materials exposed in Zircaloy-2 autoclaves.[7] In in-pile loops, however, analysis of scales from specimens of various materials has shown that most of the zirconium oxide is associated with the scale deposited outside the intensely irradiated section. The specimens in the irradiated section are free of the heavy, brass-colored scale. Previous experience, then, indicates that the Zircaloy-2 scale is mobile, at least under irradiation.

The present experiment was designed, primarily, to provide information on the transport of Zircaloy-2 corrosion products in autoclaves and on the effects, if any, of such transport on the radiation corrosion of Zircaloy-2. In the experimental system used, three Zircaloy-2 and three titanium coupon specimens were exposed in a titanium autoclave. Titanium corrodes slowly relative to Zircaloy-2, so that comparatively little titanium scale was expected to form. The Zircaloy-2 constituted only about 10% of the area, and the Zircaloy-2 scale which formed was expected to be distributed over the entire area exposed to the solution and thus reduce the scale buildup per unit area of Zircaloy-2 to as little as 10% of that in the usual all-Zircaloy-2 autoclave test.

The autoclave was of the type in which a series of six coupons is exposed to a range of intensities of neutron flux and, hence, to a range of fission power densities. Information regarding the transport of oxides was sought in comparisons between the amount of zirconium oxide formed during exposure and the amounts of the oxide on the Zircaloy-2 and titanium specimens. Evidence for possible

corrosion effects was sought in comparisons between the Zircaloy-2 average corrosion rates in this and in previous experiments, and was also sought in the data for the rate of oxygen consumption during exposure. Any effects of oxide transport on Zircaloy-2 corrosion would be expected to become less pronounced as the total amount of Zircaloy-2 corrosion products in the autoclave becomes sufficient, even when uniformly distributed over all surfaces, to coat the Zircaloy-2 surfaces with the usual amounts of corrosion products. Hence, an effect of transport on corrosion might be apparent in a change in the rate of oxygen consumption during exposure.

The experiment was also utilized to obtain further information on the sorption of uranium in the heavy, loose corrosion scales as distinct from adherent surface films and scales.

The exposure and postirradiation procedures were similar to those in previous experiments.[3] All the specimens were subjected to the drying procedure for removal of bulk scales. Scales from the three Zircaloy-2 specimens were collected together in one operation; those from the three titanium specimens were collected together in a separate operation. The bulk scales were submitted for chemical analyses. Two specimens of Zircaloy-2 and two of titanium were subjected to cathodic defilming after drying. The two specimens which were not cathodically defilmed and one specimen each of Zircaloy-2 and titanium which were cathodically defilmed were submitted for analyses for uranium and some other elements in the adherent materials remaining on the surfaces.

Pertinent information about the solution employed, the irradiation, and results of corrosion measurements are given in Table 15.1. The Zircaloy-2 corrosion-rate - power-density results are plotted in Fig. 15.1. The Zircaloy-2 corrosion shown by weight-loss measurements was sufficient to account for 53% of the 65 cc(STP) total oxygen consumed. Based on oxygen consumption, the total corrosion in the autoclave was 18% greater than the corrosion calculated by using specimen weight data and the assumption that the corrosion of the titanium autoclave at a given power density was the same as that determined from extrapolation of weight-loss data. As noted in Table 15.1, it is assumed that this additional oxygen was consumed in titanium corrosion. This assumption is made because a small and quite possible error of a fraction of a milligram per square centimeter in the determination of the true weight loss of a titanium specimen could account for the difference between the specimen and oxygen data; whereas the Zircaloy-2 weight-loss results would have to be in error by the unlikely amount of several milligrams per square centimeter to account for the difference. The results of oxygen depletion measurements did not show any unusual deviations from a constant rate of loss of oxygen during radiation exposure.

Visual inspection of the specimens after exposure revealed that the Zircaloy-2 specimens were only partially coated with the loose, bronze-colored scale. The titanium specimens (usually gray after exposure) were partially coated with a similar material (described as a dark gold-colored scale). Data pertaining to the amounts of scale removed from the different specimens in the descaling operations are shown in Table 15.2. Also included in the table are calculated values for the amount of ZrO_2 formed during exposure and for the amounts of ZrO_2 removed from the titanium specimens. For the latter calculation it was assumed that all the TiO_2 formed in corrosion remained on the titanium specimens until removed by defilming and that the true amount of corrosion of a titanium specimen was greater than the amount shown by the weight loss by a factor of about 1.5, deduced from the oxygen consumption data as described above.

Table 15.1. Solution Compositions, Average Exposure Conditions, and Corrosion Rates

Experiment Designation	Solution Composition					Exposure		Av. Soln. Power Density	Corrosion Rate (mpy)	
	UO_2SO_4 (93.2% U^{235}) (m)	$CuSO_4$ (m)	H_2SO_4 (m)	Other Solute (m)	Solvent	Temp. (°C)	Time (hr)	(w/ml)	from O_2 Consumed	from Spec. Wt. Losses
L53T-132	0.170	0.044	0.040	---	D_2O	280	1097	6.9[a] 7.3[a]	---[c] ---	0.5 (Ti) 11.2 (Zr-2)
L6Z-133	0.172	0.002	0.030	---	H_2O	280	172	6.7	12.4 (Zr-2)	15.2 (Zr-2)[b] 13.8 (347 SS)
L52Z-136	0.170	0.040	---	---	D_2O	270	40	8.8	12.2 (Zr-2)	--
						300	91	8.3	17.7 "	--
						310	30	8.1	19.0 "	--
						320	9	7.9	18.8 "	--
						270	13	8.8	2.0 "	--
						270	19	8.8	10.5 "	--
						320	1	7.9	--	--
L51Z-137	0.186	0.021	0.044	0.4 CO_2	H_2O	280	272	9.2[a]	14.6 (Zr-2)	14.0 (Zr-2)

a These are average power-density values corresponding to the average location of the specimens of the material (Ti, Zr-2, or 347 SS) indicated.

b The Zr-2 specimen weight-loss data given are for two specimens which were sandblasted prior to exposure; two as-machined specimens were also included but were broken in dismantling.

c Pressure data indicated that 65 cc(STP) of oxygen was consumed, compared with 55 cc(STP) equivalent to extrapolation of specimen weight losses; as described in the text, it is assumed that this difference was due to incomplete removal of scale from the titanium specimens. On this basis the average titanium corrosion rate was 0.8 mpy instead of 0.5 mpy.

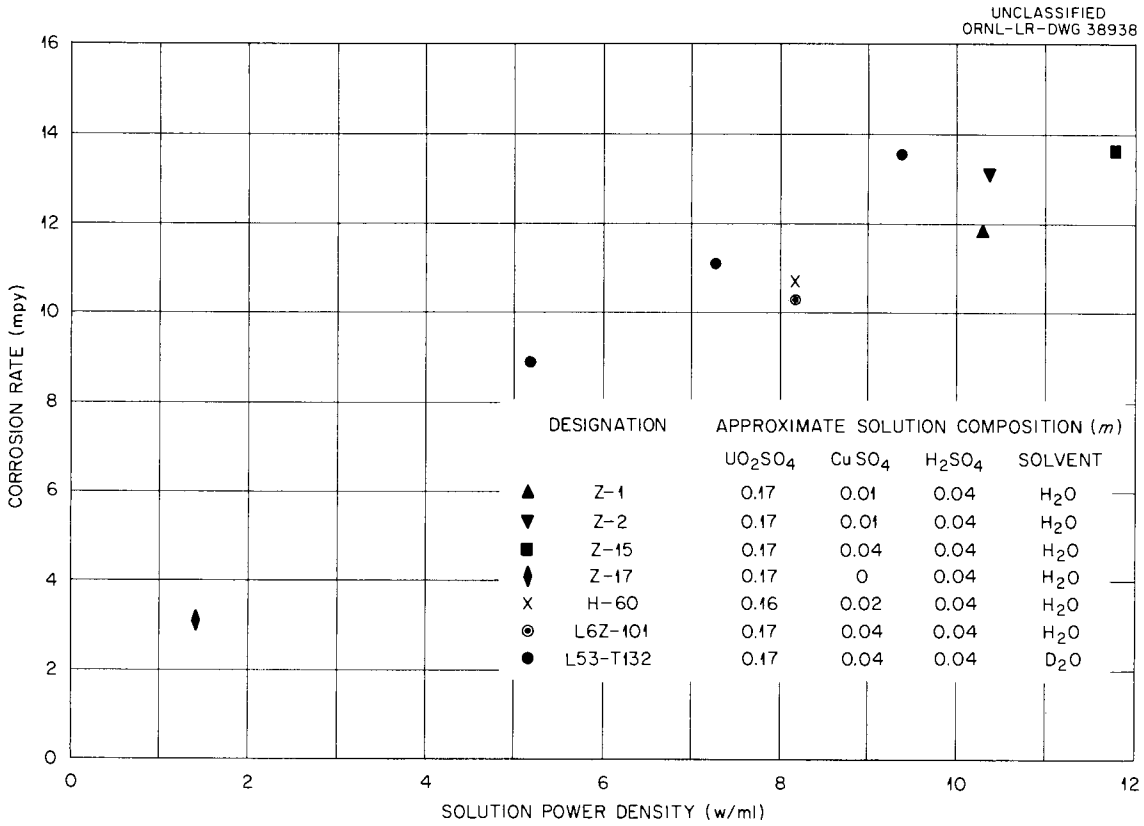

Fig. 15.1. Zircaloy-2 Corrosion in L53T-132.

Table 15.2. Summary of Data and Calculations for the Amount of Zirconium Oxide Formed During Exposure and the Amounts Found on Specimens

1. Amount of ZrO_2 formed, calculated from weight loss of Zircaloy-2	191 mg	
2. Amount of ZrO_2 per unit area		
a. Assuming all oxide remained on Zircaloy-2 (191 mg ZrO_2; 6.08 cm^2 of Zircaloy-2 area)	31.4 mg/cm^2	
b. Assuming oxide distributed uniformly over Zircaloy-2 and titanium surfaces (191 mg ZrO_2; 66.9 cm^2 of total area)	2.9 mg/cm^2	
3. Amount of oxide removed from Zircaloy-2 Specimens		
a. During drying (average from three specimens)	2.1 mg/cm^2	
b. During cathodic defilming (average from high- and low-flux specimens)	0.2 mg/cm^2	
4. Calculated amounts of oxide removed from titanium specimens	High-Flux Specimen	Low-Flux Specimen
a. Amount of oxide removed during drying (average from three specimens)	0.7 mg/cm^2	0.7 mg/cm^2
b. Amount of oxide removed during cathodic defilming	2.8 mg/cm^2	0.5 mg/cm^2
Total zirconium and titanium oxides	3.5 "	1.2 "
c. Calculated amount of TiO_2	2.0 "	0.7 "
d. Amount of zirconium oxide	1.5 "	0.5 "

The results of analyses for uranium in the scales removed during drying and in the samples derived from specimen surfaces after removal of the heavy scales are shown in Table 15.3.

(b) Transfer of Oxides.--The observation that both the Zircaloy-2 and titanium specimens were only partially coated with bulk oxide when inspected probably signifies that some oxides were lost from the specimens during the operations of opening the autoclave and removing the specimens. An exact comparison of the amounts of zirconium oxides on the Zircaloy-2 and titanium is thus precluded. However, the large difference between the values for the calculated amount of zirconium oxide formed and for the amount of scale found on the Zircaloy-2 specimens indicates that an appreciable fraction of the Zircaloy-2 corrosion products was not on the specimen surfaces during exposure. The weight results for the titanium specimens show that some zirconium oxide remained on the titanium specimens when they were descaled by drying but was removed in defilming. For the high- and low-flux titanium specimens, respectively, the total amount of zirconium oxide deposited was about 75 and 20% of the average amount found on the Zircaloy-2.

To summarize, it appears that appreciable amounts of the Zircaloy-2 corrosion products were transferred from the Zircaloy-2 specimens to titanium surfaces during exposure. The results do not provide quantitative information on the amounts transferred.

(c) Corrosion Rates of Zircaloy-2.--There is no evidence that the transfer of zirconium corrosion products in this experiment had any beneficial effect on the Zircaloy-2 corrosion. No Zircaloy-2 corrosion results from previous experiments in equivalent D_2O solutions are available for comparison with the present results. However, many past results[8] are available for H_2O solutions which were otherwise similar to the present solution. These H_2O results are illustrated in Fig. 15.1. The corrosion rates for Zircaloy-2 in the present experiment, at the solution power densities employed, are somewhat greater than those found in the previous H_2O experiments. As mentioned previously, there was no evidence in the oxygen data for other than normal deviation from a constant rate of oxygen loss during radiation exposure.

(d) Uranium in Corrosion Scales and Films.--As discussed previously,[6] the location and amounts of uranium sorbed on and/or in corrosion scales are important factors in consideration of the effects of the sorbed uranium on Zircaloy-2 corrosion. A given amount of uranium located very near the surface probably has a greater effect on corrosion than the same amount of uranium located in the bulk scale, because of differences between the numbers and energies of fission-fragment recoils which reach the specimen surface from the different locations. A correlation of Zircaloy-2 radiation-corrosion results[10] obtained in autoclave and loop experiments has led to the tentative conclusion that in many autoclave experiments uranium is sorbed in appreciable amounts near the corroding Zircaloy-2 surface. In this experiment the analytical result for uranium on the surface of the Zircaloy-2 specimen which was analyzed after the heavy scale was removed by drying and brushing appears to verify this conclusion. As shown in Table 15.3, the analysis showed 22 g of uranium per square centimeter. Consideration of geometries and ranges of fission fragments shows that this amount of uranium, located immediately on the specimen surface, can lead to the deposition of amounts of fission-fragment recoil energy in the surfaces which are as much as 1 to 1.5 times those from uranium in a 0.17 m UO_2SO_4 solution in contact with the surface. The Zircaloy-2 specimen which was cathodically defilmed before the surface was analyzed retained 5.8 g of uranium per square centimeter. This lower value may be a result of removal of some of the surface uranium in the cathodic defilming.

Table 15.3 Uranium Content of Bulk Scales and Surface Materials Removed from Autoclave Specimens

Autoclave and Type of Specimen	Weight of Sample Removed by Drying (mg/cm^2, average)	Uranium in Sample (wt %)	Weight of Uranium in Bulk Scale Removed by Drying (g/cm^2, average)	Weight of Uranium in Material Adhering to Surface (g/cm^2)
L53T-132				
Bulk scale				
3 Zircaloy-2 specimens	2.1	0.06	1.3	
3 titanium specimens	0.7	0.7	4.9	
Surface material after drying and brushing				
1 Zircaloy-2 specimen, average-flux position				22
1 titanium specimen, average-flux position				11
After drying, brushing, and cathodic defilming				
1 Zircaloy-2 specimen, high-flux position				5.8
1 titanium specimen, high-flux position				12
L51Z-137				
Bulk scale				
6 Zircaloy-2 specimens and rack	4.1	3.3	135	
After drying and brushing				
1 Zircaloy-2, high flux				3.1
1 Zircaloy-2, low flux				34
After drying, brushing, and cathodic defilming				
1 Zircaloy-2, next-to-highest flux position				1.9
1 Zircaloy-2, next-to-lowest flux position				3.2

It is worth noting that these results for uranium on the Zircaloy-2 surfaces are relatively free of some uncertainties associated with the results of similar determinations[9] in other autoclave experiments. In these other experiments, the bulk scales contained appreciable amounts of uranium, and it was possible that errors in the analyses for surface uranium could arise from a failure to remove all bulk scale prior to sampling the surface, or from a removal of some of the surface material along with the bulk scale. The Zircaloy-2 corrosion scales removed by drying in this experiment contained a negligible amount of uranium compared with the 22 g/cm^2 on the dried-and-brushed specimen and about 20% of the amount found on the cathodically defilmed specimen.

The explanation for the low uranium content of the Zircaloy-2 scales removed by drying is unknown. A much larger content was predicted from comparisons with past results with similar H_2O solution.[5] The low uranium may be connected in some way with the transport of oxides, but the mechanism for such an effect has not been visualized.

The accuracy of the analytical results for uranium near the surface of the titanium specimens is more uncertain than for the Zircaloy-2 specimens since an appreciable amount of titanium oxide scale presumably was removed during cathodic defilming of the titanium specimens, and the uranium content of this scale is unknown. However, the fact that the cathodically defilmed specimen and the specimen which was only dried and brushed exhibited about the same amount of uranium suggests that scale removed in defilming contained little uranium, and that significant amounts of uranium were sorbed fairly close to the surface of the specimens.

15.2.3 Test of CO_2 As a Chemical Additive to Deter Zircaloy-2 Corrosion--Experiment L51Z-137

The corrosive attack of fuel solution in-pile is related to fission-fragment damage and is increased by accumulation of uranium-containing species on the corroding surfaces. Uranium species are found on the surface layers of the metal and in the scale removed from specimen surfaces, illustrating that sorption of uranium does occur. Presumably a very strongly absorbed species might compete successfully with the uranium and thereby keep the surfaces clean of the damaging fissioning atoms. The objective of this test was to determine if CO_2 has this desirable ability.

An all-Zircaloy-2 autoclave system of the current type which exposes six coupons at a range of power densities was used. The solution was similar in content (Table 15.1) to several of those exposed in the past with the exception that CO_2 at an estimated concentration of 0.4 m (194 psi at room temperature) was included.

Data pertinent to the exposure and corrosion are found in Table 15.1. The results of analyses for uranium in the bulk scales removed during drying of specimens and on the surfaces of specimens after descaling are given in Table 15.3.

The six specimens were exposed to a range of solution power densities from about 5.6 to 12.9 w/ml for 272 hr. The rate of oxygen consumption was linear. The pressure data (observed at 25°C) indicated an average corrosion rate of 14.6 mpy; the average rate calculated on the basis of the six specimen weight losses was 14.0 mpy. The specimen results are shown graphically in Fig. 15.2 together with corrosion results obtained in previous experiments with solutions containing

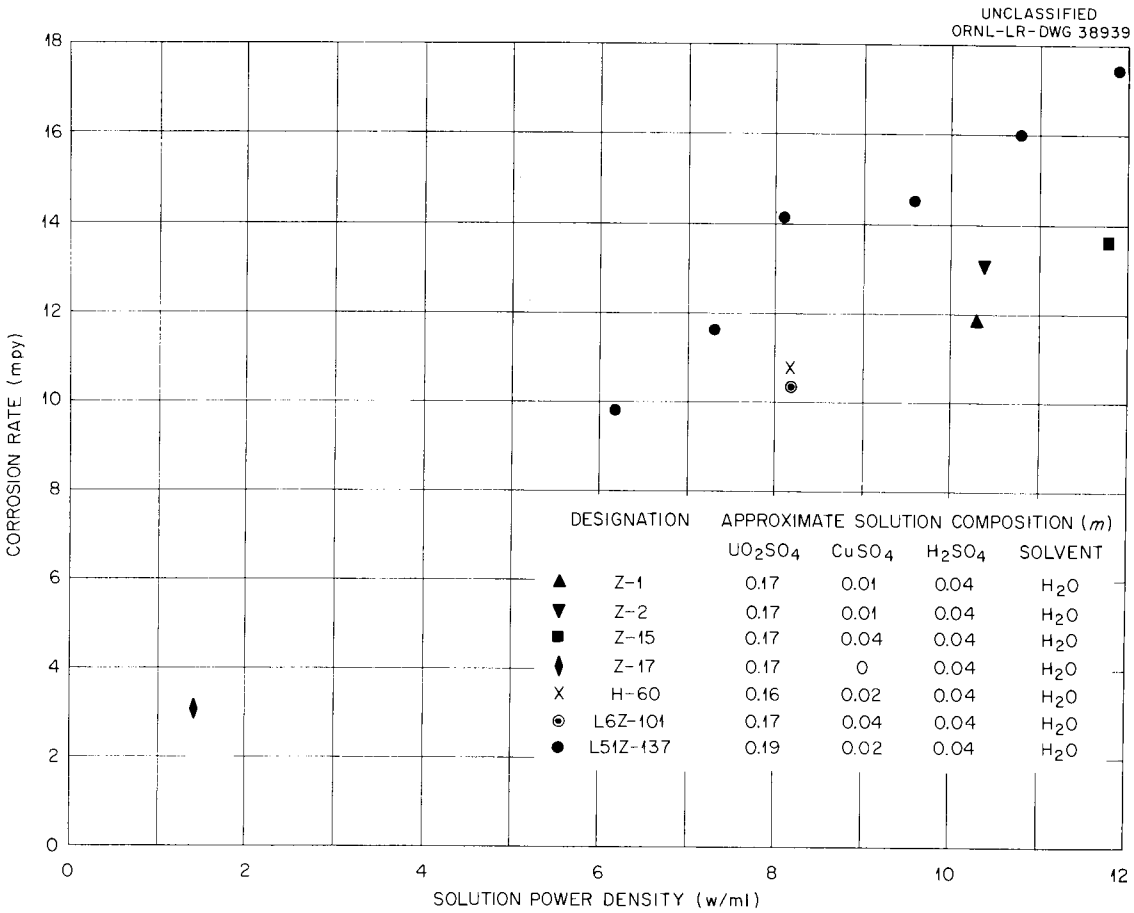

Fig. 15.2. Zircaloy-2 Corrosion in L51Z-137.

no CO_2 but which were otherwise similar to the present solution. However, the previous experiments were in vertically oriented autoclaves and differed in that respect also from the present axially oriented autoclave experiment.

On postirradiation examination, the solution was found to contain almost all the uranium originally charged, 90% of the sulfate, and 45% of the copper. A large amount of the normal brass-colored scale was found on the specimens, and a 115-mg sample of this scale was collected from drying the six coupons and rack.

The value of 3.3% (Table 15.2) for the uranium in the scales removed by drying the Zircaloy-2 specimens is on the high side of the range of 1-3% found in scales from the previous non-CO_2 experiments,[8] the results of which are used for corrosion comparison in Fig. 15.2. The 34 g of uranium per square centimeter found on the surface of one of the specimens which was sampled after drying and brushing could account for an appreciable fraction of the effective power density at the specimen surface if this uranium was located directly on the surface during exposure (see Sec. 15.2.2). The 3.1 g of uranium per square centimeter found on the surface of the other, similarly prepared, specimen could have a proportionately smaller (nearly negligible) estimated contribution to the effective power density. The reason for the difference between the amounts of uranium found on the two specimens is unknown, but it may be associated with sampling procedures since the bulk scale contained an appreciable amount of uranium (see Sec. 15.2.2).

As shown in Fig. 15.2, the Zircaloy-2 corrosion rates at a given solution power density are somewhat greater than those observed in the previous similar experiments used for comparison.

In general, it appears that the presence of CO_2 in this experiment had no beneficial effect on Zircaloy-2 corrosion. The CO_2 may, indeed, have exercised a small adverse effect, as indicated by the high uranium content of the bulk scales and by the Zircaloy-2 corrosion rates.

15.2.4 Correction of Data Reported in a Previous Quarterly Report

Important corrections to the solution power densities previously reported for experiments L52Z-136 and L6Z-133 are included in Table 15.1. The previously reported values were about twice too large.

In the case of L52Z-136[11] the conclusions drawn from the results are unaffected by the corrected power density; that is, it still appears that the separation of the solution into two phases did not alter the corrosion of Zircaloy-2.

In the case of L6Z-133[12] the conclusions are definitely altered by the correction in the power-density value. L6Z-133 was run to test a hypothesis that increased hydrogen pressure in the system would reduce the rate of type 347 stainless steel corrosion. The system was a Zircaloy-2 autoclave with two stainless steel pins and four Zircaloy-2 pins. The solution employed contained only 0.002 m $CuSO_4$, and the radiolytic-gas pressure varied from 440 psi at the start to 960 psi at the finish. At the solution power density of the exposure, the corrosion rate was considerably higher (not lower as previously concluded) than comparable results[8] from experiments (L6Z-104, -106, and -112) with more moderate (about 50 psi) radiolytic-gas pressure values.

15.3 ADSORPTION OF URANIUM ON HYDROUS ZIRCONIUM OXIDE FROM UO_2SO_4 SOLUTIONS

In-pile loop and bomb experiments have shown that the corrosion scales and oxide films on zirconium and zirconium-alloy specimens are capable of sorbing uranium from uranyl sulfate solutions. Since hydrous zirconium oxide is known to act as an ion exchanger, it seems quite likely that its adsorptive property may be a major contributor to the inclusion of uranium in these scales and films.

Heston[13] has performed batch-type experiments which yielded data for the adsorptive capacity of hydrous zirconium oxide for uranium. These data were obtained by equilibrating small amounts of a uranyl sulfate solution with small amounts of the oxide at temperature for 1 hr and then measuring the change in the solution concentration caused by adsorption. He further found that the area of the hydrous oxide was decreased considerably by exposure in high-temperature water for 1 hr.

It was the purpose of the present research to extend Heston's work by a method utilizing a special, high-temperature, ion-exchange column with the objective of possibly employing this technique for the characterization of the adsorption with respect to temperature, solution composition, and other variables.

The high-temperature ion-exchange apparatus is represented schematically in Fig. 15.3. The basic design, made by Heston and described in detail elsewhere,[13] was modified for the present work.

About 250 ml of a uranyl sulfate solution of a given uranium concentration and 0.02 m in H_2SO_4 was added to the reservoir while all valves were closed. A small wad of glass wool was placed at the lower, constricted end of the column, and a given amount of the hydrous oxide was then added to the column on top of this plug. The apparatus was completely assembled, and valve 1 was opened to admit the solution to the column. The furnace was then regulated to 250°C, and the solution was allowed to flow through the column by opening valve 4.

The flow rate was regulated such that a 50-ml sample of the effluent solution could be collected over a period of several hours. The subsequent 20 ml of effluent was collected as a separate sample. Both these samples, as well as a sample of the original solution, were then analyzed for uranium content. The analyses yielded data which allow calculation of the adsorption capacity of the hydrous oxide. The experimental results are summarized in Table 15.4.

It had been anticipated that the trailing 20-ml sample in all cases would have the same concentration as the initial solution, thus indicating that the oxide had been saturated with adsorbed uranium during the course of the experiment. However, in all experiments except 5 and 7, the concentration of this sample was higher than the initial concentration. This indicated that an excess of uranium had been added to the sample above that contained in the original solution. On the other hand, experiment 5 gave the anticipated results, while in experiment 7, the 20-ml sample was less concentrated than the original solution. The reproducibility appears to be poor upon comparison of results from experiments with solutions of nearly the same concentration. However, the concentration discrepancies between the initial solutions and the 20-ml trailing samples give rise to rather large relative errors in the calculated adsorption capacities. This factor may make the interpretation of the results somewhat questionable but does not necessarily invalidate the technique.

The concentration discrepancy between the original solutions and the 20-ml samples in experiments 2, 3, 4, and 6 might be attributed to the decrease in sur-

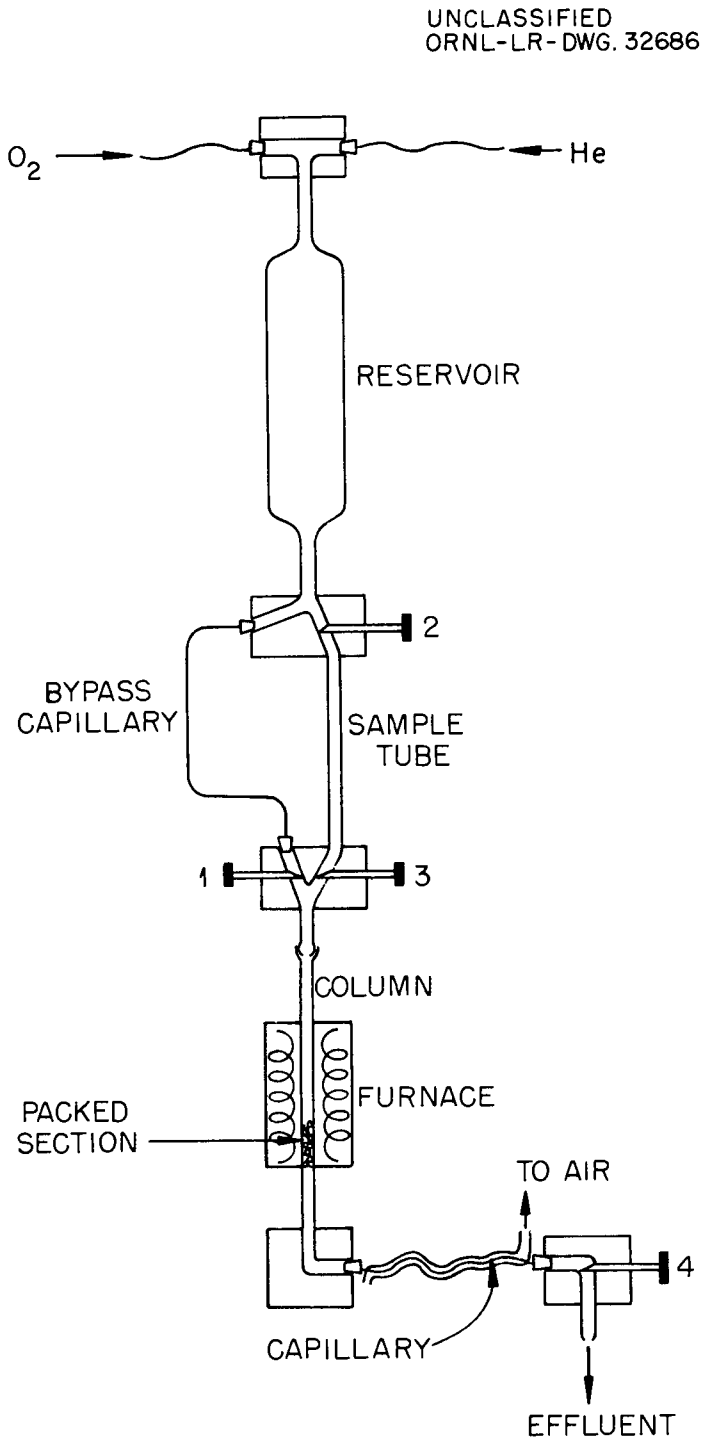

Fig. 15.3. High-Temperature Ion-Exchange Apparatus.

Table 15.4. Test Conditions and Results for Uranium Adsorption Experiments

Experiment No.	Uranium Concentration Initial (mg/ml)	50 ml (mg/ml)	20 ml (mg/ml)	Weight of Oxide (g)	Length of Experiment (hr)	Amount of Uranium Sorbed (mg U/g Oxide)
1	4.97	4.48	--	1.66	$3\frac{1}{2}$	14.8
2	5.04	4.45[a]	5.18	1.00	$3\frac{1}{2}$	27.9
3	52.8	51.1	53.2	1.00	$3\frac{1}{2}$	77.0
4	37.8	35.7	38.6	1.00	$3\frac{1}{2}$	89.0
5	10.25	9.00	10.25	1.00	6	62.5
6	42.4	40.7	43.1	1.00	6[b]	71.0
7	39.1	38.4	37.8	1.00	$6\frac{1}{2}$	61.0

a This sample had a volume of 52 ml.

b Time at temperature was considerably less than 6 hr.

face of the oxide upon prolonged heating. Since the adsorption is, in part at least, a surface phenomenon, the amount of uranium adsorbed is dependent on the surface area of the oxide available for such adsorption. As a particular experiment progressed, the surface area of the oxide could have been decreasing with time (in accordance with Heston's results previously mentioned) and at the same time the oxide would have been adsorbing uranium from the solution. If during the course of an experiment the available surface area was saturated with uranium before the decrease in surface area had ceased, then a further reduction in surface area might have caused desorption of uranium into the solution passing through the column. This portion of the effluent solution would then be more concentrated than the original solution. On the other hand, it is possible that some of the adsorbed uranium could have been permanently incorporated in the oxide by the process involved in the change in area.

Experiments 5, 6, and 7 were made in an attempt to clarify this point by increasing the length of the experiments. The agreement between the 20-ml sample and original solution in experiment 5 was interpreted as indicating that the surface area had stopped decreasing at some point during collection of the 50-ml sample. Experiments 6 and 7, on the other hand, did not show this agreement. However, trouble was encountered in regulating the temperature in experiment 6, and it was maintained at 250°C for considerably less than the 6 hr. The disagreement in experiment 7 might indicate that the oxide had not been completely saturated with adsorbed uranium during the run. No explanation for this is apparent.

If Heston's data at 250°C are plotted on a Langmuir-type plot as a ratio of uranium concentration in solution to the concentration on ZrO_2 (U_s/U_g) vs the uranium concentration in solution at room temperature (U_s), a straight line is

obtained as shown in Fig. 15.4. A similar treatment is also given the data reported here. These data may also be approximated by a straight line, which falls lower than the one through Heston's data, although the treatment suffers from the inconsistencies in the data.

The difference between the Langmuir-type plots of Heston's data and the present data at higher concentrations may be partially explained by differences in technique. Whereas in the present work the oxide was at temperature throughout an experiment, Heston cooled the equilibrated mixtures of oxide and solution before separating them for analyses. The results thus obtained might represent only the amount of uranium that was held irreversibly if the adsorption process is partially thermally reversible and some desorption had occurred during the 10 min required for the cooling and separation. Then, too, the exposure period of 1 hr may not have been sufficient to completely saturate the oxide with adsorbed uranium. Both of these factors could lead to erroneously low adsorption capacities.

The present data, although apparently not highly accurate, indicate that an improved technique could well yield valuable information concerning the adsorption of uranium by hydrous zirconium oxide. Further experimentation is planned.

REFERENCES

1. H. C. Savage et al., HRP Quar. Prog. Rep. Oct. 31, 1958, ORNL-2654, pp 164-165.
2. G. H. Jenks et al., HRP Quar. Prog. Rep. April 30, 1957, ORNL-2331, p 113.
3. K. S. Warren and R. J. Davis, In-Reactor Autoclave Corrosion Studies - LITR I. Outline of Methods and Procedures, ORNL-CF-57-5-110 (May 22, 1957).
4. H. C. Savage et al., HRP Quar. Prog. Rep. Jan. 31, 1957, ORNL-2272, p 110 and Figs. 13.1, 13.2, and 13.3.
5. G. H. Jenks et al., HRP Quar. Prog. Rep. Oct. 31, 1957, ORNL-2432, pp 120-126.
6. G. H. Jenks et al., HRP Quar. Prog. Rep. Jan. 31, 1958, ORNL-2493, pp 125-126.
7. Ibid., pp 135-137.
8. R. J. Davis, Tabular Summary of Zircaloy-2 In-Pile Rocking Autoclave Corrosion Data, ORNL CF-58-6-92 (June 18, 1958).
9. G. H. Jenks et al., HRP Quar. Prog. Rep. April 30 and July 31, 1958, ORNL-2561, pp 233-234.
10. G. H. Jenks, topical report (in preparation).
11. G. H. Jenks et al., HRP Quar. Prog. Rep. Oct. 31, 1958, ORNL-2654, pp 166-173.
12. Ibid., pp 173-176.
13. B. O. Heston, Adsorption of Uranium on Hydrous Zirconium Oxide, ORNL CF-58-11-39 (in press).

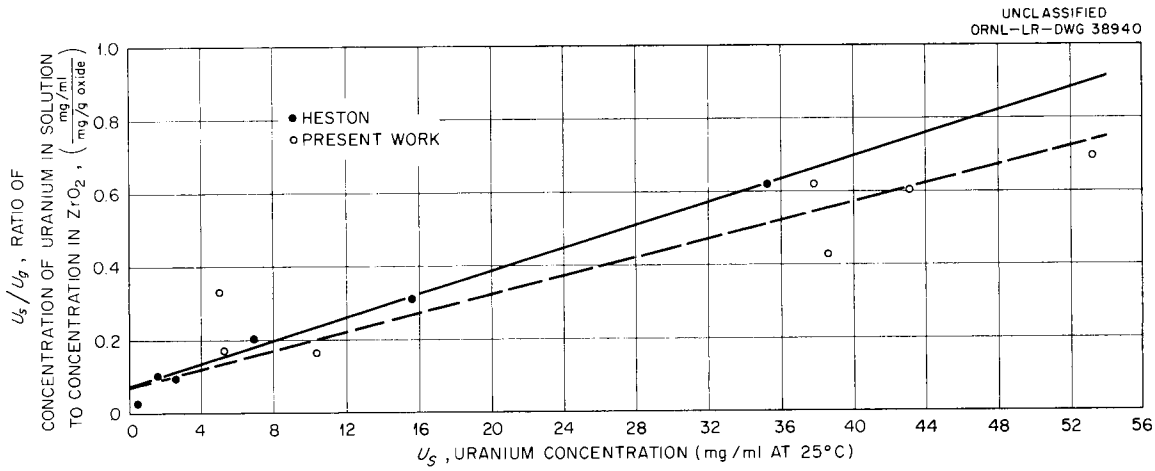

Fig. 15.4. Langmuir-Type Plot of Data for Adsorption of Uranium on Hydrous ZrO_2 at 250°C.

16. METALLURGY

G. M. Adamson

R. G. Berggren
E. S. Bomar
F. W. Cooke
T. M. Kegley, Jr.
W. J. Leonard
M. L. Picklesimer
J. J. Prislinger
P. L. Rittenhouse
R. L. Stephenson
J. K. White
J. C. Wilson
C. H. Wodtke

16.1 HRT REPAIR AND EXAMINATION

16.1.1 Examination of Specimens Removed from the HRT after Run 17

After completion of HRT run 17, disk specimens cut from five of the six top screens of the HRT core tank, the high-flux end of the titanium specimen holder that had been in the core tank during the run, and four of the mechanical-property specimens recovered from the top screen were submitted to the HRP Metallurgy Group for macro- and microexamination. The examinations have been completed, and a detailed report is in preparation. In the last report,[1] the conditions of the screen specimens and the titanium specimen holder were described, and conclusions regarding the causes of those conditions were presented. None of the conclusions have been changed by the more complete examinations made during the past quarter.

Figure 16.1 shows a section from a screen, as removed from the reactor, illustrating the exfoliation which has occurred primarily in the fabrication cracks. The typical microstructure found in all screens, both before and after use in the HRT, is pictured in Fig. 16.2, showing a cold-worked structure with extensive cracking and intermetallic stringers. This sample was cut from an area only 1/4 in. from the center of the "molten spot" and shows how restricted the affected area was. Recrystallization of such a structure would have occurred in a few seconds at temperatures of 550 - 600°C, or above.

The structures in the vicinity of the "molten spot" found on the top screen offer information about the temperatures attained and their duration. During previous reactor operation, many of the cracks in the screens had become filled with oxides. Such oxides are soluble in zirconium at elevated temperatures and will cause changes in the microstructure. Microstructures found under the molten spot are shown in Fig. 16.3. The dissolving oxide and related structures are shown. The order of structures from the oxide into the parent metal is:

1. dissolving oxide,
2. oxygen-stabilized alpha,
3. oxygen-contaminated beta phase (at temperature),
4. uncontaminated beta phase (at temperature).

UNCLASSIFIED
PHOTO 2402

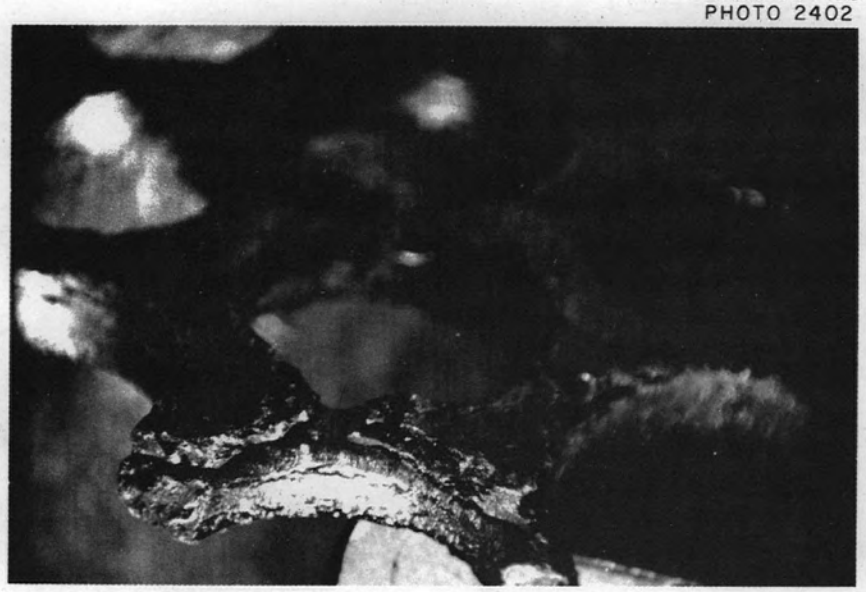

Fig. 16.1. Cracking and Exfoliation in Zircaloy-2 Screen from HRE-2 (Bright Field, 3.3X, 2402).

UNCLASSIFIED
PHOTO 46960

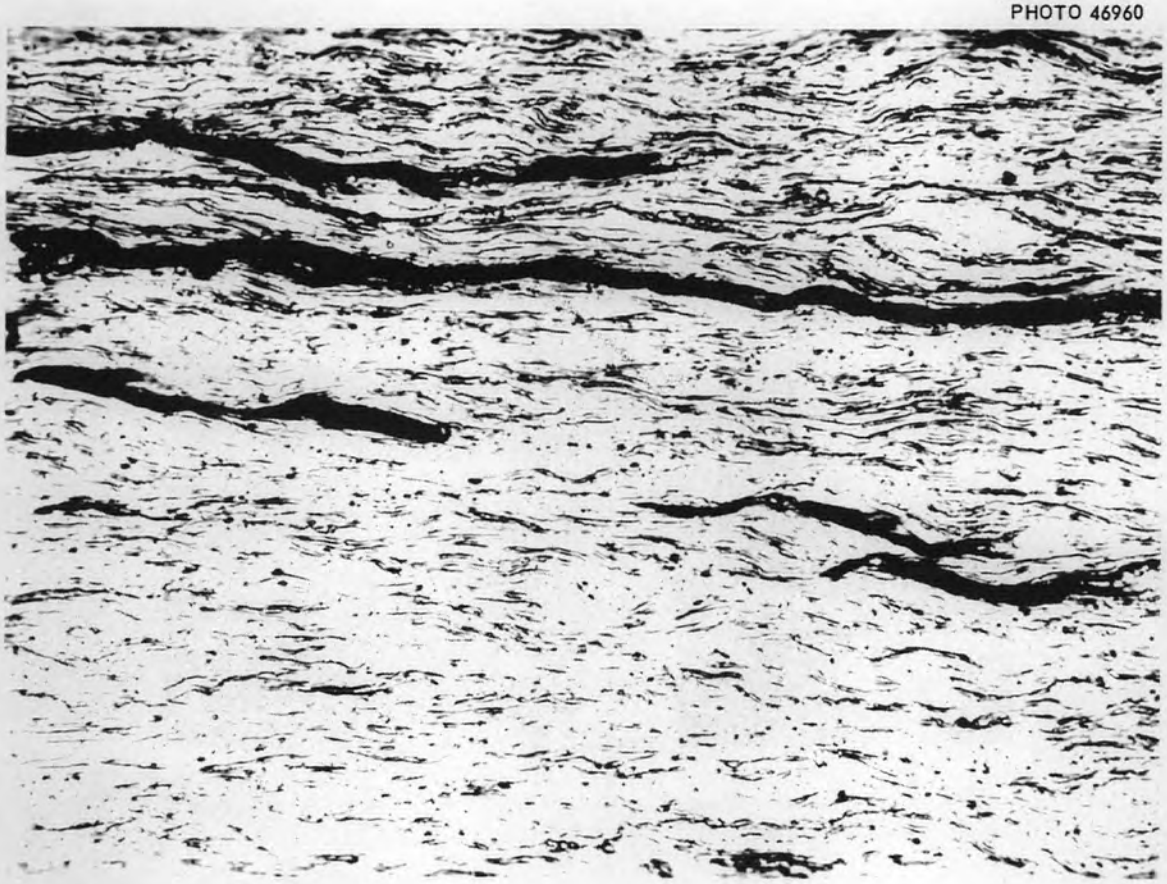

Fig. 16.2. Base Metal Structure of Zircaloy-2 Screens. Structure did not change during exposure in HRT. Bright field, 500X.

UNCLASSIFIED
PHOTO 46961

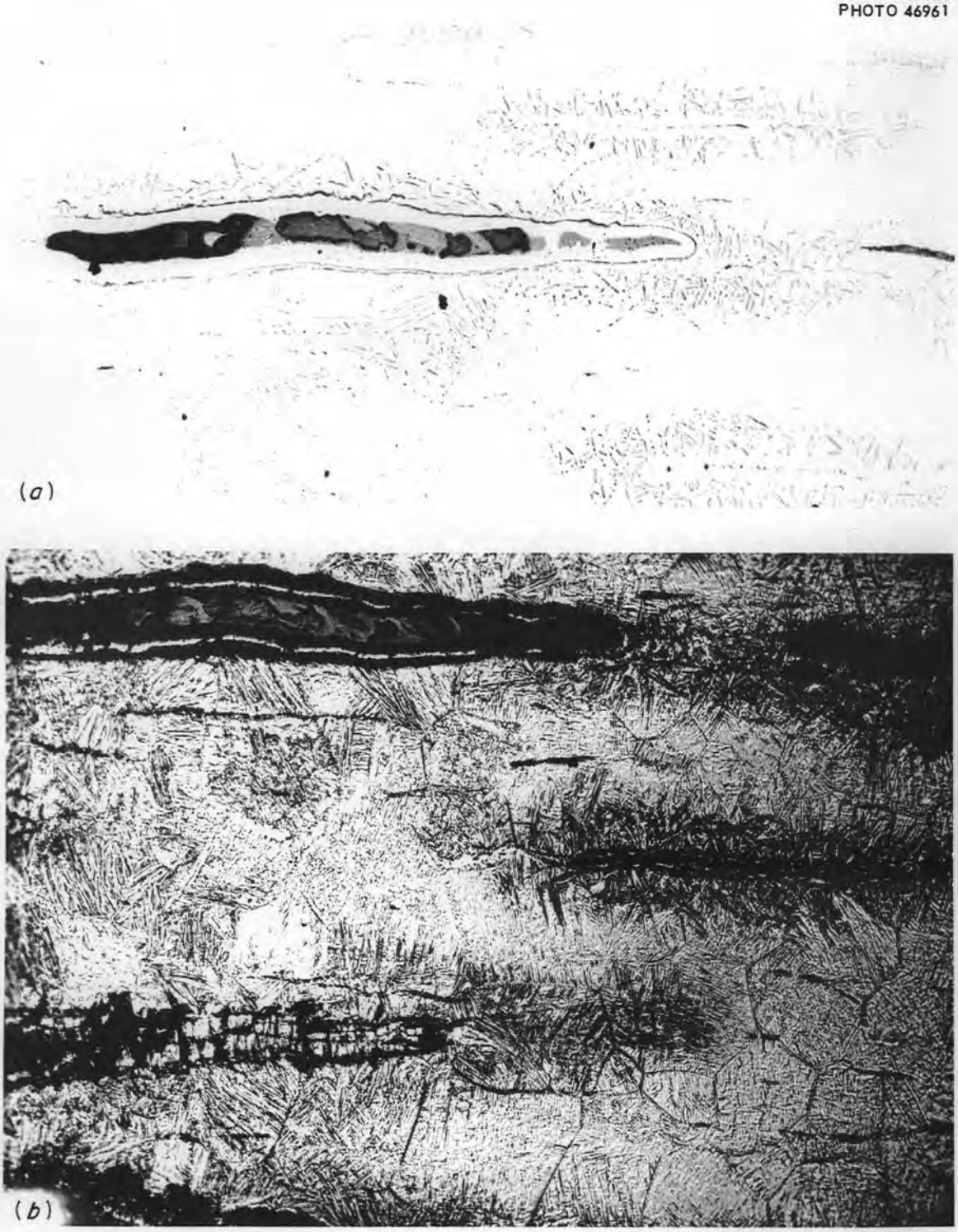

Fig. 16.3. Structure of Zircaloy-2 Screen Under Molten Area, Showing Dissolving Oxides and Altered Structure. Bright field, 100X. (*a*) As-polished. (*b*) Etched.

The structures shown in Fig. 16.4 were located at the top and bottom corners of the screen hole, nearest the high-temperature area of the "molten spot." Figure 16.4a, the top edge of the specimen, shows an oxygen-stabilized alpha rim, oxygen-contaminated beta phase (at temperature), and uncontaminated beta phase (at temperature) in that order. The lower corner (Fig. 16.4b) shows only the two beta structures and is primarily the fine beta. The very fine martensitic structure of the prior beta phase is characteristic of very rapid quenching from temperatures in the beta field, and the small, prior-beta grain size is an indication that temperatures above 1200°C existed at this area during only a very few seconds of the temperature excursion.

A series of controlled heating, melting, and burning experiments with annealed and cold-worked Zircaloy-2 have shown that the range of structures observed in the screen specimen may be reproduced by melting a specimen in 2 sec under water but not by melting in approximately 30 sec.

Three Zircaloy-2 and one A40 titanium multiple tensile specimens, originally located on the titanium specimen holder in the core, were submitted for macro- and microexamination after recovery from the top screen of the HRT core tank at the end of run 17. The Ti-A40 showed no damage or corrosion, except at the ends which were located in the supporting bracket or in the positioning screw. Both ends showed evidence of having been heated into the beta field, above 900°C, for a very short time. The minor damage observed was believed to have been caused by the "burning" of the positioning screw and supporting bracket. The specimen is scheduled to be tensile tested shortly. Metallographically, no increase in deuterium was detected in the sample.

The three Zircaloy-2 specimens recovered showed varying amounts of damage to the surface and to the underlying metal, ranging from corrosive pitting of the surface, to "burning" analagous to that produced by flame cutting with an oxyacetylene torch. Corrosion pits (free of deposit, smooth, shiny, and rounded) were observed in sections of the specimens that (1) had been heated to very high temperatures but not "burned," (2) had been "burned," (3) had not been heated to temperatures above 800°C--probably not above 400 - 500°C. The pits were also observed to have been formed both before and after high-temperature excursions, as shown by the presence of oxygen-stabilized alpha rims in some pits but not in others, even in the same field under the microscope. Analyses have shown that none of these samples picked up deuterium during exposure in the reactor.

Macrophotographs of an original specimen and of the most extensively damaged tensile specimen, W-1-b, are shown in Fig. 16.5. The T-head end of the specimen had been "burned" to the extent that a grip section had been reduced from 0.240 in. to less than 0.070 in. Photomicrographs are presented in Fig. 16.6 of three representative areas, cut within a 1/4-in. length on the specimen: 16.6a near the smallest cross-section of the "burned" section; 16.6b at a section which had been heated just into the beta field; and 16.6c at a section which had not been heated above 800°C and which shows a structure typical of the remainder of the specimen. The very small size of the prior-beta grains, shown in Fig. 16.6b, no larger than the alpha grains from which they were formed (Fig. 16.6c), shows that the duration of the excursion was not more than a few seconds. Careful examination of the area represented in Fig. 16.6b revealed that no later temperature excursion above 800°C occurred, as shown by the absence of precipitation of the intermetallics or the rounding of the martensite needles in the quenched beta structure.

The damage seen on the other specimens was similar in nature but much less extensive.

UNCLASSIFIED
PHOTO 46962

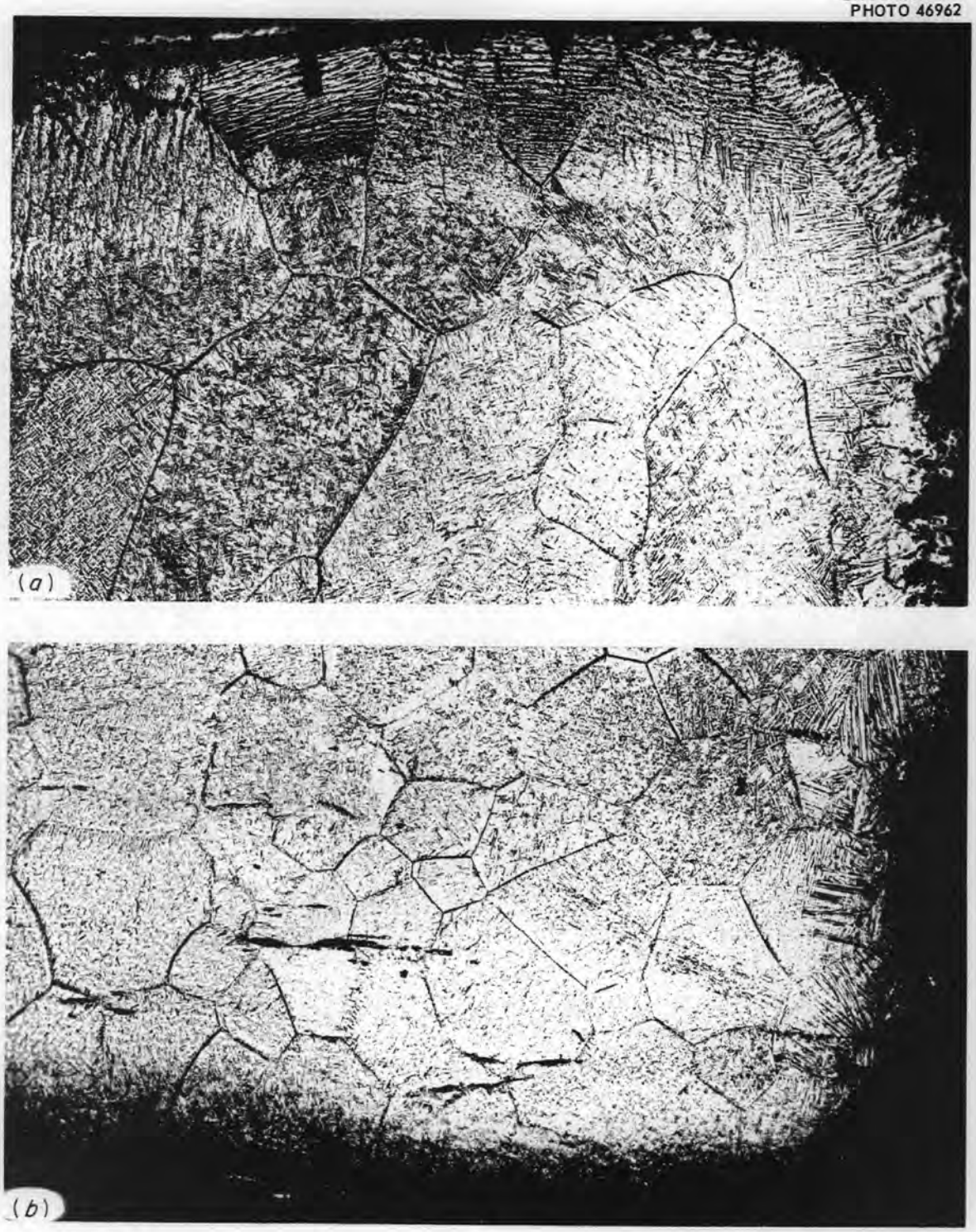

Fig. 16.4. Structure of Zircaloy-2 at Edges of Screen Hole Adjacent to Molten Area. Bright field, 100X. (*a*) Top corner. (*b*) Bottom corner.

UNCLASSIFIED
PHOTO 46963

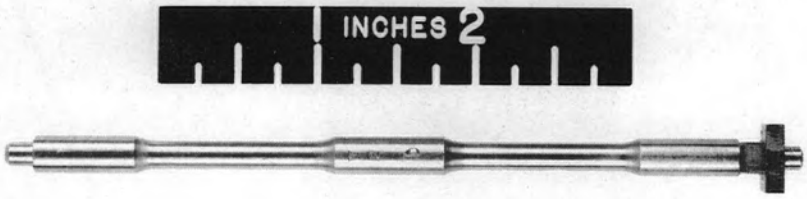

Fig. 16.5. Original and Burned T-Head of Zircaloy-2 Tensile Specimen w-l-b, After Exposure in HRE-2.

UNCLASSIFIED
PHOTO 46964

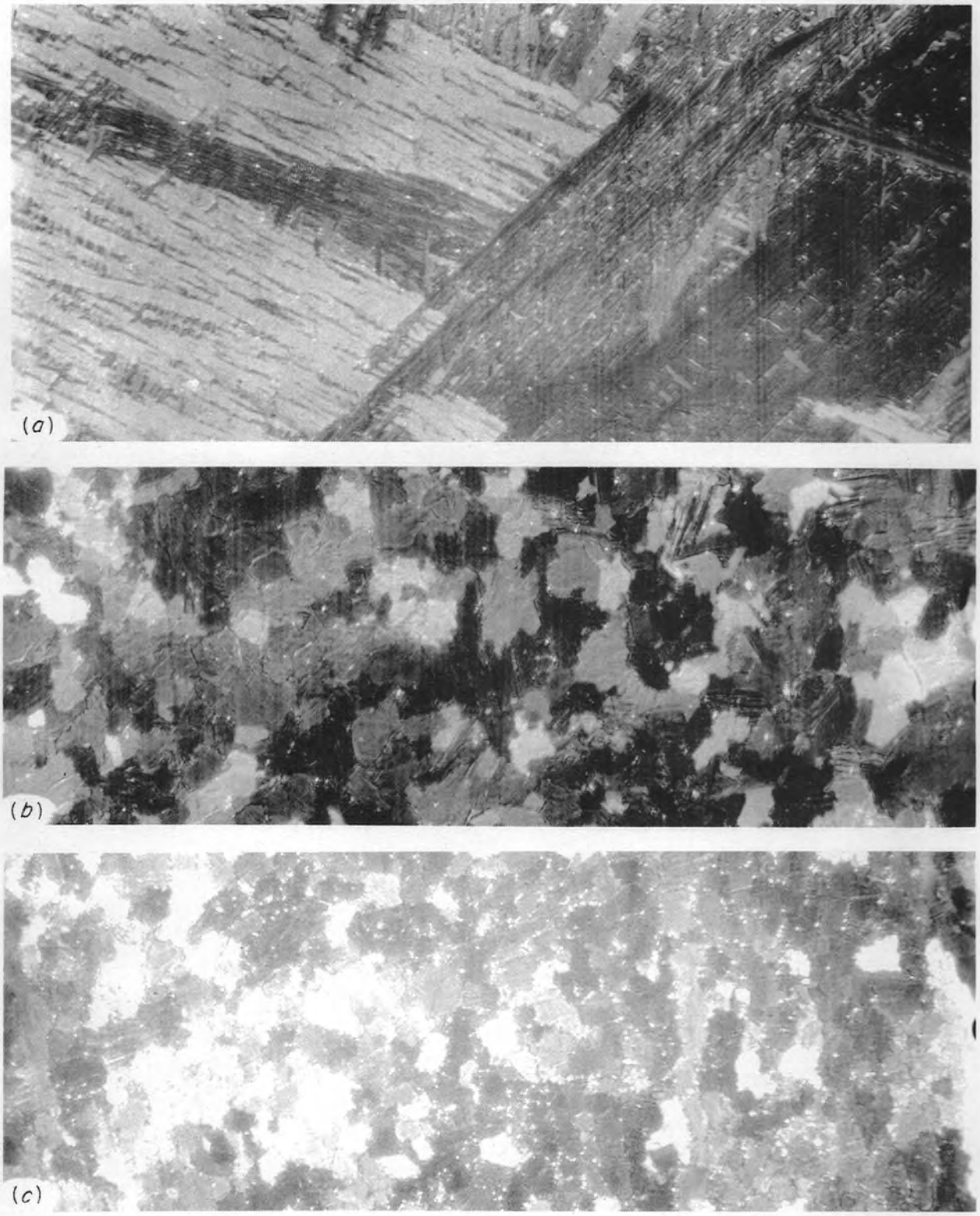

Fig. 16.6. Microstructures Observed in Burned Zircaloy-2 Tensile Specimen. Polarized light, 500X. (*a*) Very high temperature; prior beta area. (*b*) Low temperature; prior beta area. (*c*) Neighboring unaffected alpha area.

Sections from the titanium specimen-holder inserted in the core region of the reactor during run 17 were examined macroscopically and microscopically. Macrophotographs of the spike and of the hole formed at the lower part of station H of the holder are shown in Fig. 16.7. All specimen support brackets were burned off at station H, and the stubs visible in Fig. 16.7a were typical of the portions remaining. The conditions of the surface around the hole, as shown in Fig. 16.7b and 16.7c, indicate that the hole was probably formed by two temperature excursions. Microstructural examination of specimens cut to show different sections of the region of the hole confirm that conclusion by showing appreciable differences in the depth of the oxygen-contaminated layer. Measurements of the spike length after the run show that 11/16 in. of the spike had disappeared, and microstructural examination of the remaining portion indicates that the missing part burned off. The highly polished surface of the tip, evident in Fig. 16.8, was produced from a surface layer formed from molten and oxygen-contaminated titanium. Microstructural examination of the bracket stubs (Fig. 16.9) showed that the brackets had been burned off, producing surface layers, at temperature, of mixed oxide and molten titanium, oxygen-stabilized alpha titanium, and oxygen-contaminated prior-beta phase. The interior structures of all specimens examined, at station H, were those of large-grained alpha titanium plus large amounts of the deuteride, equivalent to approximately 1000 ppm H. Thermal cycling over a temperature range from 250 to 350°C with approximately 2000 ppm D present (equivalent to 1000 ppm H) apparently destroyed all evidence of prior high-temperature excursions except in the surface layers where the oxygen contamination was sufficiently high to prevent any high concentration of deuterium. Control experiments, conducted with titanium A40 specimens containing 1000 and 2000 ppm H, confirmed the conclusion that the prior structure was destroyed when specimens were thermally cycled from 250 to 350°C six times.

Using heat transfer coefficient calculations, H. C. Claiborne[2] has shown that a surface layer or deposit less than 0.060 in. thick and containing a high concentration of uranium could, during reactor operation, produce localized overheating to the extent that melting of the base metal could occur. Since all of the damage by "burning" or high-temperature excursions was observed to have occurred at areas on the specimen holder where poor cooling or eddies would be suspected, it was therefore concluded that the high-temperature excursions were caused by such a deposit and not by direct chemical reaction of the metals with the fuel solution.

In summary, it was concluded that:

1. Localized sections of the titanium specimen holder had been heated to a temperature above the melting point during reactor operation, causing a reaction between the holder and the steam - heavy water environment.

2. When the heat source (probably a deposit containing a high concentration of uranium) was removed as a result of the reaction, the reaction quenched out, indicating that the reaction was not self-sustaining.

3. The damage observed on the Zircaloy-2 mechanical-property specimens, originally supported on the titanium specimen holder, was caused by the "burning" of the specimen holder and not by a reaction of the specimens with their environment.

UNCLASSIFIED
PHOTO 46965

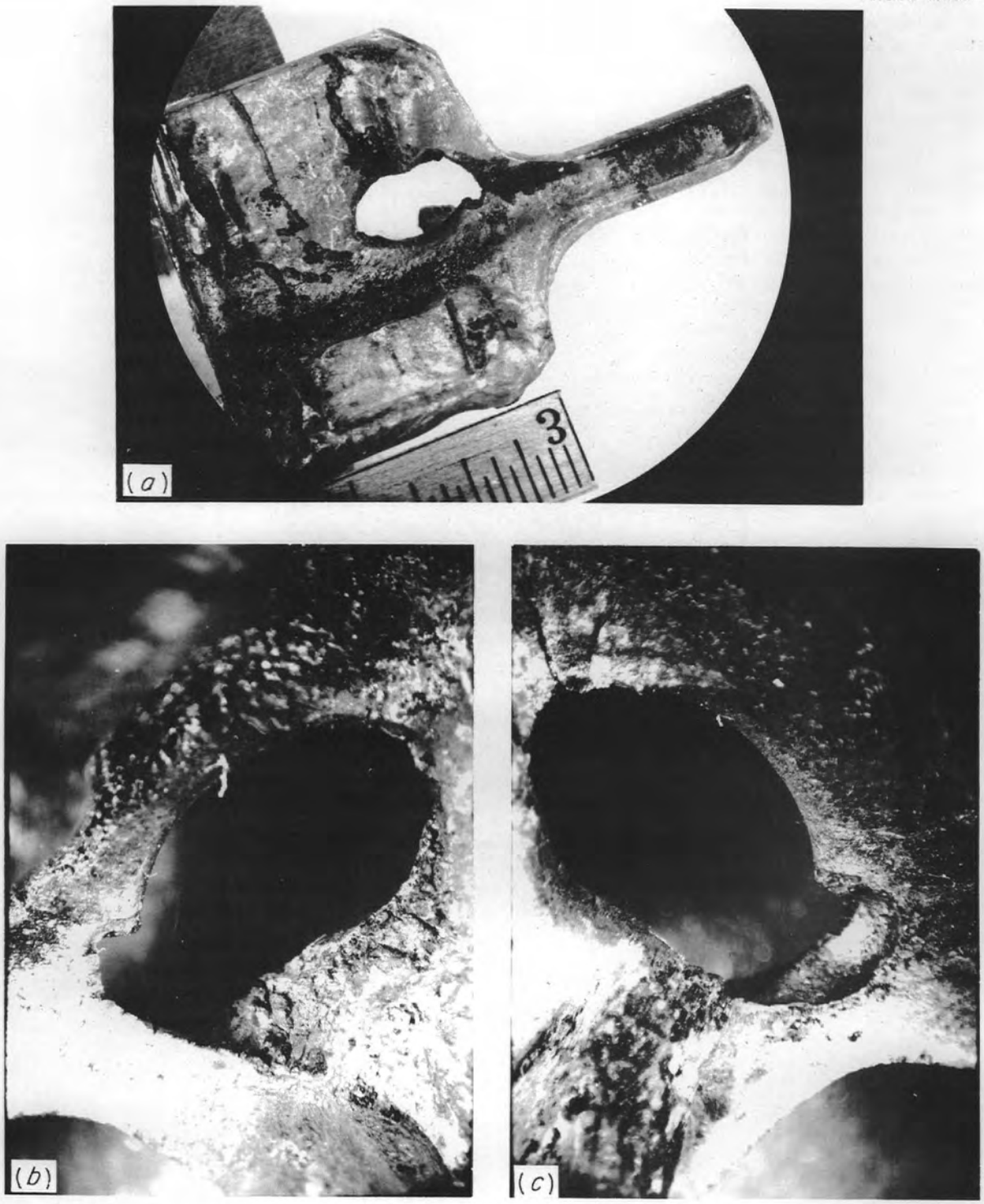

Fig. 16.7. Lower End of Titanium Specimen Holder After Reactor Exposure, Showing Burned Tip and Holes. (*a*) Macrophotograph tip section. (*b*) Burned hole in web, side A. 4.5X. (*c*) Burned hole in web, side B. 4.5X.

UNCLASSIFIED
PHOTO 46966

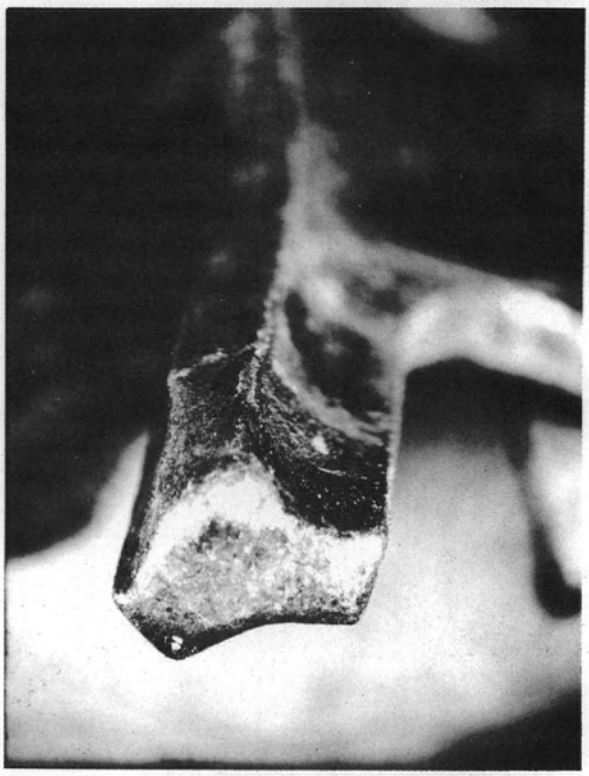

Fig. 16.8. View of Burned Titanium Spike on Bottom of Specimen Holder. 4.5X.

UNCLASSIFIED
PHOTO 46967

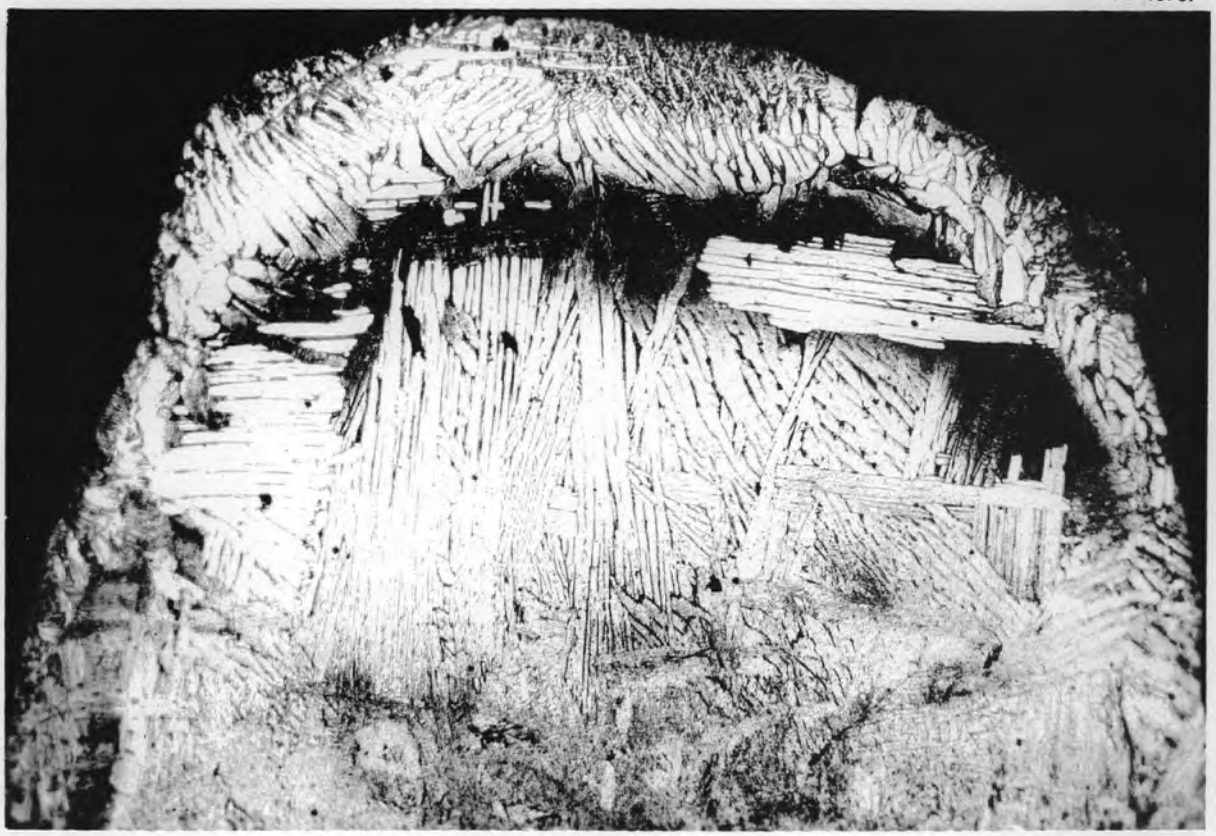

Fig. 16.9. Cross-Section of Burned Titanium Bracket-Stub from Specimen Holder. Bright field, 50X.

4. The damage observed on the top screen of the core tank, due to a high-temperature excursion, was caused by an event associated with the titanium specimen-holder spike.

5. The exfoliation observed on the screen specimens was caused primarily by corrosion or hot spots occurring in the cracks and laminations that existed in the screens as installed in the vessel. The cracks and laminations were formed primarily during the punching of the holes during manufacture.

16.1.2 Screen Removal

(a) Tungsten-Arc Submerged Cutting.--Electric-arc cutting is under consideration as a means of cutting the Zircaloy-2 diffuser screens into strips for removal from the core vessel. The most promising method investigated to date is tungsten-arc cutting under water.

Early trial cuts were made by using a standard Linde Heliarc cutting torch and control equipment. The manual torch was moved mechanically across a submerged screen. The 1/8-in.-thick-screen could be readily cut at nearly 100 in./min with 420-amp current. Zircaloy-2 spatter produced under these conditions has been shot-like, ranging from very fine to about 1/8-in.-dia spheres with no tendency to stick together. Spatter removal should thus be facilitated.

An experimental torch (Fig. 16.10) small enough to be passed through the 2-in.-ID access pipe at the top of the core was designed and built. The greatly simplified torch retained only the features believed essential to the cutting process. The orifice dimensions of the Heliarc torch were preserved, while cooling-water lines, the "pilot arc" circuit, and other automatic circuits were eliminated. The experimental torch has performed satisfactorily during trials. Submerged Zircaloy-2 screen has been cut at the rate given above. Life of the torch appears adequate to cut the largest screen into strips.

Future effort will be concentrated on operating the experimental torch for extended periods to check reliability, optimize operating conditions, and make necessary changes in design.

16.1.3 Tungsten-Arc Melting

Preliminary tests were made by using the tungsten-arc melting method to melt a path through the screen under an inert-gas atmosphere. An ordinary welding torch was rigged mechanically to move upward across a vertical screen. At about 120 amp and 15 in./min travel, webs were melted with a minimum of dropping spatter. In most cases, each melted web, after parting, resolidified as two distinct drops on the edges of the cut. However, when drops did fall they were usually of appreciable size and often fused together.

A modification in the tungsten-arc melting method was conceived whereby a cut could possibly be made without moving the torch. A multiple-electrode holder (Fig. 16.11) was designed to hold 12 electrodes spaced 1/2 in. apart in a row. The holder was positioned with electrodes in a vertical row normal to a vertical screen.

Original trials were made with self-control of the arc. When the circuit was energized, the arc at 140 amp established itself at one electrode, melted a hole in the screen, automatically jumped to another electrode, and repeated this to melt a rather wide path and thereby free a section of screen. A large

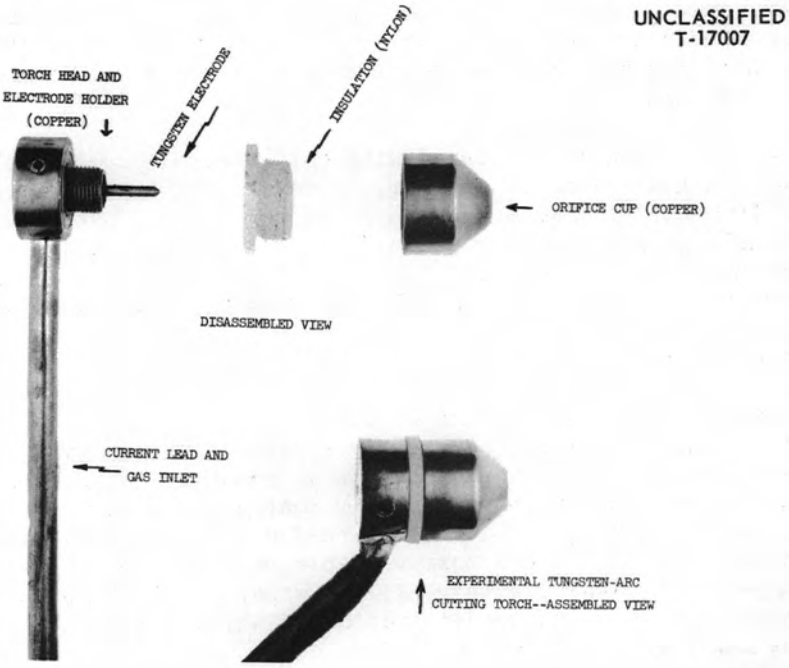

Fig. 16.10. Small Tungsten-Arc Cutting Torch for Removing HRE-2 Screens.

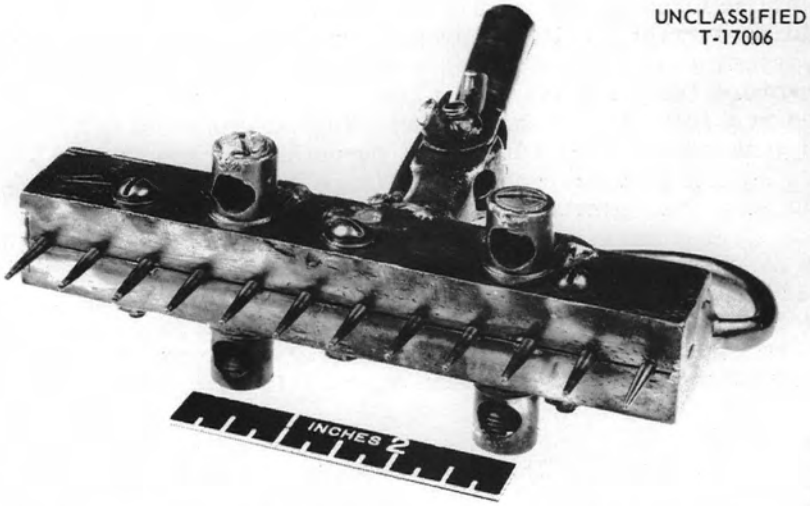

Fig. 16.11. Multiple-Electrode Tungsten-Arc Melting Torch.

volume of spatter in the form of drops was produced.

In an attempt to limit the width of the cut and reduce the volume of spatter, two methods of arc-duty cycle control were established. With time control, cuts were produced at 360 amp, with about 1/2 sec arc-on time, 8 sec arc-off time. With arc-voltage control, cuts were produced at 140 amp by momentarily breaking the circuit when arc voltage increased to about 24--about 4 over the initial voltage.

These control methods, compared with self-control, successfully reduced the width of cut and volume of spatter. However, the individual drops of spatter remained quite large and often fused together. This disadvantage, plus foreseeable difficulties in positioning the holder and in achieving reliable arc control have resulted in work on the multiple-electrode device being discontinued in favor of the Heliarc-cutting method described above.

16.1.4 Core-Tank Repair

Preliminary development work has been done on a method to plug the hole in the HRE-2 core tank by welding a Zircaloy-2 patch into the wall of the vessel. Since the welding operations would have to be remotely controlled, an operation requiring the minimum number of exteriorly controlled welding variables would be most desirable. A tungsten-inert-gas fusion weld using no filler wire appeared to be the simplest and most workable method. Previous work had shown that Zircaloy-2 root passes, without filler wire, could be made successfully. A joint design combined with welding variables which would result in a single-pass weld of maximum thickness and minimum curvature on the face was the goal. With these objectives, 2-in. circles were cut from a 5/16-in. Zircaloy-2 plate; the interior pieces (plug) were prepared by using various root faces and bevel angles. The exterior pieces (the vessel wall) were left as cut. No root gap was used in the welding. The torch was mounted on an arm extending from a center guide rod (positioned at patch center) and motor driven to describe a 360° arc. All welding was done with the plate in a vertical position. Joint design, welding current, and welding-head speed were the variables investigated. In general, closing up the bevel angle tended to produce a face surface of minimum curvature (maximum smoothness) but at the sacrifice of weld thickness and with the requirement of a higher heat input. Increasing the bevel angle gave a weld face of greater width, more curvature, not as flush with the surface, but having greater penetration (more effective weld thickness). None of the welds were full-penetration, full-thickness welds, but they appear to be adequate.

Although basic welding procedures have been developed which appear feasible for welding circular Zircaloy-2 sections in a vessel, it is not known whether proper welding control can be achieved remotely in a limited-access vessel. Work on this method of repair has been stopped in favor of a mechanical patch.

16.2 ZIRCALOY-2 FABRICATION STUDY

The directionality of mechanical properties in sheet or plate Zircaloy-2 is known to be a function of preferred orientation and of defects such as gas stringers and intermetallic stringers which are formed during fabrication.[3] A fabrication schedule developed at ORNL,[3] which includes the step of water-quenching from 1000°C, produces material free of intermetallic stringers (but not gas stringers) and with much less preferred orientation and anisotropy of mechanical properties than that produced by the generally accepted commercial schedule.

Although the new fabrication schedule produced material with better properties, it had not been shown that material with optimum properties was produced, nor was it shown how the anisotropy of mechanical properties varied with changes in the fabrication procedure. A study of the effects of fabrication variables on the preferred orientation and anisotropy of mechanical properties was undertaken for the following reasons:

1. To attempt to improve the current HRP fabrication schedule.

2. Isolate the effects of the fabrication variables so that it might be possible to predict the anisotropy of properties produced by a given schedule and to devise a fabrication schedule for producing the desired degree and type of anisotropy.

3. Provide sufficient background information on preferred orientation and fabrication variables to enable analyses to be made of production fabrication problems and to provide their solution from examination of failed material.

4. Possibly to provide a means of evaluating production material for quality control and for setting manufacturing specifications.

Sixteen experimental fabrication schedules were designed, and approximately 1/4 to 1/2 ft^2 of 1/4-in.-thick Zircaloy-2 was rolled to each schedule. The variables were:

1. the number of beta quenches,
2. the location of beta quenches in the schedule,
3. the proportion of beta rolling,
4. the alpha-rolling temperatures,
5. the amount of final warm rolling,
6. the degree of cross-rolling,
7. the location of cross-rolling in the schedule.

Complete tensile and impact energy data have been obtained for ten of the sixteen experimental schedules and for two commercially fabricated lots from large Zircaloy-2 ingots, one straight-rolled to the present HRP schedule, and one cross-rolled during ingot breakdown.

Analysis of the tensile data has shown, as reported previously,[4] that the effects of the fabrication variables on anisotropy cannot be separated by use of the values for yield strength, tensile strength, elongation, or reduction of area. Such anisotropy is present, however, since all fractured specimens had elliptical cross sections. Optical comparator measurements made on the cross sections of the gauge area of the fractured specimens showed that the cross sections were always ellipses; these ellipses varied with fabrication schedule and are reproducible; the eccentricity varied from fracture to shoulder; and the change in eccentricity with distance from the fracture varied with fabrication procedure.

As an aid in separating the fabrication variables, an empirical equation was formulated for a calculation involving the amount of plastic flow in the major and minor axes and the reduction of area in order to yield a dimensionless number, called the "elliptical index." The equation defining the elliptical index (EI) is:

$$EI = \frac{\frac{a}{r - a} \Big/ \frac{b}{r - b}}{1 - \frac{ab}{r^2}},$$

where

a = length of major semiaxis of the ellipse of cross section,
b = length of the minor semiaxis of the ellipse of cross section,
r = radius of original specimen gauge section.

The dimensions concerned in the calculation are represented graphically in Fig. 16.12.

The elliptical index number thus has the following properties:

1. It can be calculated at any point along the length of the tensile specimen.

2. For a given reduction in area, the index number approaches a low value as the eccentricity of the ellipse of cross section decreases.

3. If the eccentricity of the ellipse of cross section is relatively high, the index number will be large, even for a high reduction of area.

4. A plot of elliptical index number vs distance from the fracture toward the shoulder will show double-necking and uniform elongation (when they occur) and the change in the anisotropy of plastic flow with degree of strain.

5. Comparison of these numbers taken from the fracture of specimens will provide information on the effects of fabrication on isotropy.

Values for conventional tensile properties and for the elliptical index at the fracture for four fabrication schedules are presented in Table 16.1. Three of these schedules (62, 10, and J) are basically the present HRP schedule, and differ only in the degree and location of cross rolling in the fabrication procedure; the other schedule (schedule 8) is from plate which was alpha-rolled at 1000°F and annealed at 1470°F. With schedule J, the ingot was cross rolled during the initial breakdown; while with schedule 10, the cross rolling was performed as the final warm-working step after the beta quench. No cross rolling was used with schedule 62. From the tensile data it would appear that schedule 8 produces the more nearly isotropic material; however, the index data show that this is far from true.

A more complete study of anisotropy may be obtained by a study of plots of the index numbers vs distance from the fracture. Such data for the four schedules are shown in Fig. 16.13. Variations in the location and the shape of the curves show that the elliptical-index data can provide effective separation of the fabrication variables under study. They are capable of revealing differences in the development of anisotropy of flow properties both within and between fabrication schedules. Differences may occur in samples which would not be revealed by comparing only the index number at the breaks but which are revealed by the different shapes of the curves.

Impact energy vs temperature data, using subsize Izod V-notch specimens with notches oriented in both the rolling plane and normal to the rolling plane,[5] have been obtained on ten of the experimental schedules and on one

UNCLASSIFIED
ORNL-LR-DWG 38672

$$\text{ELLIPTICAL INDEX} \equiv \frac{\dfrac{a}{r-a} \Big/ \dfrac{b}{r-b}}{1 - \dfrac{ab}{r^2}}$$

r = GAGE SECTION RADIUS OF TENSILE SPECIMEN

a = MAJOR SEMI-AXIS OF TENSILE SPECIMEN CROSS-SECTION AFTER FRACTURE

b = MINOR SEMI-AXIS AFTER FRACTURE

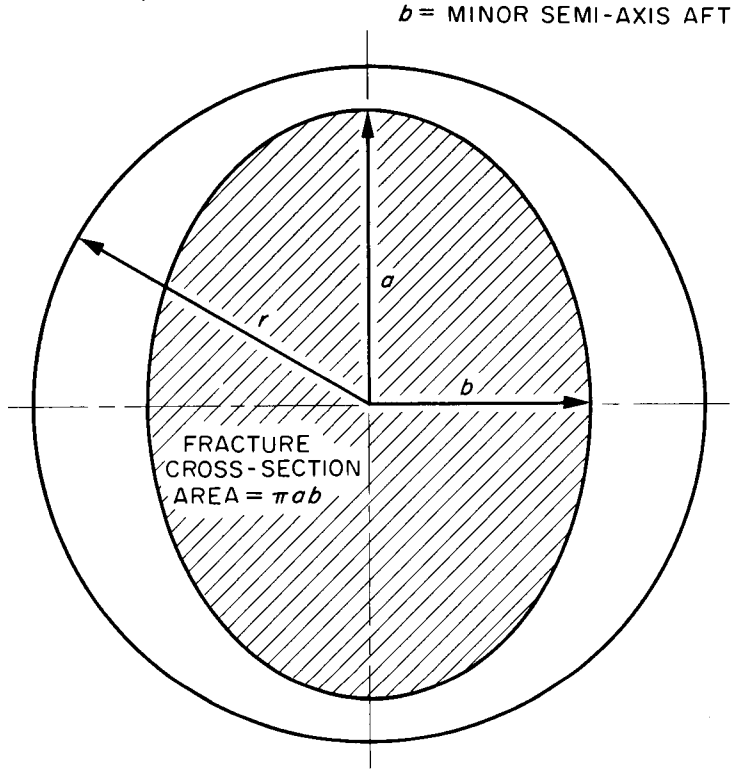

Fig. 16.12. Definition of Elliptical Index Terms.

Table 16.1. Tensile Properties of Zircaloy-2 at Room Temperature

Specimen No.	Orientation	Tensile Strength (psi)	Yield Strength (psi)	% Extension in 1 in.**	% Reduction in Area	Elliptical Index at Fracture
62-1	Transverse	74,500	63,000	22.0	43.3	6.08
62-2	Transverse	74,000	63,400	22.5	44.0	5.99
62-5	Longitudinal	75,700	55,400	22.5	45.5	3.42
62-6	Longitudinal	75,900	56,200	22.5	43.8	3.47
10-7	Transverse	73,200	66,000	22.5	52.6	8.17
10-8	Transverse	73,700	67,100	21.0	51.6	7.30
10-1	Longitudinal	75,000	56,600	22.5	48.3	4.86
10-2	Longitudinal	75,000	57,500	22.5	50.0	4.38
J-7	Transverse	78,100	69,400	21.5	44.6	3.38
J-8	Transverse	78,100	70,500	21.5	44.9	3.16
J-1*	Longitudinal	74,800	51,800	23.0	36.0	6.96
J-2*	Longitudinal	75,000	52,300	21.0	31.2	7.27
8-1	Transverse	67,900	58,200	19.0	42.0	22.65
8-2	Transverse	68,200	58,400	20.0	45.3	21.32
8-27	Longitudinal	68,500	56,100	22.5	45.5	21.50
8-31	Longitudinal	67,100	53,700	26.0	48.2	15.07

*Minor axis of elliptical fracture cross section normal to the plane of the plate. Major axis normal in all other cases.

**Measured on sample.

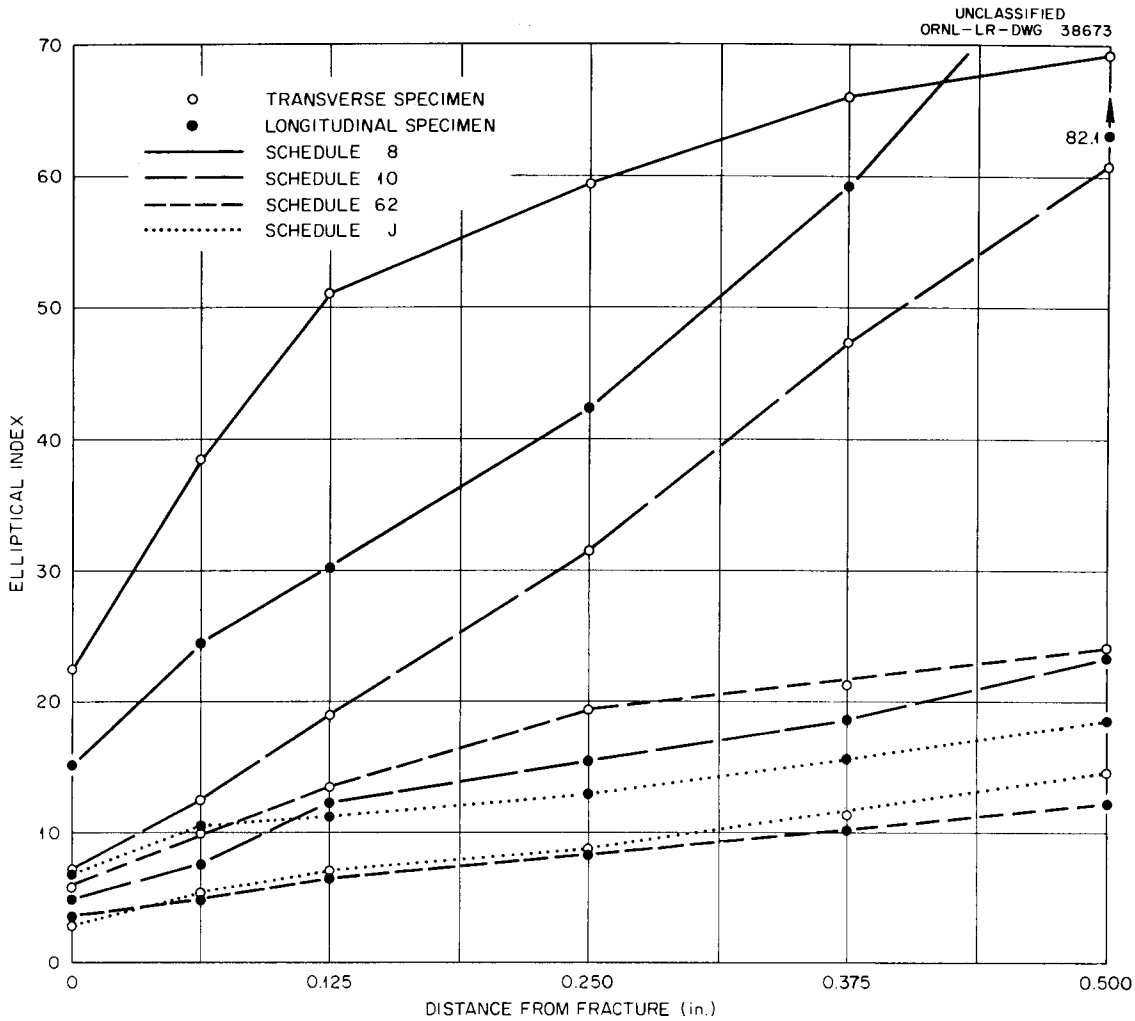

Fig. 16.13. Plot of Elliptical Index vs Distance-from-Fracture for Zircaloy-2 Tensile Samples Fabricated According to Various Schedules.

of the two commercial schedules. Examination of the curves plotted from the data has shown that the impact-energy test modified to provide for variation of notch orientation provides a better separation of the effects of anisotropy in the fabricated plate than does the normal tensile test. Comparison of the plots of impact energy vs temperature, presented in Fig. 16.14 for three of the schedules, will show the differences developed by the fabrication schedules previously discussed. The principal effect observed is that the energy values for the L_V orientation are shifted from a low-energy level to a considerably higher level at temperatures above 100°C. The material produced by schedule 10 is more isotropic in its mechanical properties, although the preferred orientation is, in one way, more highly perfected.

Examination of the impact energy vs temperature curves obtained for the other schedules has shown that the principal effect observed for the fabrication variables is that fabrication in the alpha field without intermediate beta quenches causes a rather large divergence of the curves for vertical- and horizontal-notch orientations. Higher energy absorption but much lower transition temperatures occur for alpha-rolled material in specimens with notches normal to the rolling plane.

Preferred-orientation data are being collected by means of conventional and inverse-pole-figure determinations. Such data have been obtained on three schedules previously discussed and are shown in the pole figures presented in Fig. 16.15. The pole-figure plots show the intensity of orientation of the pole of the basal plane (002) and of a plane (110) equivalent in distribution to the prism plane $(10\bar{1}0)$ of the close-packed hexagonal unit cell for Zircaloy-2. In the schedule-62 material, the basal poles are oriented almost at random in a band containing the transverse and normal directions and are completely absent from the region around the rolling direction. The other pole figures determined on the same material have shown that the pole of the prism plane $(10\bar{1}0)$ is almost randomly oriented in the plane of rolling except for being absent in the small high-intensity area occupied by the basal poles. Thus, knowing the distribution of the deformation systems available for flow in all directions, it is possible to predict the following:

1. The ductility in the thickness direction will have a reasonable value but not as great as those in the rolling and transverse direction.

2. There will be an ellipticity of cross section, about the same in all orientations of specimens, which will not be large and in which the major axis of the ellipse will be parallel to the normal to the rolling plane.

3. The normal tensile values will be approximately the same for all orientations of tensile specimens in the plane of the plate.

Similar determinations on the material of schedule J show that cross rolling during ingot breakdown concentrated the basal-plane poles around the transverse direction and the prism-plane poles around the rolling direction. Cross rolling during the final warm-working operation (schedule 10) concentrated the basal-plane poles around the normal to the rolling plane and randomly distributed the prism-plane poles in the rolling plane except for a relatively small area around that normal. These data permit the prediction that, in the schedule J material, the major axis of the ellipse of cross section rotates from the direction of the normal to the rolling plane for the transverse specimen to the transverse direction for the longitudinal specimen, providing,

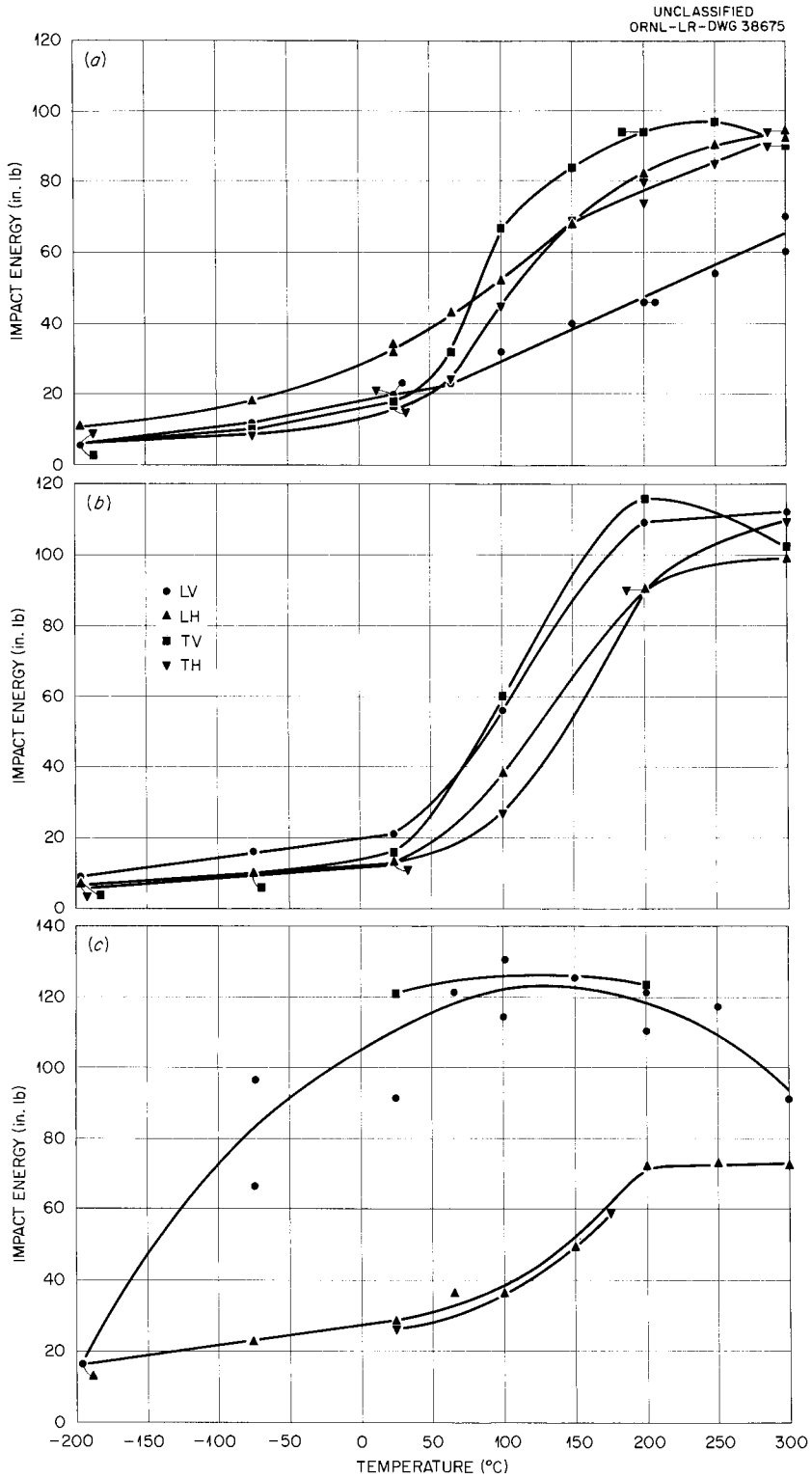

Fig. 16.14. Subsize Izod Impact Curves for Zircaloy-2 Fabricated According to Various Schedules. (*a*) Schedule J – HRP schedule with cross-rolling during breakdown. (*b*) Schedule 10 – HRP schedule with cross-rolling after beta quench. (*c*) Schedule 8 – alpha rolled plus anneal at 1470°F.

UNCLASSIFIED
ORNL-LR-DWG 38678

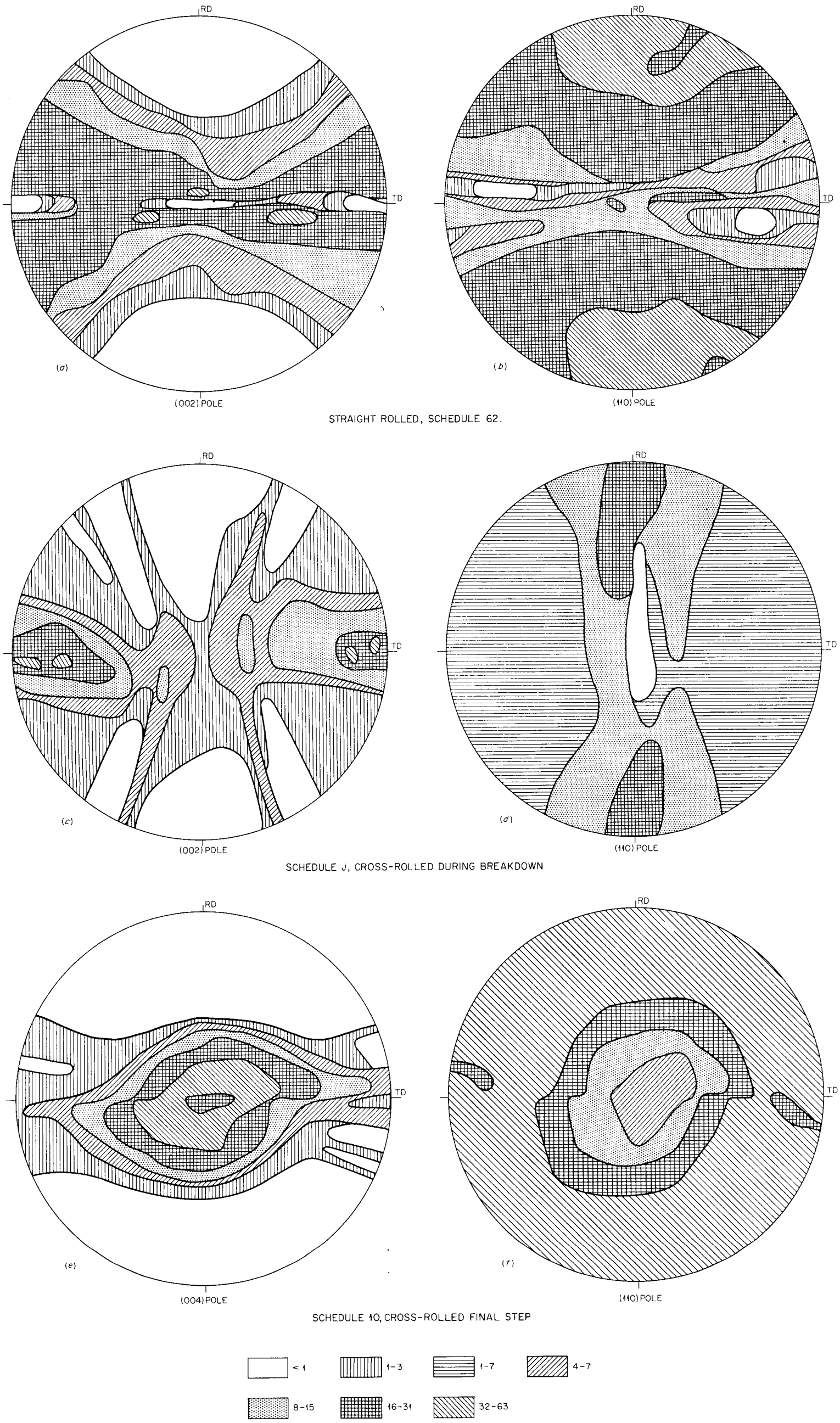

Fig. 16.15. Pole Figures Showing Effect of Cross Rolling in Fabrication of Zircaloy-2.

for the first time observed, greater ductility in the thickness direction of the plate. It would also be predicted that the ductilities in all directions would have reasonable values. For the schedule 10 material, it would be predicted that (1) the ductility in the thickness direction would be decreased appreciably in comparison with the other schedules, causing increased ellipticity; that (2) the ellipticity at the fracture would not change greatly with orientation of the specimen in the rolling plane; and that (3) the tensile properties would not change appreciably with specimen orientation in the plane of the plate.

Examination of the tensile data and the elliptical index plots shows that the above predictions, made from the preferred-orientation data, are borne out. Complete analyses of the above types are being made on all the experimental fabrication schedules. The cross comparison of the different types of information obtained for all the fabrication variables should provide a guide, as indicated by the correlations that can be made between the preferred-orientation data and the elliptical-index data presented, for extrapolation of the results to other fabrication schedules.

No explanation or prediction of the impact-energy curves can yet be made from either the elliptical-index or the preferred-orientation data according to the examinations made to date. It is hoped that a better analysis of the stress system operating in the impact specimen during fracture can be made, allowing prediction of the energy absorption values according to the preferred-orientation data, and then according to the elliptical-index data.

The data obtained to date are not sufficiently complete to permit major conclusions to be drawn, although some trends have been established. It has been shown that the types of analyses being made are quite useful and probably necessary for the understanding of the development and effects of anisotropy in the fabricated plate. It has been shown that the elliptical-index analysis permits considerably more useful information to be obtained from the conventional tensile test specimens.

16.3 ZIRCALOY-2 FORMING STUDY

16.3.1 Fabrication of a Spherical Vessel

An evaluation has been completed of the study to determine the feasibility of forming Zircaloy-2 hemispheres by power spinning. The details of this study, in which successful hemispheres were made, were discussed in the last HRP Quarterly Progress Report.[5]

Plates of three different thicknesses, 1/8 in., 1/4 in., and 5/16 in., were hot spun on 15-in.-dia hemispherical dies. Table 16.2 lists the variation in thickness of the spun area, the average thinout at the equator, the average inside diameter at the equator, and the eccentricity (out-of-roundness) at the equator. The equatorial diameter was only reproducible within 0.185 in. for shells of the same starting thickness. It should be noted that all the dimensions evaluated varied from the desired values more in the case of the thicker plate than in the thinner. This was not expected, since the greater amounts of deformation possible and better control in the thicker material were expected to have promoted a closer approach to ideality.

The necessity of welding the hemispheres together to form a spherical vessel makes the eccentricity a most significant variable. Weld "fitups" of

Table 16.2. Average Dimensions of Zircaloy-2 Hemispheres

Effect of Spinning	Starting Thickness		
	1/8	1/4	5/16
Variation in thickness, in.	0.032	0.037	0.159
Thinout at equator, in.	0.035	0.050	0.100
Inside diameter at equator, in.	15.172	15.488	15.544
Eccentricity, in.	0.050	0.058	0.078

less than 0.025 in. would obviously necessitate machining of the surfaces near the equator. While such tolerances were not obtained, it was possible by hand fitting and a minimum of machining to obtain joints that could be welded. Two 1/4-in.- and one 1/8-in.-thick spheres were successfully welded.

While this method is capable of satisfactorily forming hemispheres of the required size, it is not giving the very close tolerances expected. It is possible that closer tolerances could be obtained by additional development work that does not now appear to be warranted. Since this process will require machining to the desired tolerances, other fabrication methods (hot pressing and pack pressing) which originally did not look so promising will also be investigated.

16.3.2 Fabrication of Pipe-to-Vessel Transition

In connection with the program discussed above, a limited study has been conducted to determine the amenability of Zircaloy-2 pipe and hemispherical shells to flaring by hot pressing. This effort was motivated by a desire to effect a transition from a pipe to a spherical vessel requiring only a single weld. A pair of formed, carbon steel dies were used to press a preheated pipe, or shell, into the desired shape (Fig. 16.16). A pipe, 3.43 in. OD and having a 0.215-in. wall, was flared to a maximum outside diameter of 5.91 in., at which point slight discontinuities appeared (Fig. 16.17a). These size ratios are similar to ones that would be required for fabrication of presently conceived HRE-3 type core tanks. The wall thickness at the point of maximum deformation was 0.181 in., representing only 35% of the thinout calculated on a simple stretching model. Since the wall thickness of the vessel must be maintained throughout the transition, it is a most desirable effect. It is believed that compressive loading of the pipe during pressing caused thickening of the wall (upsetting) which accounts for the reduced thinout.

A hemispherical shell 15 in. in diameter and having a 0.207-in. wall at the pole was also flared. A 2.10-in. hole at the pole was expanded to 3.96-in. with no difficulty and practically no thinout (Fig. 16.17b).

A pipe-and-hemisphere pair, successfully pressed in a similar manner, will be welded into a completed pipe-to-vessel transition mockup. Specimens will also be prepared for x-ray analysis of the deformation textures produced.

The results of this study are encouraging, and it appears that a full-size transition can be made by a relatively simple pressing operation and with only a moderate development program.

UNCLASSIFIED
ORNL-LR-DWG 38684

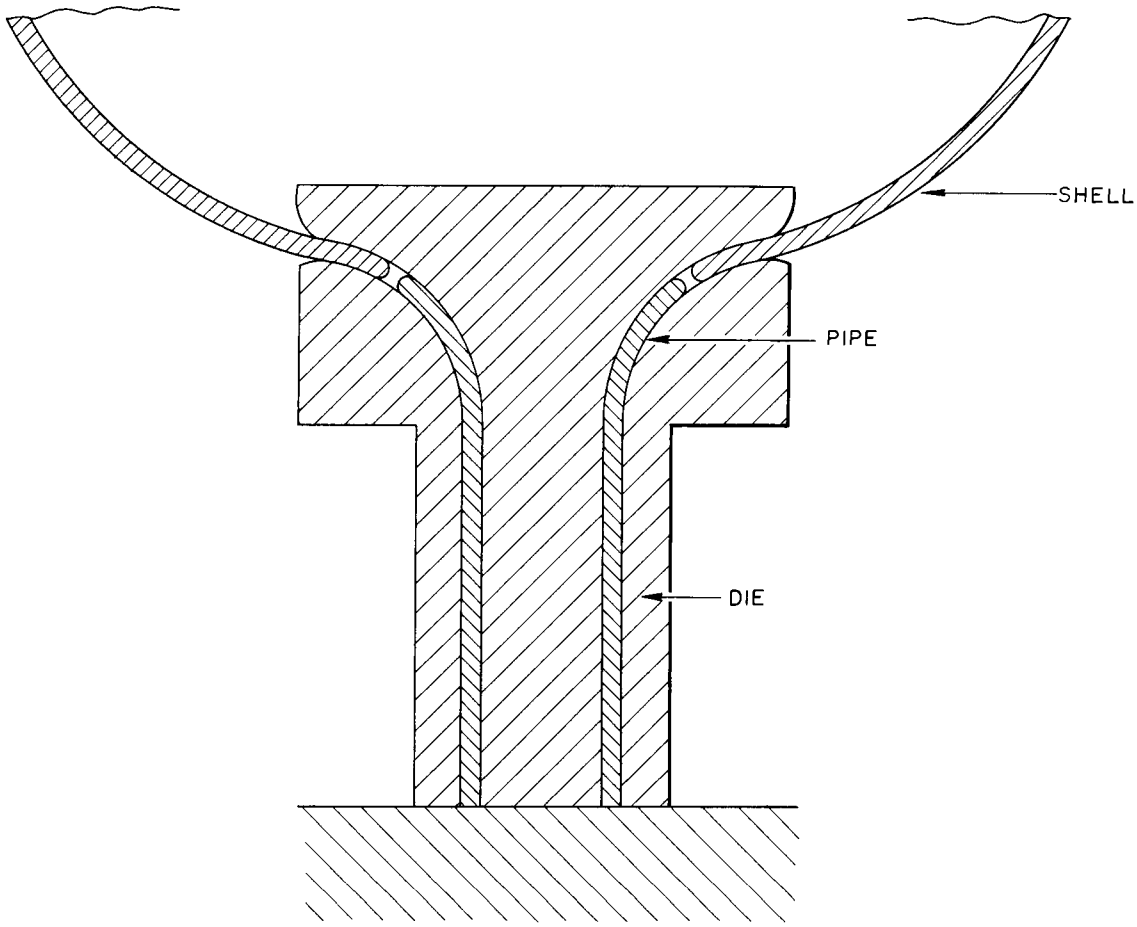

Fig. 16.16. Flared Zircaloy-2 Pipe and Shell in Die.

UNCLASSIFIED
T-16986

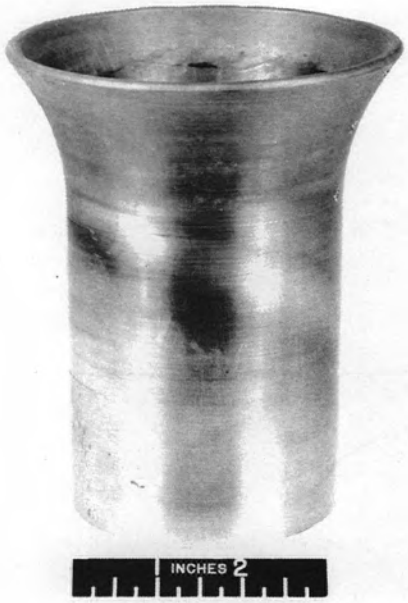

UNCLASSIFIED
T-16985

Fig. 16.17. Zircaloy-2 Parts Formed by Warm Pressing. (*a*) Flared pipe. (*b*) Reverse curvature in hemisphere.

16.4 WELDING DEVELOPMENT

16.4.1 Composite Welds

The use of heat exchangers constructed from composite tubing and tube sheets could be desirable in homogeneous-reactor environments for obtaining a system with maximum corrosion resistance to both of the media which must be contained. However, previous work on the welding of type 347 stainless steel tubes clad exteriorly with Inconel into a type 347 stainless steel Inconel-clad tube sheet had not been successful.[5] Invariably, cracking had been found in the type 347 cover passes. The use of such materials as Incoloy, Hastelloy W, and Inor 8 as barrier passes between the Inconel and stainless steel reduced the general cracking in the cover deposit, but it was still present in craters.

Additional tube-to-header welds have been made by using composite 1/2-in.-dia., 1/16-in.-wall tubing with an Inconel-to-type-347-stainless-steel ratio of 60/40. Successful welds were made using the configuration shown in Fig. 16.18. All welding was performed by using the tungsten-inert-gas process with filler-wire additions and with current tapering in extinguishing the arc over a crater. The use of a stainless steel containing less nickel, type 312 (29% Cr, 9% Ni), as the barrier eliminated the cracking difficulties, both in the deposit and in the craters. With this barrier material deposited on the Inconel root passes, successful cover passes were made by using types 347, 308L, and 312 stainless steel. While it may be desirable to strip the Inconel from the tube where it contacts the cover pass, this would not eliminate the necessity of a barrier pass, and in this work was not necessary for a satisfactory weld.

16.4.2 Zircaloy-2

Welding procedures for Zircaloy-2 now in use in the Homogeneous Reactor Project are quite rigid in terms of the machining tolerances on the joint design. The required land is 0.025 in., and the maximum misfit of the two sides must be less than 0.010 in. Such tolerances actually reflect the tolerance allowed on the inside diameter of shapes such as pipes, cylinders, cones, and spheres. This degree of precision in preparation is necessary to secure uniform-quality weldments. The trend in vessel design has been toward the elimination of welds by the direct formation of shapes by hot pressing, spinning, and flaring. The acceptability of these methods would be greatly increased by relaxation of final dimensional requirements. With this in view, work was started on mechanical welding procedures which have shown promise of yielding successful welds with less-stringent joint specifications.

Mechanized tungsten-inert-gas (TIG) equipment with a trailer shield and grooved plate for inert-gas coverage on the face and root side of the weld, respectively, was used for this work. Zircaloy-2 plate, 0.210 in. thick, with root faces of 0.062, 0.083 and 0.125 in. was used in various conventional joint designs. Plates were butted to facilitate fitup, and the root passes were straight fusion passes without filler wire. Full-penetration root passes were achieved with misfits of 0.025 in. on the root surface of plates having a 0.125-in. land. Figure 16.19 is a photograph from the root side of one test weld made under the following welding conditions: 215 amp; 2-1/4-in./min head speed; argon torch gas, 25 ft^3/hr; No. 12 gas cup; argon backup gas 30 ft^3/hr; trailer argon, 50 ft^3/hr; 0.125-in. lands; misfit, 0.010 in. A full-penetration, uncontaminated root pass was obtained, as determined by metallography.

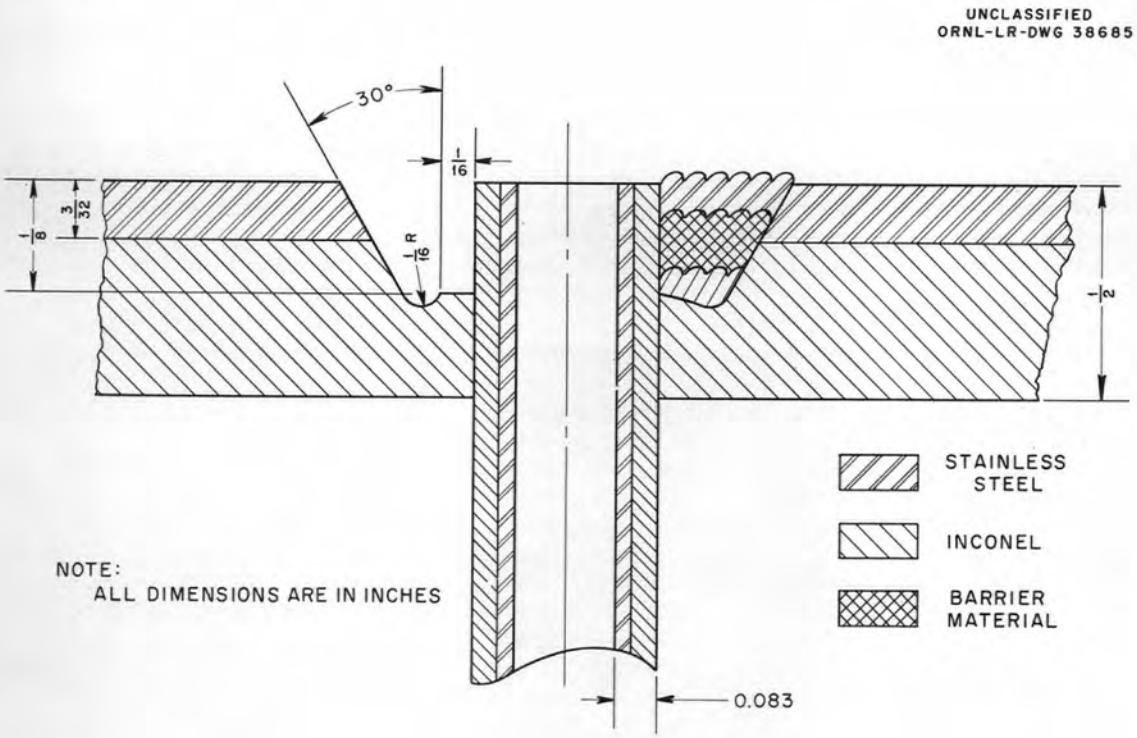

Fig. 16.18. Weld Joint Configuration for Inconel Clad Stainless Steel Tubes and Stainless Steel Clad Inconel Tube Sheet.

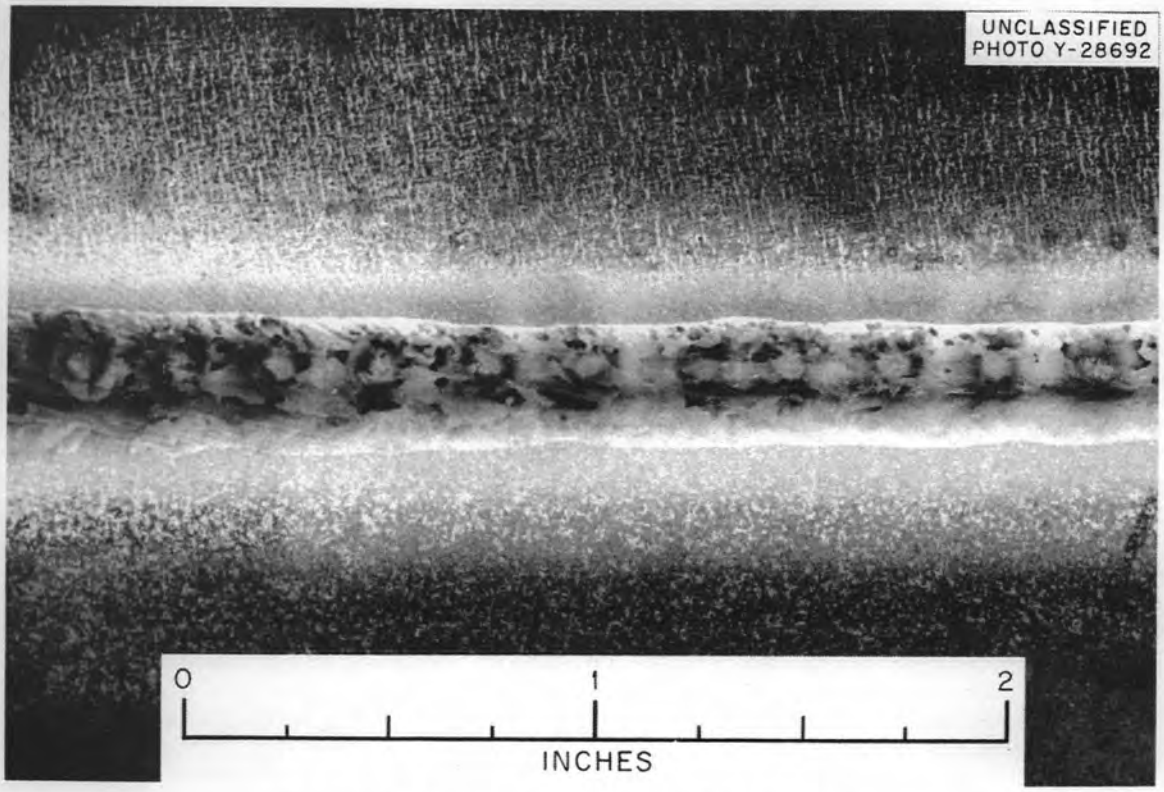

Fig. 16.19. Photograph of Zircaloy-2 TIG Machine Weld.

16.5 COMBUSTION OF TITANIUM AND ZIRCONIUM

A final report on present phases of the work on combustion of titanium and zirconium has been issued by Stanford Research Institute.[6] For titanium, a curve has been developed which shows a marked reduction in oxygen pressure required for ignition as the temperature increases.

Difficulty is still being encountered in obtaining reproducible data from Zircaloy-2. As the methods are improved, the critical oxygen pressure keeps decreasing. The lowest values obtained so far have been 250 psi oxygen in a static system and 50 psi in a dynamic system.

Prime responsibility for this contract has now been assumed by the Reactor Safety Branch of the AEC. At this time no additional work is scheduled within the Laboratory.

16.6 NONDESTRUCTIVE TEST DEVELOPMENT

16.6.1 Resonance Measurements of HRT Core Vessel

An internal-positioning rig has been fabricated for obtaining measurements of the resonant frequency of the HRT core vessel and, hence, of its thickness. Trials in the HRT mockup indicate that, mechanically, the rig is satisfactory.

16.6.2 Attenuation of Ultrasonic Energy in Zircaloy-2

Measurements of the attenuation of ultrasonic energy in the range of frequencies most often used for inspection have been made by using ultrasound of both longitudinal and shear modes. As might be expected, shear attenuation (α_s) is considerably greater than longitudinal attentuation (α_l); and both modes attenuate directly as the fourth power of frequency, as predicted by the Rayleigh law. The exact relationship of α_s to α_l has not been determined in the general case, but, for the data presently available α_s/α_l is greater than 2 and less than 4. A more exact determination of this relationship should reveal additional information about the basic mechanisms of attenuation.

16.6.3 Measurement of Ultrasonic Velocity in Metals

The velocity of elastic waves in metals is important in determining the elastic constants of the metals and in observing changes in these elastic properties. Several techniques are in use. In essence, a pulse of high-frequency sound is directed into a metal specimen and then echoes between two opposite parallel faces. The time of passage either is measured directly by a time intervalometer or is obtained indirectly by measurement of the length of a water column required to produce an identical time delay.

Both the velocity of a longitudinal mode of vibration (V_l) and the velocity of the shear mode (V_s) are required to define the full set of elastic properties. A shear mode can be produced by use of a Y-cut quartz crystal, or configuration of the specimen may be chosen so that normal beam divergence from an X-cut crystal causes a conversion to shear mode. Either of the methods is straightforward at room temperature, but special couplants and remote access rods must be used for elevated-temperature measurements. At room temperature, V_l for Zircaloy-2 falls between 180,000 and 185,000 fps. Further measurements as well as technique refinements are being made.

16.7 EFFECTS OF RADIATION ON STRUCTURAL METALS AND ALLOYS

All work on the effects of radiation on pressure vessel steels is now supported by the Gas-Cooled Reactor Project, and data will be reported in publications of that project. The limited remaining HRP funds will be used for an elevated-temperature irradiation of zirconium alloys, starting with the May shutdown of the ORR and completion of testing of samples (other than steels) already irradiated.

REFERENCES

1. G. M. Adamson et al., HRP Quar. Prog. Rep. Jan. 31, 1959, ORNL-2696, p 152.
2. H. C. Claiborne, Hole Formation in HRT Core Tank, ORNL CF-58-11-49.
3. M. L. Picklesimer and G. M. Adamson, Development of a Fabrication Procedure for Zircaloy-2, ORNL CF- 56-11-115.
4. G. M. Adamson et al., HRP Quar. Prog. Rep. Oct. 31, 1958, ORNL-2654, p 184.
5. G. M. Adamson et al., HRP Quar. Prog. Rep. Jan. 31, 1958, ORNL-2493, p 146-159.
6. F. E. Littman and F. M. Church, Reactions of Metals with Oxygen and Steam, Stanford Research Institute Final Rep. No. AECU-3882, Feb. 15, 1959, SRI Project No. SD-2116.

Part V

CHEMICAL ENGINEERING DEVELOPMENT

D. E. Ferguson

17. URANYL SULFATE FUEL PROCESSING

R. A. McNees P. A. Haas

M. H. Lloyd S. Peterson E. L. Youngblood

17.1 FUEL-SOLUTION BEHAVIOR

When simulated HRT fuel solution containing 1200 ppm of nickel is heated to 335°C, a blue-green solid is formed which, when the solution is cooled, is converted to a light yellow-green solid that redissolves very slowly at 25°C.[1] Analysis showed it to be nickel sulfate containing only trace amounts of uranium and copper.

17.2 SOLIDS BEHAVIOR

In further study of the effects of variables on the performance of hydroclones in removing corrosion-product solids from a circulating loop, a 3-in.-dia hydroclone with a feed rate of 30 gpm was substituted for the smaller hydroclone (0.6-in.-dia, 1-gpm flow rate) used in previous tests.[2] Under conditions reproducing as nearly as possible the conditions of previous runs, the amount of solids collected was not greater than 10% of the solids produced by corrosion, about the same as was removed by the smaller hydroclone.

17.3 HRT SOLIDS

In order to determine the isotopic composition of the uranium in different solids removed from the HRT, various methods were tested for recovering and decontaminating the uranium from such solids. Of the methods tested, complete dissolution of solids was obtained by boiling with 10.8 M H_2SO_4 and then diluting to 4 M and boiling again, or by fusion with potassium-hydrogen fluoride followed by dissolution of the melt in 6 M HCl. The best recovery (60%) of the 1 mg of uranium contained in 100 mg of solids was obtained by passing the diluted (0.25 M) sulfuric acid solution through Dowex 1 resin in the chloride form, washing the resin with 6 M hydrochloric acid, and finally eluting with 0.1 M acid. By a similar ion-exchange method, less than 30% of the uranium was recovered from the bifluoride fusion - hydrochloric acid dissolution. A solvent-extraction scheme was not found which is sufficiently dependable and simple for remote operation in a hot cell. The sulfuric acid dissolution and ion-exchange method will be used to isolate and decontaminate uranium from actual HRT chemical plant solids and scale.

Small segments of the titanium holder used to support corrosion test specimens in the core of the HRT during run 17 were subjected to various descaling treatments, and portions of the scale were analyzed. Three different solutions

completely removed HRT scale from titanium: (1) 0.8 M $CrSO_4$ - 0.5 M H_2SO_4 solution at 85°C, (2) boiling Turco 4502 solution followed by 30% HNO_3, (3) a 1:1 volume mixture of Deoxidine 170 and water at 104°C. The action of both the chromous sulfate solution and Turco reagents was essentially complete in 1 hr, but about 20 hr was required for the diluted Deoxidine. Not effective as descaling agents were dilute oxalic acid at 25°C, dilute or concentrated nitric acid, either hot or cold, and a dilute nitric acid - hydrogen peroxide mixture at 25°C. The latter reagent partially removed some scale, which contained copper, chromium, titanium, zirconium, and iron in the weight ratio of 1/5/17/23/25. No uranium was found in this batch of solids, but since the solids had been loosened from the metal by the nitric acid - hydrogen peroxide treatment, uranium initially present could have been leached out prior to analysis.

17.4 NICKEL REMOVAL FROM FUEL SOLUTION BY ELECTROLYSIS

Laboratory studies showed that an attractive method for controlling the buildup of nickel and manganese in HRT fuel solution as the result of corrosion of stainless steel is to remove these elements from solution electrolytically. A platinum anode and mercury cathode gave best results. When the mercury cathode was used, the combined concentration of nickel and manganese in the concentrated fuel solution was decreased to less than 50 ppm. Concentrating the fuel solution to 60 g of U per kg of D_2O increases the sulfuric acid concentration to 0.2 M and thereby prevents hydrolytic precipitation of the tetravalent uranium produced during electrolysis. When a solid-metal cathode was used, the nickel concentration could not be decreased below about 4 g of Ni per kg of D_2O; manganese was usually not removed at all, although precipitation of some manganese dioxide at the anode was observed. After electrolysis, the tetravalent uranium formed during electrolysis can be reoxidized to the hexavalent state by contacting with an O_2-O_3 gas mixture.

When the amount of combined nickel, copper, and manganese in the mercury cathode is greater than about 1%, the mercury cathode begins to solidify and a solid amalgam phase is formed. Removal of nickel, copper, and manganese from the mercury so that it could be re-used in the electrolytic cell was best accomplished by treating the cathode material at 25°C with 0.5 M HNO_3 containing 1.5% H_2O_2. Stronger oxidizing reagents at times gave satisfactory results but sometimes resulted in excessive attack on the mercury.

Installation of equipment was completed in order to test the electrolytic removal of nickel from 30-gal batches of 0.4 m UO_2SO_4 solutions simulating concentrated HRT fuel. Preliminary runs were made with solutions of copper, nickel, and manganese sulfates in water - sulfuric acid without uranyl sulfate. When amalgam concentrations of about 1% were reached, the electrodes shorted via a solid amalgam which floated on the mercury cathode. Careful cell design will be necessary to avoid this problem as well as that of the localized electrolytic corrosion and excessive leakage currents observed in these preliminary experiments.

REFERENCES

1. R. A. McNees, et al., HRP Quar. Prog. Rep. January 31, 1959, ORNL-2696, p 170.

2. Ibid., p 171.

18. EQUIPMENT DECONTAMINATION

R. A. McNees J. F. Manneschmidt A. B. Meservey

A canned-rotor pump from the HRT chemical plant was descaled and partially decontaminated by two cycles of $CrSO_4$ (0.8 M) - H_2SO_4 (0.5 M), alternated with dilute HNO_3 containing 3% H_2O_2. The beta-gamma activity of the inlet flange was reduced from over 200 to 10 r/hr at the HRT site. Further decontamination of the pump flange with chromous sulfate solution in the laboratory decreased the activity to about 70 mr/hr.

Two objections to the use of chromous sulfate solutions have been the difficulty of preparation and the excessive corrosion rate on titanium. Gallon amounts of solution were quickly prepared by heating a slightly acidified solution of chromic sulfate to 80°C in contact with mossy zinc, under nitrogen. The corrosiveness of the solution was decreased by lowering the H_2SO_4 content from 0.5 to 0.1 M. At this lower acidity, the corrosion rate is 40 mpy for titanium. Also, at the lower acidity (0.1 M), oxidation of chromous to chromic ion by water at 100°C is only 8% as fast as at the higher (0.5 M) acidity.

Specimens of HRT pipe were descaled and decontaminated by Deoxidine 170, a proprietary reagent containing inhibited phosphoric acid. When a piece of pipe was exposed for 92 hr in a boiling (104°C), equal-volume mixture of Deoxidine 170 and water, the scale was dissolved, and the gamma decontamination factor was 10^3. Corrosion rates were 0.7 mpy for type 347 stainless steel and Zircaloy-2, and 42 mpy for titanium.

19. THORIUM OXIDE SLURRY DEVELOPMENT

J. P. McBride	P. A. Haas	W. H. Lewis
S. D. Clinton	N. A. Krohn	R. L. Pearson
C. C. Haws	K. H. McCorkle	C. E. Schilling
K. O. Johnsson	L. E. Morse	R. H. Winget

19.1 SLURRY IRRADIATION STUDIES

19.1.1 Slurry Irradiations in the LITR

Two short-term slurry irradiations were made in the C-44 vertical-tube facility of the LITR. The first test (LITR-53) was on a slurry of unpumped Westinghouse 650°C-fired ThO_2, containing 250 g of Th per kg of D_2O, with 145 ppm of palladium and 0.5 wt % of U^{235} (based on Th). The slurry was irradiated at 290°C under oxygen pressure (250 psi at room temperature) for 242 hr; it was removed because of failure of the solenoids which drive the stirrer. No accumulation of radiolytic gas was noted at temperature, and 228 psi of residual gas pressure was found upon cooling at the end of the experiment.

The second test (LITR-54) was on a slurry (250 g of Th per kg of D_2O) of ThO_2 - 8% natural uranium prepared by the adsorption method and fired at 1050°C. It was sealed in air and irradiated for 335 hr at temperatures from 265 to 300°C. No radiolytic gas was detected at these temperatures, although a residual pressure of 105 psi at 45°C was found at the end of the test.

19.1.2 Postirradiation Examination

Three previously irradiated slurries (LITR-50, 51, and 52)[1] were recovered for analysis. The first two were analyzed in the usual way for fission-product distribution (Table 19.1), which was in agreement with previous results. The entire sample for LITR-52 was used in an unsuccessful effort to determine the amount and distribution of the palladium catalyst, but the amount was too small for determination.

19.1.3 Slurry Irradiations in the Graphite Reactor

A slurry of 500 g of Th per kg of D_2O of Th - 2.8% U^{235} was irradiated in Hole 11 of the Graphite Reactor under an initial D_2 gas pressure of 250 psi at room temperature. The slurry was irradiated for a week at temperatures from 164 to 200°C, generating small amounts of radiolytic gas ($<$ 100 psi). At this point the stirrer stopped, and an increased rate of gas generation made it necessary to increase the temperature to 250°C in order to increase the rate of back reaction. The stirrer restarted after $\sim$24 hr, and the experiment continued at

Table 19.1. Distribution of Fission Products in Irradiated Slurries

Slurry: 500 g of Th per kg of D_2O, 650°C-fired; 3% natural uranium; 122 ppm Pd; pump-loop sample from Pennsylvania Advanced Reactor Project
Conditions: irradiated at 300°C in the LITR

Experiment No.	Amount in Supernatant (%)								
	Gross β	Gross γ	Sr	Cs	Ru	TRE	Zr-Nb	I	Pa
LITR-50*	1.0	1.2	22.0	8.0	<0.1	1.6	<0.1	<0.1	<0.1
LITR-51*	1.1	1.1	4.5	13.5	5.4	2.9	0.8	<0.1	1.0

*See ref 1 for descriptions of the experiments.

temperatures varying from 200 to 282°C. Equilibrium pressure observed during the next several weeks was about 1200 psi of radiolytic gas at 200°C. This pressure was higher than found early in the test and agreed with that previously determined without a D_2 overpressure.

19.1.4 Oxygen Solubility in Aqueous Slurries

As a preliminary to measuring the solubility of oxygen in aqueous slurries, the solubility of oxygen in water was determined in the equipment intended for use in the study.[2] The isotherms obtained were shown in Fig. 19.1a. A cross plot of the data from the isotherms was made in order to give the isobars shown in Fig. 19.1b. Henry's law constants calculated from the isotherms are given in Table 19.2. The data are in good agreement with data obtained by a direct sampling technique and reported in the literature.[3]

19.1.5 Equipment Development: Capillary Cooling System for Irradiation Bombs

Efforts to develop improved methods for cooling in-pile experiments continued with further studies on heat removal from and temperature distribution in slurry irradiation bombs or bomb mockups cooled by water flowing through steel capillaries wound around the bombs.

(a) Heat Removal Studies.--In tests with total water flow rates of 80 g/min through two 10 ft stainless steel capillaries, 20 mil ID, which were wrapped separately around each half of a simulated slurry irradiation bomb (Fig. 19.2), 1800 w of heat was removed at a maximum bomb wall temperature of 300°C. The heat generation expected in the LITR is only 300 w. The increase in bomb weight due to the cooling coils was 23 g. The primary limitation on the rate of heat removal was pump output. A second limitation was preferential water flow, and hence preferential cooling, in one of the capillaries caused by vapor binding in the other capillary.

At certain locations on the bomb, severe local temperature cycling with the pump pulse frequency occurred. This was greatly reduced by adding a gas cushion to the pump discharge. The cycling was localized: usually at the inlet point

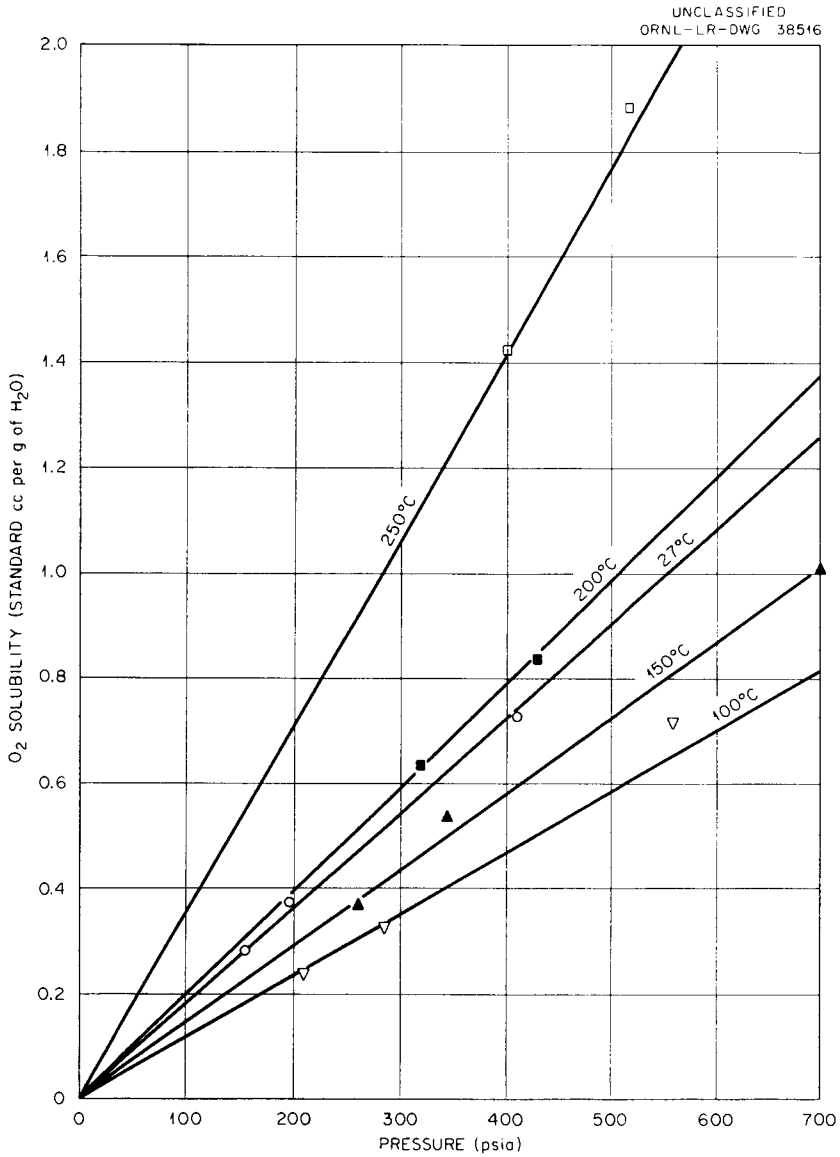

Fig. 19.1*a*. Solubility Isotherms for Oxygen in Water.

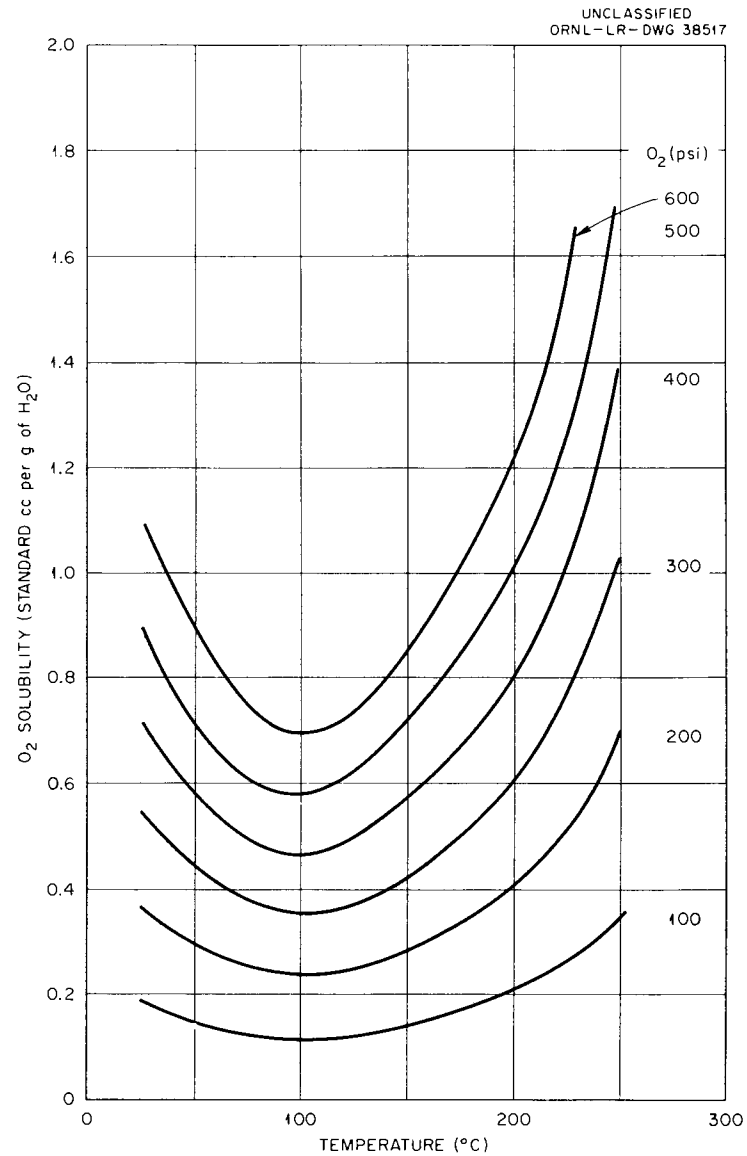

Fig. 19.1*b*. Solubility Isobars for Oxygen in Water.

UNCLASSIFIED
ORNL-LR-DWG 38518

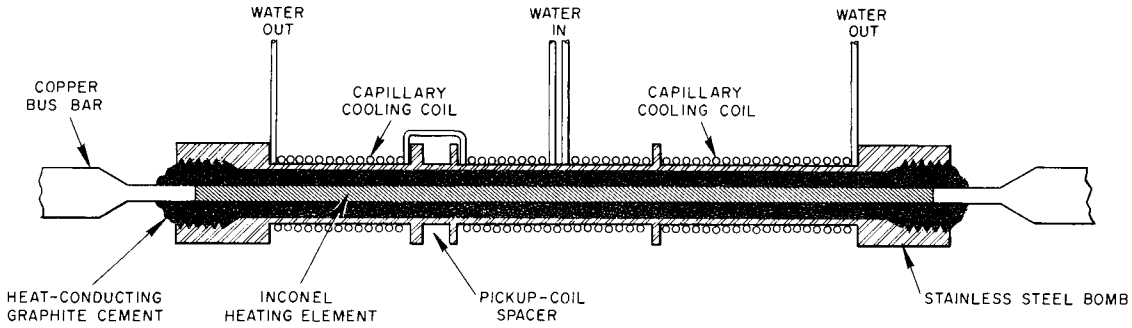

Fig. 19.2. Bomb Mockup for Heat Transfer Test.

Table 19.2. Henry's Law Constants for Oxygen in Water

Temperature (°C)	K*
	(x 10^5)
27	6.97
100	10.88
150	8.72
200	6.31
250	3.55
311**	1.64

*K = P_A/N_A, where P_A = partial pressure of gas in psi, and N_A = mole fraction of gas in solution.

**Single measurement.

and the outlet of the capillary---the latter was subject to vapor binding. The cycling of the capillary outlet temperature became severe only when its temperature exceeded 220°C, the temperature at which disproportionation of flow in the capillaries became evident.

(b) Temperature Distribution in Dash-pot-stirred Bomb.--Additional studies were carried out to determine the effect of capillary cooling of the dash-pot-stirred bomb on the ability to determine steam pressure in the bomb from the temperature read by the bottom thermocouple. A standard dash-pot bomb[4] was wrapped with stirring coils and a pickup coil in the usual way. The bomb was equipped with a stirrer, loaded with approximately 6 ml of water, and placed in a heating jacket. Cooling water at room temperature was supplied to the coils by a Zenith gear pump.

When the bomb was cooled by water flowing down over the bomb, the difference between the observed pressure and steam pressure corresponding to the temperature indicated by the thermocouple in the bottom of the bomb was small. When the cooling water was introduced at the bottom of the bomb, however, the difference was large. (Table 19.3)

19.2 GAS RECOMBINATION STUDIES

Development of a catalyst for the internal recombination of radiolytic gas in thorium-uranium oxide slurries continued, with a study of the effect of pumping in both argon and oxygen atmospheres on the catalytic activity of a slurry containing a palladium catalyst. The study was carried out in cooperation with the Slurry Corrosion Section of the Reactor Experimental Engineering Division. The slurry contained 454 g of Th per kg of D_2O of a 650°C-fired thoria to which uranium ($UO_3 \cdot H_2O$) and palladium catalyst were added in the ratio of 5.15 mg of U and 0.158 mg of Pd per g of Th. The palladium was deposited on the thorium oxide by a method developed at Westinghouse Electric Corporation.[5]

Table 19.3. Operating Conditions and Data for Temperature-Distribution Tests

Run No.	Direction of Water Flow	Total Heat Generated (w)*	Water Flow Rate (ml/hr)	Measured Bomb Temp. (°C)	Bomb Press. (psi)	Observed Pressure Minus Pressure Corresponding to Measured Temp. (psi)
1	-	70	0	300.25	1310	-40
2	Down	200	40	298.5	1270	-16
3	Up	385	75	300	1885	+600

*Not corrected for heat losses.

In the first run, BS-25,[6] the loop was pressurized with argon and the slurry was pumped 478 hr at 280°C. A partial pressure of deuterium gradually developed as a result of the corrosion process (35 std cc per liter of slurry at the end of the run). In the second run, BS-25A,[7] 400 std cc of oxygen per liter of slurry was substituted for the argon-deuterium atmosphere, and pumping was continued at 280°C for an additional 526.8 hr. Slurry samples were withdrawn from the loop from time to time, and their catalytic activity for combining deuterium and oxygen was determined in laboratory tests at various temperatures, first at low temperature and then at high temperature, in successive experiments.

The catalytic activities of the initial samples of the slurry pumped in an argon atmosphere were such that 250°C could not be reached in the gas recombination tests without detonating the gas (Table 19.4). After 214 hr pumping, the catalytic activity had dropped to the point where it was possible to make measurements in the 250-285°C region, and from this point on there was no apparent change in catalytic activity. The reaction rate in the region of 150°C decreased from an initial value of 10.4 moles D_2/liter-hr to a final value of 4 to 5 moles D_2/liter-hr, both at 100 psi D_2 partial pressure. At reaction temperatures above 250°C and pumping times of 200 hr or more, the recombination rates were less than 0.5 mole D_2/liter-hr at 100 psi D_2 partial pressure. After the recombination experiment at 285°C with the 478-hr-pumped sample, subsequent experiments with this sample at 155°C showed essentially no activity. It is assumed that the high activities at 150°C shown by the samples are of temporary duration and may be associated with the presence of reduced species of uranium or with corrosion products which are oxidized and hence deactivated by heating under stoichiometric proportions of gases. Only the sample taken after 22.5 hr of pumping showed an increase in activity with increasing recombination temperature. In subsequent samples the activity decreased. Slurries treated under reducing conditions in static bomb tests have shown similar high catalytic activities. The deactivation effects of pumping in a reducing atmosphere on catalytic activities noted above may have resulted from corrosion-product accumulation.

As indicated above, after the 478 hr of pumping under the argon-deuterium atmosphere, an oxygen atmosphere was substituted for the argon-deuterium. Only

Table 19.4. Effect of Pumping on Slurry Catalytic Activity

Slurry: 450 g of Th per kg of D_2O (650°C ThO_2); 5.15 g of U per kg of Th ($UO_3 \cdot H_2O$ rods); 0.123 g of Pd per kg of Th (0.58% Pd on 650°C ThO_2)

Pumping temperature: 280°C

D_2/O_2 (charging ratio): 2/1

Pumping Time (hr)	Recombination Experiment: Temperature (°C)	Recombination Experiment: Moles D_2 Reacted per Hr per Liter Slurry (P_{D_2} = 100 psi)
Phase 1. System Pressurized with Argon (120 psig at Room Temperature)		
22	129.5	5.4
	151.0	10.4
	184.0	12.0
47	131	11.6
	190	7.6
	216	Detonation
70	156	7.8
	178	5.1
	150	Detonation
142	153	4.9
	176	1.7
	143	Detonation
	165	Detonation
214	121	5.1
	208	0.3
	170	Detonation
	258	0.4
310	162	4.1
	181	Detonation
	218	Detonation
	257	0.2
382	151	4.8
	200	1.4
	160	Detonation
	253	0.1
478	155	5.5
	207	0.1
	265	0.3
	285	0.2
Phase 2. System Pressurized with Oxygen (120 psig at Room Temperature)		
22.8	280	0.07
	280	0.04
	279	0.04
526.8	280	0.08
	280	0.08

the 22.8- and 526.8-hr samples from the oxygen run were analyzed for catalytic activity. At 280°C the recombination rates in both samples at a deuterium partial pressure of 100 psi were less than 0.1 mole D_2/liter-hr (Table 19.4). Very little activity was observed with these samples in the range 150-200°C.

No difficulties were experienced with the BS-25A samples during the recombination tests, but detonations in the 150-220°C region were a frequent source of difficulty with the BS-25 samples. The difference in behavior was probably the result of uranium and/or corrosion products which were reduced and hence rendered catalytically active by the treatment under the argon-deuterium atmosphere in the loop, but rendered inactive by the subsequent oxygen treatment in BS-25A.

19.3 ROLLING-BALL VISCOMETER

Development studies were continued on a rolling-ball viscometer[1] designed for use with small volumes of slurry at room temperature and at elevated temperatures and ultimately for remote use with irradiated slurries. Data on terminal velocities at various angles of incline were obtained for slurries of 650°C-fired thoria at concentrations from 250 to 600 g of Th per kg of H_2O (Fig. 19.3). At 800 g of Th per kg of H_2O, the ball would not roll.

Values of yield stress (Table 19.5) were calculated from rolling-ball

Table 19.5. Yield Stress of DT-7-650 Thoria Slurries

Slurry Concentration (g of ThO_2 per kg of H_2O)	Yield Stress (lb/ft^2)	
	Rolling-Ball Viscometer	Capillary Viscometer
204		0.008
250	0.008	
400	0.04	0.04
600	0.18	0.16
800	> 0.31	
853		0.28

viscometer data by extrapolating the maximum slope of the laminar-flow segment of the terminal-velocity curves to zero velocity, multiplying the value of

$$\frac{3}{4}\,\frac{\rho_{ball} - \rho_{slurry}}{\rho_{ball}}\,\sin\theta \qquad (\theta = \text{angle of incline})$$

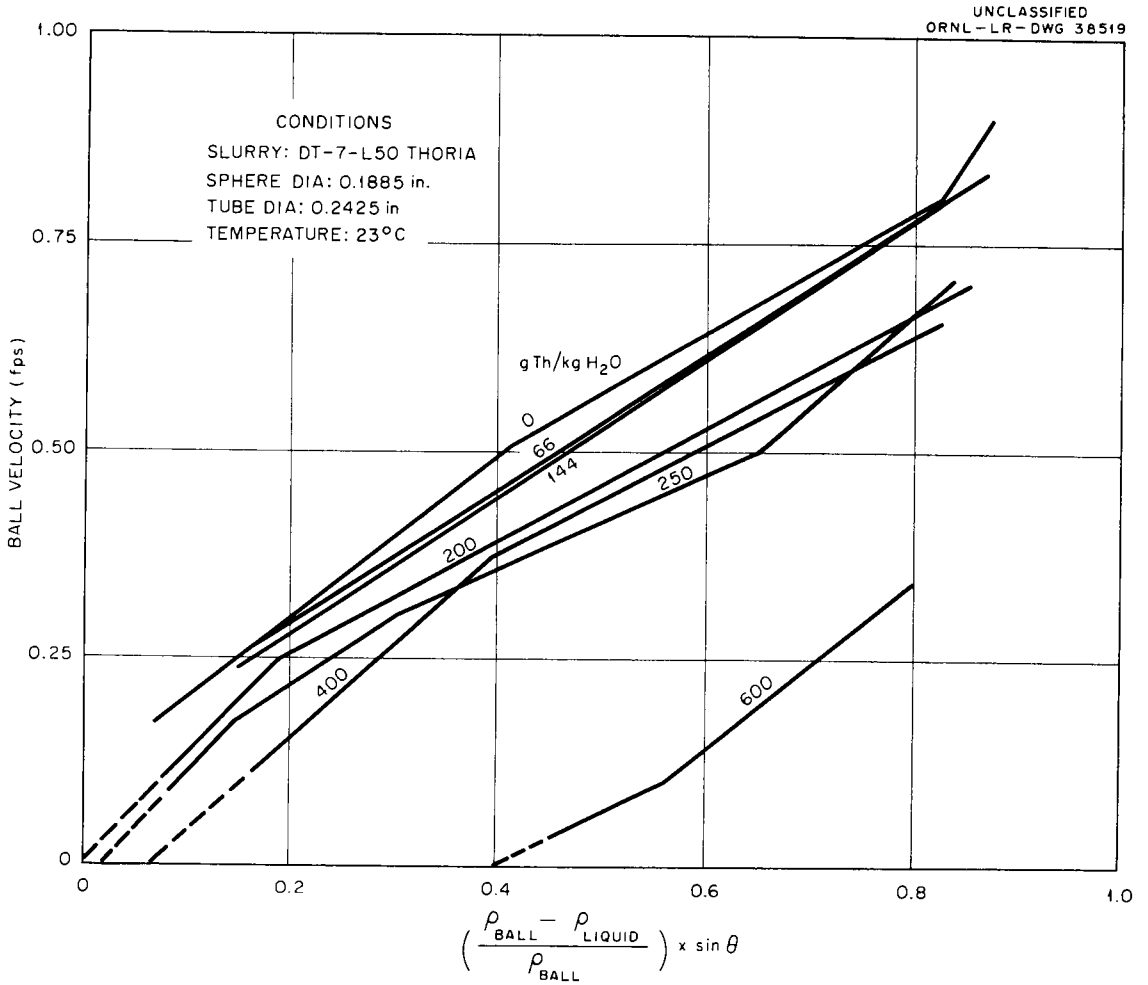

Fig. 19.3. Effect of Driving Force on Terminol Velocity of Ball Falling Through Thoria Slurries.

at this point by the weight of the ball, and dividing the result by the area of the ball plus the area of the tube parallel with the ball. In making this calculation, it is assumed that slurry is in motion only in the section of tube parallel with the ball and that all surface elements subjected to fluid motion contribute the same drag per unit area. These assumptions are not strictly satisfied if the ball is in motion, but they appear reasonably applicable at low velocity.

For purposes of comparison, rate of shear vs wall stress for DT-7-650 slurries was measured with a capillary-tube viscometer (Fig. 19.4). Agreement was good between the yield stress computed from the rolling-ball data and that from the capillary-tube data (Table 19.5).

The derivation of the coefficient of rigidity (η) from rolling-ball viscometer data does not parallel the calculations appropriate for the capillary-tube viscometer. Maximum slopes of the laminar-flow segments of the curve do not show the expected trend toward decrease with increasing slurry concentration. However, if the onset of turbulent flow can be determined, η can be estimated from the plot of Hedstrom's S factor vs the Reynolds number. The values of η can only be estimated because the onset of "effective" turbulence is not clearly defined in the rolling-ball viscometer--the fluid velocity changes from point to point over the surface of both the ball and the tube. Coefficients of rigidity equal to 1.1 centipoises for 250 g of ThO_2 per kg of H_2O and 1.4 centipoises for 400 g of ThO_2 per kg of H_2O were estimated by use of the average of the fluid velocities with respect to the ball and to the wall at the smallest cross section for flow, as calculated for the point of initial curvature in the velocity - driving-force curve. The values agree with those derived from the capillary-tube viscometer, but more data are needed to define the range of slurry properties over which this empirical velocity-averaging procedure is useful. Typical scatter of the data is illustrated in Fig. 19.5, which shows the $\pm 2\ \sigma$ interval of confidence for a 250 g of ThO_2 per kg of H_2O slurry (DT-7-650).

19.4 BORON ADSORPTION STUDIES

One method of keeping a slurry reactor subcritical during startup would be to add to the slurry boric acid, which could be removed when operating conditions were reached. Calculations based on a slurry reactor with a 2.5-ft core, 400 g of Th per liter and 0.1 g U^{235} per g of Th, indicate that the molar ratio of boron to thorium and uranium required for subcriticality under all conditions should be 0.02. For successful reactor operation after startup less than 0.029 mg of boron per gram of solid (equivalent to 1% neutron loss to the boron) should remain adsorbed on the solid after removal of the boric acid from the system.[1,9]

Initial experiments with a slurry of 650°C-fired thorium-uranium oxide indicated that the adsorption of boron by the solid and the removal efficiency of the boron were such that boric acid could not be used as a soluble poison for criticality control.[1] It appeared, however, that in a slurry of 1100°C-fired thorium-uranium oxide such a method of operation was feasible. Additional experimentation has confirmed this indication.

In a slurry (270 g of Th per kg of H_2O) of the 1100°C-fired mixed oxide having an initial boron concentration of 370 ppm in the supernatant, 33% more than the amount required for subcriticality, less than 0.029 mg of boron was

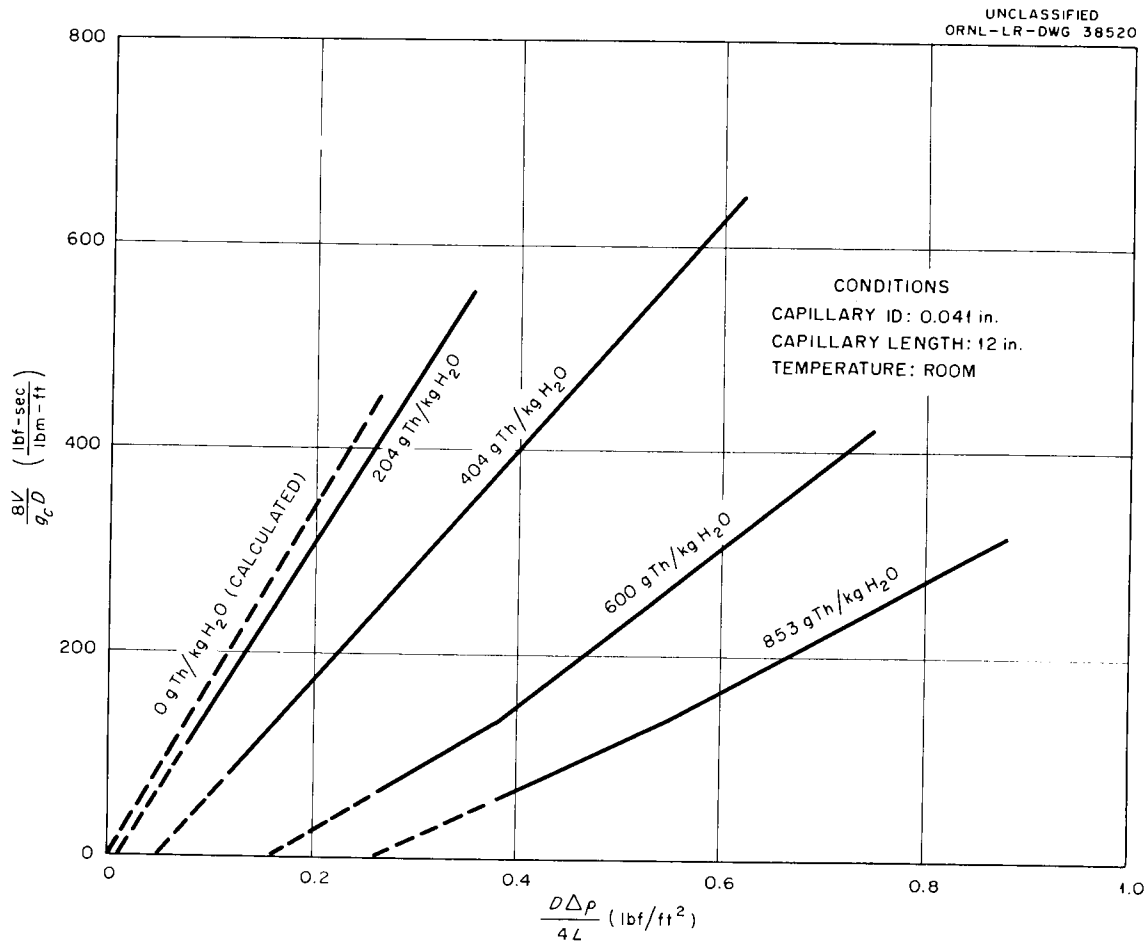

Fig. 19.4. Rate of Shear vs Wall Stress for DT-7-650 Thoria Slurries According to Capillary Tube Viscometer.

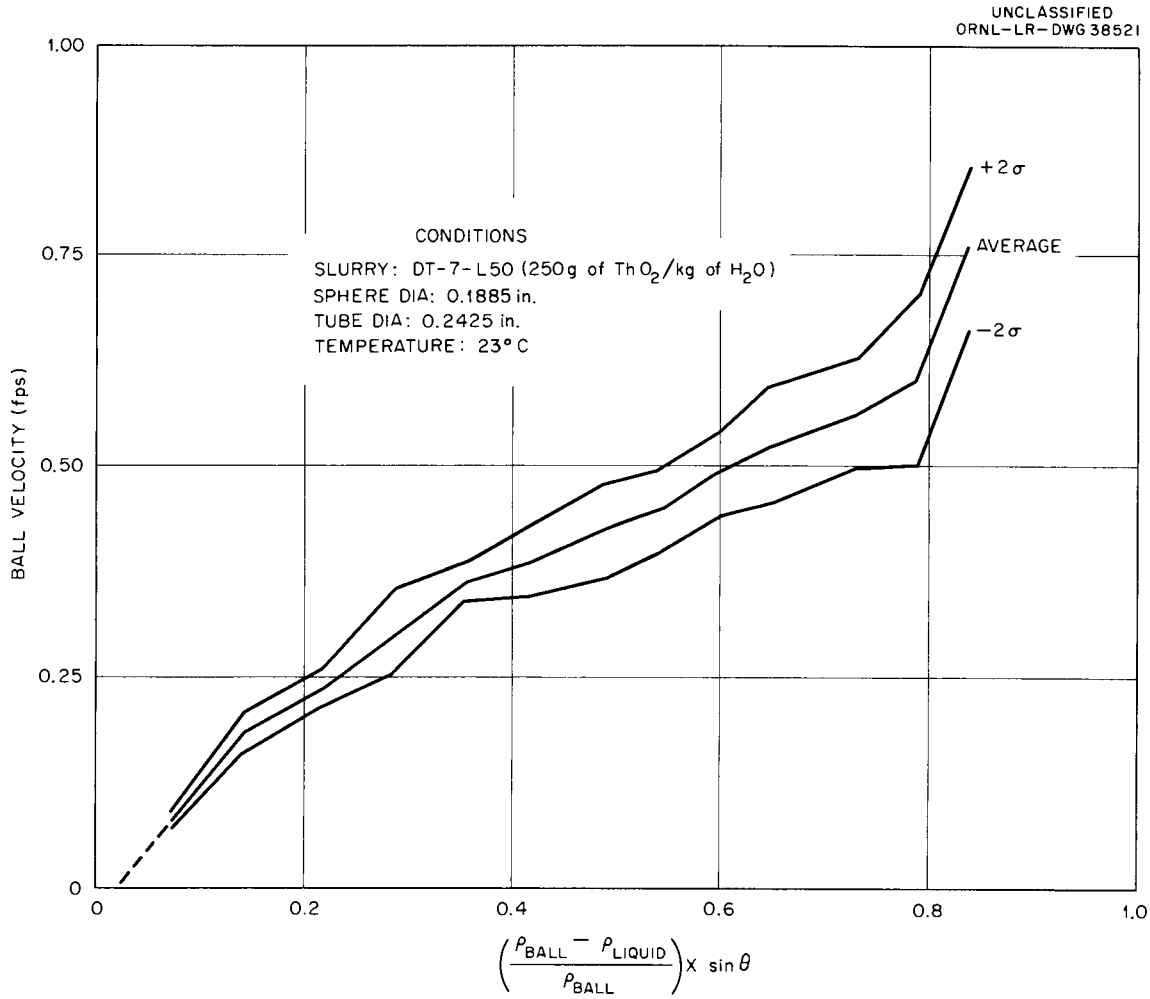

Fig. 19.5. Scatter of Driving-Force-vs-Terminal-Ball-Velocity Data According to Rolling-Ball Viscometer.

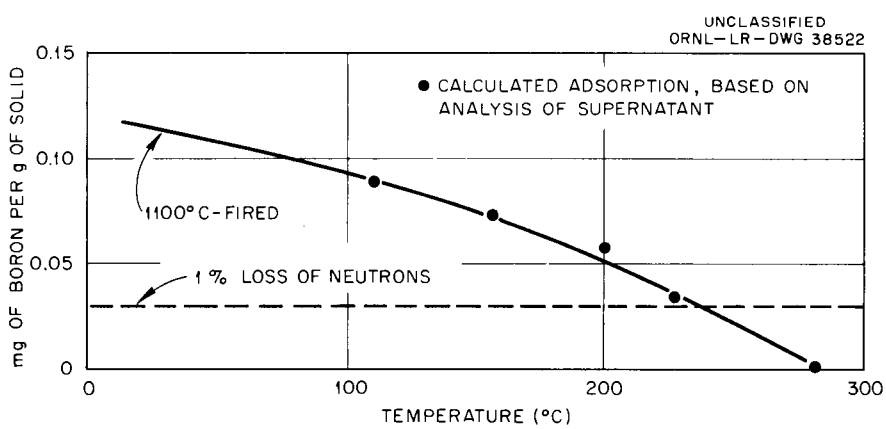

Fig. 19.6. Boron Distribution in Thorium-Uranium Oxide Slurries. Conditions: U/Th = 0.10; 238 g Th per kg H_2O; 0.713 g boron per kg H_2O.

adsorbed per gram of solid at temperatures above 60°C. About 60% of the adsorbed boron could be desorbed from the solid in fresh supernatant at 100°C in less than 2 hr. When a slurry (238 g of Th per kg of H_2O) of the 1100°C-fired mixed oxide contained 713 ppm boron in the supernatant, less than the 0.029 mg of boron was adsorbed per gram of solid at 240°C and above (Fig. 19.6).

19.5 DEVELOPMENT OF OXIDE PREPARATION METHODS

Developmental studies for the preparation of oxides included further work on the production of mixed oxides by flame calcination, with emphasis on the production of spherical particles; final work on the fluidized-bed denitration process for the production of 50- to 500-μ thoria particles; and continued study on the production of oxide enriched in particles less than 0.5 μ by hydroclone classification of thoria slurries.

19.5.1 Flame-Calcination Experiments

Electron micrographs of shadow-cast particles showed that spherical particles were obtained by flame-firing at 1400°C alcoholic solutions of thorium-uranium-aluminum nitrates having a U/Th weight ratio of 0.08 and Al/Th weight ratios of 0.025 and 0.05 (Fig. 19.7). These observations confirm the spheroidizing effect first reported[10] for a similar experiment with a mixture containing an Al/Th weight ratio of 0.1. Average particle sizes for the preparations containing Al/Th ratios equal to 0.025 and 0.1 were 1.7 and 1.8 μ, respectively. Yield stresses for slurries (1200 g of Th per kg of H_2O) of the same materials were 0.02 and 0.2 lb/ft^2, respectively.

Corrosion rates, particle degradation, and uranium solubility of Th-U oxides were measured in toroid tests with slurries having 200 g of Th per kg of H_2O (Table 19.6). Type 347 stainless steel under oxygen overpressure corroded at rates of 2.7 to 7.0 mpy. Corrosion rates with the flame-fired materials were about the same as those obtained with the 1050°C-fired pilot-plant production material. Particle degradation appeared to be slight under oxygen, but there was some growth under deuterium.[1] This apparent increase in particle size may be due to analytical error. Uranium solubility in the supernatant was below the limits of detectability for three of the four samples under deuterium, and low for the samples under oxygen. Analytical results (Table 19.7) showed high values for yield stress (0.45 to 0.94 lb/ft^2) and surface area (6 to 8 m^2/g) for flame-calcined mixed Th-U oxides. Values for similar furnace-fired materials are 0.2 to 0.3 lb/ft^2 and 2 to 3 m^2/g, respectively.

19.5.2 Fluidized-bed Denitration

Development studies on the use of fluidized-bed denitration in producing 50 to 500-μ-dia thorium oxide particles for fluidized-bed reactor fuels were completed.[1] A final report is being written in which the fluidized bed and the agitated trough for denitrating an aqueous solution of thorium nitrate will be compared.

Four fluidized-bed runs were made by spraying aqueous thorium nitrate or uranyl nitrate solution into a bed of classified sea sand (Table 19.8). The bed caked below the spray nozzle in runs T-9 and T-10 but remained fluidized in runs T-8 and T-11 (the latter run used uranyl nitrate feed and was made in order to duplicate results reported by Argonne National Laboratory). There was a high yield of ThO_2 fines in all three of the runs with aqueous thorium nitrate

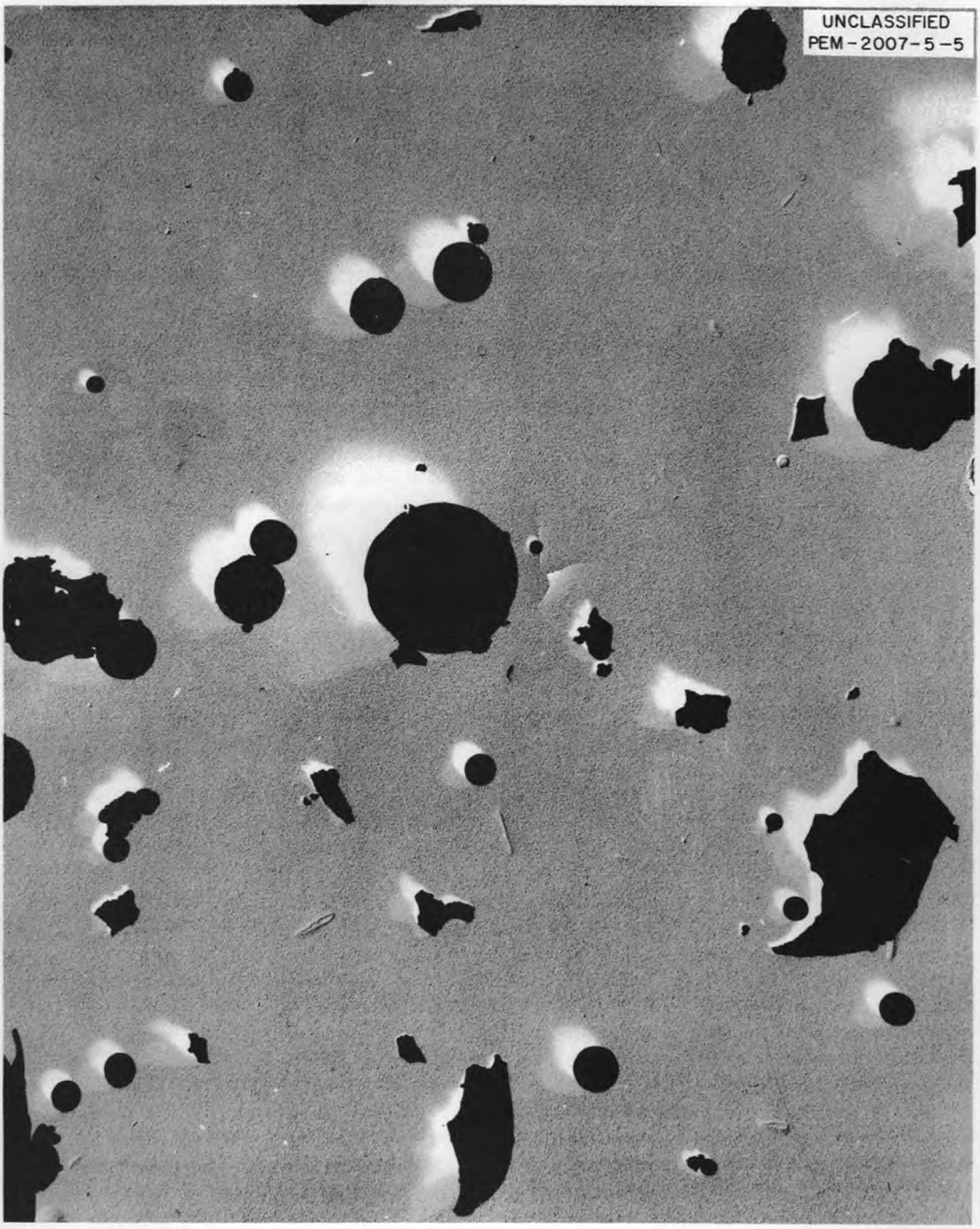

Fig. 19.7. Flame Calcination Experiments: Flame-Fired Mixed U-Th Oxides Containing 5 wt % Alumina. 10,000X.

Table 19.6. Flame-Calcining Experiments: Results of Toroid Tests on Th-U Mixed Oxides

Operating temperature: 280°C
Exposure time: 300 hr
Velocity: 26 fps
Concentration: 200 g of Th-U per kg of D_2O

Run No.	Average Particle Size (μ) Prerun	Postrun	Atmosphere	Corrosion Rate (mpy) 347 SS	Ti-75A	Inconel	Zircaloy-2	U Loss to Supernatant (ppm)	U/Th Ratio
35	1.0	1.2	O_2	6.9	0	12.3	0.2	<2	0.058
	1.0	2.0**	D_2	11	1.0	1.5	0.4	<2	
36	1.5	1.3	O_2	7.0	1.1	22	0	5	0.075
	1.5	5.4**	D_2	14	1.6	2.4	0.5	<2	
39C*	1.5	0.7	O_2	3.2	1.6	21	0.2	29	
39RC	1.0	1.0	O_2	6.3	1.6	35	0.3	84	0.076
45	0.6	1.0	O_2	2.7	1.5	17	+	3	0.077
	0.6	1.0**	D_2	0.8	1.1	0.2	0.2	<2	

*Run 34 product was classified to $d_{50} = 1.5\,\mu$ (39C); reclassified (39RC) to $d_{50} = 1.0\,\mu$.

**This increase in apparent particle size probably is due to poor dispersion of the reduced oxide before particle size analysis by sedimentation.

Table 19.7. Analytical Results Th-U Mixed Oxides Prepared by Flame Calcination

Run No.	Reflector Temp. (°C)	Average Particle Size* (μ)	Yield Stress** (lb/ft^2)	Surface Area (m^2/g)
46	1000	1.7	0.94	7.6
47	800	2.2	0.45	6.5
48	1440	2.5	0.8	6.2
49	1220	1.8	0.675	7.7
50	1425	1.7		7.7
51	1200	1.6		7.8

*After classification to remove the particles $>5\mu$ in diameter.

**These values corrected to a density of 2, from a lower sample density.

Table 19.8. Operating Conditions and Product Nitrate Content for Fluidized-Bed Denitration

Run No.	Aqueous Feed	Bed Temperature (°C)	Superficial Velocity of Fluidizing Air (fps)	Nitrate in Product (wt %)
T-8	1.8 M $Th(NO_3)_4$	700	0.8	0.06
T-9	2.5 M $Th(NO_3)_4$	500	0.8	0.34
T-10	2.5 M $Th(NO_3)_4$	400	1.3	0.51
T-11	2.5 M $UO_2(NO_3)_2$	390	1.3	0.26

feed, as indicated by a rapid buildup of the pressure drop across the metallic bayonet filters. The yield of UO_3 fines in run T-11 was so low that there was no increase in pressure drop across the filters.

Photomicrographs were made of the classified product from the two most successful fluidized-bed runs, T-8 and T-11 (Figs. 19.8 and 19.9). Sample A-UO_3 was classified between 250 and 500 μ, and sample B-ThO_2 between 500 and 840 μ. Each figure contains photomicrographs showing the particles as removed from the fluidized bed after being washed with water and sectioned to show the internal structure. In the sectioned samples, the UO_3 coating on the sand particles appeared denser and more homogeneous than the ThO_2 coating. Owing to the poor contrast between ThO_2 and sand, the composition of the ThO_2 particles is not shown clearly in the photomicrographs of cross-sectioned samples. However, visual inspection of the sectioned samples showed that each "particle" consisted of sand and loosely bound agglomerates of smaller ThO_2 particles. The UO_3, however, formed a continuous coating around the sand particles and was not readily removed by attrition. These observations are consistent with the higher yield of fines in the thorium runs than in the uranium run.

Particle-size analyses, by sedimentation and neutron activation, of the product from run T-8 also indicated the presence of loosely bound ThO_2 agglomerates. The average particle size of ThO_2 in sample C-ThO_2 (screen classified between 250 and 500 μ) was 35 μ, when dispersed in aqueous 0.001 M $Na_4P_2O_7$.

The results of these runs indicate that fluidized-bed denitration is not feasible for producing dense, high-strength 50- to 500-μ-dia ThO_2 particles. There was a high yield of fines in all the thorium runs, and bed caking was a problem in every thorium run except T-8 (bed temperature, 700°C). Neither of these troubles was encountered in the run with uranium, duplicating results reported for fluidized-bed denitration studies at Argonne National Laboratory.

19.5.3 Agitated-Trough Denitration

Tests were made on the use of an agitated-trough calciner to prepare 50- to 500-μ-dia ThO_2 by denitration of aqueous thorium nitrate in an agitated bed of ThO_2 or sea sand. The bed temperature in the vicinity of the nitrate feed line was varied between 150 and 250°C, and there was no bed caking. However, the ThO_2 did not grow on the sand particles.

A material balance for the initial agitated-trough run showed a loss of ThO_2. The initial ThO_2 bed weight was 9080 g, to which 2385 g of ThO_2 was fed as $Th(NO_3)_4$. No ThO_2 was found in the product tank, and there was only 8790 g in the bed. The lost oxide (2675 g) was probably carried from the trough by entrainment in the off-gas and discharged with the off-gas scrubber solution.

In an effort to use a nitrate feed that would give a cohesive oxide, a run was made with aluminum nitrate feed to an agitated sand bed. The resulting bed material contained a high percentage of Al_2O_3 particles between 200 and 800 μ in diameter. A feed solution equivalent to 5 wt % Al_2O_3 - 95 wt % ThO_2 gave a product consisting of fines similar to those obtained in the absence of aluminum.

19.5.4 Hydroclone Classification of ThO_2

A 40.6-kg batch of LO-42 thorium oxide was passed once through a 0.5-in.-ID hydroclone in order to enrich the overflow stream in small particles ($<0.6\mu$). The product contained over 60% of the original material that was $<0.6\mu$ and about 6% of the material $>1\mu$. Oxalic acid was used as a dispersing agent. A

UNCLASSIFIED
PHOTO 46448

B-ThO_2 MAGNIFICATION 15X

B-ThO_2 (WASHED WITH H_2O) MAGNIFICATION 15X

B-ThO_2 (CROSS SECTION) MAGNIFICATION 34X

CONDITIONS
AQUEOUS FEED 1.8 *M* $Th(NO_3)_4$
BED TEMPERATURE: 700°C
PARTICLES SCREEN CLASSIFIED
BETWEEN 500 AND 840 microns

Fig. 19.8. Photomicrographs of Particles from Denitration of $Th(NO_3)_4$ on a Fluidized Sand Bed.

UNCLASSIFIED
PHOTO 46447

A-UO_3 MAGNIFICATION 15X

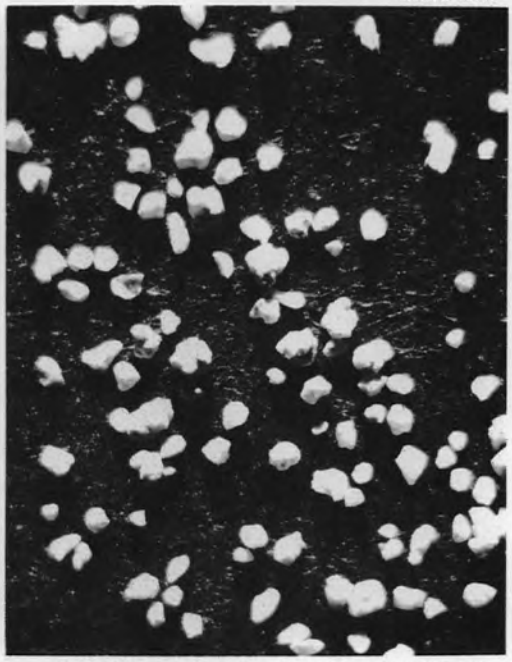

A-UO_3 (WASHED WITH H_2O) MAGNIFICATION 15X

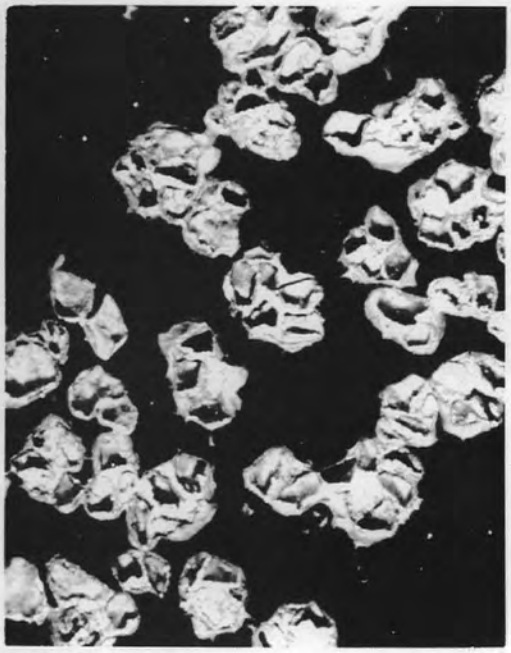

A-UO_3 (CROSS SECTION) MAGNIFICATION 34X

CONDITIONS

AQUEOUS FEED 2.5 *M* $UO_2(NO_3)_2$
BED TEMPERATURE: 390°C
PARTICLES SCREEN CLASSIFIED
BETWEEN 250 AND 500 microns

Fig. 19.9. Photomicrographs of Particles from Denitration of $UO_2(NO_3)_2$ on a Fluidized Sand Bed.

high-pressure drop, 60 psi, and a slurry temperature of 80°C were used to increase the hydroclone efficiency for small particles. These results demonstrate a practical separation factor for ThO_2 particles down to 0.6 μ. The reverse process, removing fines from larger material, is more difficult, however, since a fraction of the fines proportional to the underflow stream flow rate goes with the larger material and because dispersion of all fine particles is difficult to attain.

19.6 THORIUM OXIDE PRODUCTION

Six precipitations were made in order to prepare approximately 1200 lb of calcined thorium oxide. About 1020 lb of mixed oxide (U/Th = 0.08 and 0.16) was prepared by the adsorption method. Total shipments this quarter amounted to 2750 lb of material, of which 2000 lb was mixed oxide.

The thorium oxide equipment was cleaned and moved from Building 3019 to Building 2528. The relocated equipment is estimated to be 50% reassembled along with minor process-equipment improvements.

REFERENCES

1. J. P. McBride et al., HRP Quar. Prog. Rep. Jan. 31, 1959, ORNL-2696, p 177-198.

2. H. F. Soard, Solubility of Oxygen, Hydrogen, and Iodine in Thorium Oxide Slurries, ORNL CF-59-2-97.

3. H. A. Pray, C. E. Schweichert, and B. H. Minnich, The Solubility of Hydrogen, Oxygen, Nitrogen, and Helium in Water at Elevated Temperatures, BMI-T-25, p 15.

4. N. A. Krohn, "Radiation Studies of Thorium Oxide Slurries," in HRP Civilian Power Reactor Conference, ORNL, May 1-2, 1957, TID-7540, p 131, 1957.

5. W. D. Fletcher, Westinghouse Electric Corporation, personal communication.

6. E. L. Compere et al., HRP Quar. Prog. Rep. Jan. 31, 1959, ORNL-2696, p 106.

7. See Sec. 14.1.2 of this report.

8. B. O. A. Hedstrom, "Flow of Plastics Materials in Pipes," Ind. Eng. Chem. 44, 651-656(1952).

9. P. R. Kasten et al., HRP Quar. Prog. Rep. Jan. 31, 1959, ORNL-2696, p 40-41.

10. C. C. Haws, Unit Operations Monthly Report, Jan. 1959, ORNL CF-59-1-74 (in press).

Part VI

SUPPORTING CHEMICAL RESEARCH

H. F. McDuffie

20. HETEROGENEOUS EQUILIBRIA IN AQUEOUS SYSTEMS

W. L. Marshall

C. J. Barton G. M. Hebert R. E. Moore
J. S. Gill E. V. Jones R. Slusher

20.1 THE SYSTEM UO_3-CuO-NiO-SO_3-H_2O (D_2O) AT 300°C

The investigation of the system UO_3-CuO-NiO-SO_3-H_2O (D_2O) at 300°C was continued.[1] Currently, the study is directed toward the establishment of the binary curve along which two solids, $3CuO \cdot SO_3 \cdot 2D_2O$ (antlerite) and a newly discovered compound, $CuO \cdot 3UO_3$, are in equilibrium with solution. Experimental data were obtained for solutions containing from 0.04 to 0.5 m SO_3. The experimental approach was similar to that used previously (i.e., initial mixtures of components are so selected that two solid phases will be present at equilibrium). At the beginning of this part of the study of the five-component system, it was expected that the two solid phases along the binary curve would be $3CuO \cdot SO_3 \cdot 2D_2O$ (antlerite) and $UO_3 \cdot UO_2SO_4$ (zippeite). In actuality, however, $CuO \cdot 3UO_3$ and $3CuO \cdot SO_3 \cdot 2D_2O$ were found. Therefore, the binary curve indicated in the diagrams on page 213 of the previous HRP quarterly report[1] has been revised as indicated by Fig. 20.1, a projection on the UO_3-CuO base of a cubic representation of the five-component system UO_3-CuO-NiO-SO_3-D_2O at 300°C and 0.08 m SO_3. A detailed explanation of this mode of representation was incorporated in the previous report.[1] The further revision indicates that at least two ternary curves must exist, the one in which $UO_3 \cdot UO_2SO_4$, $3CuO \cdot SO_3 \cdot 2D_2O$, and $NiSO_4 \cdot D_2O$ are the solids and the one in which $UO_3 \cdot UO_2SO_4$, $3CuO \cdot SO_3 \cdot 2D_2O$, and $CuO \cdot 3UO_3$ are the solid phases. The additional postulated ternary point and binary point at constant SO_3 concentration are shown in Fig. 20.1 and indicate the current status of the investigation. Efforts are continuing in order to verify and establish the exact location of the additional skeletal points.

A discussion of the identification, characterization, and preparation of the solid phase $CuO \cdot 3UO_3$ is given in Sec. 20.2, and a new method of preparation of $3CuO \cdot SO_3 \cdot 2D_2O$ at low temperatures is described in Sec. 20.3.

20.2 THE COMPOUND $CuO \cdot 3UO_3$

Very small amounts of a red solid phase have been observed to precipitate from CuO-UO_3-SO_3-H_2O solutions at high temperatures[2] and also to precipitate slowly at room temperature from dilute solutions which had been heated to approximately 300°C in sealed quartz tubes for varying lengths of time without observable precipitation. The amounts of solid material produced in sealed-tube experiments were too small to permit positive identification. Larger quantities of this phase were prepared during the past quarter by equilibrating 2 or 3 g each of

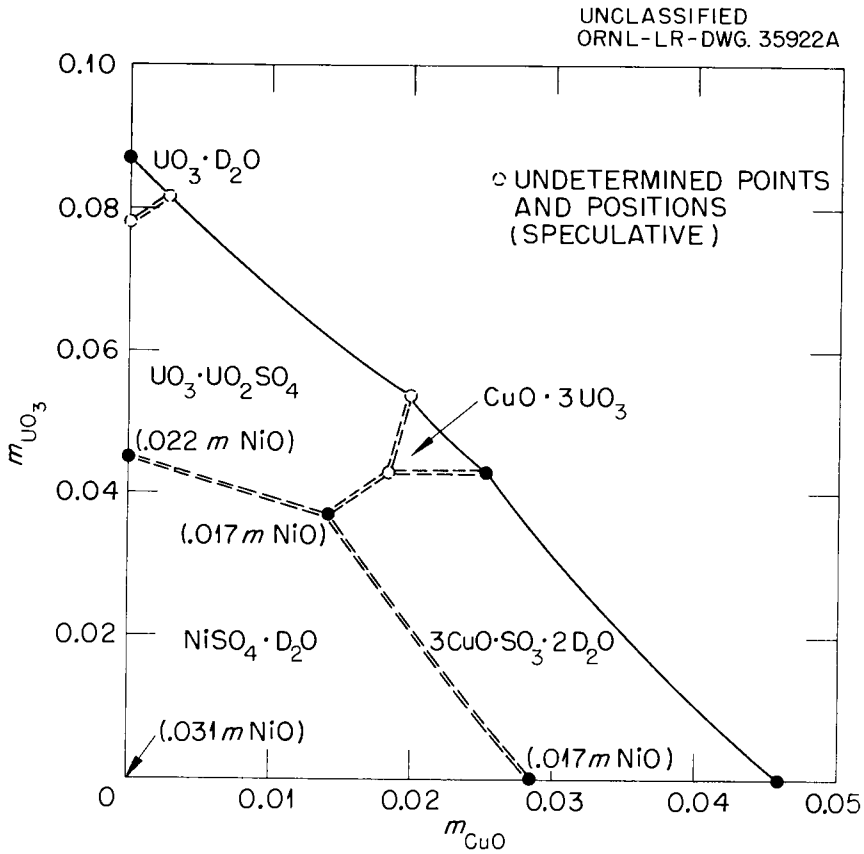

Fig. 20.1. Projection on UO_3-CuO Face of Cube Representing System UO_3-CuO-NiO-SO_3-D_2O at 300°C (SO_3 Constant at 0.08 *m*).

UO_3 hydrate and $3CuO \cdot SO_3 \cdot 2H_2O$ with 25 ml of 0.02 to 0.11 M H_2SO_4 at 300°C for 16 to 72 hr in titanium pressure vessels. Mixtures of the red solid and a green solid, $3CuO \cdot SO_3 \cdot 2H_2O$ (antlerite), were obtained; the latter was removed by slurrying the mixture several times with water and floating off the lower-density green phase. The red phase was washed thoroughly to remove residual sulfate, dried in air at 110°C, and submitted for chemical analysis and x-ray diffraction examination.

Results from chemical analysis of six separate preparations of this material are shown in Table 20.1. The average molar ratio of UO_3/CuO from these

Table 20.1. Compositions by Chemical Analysis for Six Preparations of $CuO \cdot 3UO_3$

Preparation Number	% by Weight U	% by Weight Cu	Weight % $CuO + UO_3$	Molar Ratio UO_3/CuO
1	75.76	6.92	99.7	2.92
2	76.30	7.02	100.4	2.90
3	74.72	7.05	98.6	2.83
4	73.91	7.14	98.0	2.76
5	75.18	7.23	99.6	2.77
6	73.90	6.90	97.4	2.85
Mean	74.96	7.04	98.9	2.84
Calculated*	76.15	6.77	100	3.0

* For $CuO \cdot 3UO_3$.

numbers is 2.84. The sum of UO_3 and CuO from the analytically determined metal values averages 98.9%; it is possible, though it hardly seems likely, that some water of hydration may be present. The metal ratio is farther from an integer than the possible precision of the analysis would warrant. The compound, which will receive some further study, has been tentatively assigned the formula $CuO \cdot 3UO_3$.

The importance of this compound is indicated by the fact that it has been identified by its x-ray pattern with solid material that occurred in the HRT mockup pressurizer[3] and in the HRT pressurizer line[4] during prepower operation (run 7). Since both temperature and concentration gradients occur in the horizontal pressurizer line, it would appear that conditions at this point in the reactor circuit may be favorable for the deposition and retention of slightly soluble compounds.

A plausible explanation of the formation of this compound is furnished by Sutton's suggestion[5] that the ion $U_3O_8(OH)_4^{--}$ exists in hydrolyzed uranyl solutions. The equilibria involved can be formulated as follows:

$$3UO_2^{++} + 6H_2O \rightleftharpoons U_3O_8(OH)_4^{--} + 8H^+$$

$$U_3O_8(OH)_4^{--} + Cu^{++} \rightleftharpoons Cu\left[U_3O_8(OH)_4\right] \rightleftharpoons CuO \cdot 3UO_3\downarrow + 2H_2O.$$

Arden[6] also reported evidence of trimeric uranium anions and found compounds to which he assigned the formulas $CaO \cdot 4UO_3$ and $3CaO \cdot 8UO_3$ which resulted from titration of uranyl sulfate solutions with $Ca(OH)_2$. Sutton's data indicated that the $U_3O_8(OH)_4^{--}$ ion is formed in 0.1 M uranyl perchlorate solution at a pH of approximately 6 at room temperature. The effect of temperature variations on equilibria of this type has apparently not been investigated. Assumption of the next lower member of the hydration series, $U_3O_8(OH)_3^{-}$, leads to a UO_3/CuO molar ratio of 6, and if the ion $U_3O_8(OH)_5^{---}$ is assumed to exist, the calculated UO_3/CuO molar ratio is 2.

20.3 A NEW METHOD OF PREPARATION OF ANTLERITE, $3CuO \cdot SO_3 \cdot 2H_2O$

Quantities of the compound $3CuO \cdot SO_3 \cdot 2H_2O$ (antlerite) are needed for studies of equilibria in the system $CuO-NiO-UO_3-SO_3-H_2O$. In the past, the compound was prepared by hydrolyzing large volumes of dilute $CuSO_4$ solutions at temperatures varying between 175 and 300°C. A method for preparing antlerite has also been reported by Posnjak and Tunell[7] who studied the system $CuO-SO_3-H_2O$ over the temperature range 50-200°C. Their method did not give a pure product. It was found that the compound could be prepared at atmospheric pressure by refluxing an aqueous slurry of $CuCO_3$ with a little more H_2SO_4 added than required to give a 3 to 1 CuO/SO_3 molar ratio. This method of preparation, in addition to simplifying the production of large quantities of the compound, also lends itself better to the preparation of the D_2O analog than the former method of preparation. X-ray diffraction examination of the compound formed by the new method indicated that it is identical to that prepared earlier.

20.4 THE TWO-LIQUID PHASE REGIONS OF THE SYSTEM $UO_3-SO_3-H_2O$

Investigation of the two-liquid phase regions of the system $UO_3-SO_3-H_2O$ is continuing.[1] The previously described experimental methods are being used in which heavy and light immiscible liquid phases are equilibrated at temperature in Pyrex tubes. The tubes are cooled rapidly; then the immiscible phases are separated and analyzed for uranium and sulfate content. The experimental investigation has been extended to uranyl sulfate solutions containing up to 40 mole % excess free H_2SO_4.

Averages of the most recent results are given in Table 20.2 and are shown in Fig. 20.2 using the coordinates described in the previous report.[1] All values shown in Fig. 20.2 are for solutions which were initially 1.5 M uranium and had molar ratios SO_3/UO_3 up to 1.4 (UO_3/SO_3 = 0.833). Each point shown in Fig. 20.2 represents the results of two or more experimental runs, the average difference in ratio between similar runs being of the order of less than 2%. As mentioned in the previous report, these connecting lines between heavy and light phases are not "tie" lines in the usual sense of the word, since the data are not shown on a conventional linear diagram. The results show that, in the case of solutions of high initial free-acid concentration at high temperatures, both light and heavy phases can contain excess free acid. Solutions having an initial UO_3/SO_3 molar ratio of 1 and those containing only a small excess of free acid yield a heavy phase having a UO_3/SO_3 ratio of 1 or slightly less.

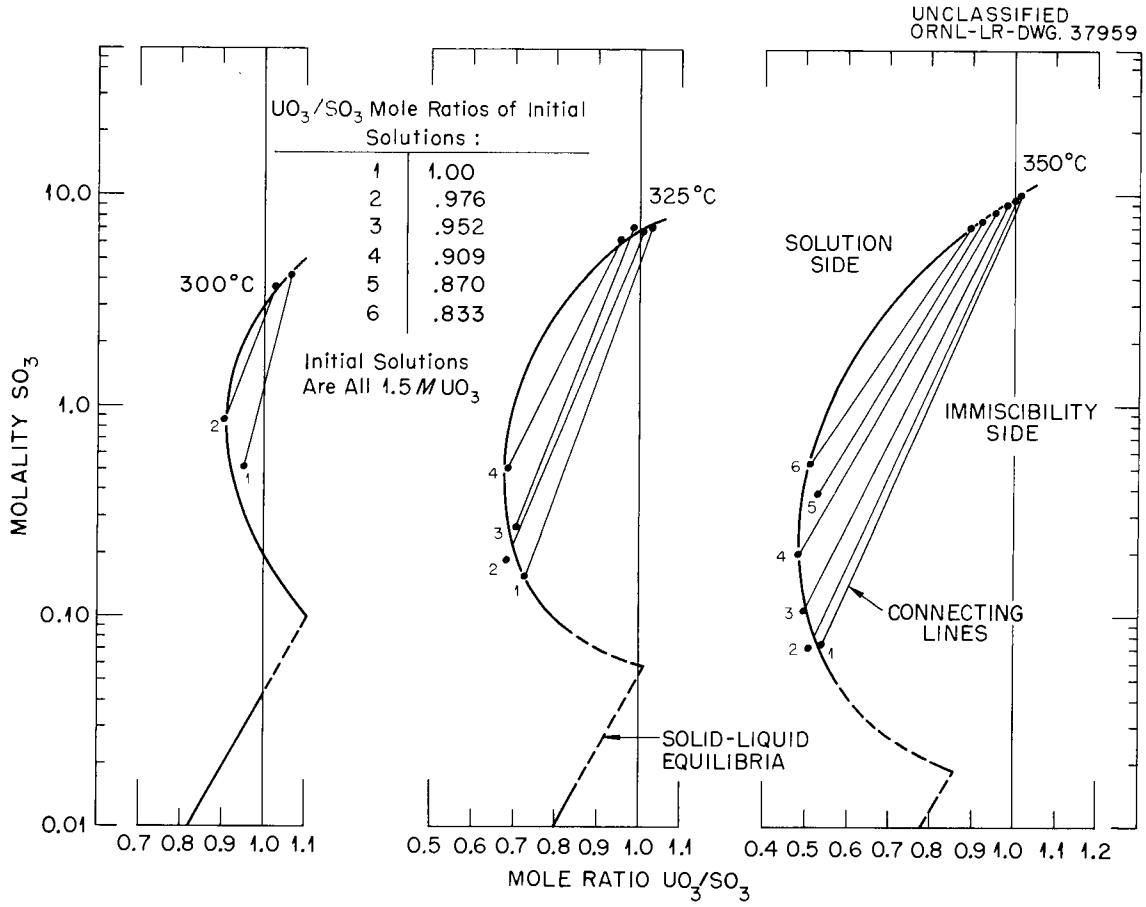

Fig. 20.2. Two-Liquid Phase Regions of the System UO_3-SO_3-H_2O.

Table 20.2 The Equilibrium Compositions of Light and Heavy Phases in the System UO_3-SO_3-H_2O

Initial $\underline{M}_{UO_3}$ = 1.5 in All Cases - (Average Values)

Temp. (°C)	Mole % Excess H_2SO_4	Light Layer		Heavy Layer	
		$\underline{m}_{SO_3}$	U/SO_3	$\underline{m}_{SO_3}$	U/SO_3
300	0.0	0.507	0.949	4.24	1.065
	2.5	0.860	0.905	3.68	1.026
325	0.0	0.153	0.724	7.111	1.031
	2.5	0.186	0.687	6.800	1.010
	5.0	0.261	0.705	7.000	0.985
	10.0	0.512	0.688	6.160	0.954
350	0.0	0.074	0.538	10.02	1.016
	2.5	0.071	0.511	9.50	1.002
	5.0	0.112	0.496	9.08	0.987
	10.0	0.196	0.481	8.44	0.956
	15.0	0.371	0.532	7.72	0.928
	20.0	0.528	0.509	7.16	0.897
	25.0	Immiscibility occurred (awaiting analytical data)			
	40.0	Immiscibility occurred (awaiting analytical data)			

20.5 INVESTIGATION OF THORIUM-CONTAINING NITRATE AND FLUORIDE SOLUTIONS FOR BREEDER-BLANKET USE

Recent efforts to find a stable thorium-containing nitrate solution which would be suitable for a breeder blanket operating at 300°C were unsuccessful. Experiments with beryllium nitrate - thorium nitrate, lithium nitrate - thorium nitrate, and beryllium fluoride - thorium fluoride solutions are described below.

20.5.1 Beryllium Nitrate - Thorium Nitrate Solutions

Several solutions prepared by mixing hydrated thorium nitrate and hydrated beryllium nitrate were sealed in glass tubes and observed visually while being heated and shaken in an aluminum block furnace. None of the solutions proved to be stable at 300°C, although solids were not precipitated until the temperature reached the 280-300°C range. It seems likely that the nitrate solutions were metastable at temperatures below that of the first appearance of a precipitate, since the precipitated solids either did not redissolve on cooling or redissolved only when the temperature had dropped below 250°C. The solution compositions and observed precipitation temperatures are given in Table 20.3.

20.5.2 Lithium Nitrate - Thorium Nitrate Solutions

A solution containing 6, 71, and 23 mole %, respectively, of $Th(NO_3)_4$, $LiNO_3$, and H_2O was observed to precipitate a solid phase at 290°C. The solid

Table 20.3. Precipitation Temperatures for Thorium Nitrate-Beryllium Nitrate Solutions

Molar Ratio $Th(NO_3)_4:Be(NO_3)_2$	Solution Composition (mole %) $Th(NO_3)_4$	$Be(NO_3)_2$	H_2O	Precipitation Temperature (°C)
2.5:1	15	6	79	294
1:1.9	8	15	77	280
1:1.9	Same molar ratio as (2) but with enough water added to dissolve the mixture at room temperature			300
1:1	11	11	78	280
1:1	Same molar ratio as (4) but with enough water added to dissolve the mixture at room temperature			290
-	0	25	75	305

did not redissolve, however, until the mixture had cooled to 240°C. Similar results were obtained with another solution containing 7.7, 61.6, and 30.8 mole % of these components.

20.5.3 Beryllium Fluoride - Thorium Fluoride Solutions

Several attempts were made to dissolve ThF_4 in moderately concentrated solutions of BeF_2 at 300°C. There was no evidence of ThF_4 solubility even in solution having a BeF_2 to ThF_4 molar ratio of 110 to 1 and containing approximately 430 g of BeF_2 per liter.

20.6 THE SYSTEM UO_3-HNO_3-H_2O AT 150-300°C

Previous investigations of the system UO_3-HNO_3-H_2O at high temperature have been restricted to studies in sealed tubes and to segments of the system which were limited to moderately high concentrations of HNO_3.[8] It was established previously[8] that $UO_2(NO_3)_2$ in aqueous solutions was thermally and hydrolytically unstable at elevated temperature as exhibited by the visual coloration of the vapor phase by the oxides of nitrogen and by the precipitation of $UO_3 \cdot H_2O$. These previous observations suggested that equilibrium concentrations of nitrogen oxides were produced in the temperature range 150-400°C, and also indicated a moderately rapid change of equilibrium (within minutes to hours) upon changing the system temperature. The removal of HNO_3 from the liquid to the vapor phase meant, however, that the use of the synthetic method for experimentation at high temperatures resulted in a rather large uncertainty in the high-temperature composition of the liquid phase. In the present investigation, metal pressure vessels are being used in which a liquid-phase sample is removed at the equilibration temperature from the solid-liquid-vapor system. This separated solution sample subsequently is analyzed for the components in solution, and no assumptions are necessary regarding loss of components to the vapor phase. In this case the vapor-phase composition and pressure are those produced by the condensed saturated solution and have fixed values, which are unknown to us at present.

A second motivating force for the current investigation is our present ability to study this system at high temperatures to very low concentrations of HNO_3 and UO_3. Boyle and Mahlmann have determined g values, in this case for the number of molecules of nitrogen produced per electron vole of fission energy[9] in aqueous nitrate systems, and from their data it appears that the g value for the production of N_2 might become very small at very low concentrations of NO_3^-. If free N_2 is not produced or is produced in only small quantity under radiation for dilute $UO_2(NO_3)_2$ solutions, $UO_2(NO_3)_2$ solutions, using N^{15} of low neutron absorption cross section, might be useful homogeneous reactor fuels.

Some of the current experimental data are included in Table 20.4 and Fig. 20.3. Our investigations of the UO_3-SO_3-H_2O system[10] and our speculations

Table 20.4. Solubility of Uranium Trioxide in Nitric Acid - Water Solutions at High Temperature

Temp. (°C)	Molality HNO_3	Molality UO_3	Saturation Mole Ratio, UO_3/HNO_3	Molarity* HNO_3	Molarity* UO_3
135	0.994	0.646	0.650	0.939	0.6104
	0.766	0.482	0.629	0.733	0.4613
	0.510	0.3281	0.643	0.494	0.3178
	0.2995	0.1965	0.656	0.2934	0.1925
	0.1505	0.0974	0.647	0.1488	0.0962
	0.1027	0.0673	0.655	0.1018	0.0667
	0.0777	0.0489	0.629	0.0771	0.0485
	0.0522	0.0326	0.624	0.0519	0.0324
200	3.102	1.858	0.599	2.678	1.6047
	1.028	0.628	0.611	0.971	0.594
	0.765	0.465	0.608	0.732	0.445
	0.514	0.3233	0.629	0.498	0.3133
	0.2519	0.1567	0.622	0.2477	0.1541
	0.1340	0.0792	0.591	0.1326	0.0784
	0.1086	0.0619	0.570	0.1078	0.0614
	0.0818	0.0469	0.573	0.0812	0.0465
	0.0587	0.03194	0.544	0.0584	0.03175
	0.0333	0.0148	0.444	0.033	0.0147
	0.0111	0.0052	0.469	0.0112	0.0052
235	0.978	0.586	0.599	0.928	0.556
	0.792	0.469	0.592	0.759	0.449
	0.523	0.3127	0.598	0.507	0.3032
	0.2879	0.1733	0.602	0.2824	0.1701
	0.1549	0.0914	0.590	0.1531	0.0903
	0.0988	0.0557	0.564	0.0981	0.0553
	0.0841	0.0435	0.517	0.0834	0.0431
	0.0546	0.0288	0.527	0.0543	0.0286

Table 20.4 (Continued)

Temp. (°C)	Molality HNO_3	Molality UO_3	Saturation Mole Ratio, UO_3/HNO_3	Molarity* HNO_3	Molarity* UO_3
270	3.172	1.808	0.570	2.753	1.568
	1.076	0.626	0.582	1.016	0.592
	0.787	0.443	0.563	0.754	0.425
	0.524	0.2932	0.560	0.508	0.2847
	0.2587	0.1428	0.552	0.2546	0.1405
	0.1287	0.0686	0.533	0.1277	0.0680
	0.1035	0.0556	0.537	0.1028	0.0552
	0.0782	0.0409	0.523	0.0776	0.0405
	0.0547	0.02741	0.501	0.0544	0.02725
	0.0374	0.0117	0.313	0.037	0.0116
	0.0142	0.0042	0.296	0.0142	0.0042
300	3.148	1.766	0.561	2.862	1.605
	1.120	0.644	0.575	1.059	0.609
	0.827	0.453	0.548	0.792	0.434
	0.543	0.3058	0.563	0.527	0.2967
	0.2683	0.1378	0.514	0.2639	0.1356
	0.1316	0.0637	0.484	0.1305	0.0631
	0.1062	0.0499	0.470	0.1052	0.0495
	0.0795	0.03617	0.455	0.0789	0.03592
	0.0546	0.02403	0.440	0.0543	0.02388
	0.0393	0.0110	0.280	0.039	0.0109
	0.0153	0.0039	0.255	0.0155	0.0039

* Molarities are on a 25°C basis.

concerning the possibility of $U_2O_5^{++}$ dimeric species existing in solution at high temperature led us to believe that similar behavior in NO_3^- media would produce saturation molar ratios of UO_3/NO_3 of 1, i.e., would indicate possible molecular species such as $U_2O_5(NO_3)_2$. However, the experimental data in Table 20.4 and Fig. 20.3 indicate saturation molar ratios UO_3:HNO_3 from 0.4 to 0.7. In view of T. F. Young's present consideration of HNO_3 in H_2O as a relatively weak acid at 300°C,[11] the saturation ratios listed above are not surprising and do not preclude the possibility of dimeric or trimeric uranium ions existing in solution at high temperature.

20.7 COMPARATIVE SOLUBILITY OF $NiSO_4 \cdot H_2O(D_2O)$ IN H_2SO_4-H_2O AND D_2SO_4-D_2O SOLUTIONS AT HIGH TEMPERATURE

The system NiO-SO_3-H_2O has been investigated extensively from 150 to 300°C and from 10^{-4} to 2 m SO_3.[12] An applied motivation for a study of this system arises from the consideration of nickel oxide as a corrosion product of stainless steel and the subsequent need for ascertaining its solubility relationships in aqueous reactor fuels. Since dilute aqueous reactor fuels are primarily D_2O solutions, solubility relationships must be evaluated in D_2O as well as in H_2O solutions. Comparative data for the solubility of $NiSO_4 \cdot H_2O(D_2O)$ in H_2SO_4-H_2O and D_2SO_4-D_2O have been obtained at 250 and 300°C. These data are shown in

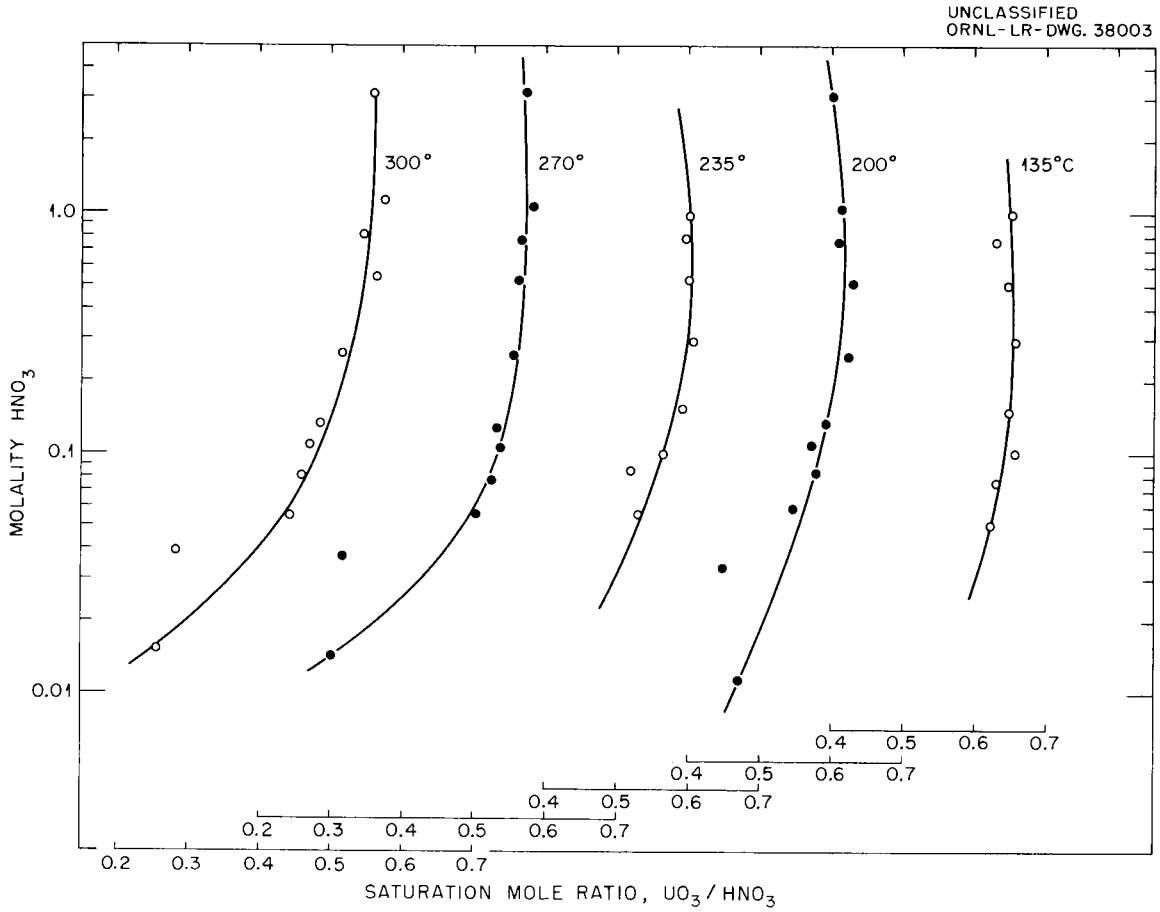

Fig. 20.3. The System UO_3-HNO_3-H_2O, 135–300°C 0.01–3 *M*.

Fig. 20.4. The very interesting aspect of these data is not so much the relative difference in solubility of $NiSO_4 \cdot H_2O(D_2O)$ in H_2O and D_2O media but rather the fact that the solubility is higher in D_2O solutions. This behavior is the reverse of the general comparative behavior at low temperatures, in which case salts in D_2O exhibit lower solubility. A possible explanation arises from Oliver and Grisard's[13] experimental data on relative vapor pressures of D_2O and H_2O, in which they observed a crossover in vapor pressure at 220.7°C. At lower temperatures H_2O has the higher vapor pressure; whereas at higher temperatures, D_2O has the higher value. It is postulated that this crossover at 220.7°C is directly related to a crossover in comparative solution-activity coefficients.

REFERENCES

1. W. L. Marshall et al., HRP Quar. Prog. Rep. Jan. 31, 1959, ORNL-2696, p 205-214.

2. F. E. Clark, J. S. Gill, Ruth Slusher, and C. H. Secoy, Journal of Chemical and Engineering Data 4, 12 (1959).

3. D. M. Richardson, ORNL CF 56-6-56.

4. D. M. Richardson, ORNL CF 57-5-36.

5. J. Sutton, "The Hydrolysis of the Uranyl Ion, Part I," J. Chem. Soc. 1949, S275.

6. T. V. Arden, "The Formation of Complex Ions in Uranyl Sulfate Solution," J. Chem. Soc. 1949, S299.

7. E. Posnjak and G. Tunell, Am. Journal Science-Fifth Series, Vol. XVIII, 1 (1929).

8. W. L. Marshall, J. S. Gill, and C. H. Secoy, Chem. Div. Quar. Prog. Rep. March 31, 1951, ORNL-1053, p 22-25.

9. J. W. Boyle and H. A. Mahlmann, Nuclear Science and Engineering 2, 492 (1957).

10. W. L. Marshall, Anal. Chem. 27, 1923 (1955).

11. T. F. Young, "Strong Acids at High Temperatures," paper presented before Division of Physical Chemistry, 135th Meeting of the American Chemical Society, Boston, Mass. (April 1959).

12. W. L. Marshall et al., HRP Prog. Rep. for Quarters Ending April 30 and July 31, 1958, ORNL-2561, p 307-311.

13. G. D. Oliver and J. W. Grisard, J. Am. Chem. Soc. 78, 561 (1956).

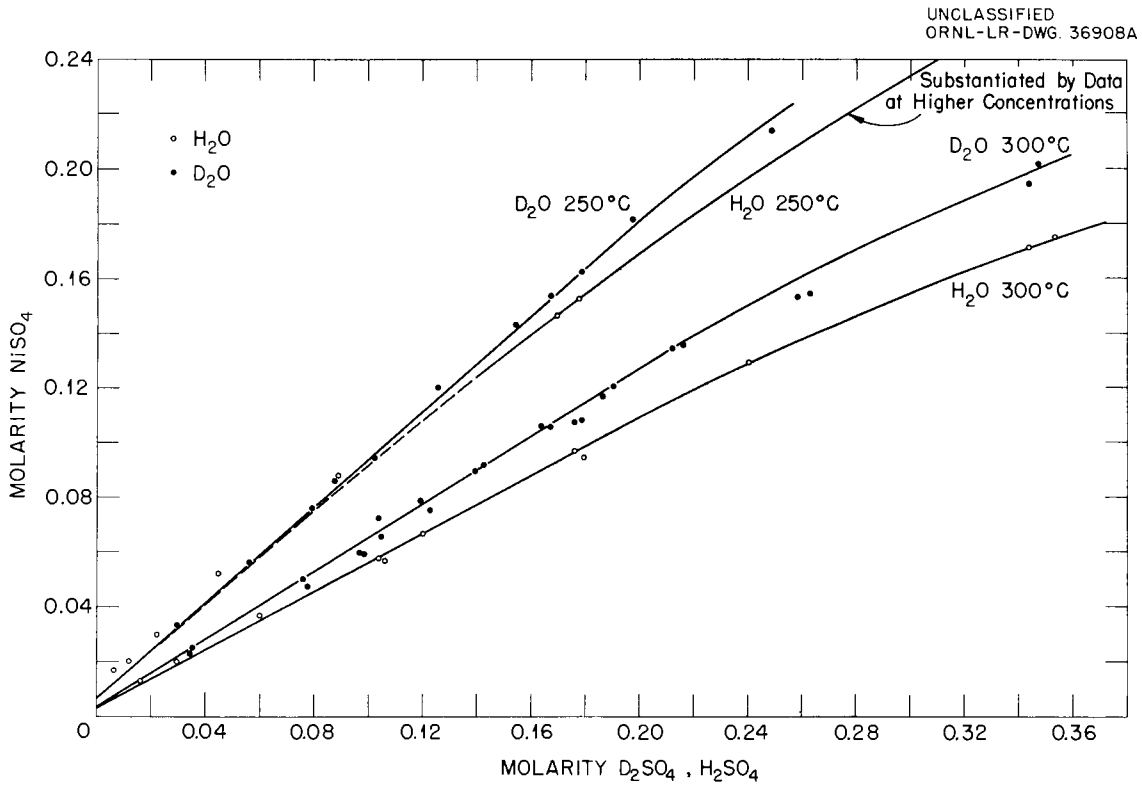

Fig. 20.4. $NiSO_4 \cdot H_2O(D_2O)$ Solubility in D_2O-D_2SO_4 and H_2O-H_2SO_4, 250 and 300°C.

21. REACTIONS IN AQUEOUS SOLUTIONS

M. J. Kelley

L. O. Gilpatrick
H. F. McDuffie
H. H. Stone
G. M. Watson

21.1 RATE OF OXIDATION OF DISSOLVED H_2 OR D_2 CATALYZED BY $Cu(ClO_4)_2$ IN LIGHT AND HEAVY WATER

The study of the mechanism of the oxidation of dissolved hydrogen by dissolved cupric salts, has continued. As explained elsewhere,[1] it is desirable to study the rates of oxidation not only of H_2 in H_2O but also in D_2O and of D_2 in both H_2O and in D_2O. During the quarter, rate constants were determined for the systems shown in Tables 21.1, 21.2, and 21.3.

The significance of the tabulated numbers in relation to possible mechanisms will be discussed when the experimental work presently in progress is completed.

21.2 URANIUM PEROXIDE PRECIPITATION AND STRUCTURE

Questions concerning the composition and structure of uranium peroxide were raised when ~6 g of lemon-yellow solid was recovered from the fuel system of the North Carolina State Reactor following a gradual loss of reactivity.[2] A disagreement was brought to light when the x-ray diffraction pattern of this material was independently compared with reference patterns[3] for $UO_4 \cdot 2H_2O$ in the files of the Analytical Chemistry and the Chemistry Divisions. This situation was resolved by the discovery that two different crystalline forms of uranium peroxide can be prepared by precipitation from the same aqueous solutions, with the occurrence of either form dependent primarily on the temperature of the precipitation.

Repeated laboratory precipitations in which 1 M hydrogen peroxide was added to 0.04 M uranyl sulfate solutions with stirring established that the low-temperature form was consistently produced below 63.5°C, while the high-temperature form was invariably produced above 64.5°C, with a mixture of both being obtained in the 63.5-64.5°C interval. Figure 21.1 illustrates the effect of precipitation temperature on the x-ray diffraction pattern and shows the actual x-ray data obtained.[4]

The low-temperature form appears to be nonhygroscopic and relatively stable in air at room temperature. Ignition to U_3O_8 established the composition of the air-dried low-temperature form as corresponding very closely to $UO_4 \cdot 4H_2O$; when the sample was exposed to sulfuric acid of density 1.50 at 24.5°C for 36 hr in a

Table 21.1. Rate of Oxidation of Dissolved H_2 Or D_2 Catalyzed By 0.1 M $Cu(ClO_4)_2$ in Different Solutions at 110°C and Low Acidity (0.01 M)

Initial Composition of Solutions:
$[HClO_4] = [DClO_4] = 0.01$ M; $[Cu(ClO_4)_2] = 0.1$ M;
$P_{H_2} = P_{D_2} = 20$ atm; $[Cr_2O_7^{=}] = 10^{-3}$ M

Experiment No.	System	k* $\frac{1}{(\text{mole})(\text{min})} \times 10^3$
34	H_2-H_2O	6.22
38	"	6.47
41	"	6.50
42	"	6.52
43	"	6.47
	Av	6.44 ± 0.06
26	H_2-D_2O	5.32
27	"	4.93
28	"	4.80
50	"	5.00
	Av	5.01 ± 0.15
44	D_2-H_2O	4.87
45	"	4.76
46	"	4.71
47	"	4.60
	Av	4.76 ± 0.08
29	D_2-D_2O	4.01
30	"	3.99
31	"	3.92
53	"	3.94
	Av	3.96 ± 0.04

*Calculated assuming equal solubilities of H_2 and of D_2 in H_2O and in D_2O and independent of acidity.

Table 21.2. Rate of Oxidation of Dissolved H_2 or D_2 Catalyzed by 0.1 M $Cu(ClO_4)_2$ in Different Solutions at 110°C and 0.505 M Acid Concentration

Initial Composition of Solutions:
$[HClO_4] = [DClO_4] = 0.505$ M; $[Cu(ClO_4)_2] = 0.1$ M;
$P_{H_2} = P_{D_2} = 20$ atm; $[Cr_2O_7^{=}] = 10^{-3}$ M

Experiment No.	System	k^* $\frac{1}{(mole)(min)} \times 10^3$
39	H_2-H_2O	3.16
51	H_2-D_2O	3.85
47	D_2-H_2O	2.15
54	D_2-D_2O	2.34

*Calculated assuming equal solubilities of H_2 and of D_2 in D_2O and independent of acidity.

Table 21.3. Rate of Oxidation of Dissolved H_2 Or D_2 Catalyzed by 0.1 M $Cu(ClO_4)_2$ in Different Solutions at 110°C and 1.0 M Acid Concentration

Initial Composition of Solutions:
$[HClO_4] = [DClO_4] = 1.0$ M; $[Cu(ClO_4)_2] = 0.1$ M
$P_{H_2} = P_{D_2} = 20$ atm, $[Cr_2O_7^{=}] = 10^{-3}$ M

Experiment No.	System	k $\frac{1}{(mole)(min)} \times 10^3$
23	H_2-H_2O	2.15
25	"	2.20
40	"	2.20
		Av 2.18 ± 0.02
52	H_2-D_2O	2.40
56	"	2.34
57	"	2.32
58	"	2.37
		Av 2.36 ± 0.03
62	D_2-H_2O	1.35
63	"	1.46
64	"	1.27
		Av 1.36 ± 0.07
55	D_2-D_2O	1.49
60	"	1.53
61	"	1.50
		Av 1.51 ± 0.02

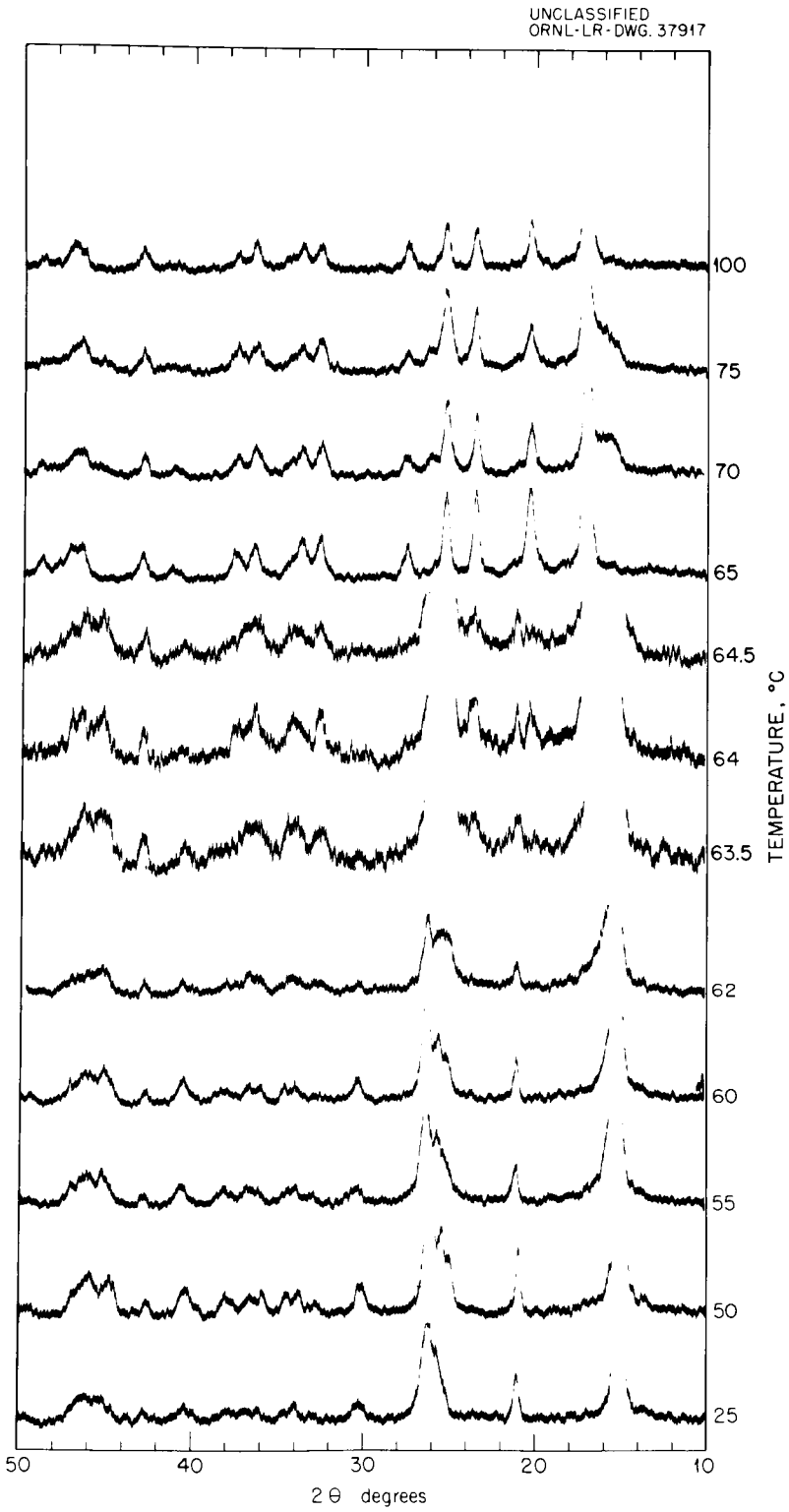

Fig. 21.1. Effect of Preparation Temperature upon Crystal Structure of Uranium Peroxide.

vacuum desiccator, exhausted initially to the onset of boiling in the acid, the loss of weight was 0.5% (from 0.4% over that calculated for the tetrahydrate to 0.1% under the calculated weight). When exposed to magnesium perchlorate overnight in an initially evacuated (25 μ) desiccator, the material was converted into the high-temperature form and lost weight equivalent to two molecules of water. The low-temperature form lost 80% of the two molecules of water, which are easily removed when heated at 50°C in the air for 1 hr; the loss of weight to the dihydrate was complete after 18 hr at 50-45°C. An unexpected stability of the tetrahydrate was noted when an attempt was made to convert it to the dihydrate by stirring in an aqueous solution of hydrogen peroxide at 70°C (above the temperature at which tetrahydrate is formed on precipitation). Stirring for 5 hr failed to convert the x-ray pattern from that of the tetrahydrate to that of the dihydrate.

The high-temperature form appears to be quite stable in the air even to temperatures as high as 90°C, at which it may be held overnight without weight change. Upon ignition to U_3O_8 the loss in weight corresponds to an original formula of $UO_4 \cdot 2H_2O$.

Attempts have been made to convert the dihydrate into the tetrahydrate by stirring an aqueous slurry of the dihydrate for extended periods of time at various temperatures. Dihydrate, which had been prepared by dehydration of the tetrahydrate over magnesium perchlorate in a vacuum desiccator, was stirred for 20 hr in distilled water at room temperature; x-ray diffraction did not reveal any reversion of the dihydrate to the tetrahydrate.

In agreement with the literature discussed below, the dihydrate was decomposed partially by heating at 150°C for 20 hr in air; the loss of weight corresponded to that required for a final formula of U_2O_7, and subsequent heating at 150°C for an additional 50 hr failed to produce further decomposition. The material was orange and liberated gas (oxygen) on contact with water as expected. Its x-ray diffraction pattern was so indistinct as to make it impossible to assert that the material is crystalline.

The literature concerning the chemistry of the oxides and hydrated oxides of uranium has been summarized and reviewed by Katz and Rabinowitch.[5] Apparently UO_4 has never been produced in an anhydrous form. Hydrates containing from "about four and one-half molecules of water" down to 1.5 molecules of water, with many intermediate values, have been reported by various investigators, but our information is quite consistent with that of the earliest investigator, Fairley,[6] who in 1877 reported that the air-dried form of uranium peroxide corresponded to the tetrahydrate but the material dried at 100°C corresponded to the dihydrate formula. No hydrates other than these appear to have been characterized sufficiently to merit serious consideration. Various project reports cited by Katz and Rabinowitch, and a recent paper by Boggs and El-Chehabi,[7] have established the thermal decomposition of the dihydrate to a compound of the formula U_2O_7. This was also confirmed by our work.

Thus the tetrahydrate and the dihydrate of uranium peroxide have now been differentiated and characterized in the same laboratory on the basis of temperature of preparation, x-ray diffraction pattern, gravimetric analysis upon heating at various temperatures, and conversion of the tetrahydrate into the dihydrate by a number of procedures. The material originally recovered from the North Carolina State Reactor was, then, the tetrahydrate; subsequent storage in a desiccator for "safety" while the various tests were performed has converted it into the dihydrate. The preparation and reactions of uranium peroxide compounds

are being studied further in connection with its occurrence and decomposition in homogeneous reactor fuel solutions at elevated temperatures.

REFERENCES

1. H. F. McDuffie et al., HRP Quar. Prog. Rep. Jan. 31, 1959, ORNL-2696, p 215.

2. Letter from M. T. Kelley to H. A. Lamonds, April 3, 1959, reporting analytical results on samples received Feb. 18, 1959.

3. Reference pattern in Analytical Chemistry Division taken from ORNL-2092, H. W. Dunn, X-ray Diffraction Data for Some Uranium Compounds. This report incorrectly attributes the formula $UO_4 \cdot 2H_2O$ to a pattern corresponding to the tetrahydrate.

   Reference pattern in Chemistry Division courtesy of R. D. Ellison based on material prepared in 1952 by H. W. Wright and identified as $UO_4 \cdot 2H_2O$.

4. The x-ray diffraction patterns were obtained through the cooperation of R. E. Thoma and his group.

5. J. J. Katz and E. I. Rabinowitch, The Chemistry of Uranium, NNES VIII-5, 1951, Chapter 11, Part A. "Uranium Oxides and Hydroxides," p 244-330.

6. T. Fairley, J. Chem. Soc. 31, 127-133 (1877).

7. J. E. Boggs and M. El-Chehabi, J. Am. Chem. Soc. 79, 4258-60 (1957).

22. GASEOUS-FISSION-PRODUCT DISPOSAL

W. E. Browning

R. D. Ackley R. E. Adams G. W. Keilholtz

Studies have been continued on disposal of radioactive fission gases by selective adsorption, with subsequent holdup and radioactive decay, from flowing streams of a sweep gas on beds of solid adsorbent. Studies during this period have included: (1) development of improved methods for evaluating the number (N) of theoretical plates in a given adsorber bed, (2) determination of the effect of sweep-gas velocity on N for Columbia G charcoal beds in pipes of 2.7-in. inside diameter, (3) evaluation of holdup time for krypton as a function of pressure of O_2 sweep gas, (4) brief examination of propagation of D_2-O_2 explosions through charcoal, and (5) measurement of dynamic adsorption coefficients for some recently acquired adsorbents.

Values of N for the Columbia G charcoal in the 2.7-in.-dia trap are shown in Fig. 22.1, with previously reported data[1] obtained with this material in 0.8-in.-dia traps. These data show that N varies with length of the bed and with linear velocity of the gas stream but not with diameter of the bed. Optimum values for N are obtained when the superficial velocity of the sweep gas is about 0.5 fpm.

Values for N shown in Fig. 22.1 were obtained by a graphical method similar to that employed in gas-liquid chromatography. With the aid of personnel from the M.I.T. Practice School, an IBM-704 program has been established for obtaining values of N from the equation developed explicitly for holdup of fission gases on solid adsorbents.[2] Subsequently it has been shown that the equation can be more conveniently used in the reduced and simplified form:

$$\frac{P}{P_{max}} = \left[\frac{t}{t_{max}} \exp\left(1 - \frac{t}{t_{max}}\right)\right]^{N-1}, \qquad (1)$$

where P is the partial pressure of the fission gas, t is time after injection of the pulse of fission gas, and P_{max} and t_{max} indicate the values at the maximum in the elution curve. Use of Eq. (1) in a logarithmic form greatly facilitates calculation of N since P/P_{max}, t, and t_{max} are read directly from the recorder chart. Values obtained with these improved methods will be reported at a later date.

The effect of oxygen pressure on holdup time of Kr^{85} on Columbia G carbon is shown as Fig. 22.2 over the range from 1 to 5 atm.

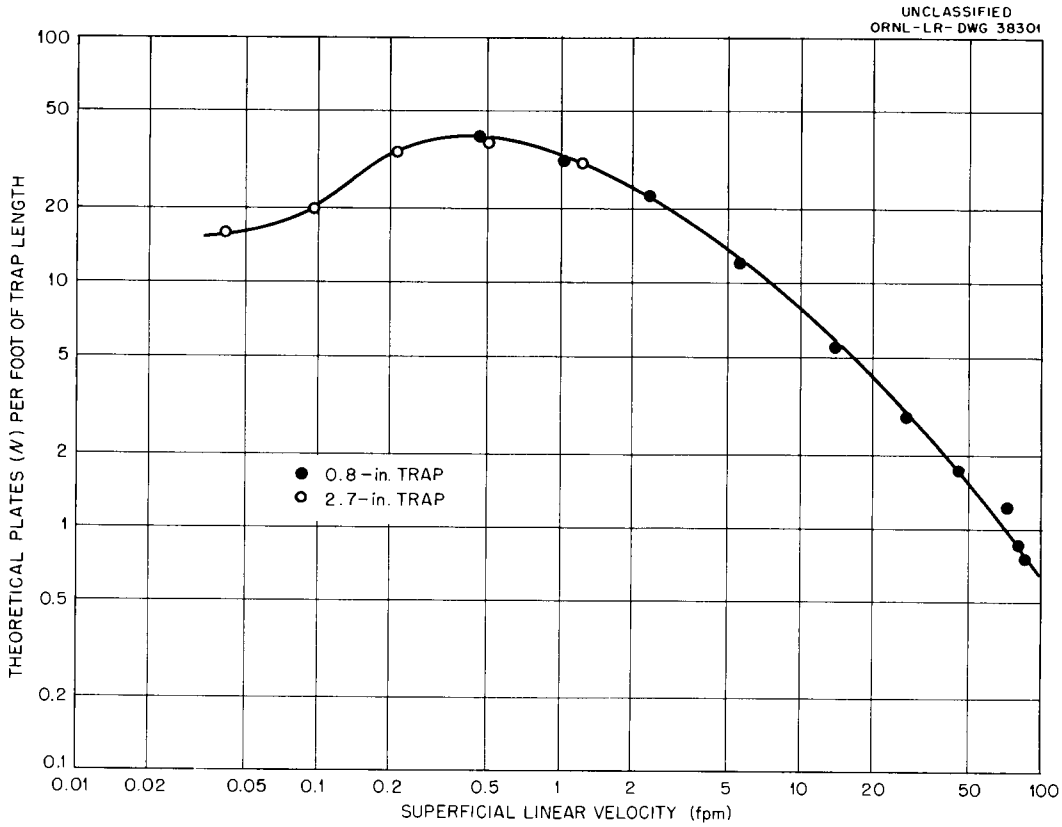

Fig. 22.1. Effect of Linear Velocity of the Sweep Gas on the Number of Theoretical Plates. Sweep gas, O_2; tracer, Kr^{85}; adsorbent, Columbia G activated carbon (at 24°C). Values of N were determined by a preliminary method.

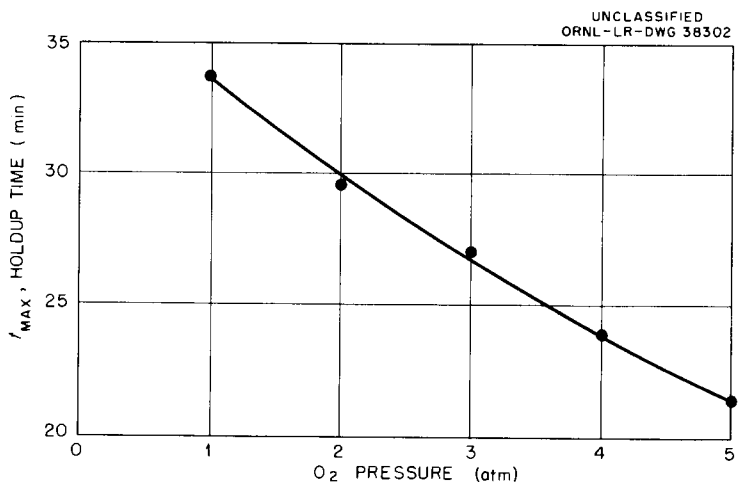

Fig. 22.2. Krypton Holdup Time Versus Oxygen Sweep-Gas Pressure. Adsorbent, Columbia G activated carbon (340 g at 24°C); superficial linear velocity, 6 fpm.

To simulate the conditions in the HRT off-gas system, a few experiments have been performed to examine propagation of explosions in D_2-O_2 mixtures through charcoal. Results indicate that limits for flammability for D_2-O_2 are very similar to those previously reported[3] for H_2-O_2.

Dynamic adsorption coefficients (k) for krypton were measured for Columbia 6G, 8/14, and Columbia CXC, 4/6, activated carbon and for two forms of porous glass. The k values for the charcoals were 55 and 49 cc/g, respectively; the corresponding figure for Columbia G is 54 cc/g. Neither sample of porous glass showed appreciable holdup of krypton.

In addition, studies to evaluate the apparent thermal conductivity of Columbia G charcoal in flowing streams of gas have been initiated. The preliminary values obtained indicate the apparent thermal conductivity to be higher by a factor of 2 than the estimated value employed in design of the HRT off-gas system.

REFERENCES

1. W. E. Browning et al., HRP Quar. Prog. Rep. Jan. 31, 1959, ORNL-2696, p 174-175.

2. W. E. Browning and C. C. Bolta, Measurement and Analysis of the Holdup Gas Mixtures by Charcoal Adsorption Traps, ORNL-2116, July 27, 1956.

3. W. E. Browning et al., HRP Quar. Prog. Rep. Jan. 31, 1959, ORNL-2696, p 173.

Part VII

ANALYTICAL CHEMISTRY

M. T. Kelley

23. ANALYTICAL CHEMISTRY

O. Menis

C. M. Boyd H. P. House D. L. Manning
G. Goldstein T. C. Rains

23.1 DETERMINATION OF SULFATE AND FREE ACID BY HIGH-FREQUENCY TITRATION: APPLICATION TO SOLUTIONS OF URANYL SULFATE

A radio-frequency titrimeter[1] was utilized in the direct titration of sulfate and free acid in solutions of uranyl sulfate. Sulfate in a typical HRT fuel solution is determined by titrating it with standard $BaCl_2$ solution. The end point of the titration is indicated by a break in the curve obtained by recording the IR drop across a fixed resistance vs the volume of titrant. Uranium must be masked by the addition of citrate or fluoride; otherwise, the break indicating the end point of the titration is obscured. For the titration of 40 to 70 mg of sulfate, the coefficient of variation is about 2%. Free acid is determined in a similar manner, utilizing NaOH as the titrant. Approximately 0.2 meq of free acid can be titrated with a coefficient of variation of 2%. Milligram quantities of uranium do not interfere. In fact, the uranium content can be estimated approximately by continuing the titration until a second break occurs. This method is not, however, recommended for the precise estimation of the uranium, because of the nonstoichiometric nature of the uranium-sodium hydroxide reaction.[2]

23.2 FLAME-PHOTOMETRIC DETERMINATION OF RARE-EARTH ELEMENTS IN THORIUM OXIDE

An investigation was made of the applicability of flame photometry to the determination of rare-earth elements in ThO_2. The rare-earth elements were separated from synthetic solutions by an extraction procedure similar to that used by Bronaugh and Suttle,[3] in which 2-thenoyltrifluoroacetone (TTA) in 4-methyl-2-pentanone (hexone) was used as the extractant. The extraction was carried out at a pH of 5.5, after which the flame spectrum of each of the rare-earth elements in the hexone extract was determined. The emissivity of the rare-earth elements in the organic medium is enhanced approximately 100-fold over that obtainable with aqueous solutions. Consequently, by utilizing an organic medium, the limits of detection can be extended significantly. The major bands or lines and their relative intensity were established over the wavelength range of 380 to 800 mμ . From these data, it seems that, with the exception of lanthanum and ytterbium, mutual interference will be encountered in the analysis of mixtures of rare-earth elements by flame photometry. A preliminary separation will be required before the individual elements can be determined.

23.3 FLAME-PHOTOMETRIC ESTIMATION OF PALLADIUM IN THORIUM OXIDE SLURRIES

A flame photometric method has been developed for the estimation of palladium in slurries of thorium oxide. The palladium is separated from interferences by extracting the Pd-α -furildioxime complex[4] with hexone from an HCl solution, after which the radiant intensity of the palladium is measured flame photometrically at a wavelength of 363 mμ . Of the various cations encountered in slurries of thorium oxide, only Cr(VI) interferes and must be reduced to Cr(III). By aspirating the palladium in an organic (hexone) rather than aqueous medium, the radiant intensity is increased tenfold. A sensitivity of 0.04 μg of Pd per ml per scale division is attainable. From 1 to 6 μg of Pd per ml in the solution used for the measurement of radiant intensity can be determined with an average coefficient of variation of 3%.

23.4 DETERMINATION OF U(IV)-U(VI) RATIO IN THORIUM OXIDE - URANIUM OXIDE MIXTURES

The controlled-potential coulometric titrator[5] has been applied to the determination of the U(IV)/U(VI) ratio in thorium oxide - uranium oxide mixtures. The samples are dissolved by refluxing them in concentrated HCl under an argon atmosphere to prevent air oxidation of the U(IV). The U(VI) is determined by coulometric reduction at -0.3 v vs the silver - silver chloride electrode. In this chloride medium, Fe(III) and Cr(VI), if present, cannot be pre-reduced at 0.0 v and, therefore, will interfere. Corrections for the interference of these elements can, however, be made, based on the concentration of each as determined by spectrophotometric analyses. A second aliquot of the HCl solution of the sample is fumed with $HClO_4$ to oxidize the U(IV) to U(VI) and the total uranium is then determined coulometrically after a pre-reduction step to remove the interference of Fe(III) and Cr(VI). The difference in the amount of U(VI) found in the original solution and in the oxidized solution is equal to the U(IV) in the sample.

The results of coulometric analyses for the ratio of U(IV) to U(VI) agree within 5% with those obtained by a method involving the dissolution of the sample in H_3PO_4 and excess dichromate followed by titration of the residual dichromate with standard $FeSO_4$.[6]

23.5 DETERMINATION OF OSMIUM IN SOLUTIONS OF URANYL SULFATE

Spectrophotometric methods were developed for the determination of microgram and milligram quantities of osmium in uranyl sulfate solutions. Samples containing milligram amounts of osmium are made strongly acid (30%) with HNO_3 to oxidize the osmium, regardless of the initial valence state, to Os(VIII). The OsO_4 is then extracted with $CHCl_3$[7] and determined spectrophotometrically. The only other element which extracts under these conditions is ruthenium. The ultraviolet adsorption spectrum of OsO_4 in $CHCl_3$ exhibits peaks at 282, 289, 297, 304, and 312 mμ with molar absorbancy indices of 1870, 1760, 1640, 1400, and 1000, respectively. Choice of wavelength will depend on the osmium concentration. From 0.3 to 3 mg of osmium can be determined with a coefficient of variation of about 3%.

In the range of 1 to 10 μg of osmium per ml of sample, the procedure is modified by the addition of a 0.2% solution of diphenylcarbazide in ethanol to

the extract. A blue-violet complex forms which exhibits maximum absorbance at 560 mμ and, after a 2-hr period for color development, the molar absorbancy index is about 31,000. The coefficient of variation is about 4%.

For osmium in extremely low concentrations, 0.2 to 2 μg/ml, the diphenylcarbazide reagent is added to an aqueous solution containing the osmium and acetic acid. The aqueous solution is then heated to 65°C, cooled to room temperature, extracted with $CHCl_3$; then, the absorbancy of the extract is measured at 560 mμ . The absorbance of the extract depends on the hydrogen ion and acetic acid concentrations of the aqueous phase; therefore, both must be carefully controlled. By extracting the osmium-diphenylcarbazide complex from an aqueous solution which is 1.4 M with both $HClO_4$ and acetic acids, a molar absorbancy index of about 100,000 can be attained. The interference of other ions in this procedure is under study.

23.6 SELECTION OF A DESCALING SOLUTION

A study was made for the purpose of finding a method for the removal of scale, in a stainless steel system, which was believed to be plugging the HRT heat exchanger. A solution suitable for the dissolution of scale composed of the oxides of iron, chromium, and other elements without doing damage to stainless steel was required. Because of the latter requirement, hot, acid solutions were ruled out. Complexing agents effective in dissolving metallic oxide were, accordingly, investigated. These included a series of compounds containing a polyaminopolycarboxylic acid group such as Versene and related compounds. In tests with a typical sample of mixed-oxide scale, the most effective solution for disintegration of the scale was a hot solution of the trisodium salt of n-hydroxyethylethylenediamine triacetate (Versenol) in an ammonium acetate buffer. From information in the literature,[8,9] it is apparent that the effectiveness of this solution in decomposing the scale is due to the formation of a soluble Fe-Versenol chelate, even in a basic solution, and also to the reduction of Cr(VI) to Cr(III) by hot Versenol, followed by the formation of a soluble Cr(III)-Versenol complex. Since it is known that acetate also forms a stable complex with Cr(III), both the Versenol and the ammonium acetate, therefore, contribute to the dissolution of the oxide scale. A test was made in which the Versenol-ammonium acetate solution was circulated in a test loop containing oxide scale, and a significant disintegration of the scale was observed. After approximately 60 hr, the solution contained 10 g of iron per liter. These results indicate that scale composed of mixed oxides can be removed effectively from stainless steel systems by utilizing the Versenol-acetate solution without doing damage to the stainless steel.

REFERENCES

1. D. L. Manning, "Determination of Thorium," Anal. Chem. Ann. Prog. Rep., Dec. 31, 1958, ORNL-2662, p 22.

2. C. J. Rodden, Analytical Chemistry of the Manhattan Project, p 74, McGraw-Hill (1950).

3. H. J. Bronaugh and J. F. Suttle, Chelation of the Rare Earth Elements as a Function of pH Using Thenoyltrifluoroacetone, LA-1561 (Aug. 1953).

4. O. Menis, T. C. Rains, "Colorimetric Determination of Palladium with Alpha-Furildioxime," Anal. Chem. 27, p 1932 (1955).

5. M. T. Kelley, D. J. Fisher, and H. C. Jones, "Automatic Electronic, Controlled-Potential Coulometric Titrator," Anal. Chem. Ann. Prog. Rep., Dec. 31, 1958, ORNL-2662, p 13.

6. O. Menis, et al., "Determination of U(IV) in Thorium Oxide-Uranium Oxide Mixtures," HRP Quar. Prog. Rep. Jan. 31, 1959, ORNL-2696.

7. R. D. Sauerbrunn and E. B. Sandell, Anal. Chim. Acta 9, 86 (1953).

8. The Versenes, Technical Bulletin No. 2, Sec. II, p 38, Bersworth Chemical Co., Framingham, Mass. (Feb. 4, 1959).

9. R. Pribil and J. Klubalova, "Use of Complexones in Chemical Analysis, VI. Colorimetric Determination of Chromium," Collection Czechoslov. Chemm. Communs. 15, 42 (1950).

OAK RIDGE NATIONAL LABORATORY
HOMOGENEOUS REACTOR PROJECT

MAY 1, 1959

PROJECT DIRECTOR
R. B. BRIGGS — D

ASSOCIATE PROJECT DIRECTOR
C. E. WINTERS** — D
A. L. GUNNELS, SEC. — REE

PROJECT EDITOR
W. D. REEL — TI

DESIGN AND ENGINEERING
R. N. LYON, ASSOCIATE DIRECTOR — REE
T. S. CARLSMITH,* SEC. — REE

DESIGN
W. R. GALL, SECTION CHIEF — REE
M. I. LUNDIN, ASSISTANT SECTION CHIEF — REE
J. R. McWHERTER, ASSISTANT SECTION CHIEF — REE

SPECIAL PROBLEMS
C. L. SEGASER — REE

HRP DESIGN
J. R. McWHERTER, ASSISTANT SECTION CHIEF — REE
R. H. CHAPMAN, GROUP LEADER — REE
E. H. GIFT — REE
R. E. SCHAPPEL — REE

MECHANICAL DESIGN, DRAFTING AND SPECIFICATIONS
M. I. LUNDIN, ASSISTANT SECTION CHIEF — REE
F. C. ZAPP, GROUP LEADER — REE
C. A. BURCHSTED — REE
J. E. JONES — REE
J. P. GILL — REE
W. ROBINSON — REE
H. H. BRADFORD — REE
R. L. CAUBLE — REE
J. P. DILORENZO — REE
F. GUNNESS — REE
T. E. HAYNES — REE
A. R. KERR — REE
W. B. KRICK — REE
L. E. PENTON — REE
C. A. ROBERTS — REE
R. D. SATTERFIELD — REE
R. H. SIGLER — REE
W. G. STERLING — REE

COMPONENT DEVELOPMENT
I. SPIEWAK, SECTION CHIEF — REE

MAINTENANCE DEVELOPMENT
J. S. CULVER, GROUP LEADER — REE
R. BLUMBERG — REE
B. D. DRAPER — TVA
P. P. HOLZ — REE
T. L. CASTILE — REE
C. JONES — REE

CIRCULATING PUMPS, HEAT EXCHANGERS
C. H. GABBARD, GROUP LEADER — REE
J. C. MOYERS — REE
I. K. NAMBA — REE
H. R. PAYNE — REE
C. C. HURTT — REE
R. J. LOCKETT — REE

FEED PUMPS AND VALVES
E. C. HISE, GROUP LEADER — REE
H. C. ROLLER — REE
J. P. HURST — REE
G. A. WINDLE — REE

CORE AND BLANKET, CHEMICAL ENGINEERING PROBLEMS
C. G. LAWSON, GROUP LEADER — REE
T. G. CHAPMAN — REE
B. A. HANNAFORD — REE
J. E. MOTT† — REE
R. P. WICHNER — REE
R. GOODMAN — REE
S. R. WEST — REE

SLURRY PROBLEMS
D. M. EISSENBERG — REE
B. J. YOUNG — REE

RESEARCH AND ANALYSIS
P. R. KASTEN, SECTION CHIEF — REE

REACTOR ANALYSIS
M. W. ROSENTHAL, GROUP LEADER — REE
S. JAYE — REE
B. E. PRINCE — REE

REACTOR PHYSICS
M. TOBIAS, GROUP LEADER — REE
C. W. NESTOR, JR. — REE

PROGRAMING
T. B. FOWLER — REE
M. P. LIETZKE — REE
H. A. MACCOLL — REE

TRANSPORT PROPERTIES OF SLURRIES
D. G. THOMAS, GROUP LEADER — REE
P. H. HAYES — REE
R. M. SUMMERS — REE

PHYSICAL CHEMISTRY OF SLURRIES
C. S. MORGAN, GROUP LEADER — REE
B. G. SUTTON — REE

SYSTEMS DEVELOPMENT
R. B. KORSMEYER, SECTION CHIEF — REE
F. N. PEEBLES, ASSISTANT SECTION CHIEF — REE

SLURRY SYSTEMS DEVELOPMENT I
R. VAN WINKLE, GROUP LEADER — REE
H. B. PIPER — REE
C. A. MCLAUGHLIN — REE

SLURRY SYSTEMS DEVELOPMENT II
L. F. PARSLY, JR., GROUP LEADER — REE
R. D. BUNDY — REE
R. J. KEDL — REE
M. RICHARDSON — REE
R. E. CARNES — REE

HRT CORE MOCKUP
P. H. HARLEY, GROUP LEADER — REE
T. R. WILSON — REE

OPERATIONS
A. N. SMITH, GROUP LEADER — REE
T. L. BOSWELL — REE
B. R. CHILCOAT — REE
J. T. DICKIE — REE
C. A. GIFFORD — REE
H. G. MOORE — REE
D. H. WALLACE — REE

INSTRUMENTATION AND CONTROLS
D. S. TOOMB, SECTION CHIEF — I&C

REACTOR I&C SYSTEM DESIGN
J. R. BROWN, GROUP LEADER — I&C
R. W. BORGERS — I&C

HRP SUPPORTING SERVICES
H. O. WILLS, GROUP LEADER — I&C
P. G. HERNDON — I&C
R. M. BURNETT — I&C

VALVE DEVELOPMENT AND SPECIFICATIONS
A. M. BILLINGS, GROUP LEADER — I&C
E. H. BELL — I&C
B. J. JONES — I&C

INSTRUMENT DEVELOPMENT
R. L. MOORE, GROUP LEADER — I&C
T. M. CATE — I&C

CHEMICAL PLANT I&C SYSTEM DESIGN
D. G. DAVIS, GROUP LEADER — I&C
S. J. BALL* — I&C
P. E. SMITH — I&C

REACTOR MATERIALS RESEARCH
E. G. BOHLMANN, ASSOCIATE DIRECTOR — REE
T. K. CARLSMITH,* SEC. — REE
R. E. WACKER, RECORDS — REE

SOLUTIONS
J. C. GRIESS, ASSISTANT SECTION CHIEF — REE

LOOPS
R. S. GREELEY, GROUP LEADER — REE
E. S. SNAVELY — REE
W. H. HINDS — REE

LABORATORY STUDIES
J. L. ENGLISH, GROUP LEADER — REE
D. N. HESS — REE
P. D. NEUMANN — REE
L. L. FAIRCHILD — REE
H. L. BARKER — REE
J. E. JACKSON — REE
B. L. JOHNSON — REE
J. L. UNDERWOOD — REE

SLURRIES
E. L. COMPERE, SECTION CHIEF — REE

LOOPS

OUT-OF-PILE STUDIES
S. A. REED,* GROUP LEADER — REE
R. B. GALLAHER — REE
H. F. HENDERSON — REE
F. E. McDANIEL* — REE
G. G. WARNER — REE

TOROIDS

OUT-OF-PILE STUDIES
S. A. REED,* GROUP LEADER — REE
L. RICE — REE
R. F. BENSON — REE
B. H. PARKS — REE

IN-PILE BOMBS
L. F. WOO — REE
F. E. McDANIEL* — REE

ENGINEERING
H. C. SAVAGE, SECTION CHIEF — REE

SOLUTIONS
S. E. BOLT, GROUP LEADER — REE
A. J. SHOR — REE
W. C. ULRICH — REE

IN-PILE MOCKUPS
J. R. HART — REE
J. W. MOSIER — REE
R. W. RAY — REE

100A LOOP OPERATIONS
J. F. WINESETTE* — REE
C. M. BURCHELL — REE
C. L. FRANCIS — REE
J. B. FRENCH — REE
J. W. GOOCH — REE

SLURRIES
J. M. BAKER — REE
T. H. MAUNEY — REE
O. G. GATES — REE

100A LOOP OPERATIONS
J. F. WINESETTE* — REE
L. L. ALLEN — REE
C. R. BENSON — REE
V. R. BULLINGTON — REE
G. A. MOORE — REE
L. G. PHELPS — REE

IN-PILE OPERATIONS
R. A. LORENZ, GROUP LEADER — REE
V. A. DECARLO — REE
C. H. BURBAGE — REE
J. P. GORDON — REE
E. H. GUINN — REE
R. A. JONES — REE
J. W. MYERS — REE
D. G. PEACH* — REE
T. R. RAYBURN — REE
C. E. ROBERTS — REE
R. G. ROSS — REE
A. L. SUTTON — REE
W. E. TEICHERT — REE
R. M. WALLER* — REE

RADIATION
G. H. JENKS, SECTION CHIEF — REE

IN-PILE LOOPS
M. D. SILVERMAN, GROUP LEADER — C
J. E. BAKER — REE
S. H. WHEELER — REE

IN-PILE BOMBS
R. J. DAVIS, GROUP LEADER — C
K. S. WARREN — C
J. L. RUTHERFORD — REE

SUPPORTING RESEARCH
A. L. BACARELLA — C
J. C. BANTER — REE
W. C. YEE — C

REMOTE EVALUATION
A. R. OLSEN — REE
B. W. McCOLLUM, SHIFT LEADER — REE
C. M. FITZPATRICK — REE
W. J. SCHILL — REE
W. H. SMITH, JR. — REE

METALLURGY
G. M. ADAMSON, SECTION CHIEF — M

METALLURGICAL RESEARCH
M. L. PICKLESIMER, LEADER — M
P. L. RITTENHOUSE — M
R. L. STEPHENSON — M
P. J. JONES — M
G. C. NELSON — M
J. J. WOODHOUSE — M

METALLURGICAL ENGINEERING
G. M. ADAMSON,* LEADER — M
F. W. COOKE — M
W. J. LEONARD — M
J. J. PRISLINGER — M
J. K. WHITE — M
C. H. WOOTKE — M
C. M. SMITH — M
M. A. SHEELER — M

METALLOGRAPHY
R. S. CROUSE,** LEADER — M
T. M. KEGLEY, JR. — M
E. R. BOYD — M
B. F. DAY** — M
R. L. FITZGERALD** — M
T. J. HENSON** — M

RADIATION DAMAGE
R. G. BERGGREN** — SS
J. C. WILSON** — SS
F. B. GRIZZEL** — SS

SUBCONTRACTS

FRANKLIN INSTITUTE
RICE INSTITUTE
UNIVERSITY OF UTAH

AC — ANALYTICAL CHEMISTRY
C — CHEMISTRY DIVISION
CT — CHEMICAL TECHNOLOGY DIVISION
O — DIRECTOR'S DIVISION
I&C — INSTRUMENTATION AND CONTROLS DIVISION
M — METALLURGY DIVISION
RC — REACTOR CHEMISTRY DIVISION
REE — REACTOR EXPERIMENTAL ENGINEERING DIVISION
SS — SOLID STATE DIVISION
TI — TECHNICAL INFORMATION DIVISION
* — DUAL CAPACITY
** — PART TIME ON PROJECT
† — ATTENDING ORSORT

INDUSTRIAL PARTICIPATION

JAPANESE ATOMIC ENERGY RESEARCH INSTITUTE
TENNESSEE VALLEY AUTHORITY

CHEMICAL TECHNOLOGY
D. E. FERGUSON,* PROBLEM LEADER — CT
I. LOOPE, SEC. — CT

CHEMICAL DEVELOPMENT
D. E. FERGUSON,* SECTION CHIEF — CT

FUEL PROCESSING
R. A. McNEES, GROUP LEADER — CT
W. B. HOWERTON — CT

THORIUM BLANKET STUDIES
J. P. McBRIDE, GROUP LEADER — CT

OXIDE PREPARATION
R. L. PEARSON, PROBLEM LEADER — CT
A. T. KLEINSTEUBER — CT
C. E. SCHILLING — CT
C. W. GREENE — CT

IRRADIATION STUDIES
N. A. KROHN, PROBLEM LEADER — CT
L. E. MORSE — CT
P. P. HAYDON — CT
W. L. PATTISON — CT
H. F. SOARD — CT

SURFACE CHEMISTRY
C. H. SECOY, GROUP LEADER — CT
H. F. HOLMES — CT
F. H. SWEETON — CT

DESIGN
W. E. UNGER, ASSISTANT SECTION CHIEF — CT

TiO_2 DEVELOPMENT DESIGN
J. C. SUDDATH — CT

HRT-CP DESIGN SUPPORT
H. O. WEEREN — CT

INSTRUMENTATION
C. S. LISSER — I&C

PILOT PLANT
R. B. LINDAUER, SECTION CHIEF — CT

SLURRY PREPARATION
W. H. LEWIS, GROUP LEADER — CT
R. H. WINGET, PROBLEM LEADER — CT
K. O. JOHNSSON — CT

UNIT OPERATIONS
P. A. HAAS, GROUP LEADER — CT

FUEL PROCESSING DEVELOPMENT
E. L. YOUNGBLOOD — CT
D. H. NEWMAN — CT

SLURRY PREPARATION DEVELOPMENT
S. O. CLINTON — CT
C. C. HAWS, JR. — CT
R. D. ARTHUR — CT
V. L. FOWLER — CT

CHEMICAL RESEARCH
H. F. McDUFFIE,* ASSISTANT DIRECTOR — RC
I. W. HODGE, SEC. — RC

HETEROGENEOUS EQUILIBRIA IN AQUEOUS SYSTEMS
W. L. MARSHALL, GROUP LEADER — RC
C. J. BARTON — RC
J. S. GILL — RC
G. M. HEBERT — RC
E. V. JONES — CONSULTANT
R. E. MOORE — RC
R. SLUSHER — RC

REACTIONS IN AQUEOUS SOLUTIONS
G. M. WATSON, SUPERVISOR — RC
M. J. KELLY, GROUP LEADER — RC
L. O. GILPATRICK — RC
H. H. STONE — RC

RADIATION EFFECTS
G. W. KEILHOLTZ, SUPERVISOR — RC
W. E. BROWNING, GROUP LEADER — RC
R. D. ACKLEY — RC
R. E. ADAMS — RC

ANALYTICAL CHEMISTRY
MYRON T. KELLEY,** DIRECTOR
C. D. SUSANO,** ASSOCIATE DIRECTOR
K. A. ODOM,** SEC. — AC
H. E. ZITTEL, COORDINATOR, HRP ANALYTICAL CHEMISTRY — AC

CORROSION ANALYTICAL LABORATORY
O. MENIS,* SECTION CHIEF — AC
H. P. HOUSE,** ASST. SECTION CHIEF — AC

RESEARCH
O. MENIS,* GROUP LEADER — AC
C. M. BOYD — AC
D. L. MANNING, GROUP LEADER — AC
R. G. BALL — AC
G. GOLDSTEIN — AC

DEVELOPMENT AND SPECIAL ANALYSES
T. C. RAINS, GROUP LEADER — AC
N. M. FERGUSON — AC

SERVICE
C. K. TALBOTT, SUPERVISOR — AC
D. E. CARPENTER — AC
F. L. LAYTON — AC
T. P. BACON — AC
W. D. CLAPP, JR. — AC
C. A. CLARK — AC
P. S. GOODWIN — AC
B. D. HICKS — AC
A. H. MATTHEWS — AC
T. G. MILLER — AC
V. S. NORMAN — AC
E. ONKST — AC
C. M. WILSON — AC

SPECTROCHEMICAL SERVICES
C. FELDMAN,** SUPERVISOR — AC
W. R. MUSICK** — AC
A. H. MARSHALL** — AC
J. A. NORRIS,** GROUP LEADER — AC
J. J. MUNDZAK** — AC

HRT AND IN-PILE LOOP ANALYSIS
U. KOSKELA, SUPERVISOR — AC
L. G. FARRAR, ASST. SUPERVISOR — AC
C. P. BAKER — AC
S. R. DINSMORE — AC
R. E. CORCORAN — AC
G. I. GAULT — AC
F. K. HEACKER — AC
M. H. McCORQUODALE — AC
H. L. WEBB — AC
H. L. WHITTINGTON — AC

RADIOCHEMICAL ANALYSIS
E. I. WYATT,** SUPERVISOR — AC

HRT DEVELOPMENT
P. F. THOMASON,** GROUP LEADER — AC
R. E. BIGGERS** — AC
F. J. MILLER** — AC
S. A. REYNOLDS,** GROUP LEADER — AC
J. S. ELDRIDGE** — AC
T. H. HANDLEY** — AC

HIGH RADIATION LABORATORY
J. E. MORTON,** SUPERVISOR — AC

NUCLEAR ANALYSIS LABORATORY
G. W. LEDDICOTTE,** SUPERVISOR — AC
L. C. BATE** — AC
W. J. HAMPTON** — AC
R. W. HARVEY** — AC

OPTICAL AND ELECTRON MICROSCOPY
T. E. WILLMARTH,** GROUP LEADER — AC

HOMOGENEOUS REACTOR TEST
S. E. BEALL, PROJECT ENGINEER — REE
B. EUBANK, SEC. — REE
O. SCOTT, JR., SPECIAL ASSIGNMENT — REE

J. W. HILL, JR., ASSISTANT SECTION CHIEF — REE
J. R. BUCHANAN, ASSISTANT FOR PLANNING — CT
J. D. FLYNN, ASSISTANT FOR OPERATIONS — REE

R. H. GUYMON, CHIEF — REE
T. G. HILL — REE
J. D. JONES — REE
R. J. HARVEY, SHIFT SUPERVISOR — REE
R. SMITH, JR., CONTROL ROOM SUPERVISOR — REE
H. L. BROWN — REE
D. T. GODWIN — REE
A. L. JOHNSON — REE
W. H. WAGNER — REE
H. F. BAUMAN, SHIFT SUPERVISOR — CT
E. W. BROWN, CONTROL ROOM SUPERVISOR — CT
J. D. BARNES — REE
E. D. BOLLING — REE
W. T. BOSTIC — CT
D. F. FRECH, SHIFT SUPERVISOR — REE
R. J. SHANNON, CONTROL ROOM SUPERVISOR — CT
P. B. DAVIS — REE
J. E. EVE — REE
L. J. SHERSKY — CT
J. E. WOLFE — REE
N. C. BRADLEY, SHIFT SUPERVISOR — CT
J. L. STEPP, CONTROL ROOM SUPERVISOR — REE
H. D. CURTIS — REE
T. W. HODGE — REE
F. L. ROUSER — REE

MAINTENANCE PLANNING
W. TERRY, SUPERVISOR — REE
G. H. JOHNSTONE — REE
L. P. PUGH — REE

INSTRUMENTATION
J. L. REDFORD, GROUP LEADER — I&C
S. J. BALL* — I&C

P. N. HAUBENREICH,* ASSISTANT SECTION CHIEF — REE

REACTOR ANALYSIS
P. N. HAUBENREICH,* GROUP LEADER — REE
S. R. BOXTON — REE
J. R. ENGEL — CT
J. HIROTA — JAPANESE ATOMIC ENERGY RESEARCH INSTITUTE
J. O. KOLB — REE
J. A. WATTS — REE

REACTOR CHEMISTRY
D. M. RICHARDSON, GROUP LEADER — REE
D. G. PEACH* — REE
R. M. WALLER* — REE

CHEMICAL PLANT
W. O. BURCH, GROUP LEADER — CT
L. B. SHAPPERT — CT
O. O. YARBRO — CT
W. A. LINDSEY — CT

PERSONNEL SUMMARY

	FULL TIME	PART TIME	INDUSTRIAL PARTICIPATION	TOTAL
ADMINISTRATION	7	3		10
ANALYTICAL CHEMISTRY	31	18		49
CHEMICAL RESEARCH	14			14
CHEMICAL TECHNOLOGY	30			30
DESIGN AND ENGINEERING	94		1	95
HOMOGENEOUS REACTOR TEST	43		1	44
REACTOR MATERIALS RESEARCH	87	7		94
TOTAL	306	28	2	336

INTERNAL DISTRIBUTION

1. C. E. Center
2. Biology Library
3. Health Physics Library
4. Metallurgy Library
5-6. Reactor Experimental Engineering Library
7-9. Central Research Library
10-14. Laboratory Records Department
15. Laboratory Records, ORNL R.C.
16. G. M. Adamson
17. A. L. Bacarella
18. J. E. Baker
19. R. G. Ball
20. S. J. Ball
21. J. C. Banter
22. R. D. Baybarz
23. S. E. Beall
24. L. L. Bennett
25. R. G. Berggren
26. G. B. Berry
27. R. E. Biggers
28. A. M. Billings
29. D. S. Billington
30. E. P. Blizard
31. R. Blumberg
32. E. G. Bohlmann
33. S. E. Bolt
34. C. J. Borkowski
35. B. F. Bottenfield
36. G. E. Boyd
37. J. C. Bresee
38. N. A. Brown
39. F. R. Bruce
40. J. R. Buchanan
41. W. D. Burch
42. C. A. Burchsted
43. S. R. Buxton
44. A. D. Callihan
45. T. A. Carlson
46. W. L. Carter
47. G. H. Cartledge
48. R. H. Chapman
49. R. A. Charpie
50. R. D. Cheverton
51. J. M. Chilton
52. C. J. Claffey
53. H. C. Claiborne
54. W. E. Clark
55. S. D. Clinton
56. T. E. Cole
57. C. W. Collins
58. E. L. Compere
59. R. S. Crouse
60. F. L. Culler
61. J. S. Culver
62. D. G. Davis
63. R. J. Davis
64. V. A. DeCarlo
65. B. D. Draper
66. J. S. Drury
67. W. K. Eister
68. L. B. Emlet (K-25)
69. J. L. English
70. D. E. Ferguson
71. J. D. Flynn
72. D. F. Frech
73. J. H. Frye, Jr.
74. C. H. Gabbard
75. J. L. Gabbard
76. W. R. Gall
77. R. B. Gallaher
78. E. H. Gift
79. H. E. Goeller
80. R. S. Greeley
81. A. T. Gresky
82. J. C. Griess
83. W. R. Grimes
84. E. Guth
85. R. H. Guymon
86. L. A. Haack
87. P. A. Haas
88. J. Halperin
89. P. H. Harley
90. R. J. Harvey
91. P. N. Haubenreich
92. D. N. Hess
93. J. W. Hill
94. E. C. Hise
95. A. Hollaender
96. P. P. Holz
97. H. P. House
98. A. S. Householder
99. S. Jaye
100. G. H. Jenks
101. D. T. Jones
102. E. V. Jones
103. K. O. Johnsson
104. W. H. Jordan
105. S. I. Kaplan
106. P. R. Kasten
107. C. P. Keim
108. M. T. Kelley
109. F. Kertesz
110. S. S. Kirslis
111. J. O. Kolb
112. U. Koskela

113. K. A. Kraus
114. N. A. Krohn
115. J. A. Lane
116. C. G. Lawson
117. R. E. Leuze
118. S. C. Lind
119. R. B. Lindauer
120. C. S. Lisser
121. R. S. Livingston
122. M. H. Lloyd
123. R. A. Lorenz
124. M. I. Lundin
125. R. N. Lyon
126. J. L. Marsh (C&CC, South Charleston)
127. W. L. Marshall
128. J. P. McBride
129. F. C. McCullough
130. H. F. McDuffie
131. H. A. McLain
132. R. A. McNees
133. J. R. McWherter
134. O. Menis
135. E. C. Miller
136. C. S. Morgan
137. K. Z. Morgan
138. L. E. Morse
139. J. E. Mott
140. J. P. Murray (Y-12)
141. I. K. Namba
142. M. L. Nelson
143. P. D. Neumann
144. R. H. Nimmo
145. A. R. Olsen
146. L. F. Parsly
147. R. L. Pearson
148. F. N. Peebles
149. Sigfred Peterson
150. H. O. Phillips
151. M. L. Picklesimer
152. R. H. Powell
153. B. E. Prince
154. J. J. Prislinger
155. L. R. Quarles
156. S. A. Reed
157. W. D. Reel
158. P. M. Reyling
159. S. A. Reynolds
160. L. Rice
161. D. M. Richardson
162. A. E. Richt
163. R. C. Robertson
164. W. Robinson
165. H. C. Roller
166. M. W. Rosenthal
167. H. C. Savage
168. C. E. Schilling
169. H. E. Seagren
170. C. H. Secoy
171. C. L. Segaser
172. E. M. Shank
173. E. D. Shipley
174. M. D. Silverman
175. M. J. Skinner
176. A. N. Smith
177. E. S. Snavely
178. A. H. Snell
179. J. W. Snider
180. I. Spiewak
181. H. H. Stone
182. R. W. Stoughton
183. C. D. Susano
184. J. A. Swartout
185. E. H. Taylor
186. W. Terry
187. D. G. Thomas
188. P. F. Thomason
189. M. Tobias
190. D. S. Toomb
191. W. E. Unger
192. W. C. Ulrich
193. R. Van Winkle
194. D. W. Vroom
195. R. E. Wacker
196. K. S. Warren
197. B. Weaver
198. H. O. Weeren
199. A. M. Weinberg
200. S. H. Wheeler
201. E. P. Wigner (consultant)
202. H. D. Wills
203. G. C. Williams
204. J. C. Wilson
205. R. H. Winget
206. C. E. Winters
207. L. F. Woo
208. W. C. Yee
209. F. C. Zapp
210. ORNL - Y-12 Technical Library, Document Reference Section
211. HRP Director's Office, Y-12

EXTERNAL DISTRIBUTION

212. Division of Research and Development, AEC, ORO
213-794. Given distribution as shown in TID-4500 (14th ed.) under Reactors-Power category (75 copies - OTS)

Reports previously issued in this series are as follows:

ORNL-527	Date Issued, December 28, 1949
ORNL-630	Period Ending February 28, 1950
ORNL-730	Feasibility Report - Date Issued, July 6, 1950
ORNL-826	Period Ending August 31, 1950
ORNL-925	Period Ending November 30, 1950
ORNL-990	Period Ending February 28, 1951
ORNL-1057	Period Ending May 15, 1951
ORNL-1121	Period Ending August 15, 1951
ORNL-1221	Period Ending November 15, 1951
ORNL-1280	Period Ending March 15, 1952
ORNL-1318	Period Ending July 1, 1952
ORNL-1424	Period Ending October 1, 1952
ORNL-1478	Period Ending January 1, 1953
ORNL-1554	Period Ending March 31, 1953
ORNL-1605	Period Ending July 31, 1953
ORNL-1658	Period Ending October 31, 1953
ORNL-1678	Period Ending January 31, 1954
ORNL-1753	Period Ending April 30, 1954
ORNL-1772	Period Ending July 31, 1954
ORNL-1813	Period Ending October 31, 1954
ORNL-1853	Period Ending January 31, 1955
ORNL-1895	Period Ending April 30, 1955
ORNL-1943	Period Ending July 31, 1955
ORNL-2004	Period Ending October 31, 1955
ORNL-2057	Period Ending January 31, 1956
ORNL-2096	Period Ending April 30, 1956
ORNL-2148	Period Ending July 31, 1956
ORNL-2222	Period Ending October 31, 1956
ORNL-2272	Period Ending January 31, 1957
ORNL-2331	Period Ending April 30, 1957
ORNL-2379	Period Ending July 31, 1957
ORNL-2432	Period Ending October 31, 1957
ORNL-2493	Period Ending January 31, 1958
ORNL-2561	Periods Ending April 30 and July 31, 1958
ORNL-2654	Period Ending October 31, 1958
ORNL-2696	Period Ending January 31, 1959